# UNIFORM ENTRY FLOW AT LOW REYNOLDS NUMBER FOR APPLICATION TO PASTE RELEASE PROCESS

Manu Dube

B.Tech, I.I.T. Bombay, 1993

THESIS

Submitted in partial fulfillment of the requirements of
the degree of Master of Science in Mechanical Engineering
in the Graduate School of
the State University of New York at Binghamton
1997

Accepted in partial fulfillment of the requirements for the
Degree of Master of Science in Mechanical Engineering in the
Graduate School of the State University of New York at Binghamton

Dr. C. Sahay ______________________
January 14, 1997
Department of Mechanical Engineering

Dr. D.C. Sun ______________________
January14, 1997
Department of Mechanical Engineering

Dr. J.H. Constable ______________________
January 14, 1997
Department of Electrical Engineering

UNIFORM ENTRY FLOW AT LOW REYNOLDS NUMBER FOR APPLICATION TO PASTE RELEASE PROCESS


## Abstract

**Entry flow for highly viscous fluids is studied for cylindrical and rectangular apertures. The Reynolds number is of the order $10^{-4}$. For the case of circular cross sections, Lew and Fung's (1969) analytical velocity distributions are used for evaluating the maximum shear strain rates. The presence of a radial velocity component which is up to 30 % of the inlet velocity is seen to be a substantial factor in the shear stress distribution in the entrance region. Finite element calculations are carried out for velocity and shear rate distributions using FIDAP. The correlation is found to be good. The numerical solution is then extended to rectangular slots, and the velocity and shear strain rates are determined. The pattern obtained differs from the one obtained for the circular cross section. In particular, as flow progresses, a region of low stress is developed near the corners. The work has potential application in fine pitch solder paste printing in electronics packaging.**

## ACKNOWLEDGEMENTS

I am extremely grateful to my advisor, Prof. C. Sahay for his invaluable help and guidance during this research. I am also thankful to Prof. D.C. Sun, Prof. J.H. Constable and Prof. J. Geer for the time and effort they devoted in helping me with the thesis. The present work would not have been possible without their guidance.

**Table of Contents**

# CHAPTER 1

# INTRODUCTION

## 1.1 Introduction

The microelectronics industry today finds increasing applications in nearly every field. As a result of the expanding scope, and the tremendous demands the new software places on the hardware, more and more computing power is essential. Space and weight constraints make miniaturization the only way feasible. A desktop of today could outperform a mainframe from a few decades ago. Besides, as the equipment finds use in diverse areas, from space and defense to medicine and business, reliability is another major factor. The industry, in the face of increasing global competition is faced with the twin challenges of miniaturization and reliability, both to be accomplished at the least possible cost.

The tremendous reduction in size of components, from vacuum tubes to the solid state transistor, to the chips of today with pitches approaching 8 mils (Socolowski, 1990), has created the need for new manufacturing techniques. One of the strongest trends over the recent years, has been a shift from Insertion Mount (Through Hole) Technology to Surface Mount Technology (SMT). Instead of components with wire shaped terminations, which were inserted through holes on the boards, the components in SMT are mounted on the surface of the board only. SMT provides several benefits over the conventional through hole technology, benefits which have ensured that SMT will continue to replace thru hole technology as the standard method of manufacture. At the same time it has certain limitations at present.

Most of the difficulties in using SMT stem from soldering problems. The problem is not amenable to analytical methods of solution because the characteristics of solder paste are not completely understood. Solder paste consists of alloy powder, with a vehicle and a flux. Thus, an understanding of paste properties would require understanding the complex interplay between the components due to their physical and chemical properties, the metallurgical properties of the alloy, and particle technology, to deal with the alloy particles in a rheologically complex vehicle. Besides, the number of variables involved is quite large. Six factors,viz., the squeegee, the stencil, the solder paste, the substrate, the printer and the post print treatment would directly seem to affect the printing process. These would be discussed in greater detail in the relevant sections.

As a result of the above, printing so far has been treated as an art based on empirical evaluations and experience, rather than on the basis of clearly outlined analytical models. This has meant that while the density of circuits has been growing at an enormous rate, printing techniques have been lagging behind in coping with the requirements. Thus, lack of a conceptual model is a serious problem as pitches get finer and finer, while the demands on reliability get more and more stringent.

## 1.2 Problem Background

Surface Mount Technology, the printing process for solder paste deposition that is a key step of SMT, and the nature of solder paste, are briefly described in this section so as to get an idea of the real problem. The simplifications required in order to make the situation amenable to analytical and numerical analysis are discussed in the next chapter.

### 1.2.1 Surface Mount Technology

As the name implies, SMT is the application of science and engineering principles to assemble at the circuit board level, by placing components and devices on the surface of the circuit board instead of through the board (Hwang, 1989). It encompasses several aspects of the process, such as designing and manufacturing of electrical circuits, designing and manufacturing of the substrates, component placement on the substrates, connecting the components to the substrates, and testing the functioning of the assemblies

The surface mount assembly process involves various steps. First the surface of the circuit board is cleaned so as to make it ready for soldering. Then solder paste is deposited on the board in the required pattern. (As a part of this printing process is of specific interest, it is dealt with in detail in later sections.) Components are then placed on the board using automated pick and place machines. Both accuracy and speed are critical here. The assembly is then baked to evaporate some of the moisture from the solder paste, so as to minimize degassing during solder reflow. The board is then assembled by reflowing the solder paste using techniques like vapor phase or infra red systems. Correct execution of this step, as far as both temperature and time are concerned, is crucial for the reliability and appearance of joints. Finally, the board is cleaned to remove the flux.

### 1.2.2 The Printing Process

Soldering is a critical process in the manufacture of surface mounted boards as it provides inherent advantages over competing techniques for most of the requirements of the electronics packaging industry (Seraphim, 1989). The most common method of soldering used is that of reflow, either vapor or infra-red. Wave soldering techniques like double wave are also used when there is a mix of insertion mount and surface mounted components. Attaching surface components usually involves using the solder paste both as an adhesive to hold the components in place, and as a path of electrical conduction. This requires a reasonably accurate placement of solder deposits over which components can be placed, the pad being reflowed later.

The most common method of paste application is that of printing. The relatively coarser size of solder particles and the geometry of the patterns required make stencil printing an excellent method for fast, economic and repeatable production. The advent of fine pitch technology has placed new demands on the deposition of solder in accurate pads, and stencil printing seems to be the best way in light of these (Figure 1.1). The advantages of stencil printing over the competing process of screen printing can be summarized as follows :

1) Stencils are more rugged than screens

2) High viscosity pastes are easier to use with stencils

3) Deposits conform more to the desirable "square" shape.

4) No-wire meshes lead to better fine line printing, up to well under 10 mils, something that

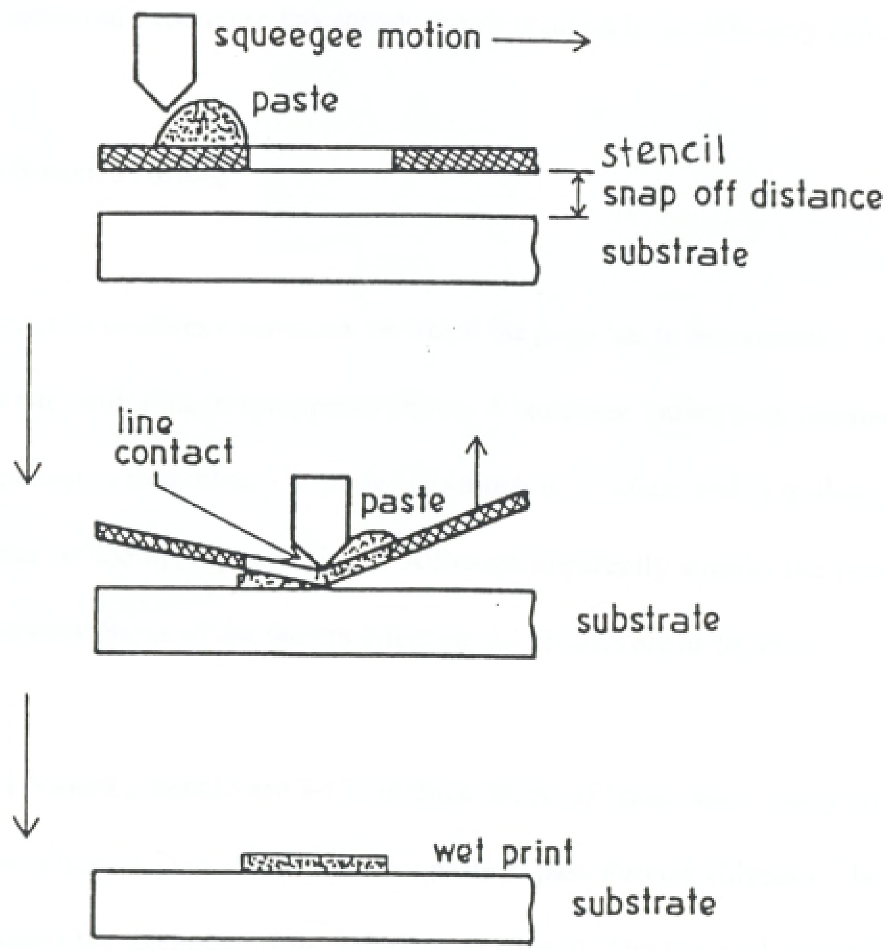


Figure 1.1 : Schematic of Stencil Printing
Ref : Hwang, J.S., "Solder Paste in Electronic Packaging"
Van Nostrand Reinhold, 1989, p164

would not be possible with screens.

5) A thick deposit would require a thick screen, which would get clogged more easily as compared to stencils. Use of lower viscosity paste would not really solve the problem, as then the print pattern definition would suffer.

Screens do have a lower initial cost, and can produce geometries like concentric circles. But overall, industrial experience has shown stencil printing to be definitely better.

### 1.2.3 Stencil Printing

In short, this involves a substrate, on which the paste has to be deposited. A stencil is placed over the substrate, with slots in appropriate places. A squeegee moves over the stencil, pushing the paste that is placed in front of it. The paste rolls along the surface, and is pushed through the slots to be deposited on the appropriate places. Although apparently simple, the process in reality is extremely complex. Some of the factors affecting the process are as follows.

**1.2.3.1 Stencil :** Stencils are 3-12 mil thick sheets of brass, steel, epoxy etc., with openings etched in areas (Figure 1.2) to allow the solder paste to pass through (Slezak). The thickness of the stencil determines the thickness of the solder paste deposit. The material used for a stencil should basically be one which can be easily etched, is somewhat resistant to abrasion from solder powder, is somewhat flexible and shows an adherence for solder powder. The last condition is required as solder would simply slip on a frictionless material instead of rolling, and thus might not be deposited


*Examples of different metal stencils with mesh border.*

Figure 1.2
Ref : Johnson, C.C., Kevra, J., "Solder Paste Technology, Principles and Applications", TAB Books Inc.,1989, p150

into the slots. Except for these requirements, the material is determined mainly by the set-up the manufacturer has to etch the stencils. Steel stencils are better to some extent than brass as far as longevity and rigidity are concerned.The print qualities are very nearly the same. Although the interaction of solder paste with the stencil does differ from material to material, the formulation of the paste is the major factor which controls the same.

**Classification of stencils :** The manufacturing process involved is used for stencil classification as this determines various characteristics of the stencil.

**1) Chemical etch :** A subtractive process, which typically uses photoresists. To minimize the etch out error, i.e. the difference in slot width as the etchant moves in from the surface towards the center, it is carried out from both the sides simultaneously. Registration errors are 1.5-2.5 mils. Aspect ratio is limited to 1-1.5. The artwork designed to create the stencil must take the effect of etch out into account.

**2) Electropolish :** An electrolytic process to smooth out the walls of a stencil produced by chemical etch.

**3) Laser cut :** Laser beam machining gives better accuracy, is cleaner, does not use hazardous chemicals.

**4) Electroforming :** An additive process. A negative pattern is formed by polymerizing a photo-sensitive film on a metal substrate. Then the stencil is formed by nickel deposition onto the substrate.

A stencil is attached to a frame via a tensioned fabric. The frame is made of aluminum out of cost and weight constraints, and thus should be tightened carefully, or else it is susceptible to deformation. Extruded aluminum is preferable to cast aluminum, and is coated with a special powder to protect it from the cleaners employed for the screen. The purpose of the epoxy screen border, which is about 1-3 inches wide, is to provide flexibility to the assembly and reduce the effect of anchoring the stencil to the frame. The recent shift towards fully aqueous or aqueous/saponifier solutions due to environmental concerns has led to increased thermal shock to the epoxy metal bond. To make sure that the squeegee never comes in contact with the fabric border, the stencil should have some extra blank area to take up the squeegee travel. The screen border is less durable, and is subject to abrasion and fraying if the squeegee comes in contact with it. Stencils are usually damaged solely because of improper set-up, misuse, or are made obsolete by design changes. Stencils rarely wear out. The border should not be too wide, otherwise it might get a permanent deformation over time, thereby causing print misregistration. The deformation of the screen as a result of friction when the squeegee moves over the stencil is important mainly for fine line prints.

**1.2.3.2 The Squeegee :** Squeegees are blades, usually made of rubber and secured in holders, which push the solder paste over the stencil. They are mainly of two kind, diamond shaped, with an angle of 45 deg. or straight, inclined at 45-60 from the horizontal (Figure 1.3). The diamond shaped squeegee is used where one blade is used to provide the stroke in both directions. The diamond

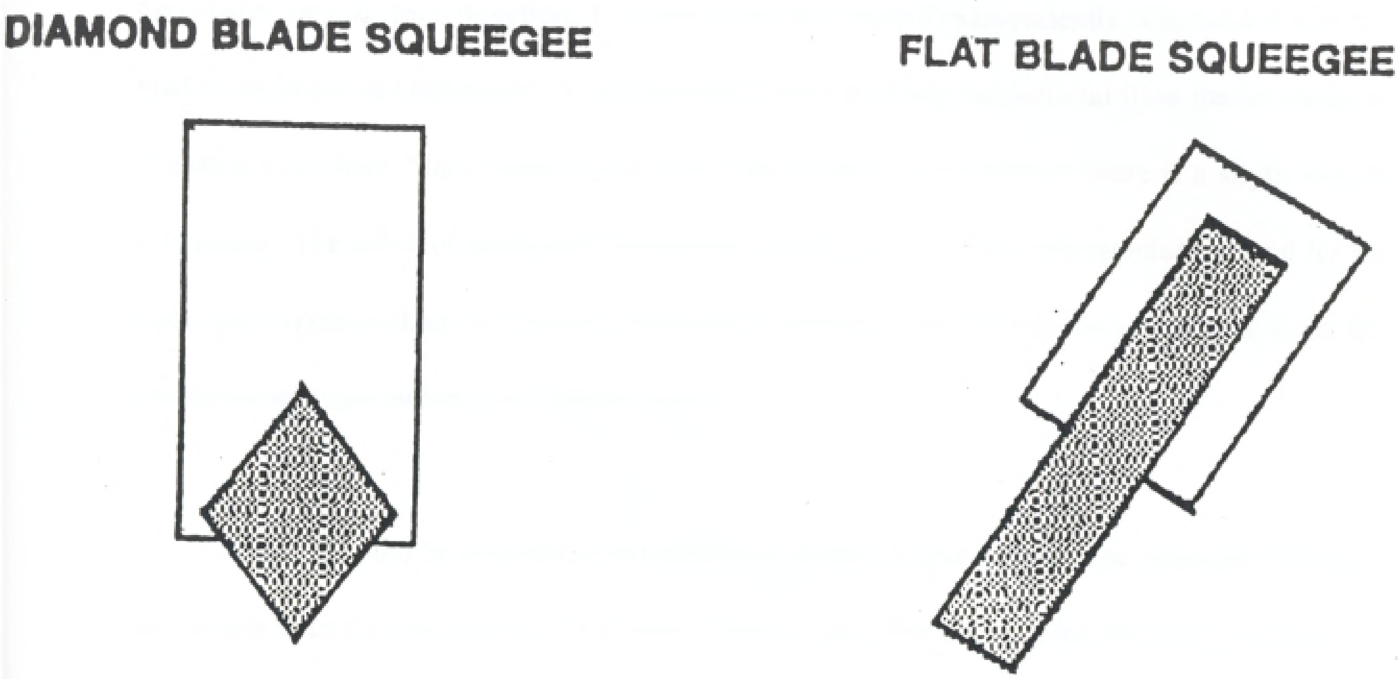


Figure 1.3 Types of squeegee blades

Ref : Dujari, P., "Study of Print Release Process in Solderpaste Printing", Masters Thesis, Department of Mechanical Engineering, Binghamton University, 1994 p. 21

squeegees are preferred as they reduce scavenging effects. At the end of one stroke, the blade hops over the paste and pushes it in the other direction. The straight blade is used in machines which use two blades, one for each direction. The angles can be adjusted independently. The hardness of the blade is an important parameter. A soft squeegee tends to scoop out material from the openings as it passes over them. Hard blades on the other hand tend to miss slots if there is a slight lack of coplanarity. The effect of squeegee load is shown in Figure 1.4. The most popular material for the squeegee is polyurethane which has a moderate hardness, is fairly abrasion resistant, and has fair resistance to hydrocarbons and fluorocarbons.

Blades should be kept sharp and straight to ensure proper wiping. The squeegee should be cut to size to fit the stencil to avoid fraying of the border. The angle of the blade is important too, as that affects the pressure acting on the paste as the latter rolls in front of the squeegee.

Since the squeegee deforms under the action of the force pushing it against the stencil, the force on the squeegee affects the paste pressure too, and hence the printing. For best results, excess pressure should be avoided.

**1.2.3.3 The Printer :** Machines vary in complexity and size. The maximum expected board size should be about 60-70% of the machine capability, so as to allow for screen borders. The quality of a printer is judged by repeatability of the print stroke, durability, and lack of design flaws.

Printing can be on contact, in which the stencil touches the substrate, or off contact, where

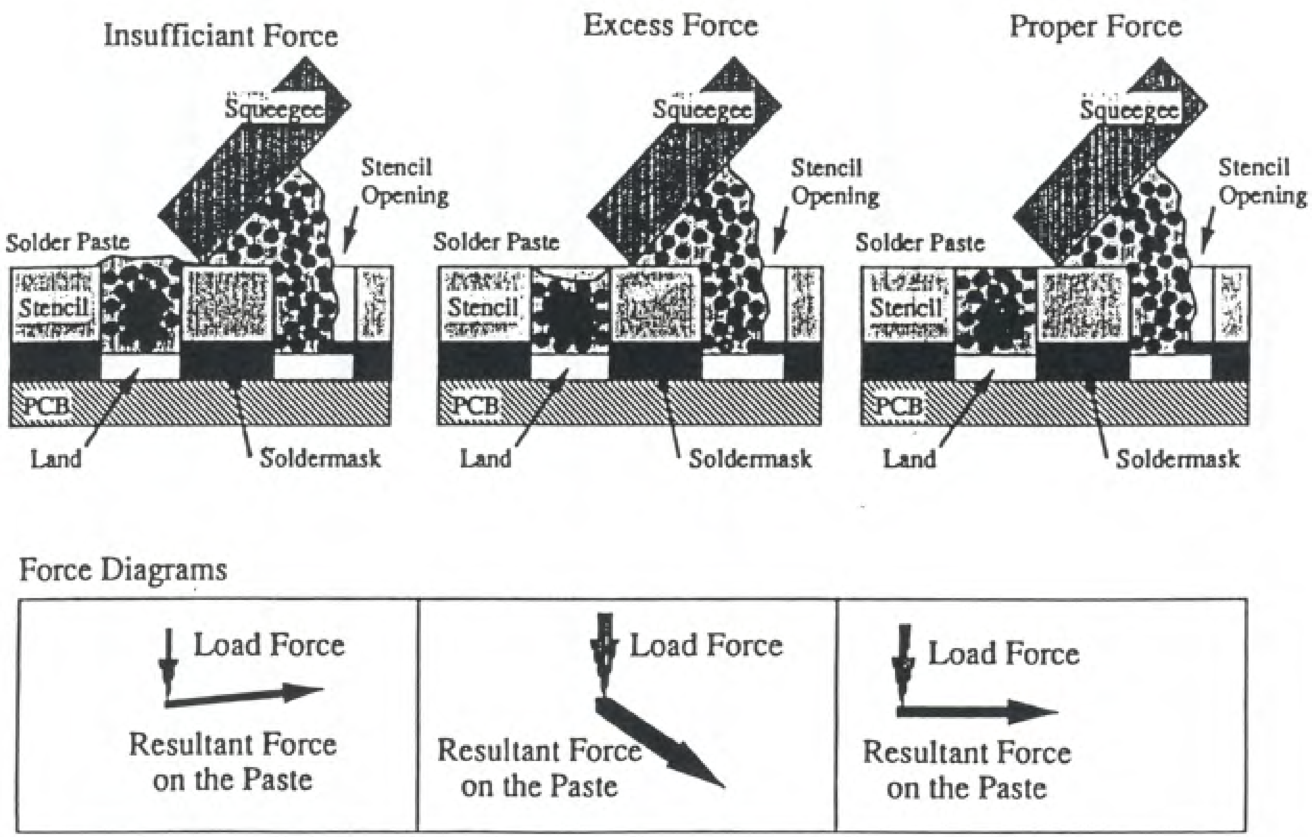


Figure 1.4 . Effects of Squeege Force on Paste Print Volume
Ref : Marcoux, P., "Fine Pitch Surface Mount Technology", Van Nostrand Reinhold, 1992,

the stencil is at a "snap off" distance away from the substrate, depending on the stencil thickness and pitch size. On contact printing is preferred as it is easier to set up, and can run with lower squeegee pressure, which helps maintain the alignment of the stencil. But as all the paste is pulled out of the stencil at one time, a lot of friction is generated, leading to cone shaped deposits. Off contact printing has the advantage that the paste is pulled out sooner after it has been deposited, as soon as the stencil snaps back. So, the paste does not have enough time to regain its viscosity, and set in the holes. Off contact printing can take care of minor non-planarity of the board. But in this case, the registration of the stencil shifts by a few mils, which could be important for fine pitch printing. Besides, the higher squeegee pressure promotes the spread of paste under the holes in case of a soldermask misregistration.

### 1.2.4 Soldering and Solder Paste

In electronic packaging, an interconnection is an electrical path or bridge between two different levels of circuitry. Soldering is, in general, a low temperature joining process that is reversible (Seraphim,1989), making it especially attractive since repair and rework are necessary considerations in the production of electronic assemblies.

**Solder Paste :** The process of soldering uses solder paste as the joining material. Solder paste can be defined as a "homogeneous and kinetically stable mixture of solder alloy powder, flux, and vehicle, which is capable of forming metallurgical bonds at a given set of soldering conditions and can be readily adapted to the automated production of reliable and consistent solder joints". Solder paste has many properties which favor its use in the industry. In the deformable viscoelastic form, it can be applied in a selected shape and is amenable to automated processes. Its tacky characteristic helps hold the parts in position without additional adhesives before permanent bonds are formed. The metallic nature provides relatively high electrical and thermal conductivity. The vehicle is primarily a carrier of the solder powder and provides the required rheology. The flux causes the surfaces and the alloy powder to be joined to maintain a clean metallic state that promotes good adhesion. At the end of the process, both the vehicle and the flux are removed, but they are crucial to the formation of a reliable and a permanent bond.

Solder paste technology is a complex interplay of various technologies and factors, and till recently, it has not been understood completely. The final test of the performance of course remains the performance of the paste in its ability to adapt to the technique used, its solderability, its physical and chemical properties, and joint integrity. Printability of the paste is critical in this regard. Also important are ease of visual inspection and simplicity of repair.

#### 1.2.4.1 Desirable Paste Behaviour for Printing

From an applications point of few, solder paste should have a desirable shelf life without gravitational separation of metal particles and the matrix. For proper print definition and deposit topography, solder paste should not have dripping tendencies as well as no stringiness. The paste should have enough tack to hold the components before reflow. The solder paste should not slump or sag, i.e. the area covered by it on the substrate should not increase due to paste flow after reflow before cooling. Besides, solder paste should be released cleanly from the stencil during the release process.

### 1.2.4.2 Factors affecting Behaviour of Paste during Printing

**Particle shape :** Particle shape plays an important role in determining the paste performance. Shape influences the rolling or flow characteristics of the solder paste during stencil printing, as well as its ability to be pushed through a stencil aperture. Shape also has an effect on the apparent density of the paste, and thus its rheology as well as viscosity. The industry has concluded virtually unanimously that the ideal shape for particles is spherical. There are several reasons for this. A sphere can be produced fairly repeatably under the correct processing conditions as surface tension naturally tries to give the drops of molten metal a spherical shape. This shape has no preferred directions, and can hence easily pass through openings. Also, the surface area to volume ratio is the least here, minimizing the opportunity for oxidation.

It has been shown that spherical particles alone might lead to some slump and flow problems. Some proportion of non-spherical particles may thus be required. Various reasons, like oxide layers and inertial forces might lead to deviations from a perfect spherical shape during production.

**Particle size and distribution :** The required size of particles depends on a number of factors, the first being the method of application. In stencil printing, the particles should be able to pass through the openings on the stencil. As a rule, the maximum particle diameter should be less than one-third to one -fourth the smallest dimension of the stencil opening so that it would be impossible for two particles to block the opening. Similar considerations exist for syringe dispensing. If a very small amount of solder paste is to be transferred, oversized particles can cause very uneven deposition. This is important when there is a need to create a thin reflowed layer of solder on a pad or land area on the board.

Too large a particle size could lead to particles being exposed over the fluxed surface, leading to oxidation and soldering problems. If particles are too fine, the surface area is larger, which could lead to oxidation. Besides, this could also lead to viscosity instability. Particles below 20 microns show a greater tendency to exhibit solder-balling.

Too wide a range of size distributions has its obvious problems. But too narrow a range also leads to stacking of particles instead of interlocking. For a good metal content of paste, as well as good printability and tack, there should be a reasonable mix of particle sizes, with the smaller ones filling the interstitial spaces between the larger particles.

Particle sizes are usually classified using "mesh sizes", the three main ones being 100, 200 and 325 mesh. A powder designated -200/+325 for instance will pass through a 200 mesh but not through a 325 mesh. 100 mesh particles are usually too coarse for surface mount processes, although stenciling can tolerate up to -100 mesh. Mesh sizes and diameters in microns can be correlated as follows:

| MS | Dia (microns) |
|---|---|
| -325 | D< 45 |
| -270 | D< 55 |
| -200 | D<75 |
| -200,+325 | 45<D<75 |

**Fluxes :** A flux is a substance that chemically cleans the surfaces to be joined by removing surface oxides and tarnishes, providing good wettability, protects the surfaces from further oxidation during the soldering process, so that a metallic continuity at the interface and a complete coalescence of the solder powder during reflow can be achieved. Besides, it should leave a residue containing the ingredients of the flux and the products of the reactions which are non-corrosive or removable by standard cleaning methods. In general, any chemicals capable of providing good reactivity with metal oxides and cleaning the metals commonly used in soldering area could be candidates.

In order to satisfy all the conditions required above, the flux itself is a paste, a mixture of various substances. A typical solder paste flux might consist of rosin/resin, solvent, activator, thickeners/rheological agents, and other additives. Complex mixtures of multiple components of each type might be present to get the right properties. Rosins improve wetting and spreading properties. Resins contribute to high temperature flow properties and impart tack. Resins also contribute to flux activity in rosin based fluxes. Resins provide the main body which determines the ultimate rheology of the paste. Synthetic resins give consistency, thermal stability, less fuming, and don't leave behind tacky deposits (Murch, 1992). Resins and rosins are dissolved using solvents.

Activators give the flux its cleaning ability, the strength of the flux being decided by the amount of the activator. Thickeners, viscosity modifiers or rheological control agents are usually added in small percentages to "thicken" the flux so as to suspend the particles, thereby preventing them from settling down. They also impart certain flow properties to facilitate consistent application. Other ingredients might include surfactants or tackifiers. The flux used affects paste rheology to a great extent.

### 1.2.5 Printing Related Properties of Solder Paste

**1.2.5.1 Rheology :** Rheology is the study of the flow and deformation of materials when subjected to a stress. This is important during application, as all processes apply some stress on the paste with the desired result being the deposition of paste in specific volumes and shapes at specific locations. The goal of rheology, as far as the field of electronics packaging is concerned, is to determine the forces required to achieve the desired transfer of paste. A brief classification of fluids has been presented in the following paragraphs to put the rheology of solder paste into proper perspective.

Fluids may be broadly classified into two, Newtonian and non-Newtonian. Newtonian fluids have a linear stress-rate of shear relationship, as against non-Newtonian, which have a non-linear one. Non-Newtonian fluids are further classified as Bingham plastic, pseudoplastic, and dilatant. Time dependant fluids are classified as thixotropic or rheopectic. Various fluid behaviors are shown in Figure 1.5. Newtonian fluids have a linear relationship as discussed, the slope of the line being

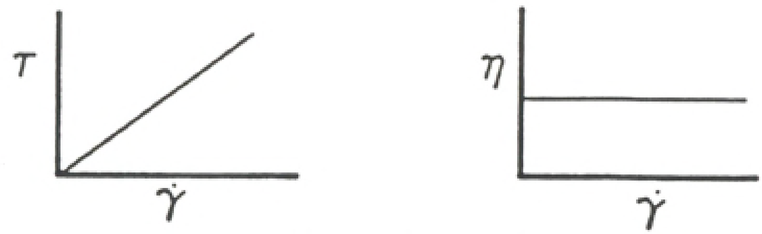


Newtonian flow.

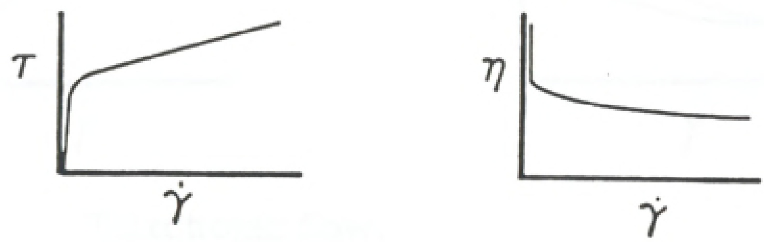


Plastic flow.

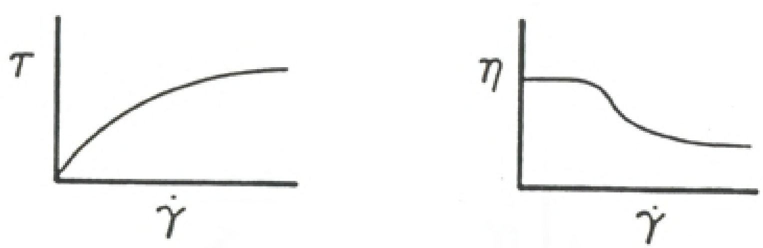


Pseudoplastic

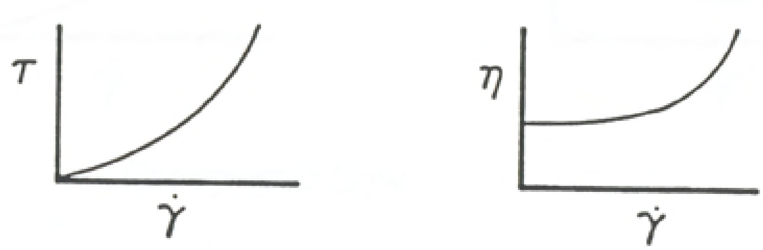


Dilatant flow.

Figure 1.5

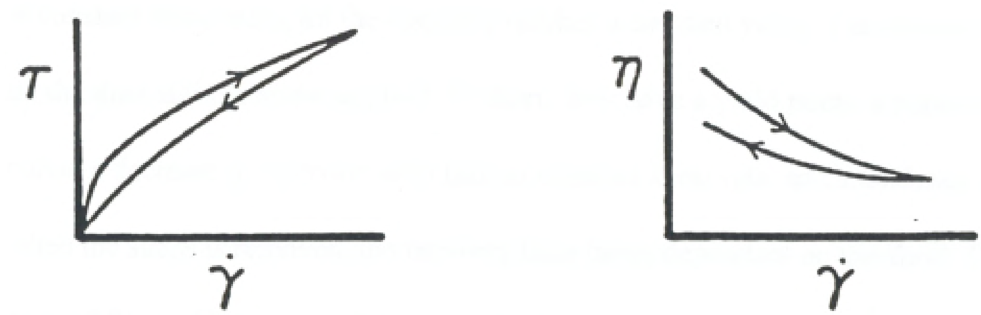


Thixotropic flow.

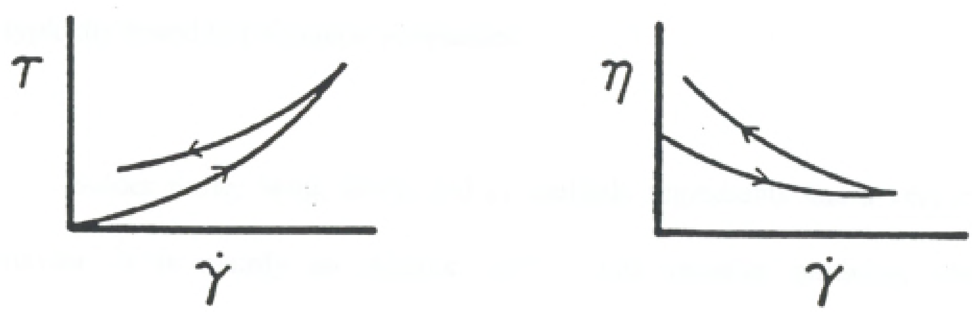


Rheopectic flow.

Figure 1.5 (cont) .
Ref : Hwang, J.S., "Solder Paste in Electronics Packaging", Van Nostrand Reinhold, 1989, p. 128

defined as the viscosity. Bingham plastics are similar but for a yield value, below which they do not flow. Pseudoplastics have the characteristic that the amount of shear stress needed for a given increase in the strain rate decreases with the strain rate. The slope of the tangent at any point gives the apparent viscosity. Dilatant fluids show a behavior opposite to that of pseudoplastic, with an increasing apparent viscosity with shear rate. Rheopectic fluids are those for which viscosity increases with time, at constant shear rates. Thixotropic fluids show a decrease in viscosity with time at constant shear rates, till the viscosity reaches a constant value. The decrease in viscosity depends on the time and the stress applied. In short, they have a yield point, a plastic or pseudoplastic flow curve, a decrease in viscosity with time at constant shear rate, and a tendency to regain the viscosity when the stress is removed, the recovery time being dependant on the fluid. Thixotropic flow is the kind of flow which is usually encountered in solder printing.

A characteristic of fluids which are used in printing processes is viscolelasticity. This signals rheological behavior somewhere between that of an ideal elastic solid, and an ideal fluid. Such a fluid can store some of its energy and can recover partially when the stress is removed. The behavior is typically found in polymeric substances.

Solder paste, being composed of multiple ingredients has a very complex rheological behavior. It is mainly an organic matrix, with metallic particles, which are distributed homogeneously in the matrix with or without the aid of dispersion agents. The drastic differences in density between the matrix and the suspended metallic particles, the relatively large particle size of spherical particles, a high load of particles, all combine to complicate paste behaviour during printing. As discussed above, solder paste behaves mainly as a thixotropic fluid.

**1.2.5.2 Viscosity :** Viscosity is the ability of a fluid to dissipate energy, and refers to the resistance offered by one layer of fluid to the motion of an adjacent layer. As has been discussed above, solderpastes show thixotropic behavior. Besides, viscosity also decreases with temperature, at lower metal content, and lower air entrapment. Typical values are 400-900 kcps for stencil or screen printing, and 100-400 kcps for syringe dispensing. Rheological modifiers are used to get the desired characteristics.

**1.2.5.3 Surface Tension :**Another important property is surface tension, which along with viscosity determines the wetting characteristics of the paste. Wetting is a must for proper formation of joints, and is determined by the dihedral angle with a solder drop on the surface as shown in Figure 1.6. Slump, tack and shelf life have already been discussed in detail in the section on desirable characteristics. Another parameter which can be used is work life, which determines the time that can elapse between paste deposition and placement of components. Usually it is based on tack, but a more detailed estimate can be obtained by including change in viscosity and percentage of solder balls with time.

## 1.3 Objective of Thesis

The flow of solder paste through a stencil consists of the fill and release process. During the fill process, the paste is pushed into the apertures under pressure generated by the motion of the

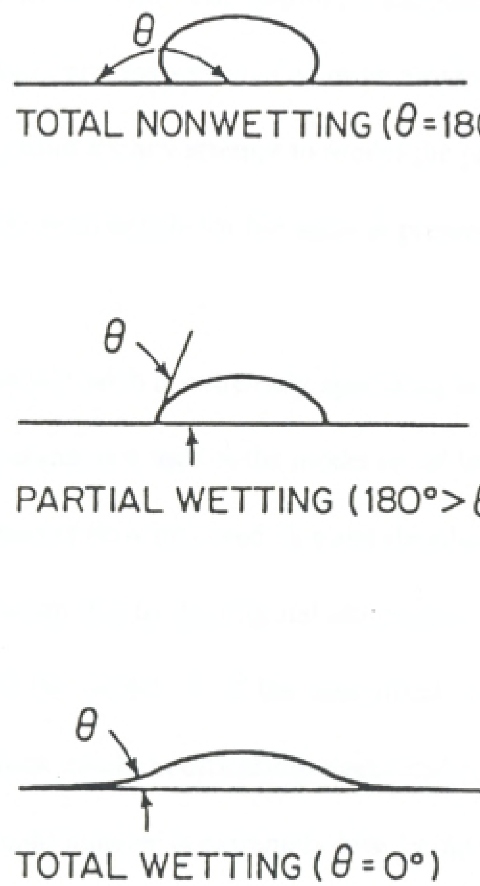


Figure 1.6. Degrees of Wetting
Ref : Dujari, P., "Study of Print Release Process in Solderpaste Printing", Masters Thesis, Department of Mechanical Engineering, Binghamton University, 1994 p. 46

squeegee. During the release process, the stencil is lifted off the substrate, and the paste is deposited on the board.

A study of the whole process of solder paste printing, the most popular method today of applying solder paste, would be extremely time consuming. So, for this work, it is proposed to concentrate on the paste release process, i.e. how the paste flows out of the stencil apertures and is deposited onto the board as the stencil is pulled off the board. The aperture is supposed to have been filled perfectly during the fill process. The release process seems to be more amenable to analytic treatment, and thus, provides a natural starting point for any attempt to model the printing process fully. Beside, not much technical work seems to be available for the same at present.

Sahay et al. (1995) have developed a model which is extremely appealing for its simplicity and ease of application. However, certain approximations used in the model could be replaced with others, which are more appropriate for the regimes of flow involved. A more detailed analysis with better approximations would show if the deviation due to the original assumptions is significant enough so as to require drastic alterations in the model, or if the simplified model could be developed further for more realistic cases, without much modification. Specifically, the formation of a boundary layer is not assumed as the Reynold number is extremely low, being of the order of magnitude $10^{-4}$. Besides, the maximum shear stress at any point, for testing if the paste has exceeded the break stress, is calculated using the eigenvalues of the stress matrix in which no terms are neglected. As will be shown later, certain terms which were ignored in the original model turn out to be the dominant terms in substantial regions of the flow.

Finite element solutions are carried out for circular apertures, and the results are compared to those obtained analytically. Rectangular apertures, for which no analytical solutions are available, are also studied using finite element techniques.

A paper based on the present work (Dube and Sahay, 1996) has been presented at the Winter Annual Conference of the ASME.

# CHAPTER 2

# PROBLEM MODELING

As described earlier, the printing process is quite involved. This chapter describes the paste release part of the process, and states simplifying assumptions so as to make the problem tractable to analysis. Assumptions can be made regarding the properties of the materials involved, the geometry of the problem, and the process conditions.

## 2.1 Material Simplifications

During the printing process, solder paste behavior could be modeled as that of a fluid although one with extremely complex behavior. Since the aim here is to create the simplest possible model, an attempt is made at approximating the behavior of the paste by a simpler fluid, and to see if it is sufficient for the purpose. Various kinds of fluid behavior are described, so that one can be selected for the paste, and the limitations of the same are clearly understood.

### 2.1.1 Fluids

A fluid can be defined to be a substance which must continue to change shape as long as there is a shear stress present, however small. An ideal fluid is a simplification which offers no resistance to shear stresses, i.e., it can take only normal compressive stresses, and shear stress is zero throughout the volume of the fluid.

Real fluids do show some resistance to shear stresses. This property is called viscosity. In general, there exists some relation (Mase, 1970) between the viscous stress tensor ($\tau_{ij}$) and the rate of deformation tensor ($D_{ij}$), expressed as:

$$\tau_{ij} = f_{ij}\,(D_{pq}) \qquad (2.1)$$

Such fluids are called Stokesian fluids. In the special case where the relationship is a linear one, the fluid is called Newtonian:

$$\tau_{ij} = K_{ijpq}\, D_{pq} \qquad (2.2)$$

The constants ($K_{ijpq}$) are called "viscosity coefficients." Using standard techniques, a relationship of the following form can be given, which is similar to Hooke's law..

$$\tau_{ij} = -p\,\delta_{ij} + \lambda^{*}\,\delta_{ij}\,D_{kk} + 2\,\mu^{*}\,D_{ij} \qquad (2.3)$$

Stokes condition gives

$$\lambda^* + \frac{2}{3}\mu^* = 0 \quad (2.4)$$

$\lambda^*$ and $\mu^*$ are viscosity coefficients of the fluids, and p is the pressure. Equation 2.4 above is a commonly used assumption which states that the "bulk" viscosity is zero.

### 2.1.2 Basic Equations for Newtonian Fluid

In Eulerian form, the basic equations which all Newtonian fluids have to satisfy are

(1) Continuity equation:

$$\dot{\rho} + \rho v_{i,i} = 0 \quad (2.5)$$

(2) equation of motion:

$$\tau_{ij,j} + \rho b_i = \rho \dot{v}_i \quad (2.6)$$

(3) energy equation:

$$\dot{u} = \frac{1}{\rho}\tau_{ij} D_{ij} - \frac{1}{\rho} c_{i,i} + z \quad (2.7)$$

(4) constitutive equation:

$$\tau_{ij} = -p\,\delta_{ij} + \lambda^{*}\,\delta_{ij}\,D_{kk} + 2\,\mu^{*}\,D_{ij} \tag{2.8}$$

(5) kinetic equation of state:

$$p = p(\rho, T) \tag{2.9}$$

and if thermal considerations are involved,

(6) Fourier law of heat conduction:

$$c_i = -k\,T_{,i} \tag{2.10}$$

(7) caloric equation of state:

$$u = u(\rho, T) \tag{2.11}$$

Here, $\rho$ is the density, $v_i$ is the velocity, $\tau_{ij}$ is the stress, $b_i$ is the body force per unit mass, u is the specific internal energy, $c_i$ is the heat flux per unit area per unit time by conduction, z is the radiant heat constant per unit mass per unit time, p is the pressure, and T is the temperature. $D_{ij}$ is the rate of deformation tensor as mentioned above. A $(\dot{\ })$ denotes differentiation with respect to time. It can be seen that there are sixteen equations and sixteen unknowns, i.e., the system is determinate.

All temperature effects are ignored, and the fluid is assumed to be incompressible, Newtonian. This simplifies the model considerably and also permits direct comparison with the model developed previously (Sahay, 1995). The approach should also help show if a Newtonian fluid model, with more appropriate assumptions would be sufficient for the process. The above equations can therefore be simplified to give the Navier Stokes equation for incompressible fluids ($v_{i,i} = 0$) as

$$\rho \dot{v}_i = \rho b_i - p_{,i} + \mu^* v_{i,jj} \tag{2.12}$$

This equation has to be solved, taking into consideration the boundary conditions, as well as the initial conditions to get the flow patterns and all the related stresses. For a viscous fluid, the velocity at fixed surfaces is zero. This condition is one that has been obtained experimentally. For an inviscid fluid, only the normal component needs to be zero.

Non dimensionalising the Navier Stokes equation gives several dimensionless parameters. The most well known of them being Reynolds number (Re), defined as

$$Re = \frac{\rho V L}{\mu} \tag{2.13}$$

where $\rho$ is the density, V is a characteristic velocity, L a characteristic length and $\mu$ the dynamic viscosity.

As is obvious the equations above are a set of nonlinear equations, and thus, are quite tedious to solve for complicated real life cases. The source of trouble is the non linear convective term on the left hand side of Eq. 2.12. In real life, various approximations are used to help solve the equations, depending of course on the conditions of flow.

Fluid flow analysis determines various regimes of flow with the corresponding approximations. Thus, flow may be steady (time independent) or unsteady, inviscid or viscous, compressible or incompressible, as the case may be. Each of these may occur in combinations, and may even have subclasses. For instance, viscous flow can be laminar, turbulent, or transitional, depending on the Reynolds number. The regimes refer more to flow conditions in specific regions of the flow rather than to the fluid itself.

### 2.1.3 Reynolds Number

Whether the fluid flow is laminar or turbulent can be determined by the Reynolds number. For pipe flow, it has been determined that Reynolds number less than 2000 indicates laminar flow, and values more than 3000 indicate turbulent flow. The intermediate range is that of "transitional" flow. This ability of dimensionless numbers to provide an insight into the nature of diverse flows constitutes their major usefulness.

Reynolds number for instance indicates where certain approximations, like those for creeping flow, could be applied, and is the indicator that the boundary layer model used in the previous analysis (Sahay, 1995) might lead to problems like the continuity equation being violated in the central core, which was treated as inviscid.

### 2.1.4 Laminar Flow through a Pipe

In flow through a pipe, the conditions near the entrance are determined by the boundary conditions. An example of a boundary condition would be a flat velocity entrance profile. As the fluid enters the pipe, the velocity on the sides goes to zero in accordance with the boundary conditions for viscous fluids. There is thus a region called "entrance length" where the fluid has a radial component of velocity in addition to the axial one, so as to satisfy the equations of motion and continuity. After some distance, the flow settles down to a parabolic linear velocity distribution. At this stage, it is described by Poiseuille flow, and is fully developed. The entrance length has been found to be a function of the pipe diameter and the Reynolds number. For the range of flows of interest, the Reynolds number, as calculated in the next chapter, shows that the flow is in the "creeping flow" regime, and that the Navier Stokes equation is simplified to Stokes equation, where the nonlinear term can be dropped. The details are given in Chapter 3.

## 2.2 Geometry Simplification

The most common geometry used for stencil apertures is rectangular. However, since circular cases are easier to analyze due to axi-symmetry, circular apertures are studied first. The previous model related more complex geometries to circular apertures using the concept of "hydraulic diameter," which would not seem to be advisable. This is because the shear rates are obtained from the differentiation of the velocity field, and thus, are highly sensitive to the actual velocity field. Finite element techniques are used for studying rectangular apertures, where calculations have been based on the same dimensions as used in the previous model to facilitate comparison.

Hydraulic diameter is defined as:

$$D = \frac{4\,A}{P} \tag{2.14}$$

where A is the cross sectional area, and P is the wetted perimeter.The concept is a powerful tool for practical analysis, however, it is defined with some specific equivalence in view. It is important to keep in mind the limitations of the analogy as we use it.

## 2.3 Process Simplification

The specific process of concern is paste release. After the stencil apertures have been filled by solder paste during the filling process, as discussed in Chapter 1, the stencil is lifted and some of the paste sticks to the walls of the stencil and is lifted off, while the rest is deposited on the board. The process thus involves a transient flow of the paste through an aperture of finite size, with another boundary at the board end.

Following the previous model, the process is modeled as a steady state uniform entry of a fluid in an infinite duct. The difference is in the approximation used to model the flow, i.e., creeping flow instead of boundary layer. The aim is to see if the results obtained would justify the previous model, or would require more accurate modeling of the material properties and process conditions. The details of the individual models are discussed in the relevant chapters which deal with the specific cases.

# CHAPTER 3

# ANALYTICAL STUDY FOR FLOW THROUGH CIRCULAR APERTURES

This chapter deals with the analytical treatment of a highly viscous, incompressible Newtonian fluid flowing through a cylindrical tube. The Reynolds number is of the order of $10^{-4}$. For such low Reynold's number, the non linear Navier Stokes equation can be simplified substantially to Stokes equation. Lew and Fung (1969) have given the solution for the velocity fields for such a flow. Here, strain rates are obtained from the velocity field obtained by Lew and Fung (1969) and the maximum shear strain rates are determined at various points. The results are used as a reference for comparison with finite element calculations discussed in the next chapter so as to validate the numerical solutions. Finite element solutions are subsequently extended to the case of rectangular apertures.

## 3.1 Problem Definition

The velocity and the strain rate fields for entry flow of solder paste into a long cylindrical tube are determined assuming steady state incompressible flow. The solder paste is assumed to be Newtonian. The aperture most widely used in electronics packaging is rectangular. An equivalent circular aperture is studied, based on the concept of equivalent hydraulic diameter discussed in Chapter 2.

### 3.1.1 Data Used

As the aim is to compare with the previous model (Sahay et. al, 1995), all dimensions used are the same as those used for sample calculations in the previous model. The radius of the tube is taken to be .00016891 m, and the length, three times the radius, is .00050673 m. The length can be assumed to be effectively infinite for calculation purposes. The assumption is borne by the calculated results which show that the flow becomes identical to Poiseuille flow after about one and a half times the radius (Lew and Fung, 1969). The fluid is assumed to have a density of 5500 $kgm^{-3}$ and a viscosity of 1000 $Nsm^{-2}$. These values are common for solder paste. The tack strength of the fluid is taken to be 50000 Pa. The inlet velocity is .203 $ms^{-1}$ in the axial direction (Figure 3.1). The Reynolds number for the flow can be calculated to be $3.77 \times 10^{-4}$. The numbers used could probably be presented more conveniently using other systems of units. However, they have been reported as above due to the fact that the finite element calculations carried out in the following chapters are seen to be sensitive to the actual numerical values input into the code. Hence it is imperative that all numbers be reported exactly, in a consistent system of units.

### 3.1.2 Governing equations

The governing equation for the problem is obtained as a simplification of the Navier Stokes equation for incompressible fluids:

$$\rho\dot{v}_i=\rho b_i-p_{,i}+\mu v_{i,jj} \qquad (3.1)$$

For extremely low Reynold's number, the above can be simplified to

$$-p_{,i}+\mu v_{i,jj}=0 \tag{3.2}$$

The inertia forces represented by the convective term (Van Dyke, 1964) may be ignored because at low speeds, being quadratic in velocity, they are ineffective. Hence the pressure forces must be balanced by viscous forces alone. The simplification is useful as the equation is linearized and is much more amenable to solution. The time derivative term vanishes as a steady state case is being considered.

As the fluid is incompressible, the continuity equation reduces to

$$v_{i,i}=0 \tag{3.3}$$

### 3.1.3 Boundary Conditions

At the inlet, axial velocity is taken to be .203 m/s while the radial velocity is zero. At the walls, the no slip condition implies all velocity components are zero. At an infinite distance along the tube, the axial velocity u tends to $u_p$ where $u_p$ is the velocity distribution given by Poiseuille flow. The radial velocity is zero in this region.

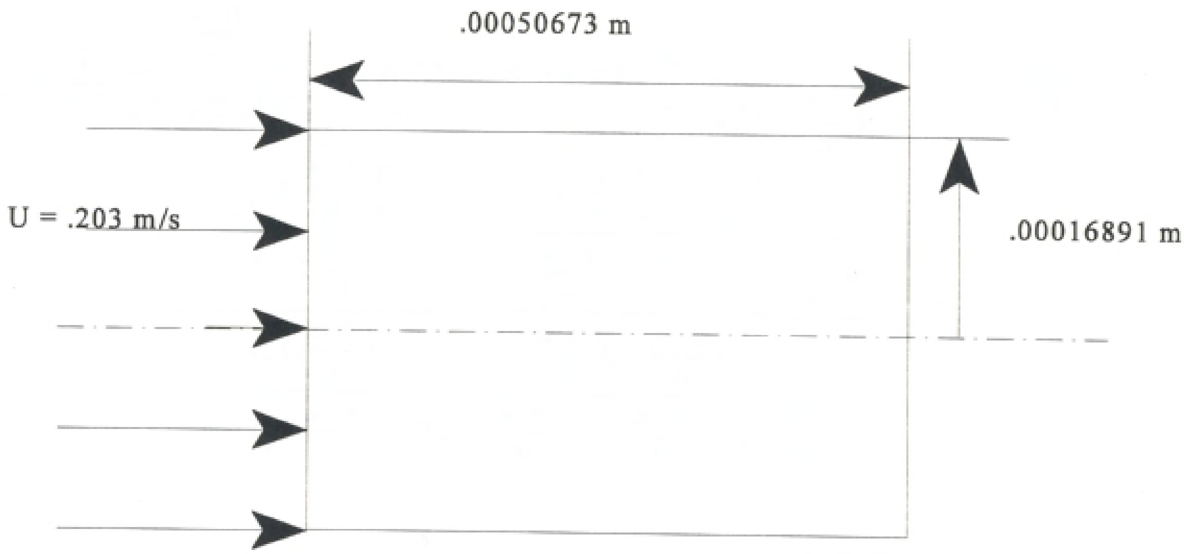


Figure 3.1 : Schematic of tube , with flow at inlet

## 3.2 Solution

The solution for the velocity field is given by Lew and Fung (1969) as follows

$$\frac{v}{U} = \sum_{n=1}^{\infty} A_n \left( k_n \frac{x}{a} e^{-k_n \frac{x}{a}} \frac{J_1 \left(k_n \frac{r}{a}\right)}{J_1 \left(k_n\right)} \right.$$

$$\frac{4}{N} k_n \sum_{m=1}^{\infty} \frac{\frac{m \Pi}{N}}{k_n^2 + \left(\frac{m \Pi}{N}\right)^2} x \left( e^{-N k} \cos (m \Pi) \left(\frac{N}{2} + \frac{k_n^2}{k_n^2 + \left(\frac{m \Pi}{N}\right)^2}\right) \sin \left(\frac{m \Pi}{N}\right) \right.$$

$$x \frac{\dfrac{I_1 \left(\frac{m \Pi}{N} \frac{r}{a}\right)}{I_0 \left(\frac{m \Pi}{N}\right)} - \dfrac{I_0 \left(\frac{m\Pi}{N} \frac{r}{a}\right) \frac{m\Pi}{N} \frac{r}{a}}{2 I_0 \left(\frac{m \Pi}{N}\right) + \frac{m \Pi}{N} I_1 \left(\frac{m \Pi}{N}\right)}}{\dfrac{I_1 \left(\frac{m \Pi}{N}\right)}{I_0 \left(\frac{m \Pi}{N}\right)} - \dfrac{\frac{m \Pi}{N} I_0 \left(\frac{m \Pi}{N}\right)}{2 I_0 \left(\frac{m \Pi}{N}\right) + \frac{m \Pi}{N} I_1 \left(\frac{m \Pi}{N}\right)}} \Bigg) \qquad (3.5)$$

$$\frac{u}{U}=2\sum_{n=1}^{\infty} A_n[(1+k_n)\, e^{\frac{-k_n x}{a}}$$

$$k_n \sum_{m=1}^{\infty} \frac{\frac{m\Pi}{N}}{k_n^2+\frac{m^2\Pi^2}{N^2}} \times \left(e^{-N k_n} \cos(m\Pi)\left(\frac{N}{2}+\frac{k_n}{k_n^2+\left(\frac{m\Pi}{n}\right)^2}\right)-k_n^2+\left(\frac{m\Pi}{n}\right)^2\right) \cos\Bigg($$

$$\times \frac{\dfrac{I_0\left(\frac{m\Pi}{N}\frac{r}{a}\right)}{I_0\left(\frac{m\Pi}{N}\right)}-\dfrac{2\, I_0\left(\frac{m\Pi}{N}\frac{r}{a}\right)+\frac{m\Pi}{N}\frac{r}{a} I_1\left(\frac{m\Pi}{N}\frac{r}{a}\right)}{2\, I_0\left(\frac{m\Pi}{N}\right)+\frac{m\Pi}{N} I_1\left(\frac{m\Pi}{N}\right)}}{\dfrac{I_1\left(\frac{m\Pi}{N}\right)}{I_0\left(\frac{m\Pi}{N}\right)}-\dfrac{\frac{m\Pi}{N} I_0\left(\frac{m\Pi}{N}\right)}{2 I_0\left(\frac{m\Pi}{N}\right)+\frac{m\Pi}{N} I_1\left(\frac{m\Pi}{N}\right)}}\Bigg)+2\left(1-\frac{r^2}{a^2}\right) \qquad (3.4)$$

The symbols in these formulas are explained as follows:

a = radius of the tube

r = radial distance of point away from tube

x = axial distance of the point downstream from the inlet

u = axial velocity at any point

v = radial velocity at any point

U = inlet axial velocity

$A_n$ are coefficients determined from the entry conditions. The first 19 coefficients obtained by applying

the inlet conditions at 19 points along the cross section have been calculated as

$A_{1\text{-}19}$ = -.41213, 0.29508, 0.23089, 0.17204, 0.12982, 0.09896, 0.07565, 0.05760, 0.04316, 0.03219,

0.02332, 0.01638, 0.01104, 0.00704, 0.00416,

0.00221, 0.00099, 0.00033, 0.00006

It can be seen that the $A_n$ decrease rapidly for increasing n, and that taking the first 19 terms would be a good enough approximation.

N = ratio of length of the tube to the radius, and is taken as 3 for calculations.

$J_i$ is the Bessel function of the first kind, order i

$I_i$ is the modified Bessel function of the first kind, order i

$k_n$ is the $n^{th}$ zero of the Bessel function $J_0$

The first seven zeroes are (CRC,1991)

2.4048, 5.5201, 8.6537, 11.7915, 14.9309, 18.0711, 21.2116

higher zeroes can be calculated using

$$k_n = \frac{1}{4}\Pi a\left(1 + \frac{2}{\Pi^2 a^2} - \frac{62}{3\Pi^4 a^4} + \frac{15116}{15\Pi^6 a^6} - \frac{12554474}{105\Pi^8 a^8} + \frac{8368654292}{315\Pi^{10} a^{10}}\right) \quad (3.6)$$

where a = 4n

The velocity field is then differentiated to give the strain rate field. A Maple program (Appendix I) has been written to carry out the differentiation. The strain rate matrix is then transformed to get the principal strain rates, and the maximum strain rate is obtained as half the difference between the maximum and the minimum eigenvalues.

## 3.3 Results

The shear strain rate distributions obtained from the velocity distributions given by Lew and Fung (1969) have been tabulated ( Table 3.1), and are plotted at various radii (Figures 3.2 - 3.12). The corresponding shear stresses are simply the viscosity times the strain rates. Lew and Fung (1969) have discussed the velocity field and have concluded that the entrance regions extend from the entrance to .7 times the diameter of the cylinder axially. In this region the radial velocity is seen to reach up to around one third the inlet axial velocity, and so it cannot be neglected as it is of the same order of magnitude as the axial velocity.

Figure 3.2 plots the maximum shear strain rate obtained from the velocity distribution given by Lew and Fung (1969), at a radius one hundreth of the tube radius. The abscissa (x/a), is the dimensionless ratio of the axial distance from the inlet (x), to the radius of the tube(a), while the ordinate denotes the maximum shear strain rate. It can be seen that the fluid is virtually free of any strains at the inlet, as can be expected for fluid near the center of the tube. In the entrance region where radial velocity components are high and the velocity distribution is quite complex, the strain rate increases appreciably, before starting to taper off, as the flow settles down to Poiseuille flow, where regions near the tube axis experience lower strain rates. The maximum value is about 1200/s at x/a ~ .3. Multiplying the values obtained with the viscosity of the paste, 1000 $Nsm^{-2}$, it is seen that in this case, the maximum shear stress at the inlet itself is (27.35)(1000) = 27350 Pa. Thus it is observed from the plot that at all axial points, the fluid is subject to shear stress levels higher than the break strength quite close to the tube axis.

Table 3.1

| r(m) | x (m) | Max Shear ($s^{-1}$) |
|---|---|---|
| **.0000016891** | **.000000000** | **27.35** |
| .0000016891 | .000016891 | 680.26 |
| .0000016891 | .000033782 | 1052.83 |
| .0000016891 | .000050673 | 1178.02 |
| .0000016891 | .000067564 | 1123.79 |
| .0000016891 | .000084455 | 967.81 |
| .0000016891 | .000101346 | 774.22 |
| .0000016891 | .000118237 | 585.32 |
| .0000016891 | .000135128 | 423.00 |
| .0000016891 | .000152019 | 294.68 |
| .0000016891 | .000168190 | 199.14 |
| **.000016891** | **.000000000** | **274.34** |
| .000016891 | .000016891 | 692.67 |
| .000016891 | .000033782 | 1049.94 |
| .000016891 | .000050673 | 1167.42 |
| .000016891 | .000067564 | 1106.91 |
| .000016891 | .000084455 | 947.61 |
| .000016891 | .000101346 | 754.29 |
| .000016891 | .000118237 | 569.42 |
| .000016891 | .000135128 | 416.36 |
| .000016891 | .000152019 | 311.64 |
| .000016891 | .000168190 | 249.47 |
| **.000033782** | **.000000000** | **553.90** |
| .000033782 | .000016891 | 761.71 |
| .000033782 | .000033782 | 1042.56 |
| .000033782 | .000050673 | 1133.47 |
| .000033782 | .000067564 | 1053.75 |
| .000033782 | .000084455 | 885.25 |
| .000033782 | .000101346 | 694.59 |
| .000033782 | .000118237 | 525.17 |
| .000033782 | .000135128 | 410.62 |
| .000033782 | .000152019 | 372.01 |
| .000033782 | .000168190 | 372.02 |
| **.000050673** | **.000000000** | **845.13** |
| .000050673 | .000016891 | 851.15 |
| .000050673 | .000033782 | 1024.66 |
| .000050673 | .000050673 | 1069.44 |
| .000050673 | .000067564 | 958.26 |
| .000050673 | .000084455 | 778.26 |
| .000050673 | .000101346 | 600.46 |
| .000050673 | .000118237 | 469.88 |
| .000050673 | .000135128 | 448.75 |
| .000050673 | .000152019 | 489.98 |
| .000050673 | .000168190 | 538.56 |
| **.000067564** | **.000000000** | **1157.55** |
| .000067564 | .000016891 | 955.08 |
| .000067564 | .000033782 | 985.11 |
| .000067564 | .000050673 | 961.94 |
| .000067564 | .000067564 | 810.06 |
| .000067564 | .000084455 | 627.97 |
| .000067564 | .000101346 | 498.80 |
| .000067564 | .000118237 | 475.18 |
| .000067564 | .000135128 | 575.86 |
| .000067564 | .000152019 | 669.11 |
| .000067564 | .000168190 | 741.40 |
| **.000084455** | **.000000000** | **1507.14** |
| .000084455 | .000016891 | 1046.96 |
| .000084455 | .000033782 | 902.90 |
| .000084455 | .000050673 | 788.10 |
| .000084455 | .000067564 | 600.69 |
| .000084455 | .000084455 | 483.5 |

| r(m) | x (m) | Max Shear ($s^{-1}$) |
|---|---|---|
| .000084455 | .000101346 | 479.31 |
| .000084455 | .000118237 | 655.21 |
| .000084455 | .000135128 | 797.68 |
| .000084455 | .000152019 | 902.52 |
| .000084455 | .000168190 | 976.01 |
| **.000101346** | **.000000000** | **1923.95** |
| .000101346 | .000016891 | 1080.47 |
| .000101346 | .000033782 | 734.58 |
| .000101346 | .000050673 | 520.73 |
| .000101346 | .000067564 | 471.95 |
| .000101346 | .000084455 | 558.43 |
| .000101346 | .000101346 | 792.20 |
| .000101346 | .000118237 | 967.02 |
| .000101346 | .000135128 | 1091.56 |
| .000101346 | .000152019 | 1177.40 |
| .000101346 | .000168190 | 1235.04 |
| **.000118237** | **.000000000** | **2471.50** |
| .000118237 | .000016891 | 950.45 |
| .000118237 | .000033782 | 474.84 |
| .000118237 | .000050673 | 593.21 |
| .000118237 | .000067564 | 866.10 |
| .000118237 | .000084455 | 1090.45 |
| .000118237 | .000101346 | 1247.19 |
| .000118237 | .000118237 | 1355.07 |
| .000118237 | .000135128 | 1427.83 |
| .000118237 | .000152019 | 1475.94 |
| .000118237 | .000168190 | 1507.20 |
| **.000135128** | **.000000000** | **3304.29** |
| .000135128 | .000016891 | 649.24 |
| .000135128 | .000033782 | 1222.78 |
| .000135128 | .000050673 | 1562.65 |
| .000135128 | .000067564 | 1683.61 |
| .000135128 | .000084455 | 1732.53 |
| .000135128 | .000101346 | 1753.06 |
| .000135128 | .000118237 | 1765.58 |
| .000135128 | .000135128 | 1772.54 |
| .000135128 | .000152019 | 1775.43 |
| .000135128 | .000168190 | 1778.42 |
| **.000152019** | **.000000000** | **4779.94** |
| .000152019 | .000016891 | 3364.38 |
| .000152019 | .000033782 | 3200.26 |
| .000152019 | .000050673 | 2809.10 |
| .000152019 | .000067564 | 2530.90 |
| .000152019 | .000084455 | 2374.78 |
| .000152019 | .000101346 | 2203.94 |
| .000152019 | .000118237 | 2140.99 |
| .000152019 | .000135128 | 2098.06 |
| .000152019 | .000152019 | 2038.74 |
| .000152019 | .000168190 | 2040.30 |
| **.0001672209** | **.000000000** | **3893.60** |
| .0001672209 | .000016891 | 6891.86 |
| .0001672209 | .000033782 | 5224.62 |
| .0001672209 | .000050673 | 3720.75 |
| .0001672209 | .000067564 | 3080.82 |
| .0001672209 | .000084455 | 2837.50 |
| .0001672209 | .000101346 | 2466.10 |
| .0001672209 | .000118237 | 2399.19 |
| .0001672209 | .000135128 | 2357.91 |
| .0001672209 | .000152019 | 2215.52 |
| .0001672209 | .000168190 | 2262.43 |

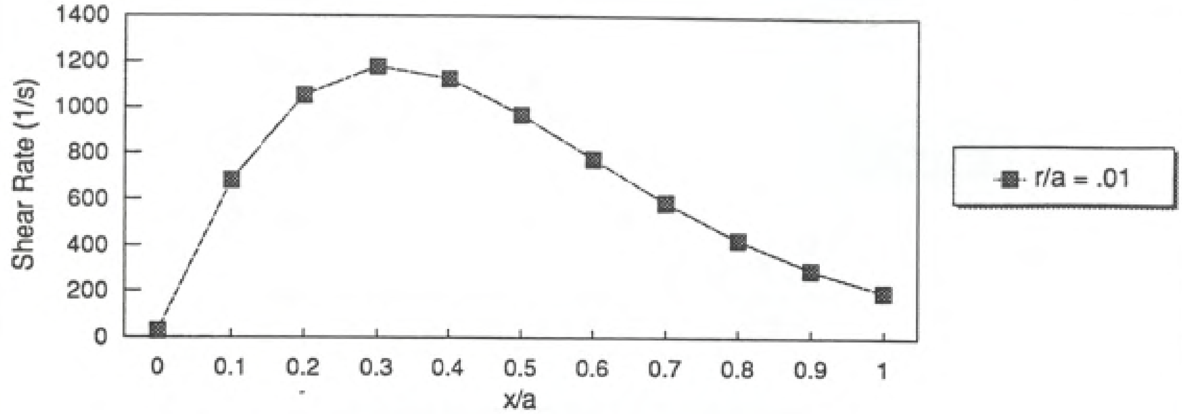


Figure 3.2 : Analytical Strain Rate
at r/a = 0.01

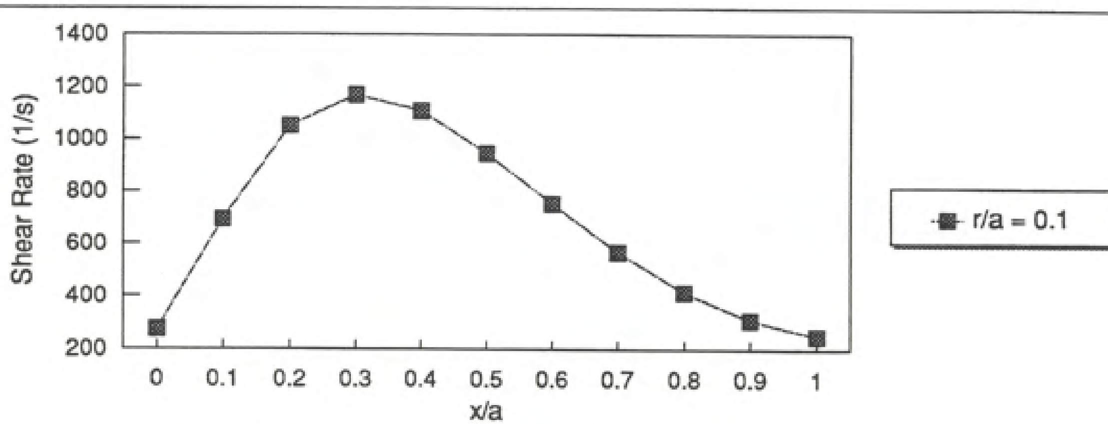


Figure 3.3 : Analytical Strain Rate
at r/a = 0.1

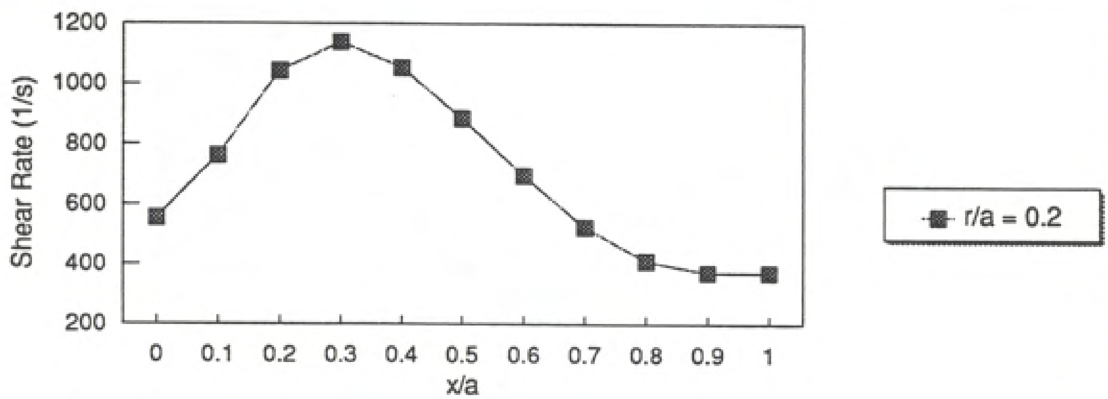


Figure 3.4 : Analytical Strain Rate
at r/a = 0.2

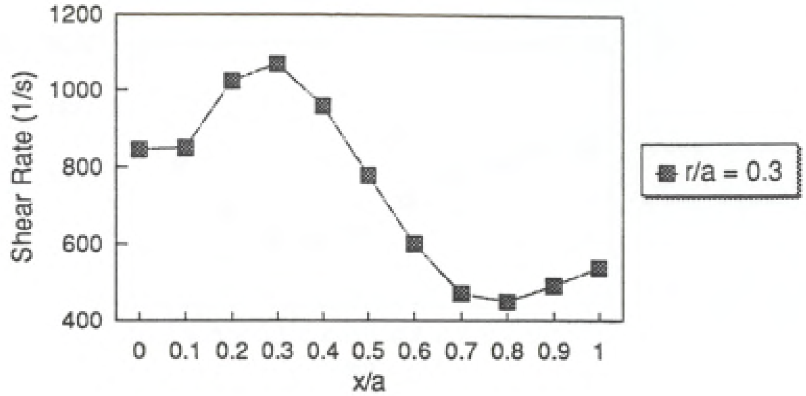


Figure 3.5 : Analytical Shear Rate
at r/a = 0.3

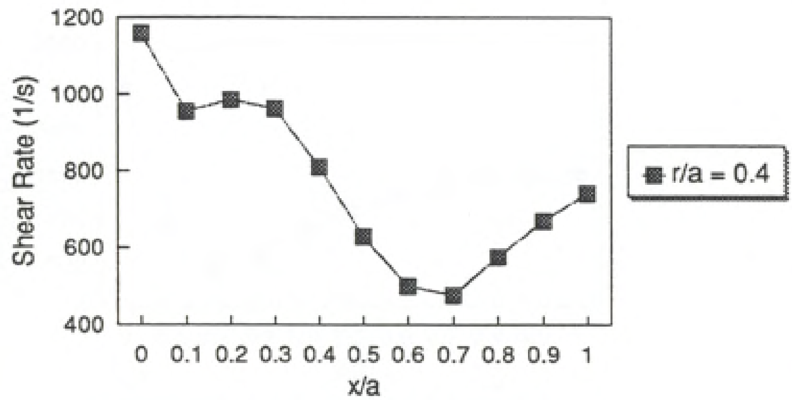


Figure 3.6 : Analytical Strain Rate
at r/a = 0.4

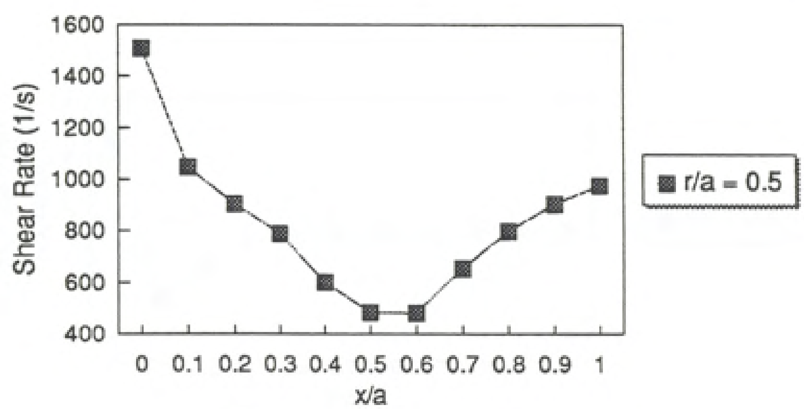


Figure 3.7 : Analytical Strain Rate
at r/a = 0.5

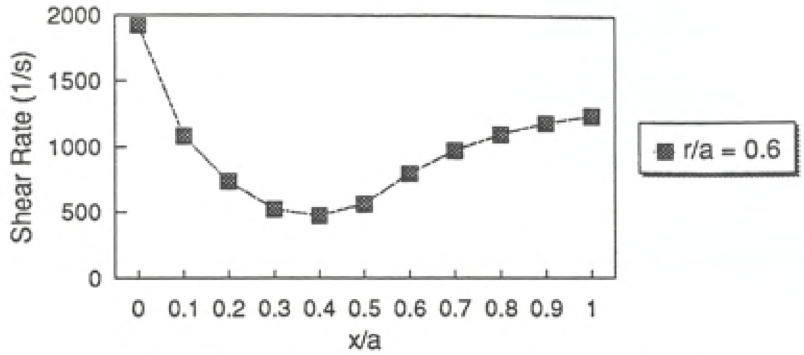


Figure 3.8 : Analytical Strain Rate
at r/a = 0.6

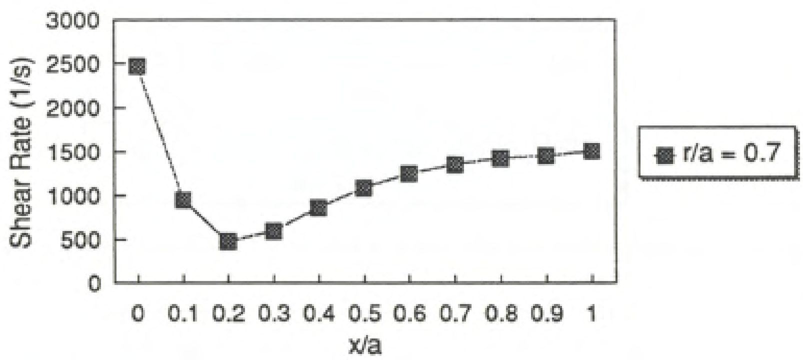


Figure 3.9 : Analytical Strain Rate
at r/a = 0.7

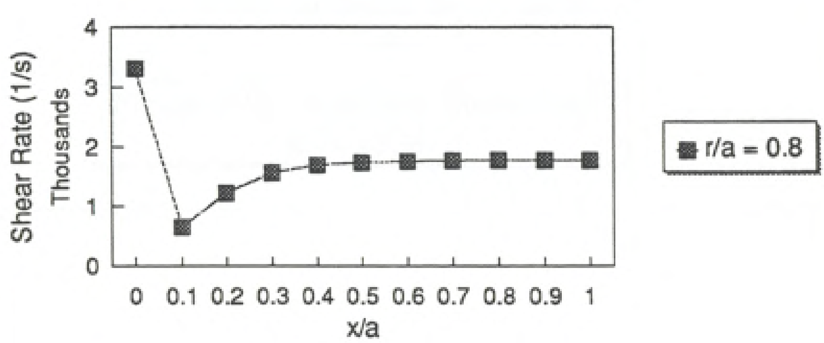


Figure 3.10 : Analytical Strain Rate
at r/a = 0.8

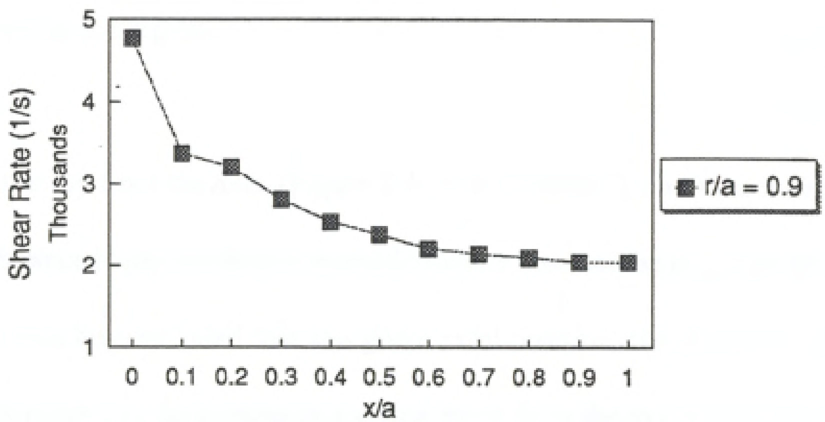


Figure 3.11 : Analytical Strain Rate
at r/a = 0.9

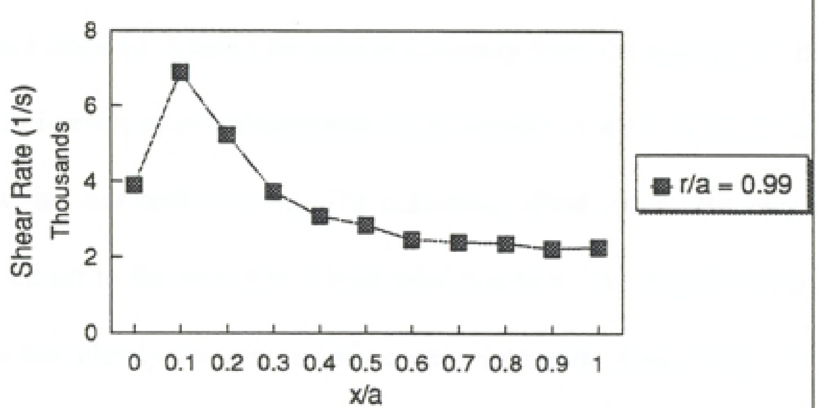


Figure 3.12 : Analytical Strain Rate
at r/a = 0.99

Figure 3.3, at a distance one-tenth the tube radius away from the center shows the same trend. However the starting shear rate is higher, showing that the discontinuity due to the wall begins to influence the flow quite close to the axis, right at the inlet. The stress levels are quite similar to the values shown in Figure 3.2, and the pattern can again be explained, as a result of the comlpex velocity distribution in the region.

On moving away from the axis, (Figure 3.4), to a distance .2 times the tube radius, the shear strain rate at the entrance begins to show a marked increase, even as the peak rate shows a slight drop (1133.47/s). It can thus be concluded that at a given axial position, the shear rate does not follow a definite trend of increasing or decreasing on moving away from the axis towards the wall. The shear rate tapers off as the flow settles down towards a Poiseuille distribution.

Figure 3.5, at a distance .3 times the tube radius away from the axis shows that closer to the wall, the distribution is even more complicated, with stresses at $x/a \sim 0.8$ decreasing below that expected from flow that has settled down. The maximum shear strain rate decreases slightly as compared to points closer to the axis at the same axial position. The discontinuous wall effects in the entrance region can clearly be seen to influence points quite away from the entrance itself, leading to a substantial entrance region. As paste release involves primarily this region, it can be seen that the actual stresses developed in the paste are quite different from any simplistic scheme.

Figure 3.6, at a radius .4 times the tube radius, the shear strain rate at the entrance is high enough to change the pattern, and the rate drops for some distance along the axial direction on moving away from the entrance. The point x/a ~ .3, which had the maximum rate for smaller radii still shows a small local maxima, lower in value than those closer to the axis, but the maximum at this radius shifts to the entrance itself. At the end away from the entrance, it can be seen that the stress decreases till about x/a ~ .7, following the trend observed for r/a = .3. However, as the final stress at r/a = .4 is expected to be higher than at r/a = .3 as the flow settles, the increase is seen to be more along the axis after x/a = .7, which is consistent with the Poiseuille distribution.

At r/a = .5, (Figure 3.7) midway between the axis and the radius, the entrance shear strain rate is high enough to dominate the pattern, with the stress decreasing monotonically till about x/a=.5. Again, as the final strain rate is higher than at smaller radii, a large increase is seen at the downstream end, where the flow approaches Poiseuille velocity distribution.

Figure 3.8, at r/a = .6 shows a continuing trend, with the strain rates at the inlet increasing quite substantially. The values are higher than the corresponding points for r/a = 0.5. The minimum shifts towards the entrance, at x/a = 0.4.

Figure 3.9 (r/a = 0.7) shows exactly the same trend, with the shear rate at the inlet increasing further, and the minima shifting even closer to the inlet.

The same trend is observed for r/a = .8 (Figure 3.10). As the minima is quite close to the inlet, the shear rate tends to level off while moving away from the inlet.

Figure 3.11 shows that extremely close to the wall (r/a = .9), the minimum is obliterated, and the stress falls continuously on proceeding away from the inlet. The values are again higher than those for lower radii, appreciably so near the inlet.

Finally, right next to the wall at r/a = .99 (Figure 3.12), the distribution shows a maximum at axial points where there was previously a minimum. The trend could be explained in part due to the changing nature of the radial velocity gradients in this region, leading to a different pattern. However, near this region, the analytical solution itself (Lew and Fung, 1969) might not be very accurate. The solution is not valid at the wall.

## 3.4 Conclusions

The most important conclusion that can be drawn from the above, as related to the problem at hand is that the value of the shear rate exceeds the break shear rate, nearly all over the flow region. The only exceptions would be the region at the inlet very close to the axis. However, the volume of this region is negligible. This indicates that there are serious drawbacks in modeling the paste release process as a steady state uniform entry flow of an incompressible, Newtonian fluid.

Another observation is that the velocity, and thus the strain rate distributions in the entrance region are quite complex, and that the radial velocity indeed is significant in determining the strain rates obtained and cannot be neglected.

# CHAPTER 4

# FINITE ELEMENT ANALYSIS FOR FLOW THROUGH CIRCULAR APERTURES

This chapter describes the creation of a finite element model to analyze the flow through a circular aperture. As mentioned earlier, the final aim is to determine the flow patterns for commonly used geometries like rectangular slots. Not much work on an analytical solution is reported in the available technical literature. In the present work, numerical finite element solutions are used. To get an idea of the validity of finite element solutions, as well as the specific quirks of the software being used, finite element analysis is carried out first for a circular slot, for which the analytical solution is already known. The software is found to be incapable of handling the problem directly due to the extremely small size of the slot. A dimensional analysis is carried out so as to determine the values for dynamically similar cases, and a set of values which does not lead to errors due to the finite digit arithmetic of the software is chosen. The relevant communications from FDI Inc., the company that created the software FIDAP are included in Appendix II-A. The program is executed for different mesh densities, and the results obtained are discussed.

## 4.1 Finite Element Model for Flow through a Circular Aperture

To compare the solution obtained using finite element techniques with that obtained via analytical methods, it is proposed to solve for the same exact case for which the analytical solutions have been obtained. Thus, the values of the various parameters are:

1) Radius of tube (a) = .00016891 m

2) Length of tube (L) = .00050673 m

3) Inlet velocity (U) = .203 m/s

4) Fluid density ($\rho$) = 5500 kg/$m^3$

5) Fluid viscosity ($\mu$) = 1000 Ns/$m^2$

6) Tack strength = 2(Maximum shear) = ($2\tau$) = 0.05 MPa = 50000 Pa

The following can be used for future reference:

Reynold number = $3.77 \times 10^{-4}$

Breaking shear rate = $\tau \mu^{-1} = 25 \ s^{-1}$

$La^{-1} = 3$

$\rho \mu^{-1} = 5.5 \ m^{-2}s$

The software used is not capable of handling such small numbers for the dimensions of the slot, and errors ranging from incorrect mesh generation, substantial continuity violations, to outright termination of the program arise.

#### 4.1.1 Dimensional Analysis

A dynamically similar flow with larger physical dimensions was studied. Dimensional similarity was obtained by dimensional analysis using the parameters given below, which would seem to be relevant to the problem:

Table 4.1

| No. | Parameter | Symbol | Dimension |
|---|---|---|---|
| 1 | Tube radius | a | L |
| 2 | Tube length | L | L |
| 3 | Inlet velocity | U | $LT^{-1}$ |
| 4 | Fluid density | ρ | $ML^{-3}$ |
| 5 | Fluid viscosity | μ | $ML^{-1}T^{-1}$ |
| 6 | Stress | τ | $ML^{-1}T^{-2}$ |

This would give an equation of the from:

$$g(a, L, U, \rho, \mu, \tau) = 0 \tag{4.1}$$

Buckingham's Π theorem gives:

No. of parameters = 6

No. of dimensions = 3

No. of dimensionless groups = 6-3 = 3

On inspection, the three dimensionless groups can be determined to be:

$$\tau a(U\mu)^{-1}, \; a(L^{-1}), \; \rho aU(\mu^{-1})$$

So, a relation of the form

$$G(\tau a(U\mu)^{-1}, aL^{-1}, \rho Ua\mu^{-1})=0 \qquad (4.2)$$

is expected to hold good between the various parameters.

### 4.1.2 Selection of Values for the Finite Element Model

Two factors are to be considered while choosing the values to be used in the FE model:

1) Dynamic similarity of the flow must be maintained. In effect, here it means holding two of the three dimensionless ratios the same, so as to ensure equality of the third.

2) Of the infinite combinations possible for dynamic similarity, the specific values chosen should

be ones that can be handled by the software without creating problems because of finite digit arithmetic.

To determine the values which satisfy condition (1) above, it is noted that the unknown parameter is the stress $\tau$. So the known parameters are adjusted to ensure the equality of the groups which do not involve $\tau$, and then the equality of the third group is used to determine the correlation between the stresses in the two cases, the finite element model and the analytical case. The analytical case is indicated with a subscript 1 while the finite element case is referred to as case 2.

Hence,

$$(\rho a U(\mu^{-1}))_1 = (\rho a U(\mu^{-1}))_2 \tag{4.3}$$

This simply states that the Reynolds number for the flows should be the same.

$$(aL^{-1})_1 = (aL^{-1})_2 \tag{4.4}$$

This ensures geometric similarity, for it indicates that the ratio of the radius of the tube to its length must be maintained the same for both cases.

As can be noted from the Eqs. 4.3 and 4.4, one ratio of parameters for the two cases, say the ratio of the radii, does not determine the other parameters uniquely except the length L, but instead, determines the ratios for a combination of parameters which could be satisfied by various values of the individual parameters.

Given Eqs. 4.3 and 4.4, Eq.4.2 implies

$$(\tau a (U\mu)^{-1})_1 = (\tau a (U\mu)^{-1})_2 \tag{4.5}$$

which gives

$$\tau_2 = (\tau a (U\mu)^{-1})_1 (a (U\mu)^{-1})_2^{-1} \tag{4.6}$$

This is as far as condition (1) regarding dynamic similarity of the cases can be applied.

Condition (2) is then used to determine the values which the software could handle efficiently. For this, problems encountered with the software must be considered.

### 4.1.3 Problems Encountered While Using FIDAP

The first model to be tried had the exact geometry of the analytical case (Figure 4.1). The mesh is seen to be incorrect, as the region is too small to be handled by FIDAP. The problem was sought to be overcome by scaling the region to a larger region during mesh generation, and getting a proper mesh, but then scaling it back to the original dimensions while solving the equations. Due

FIGURE 4.1: DISTORTED MESH

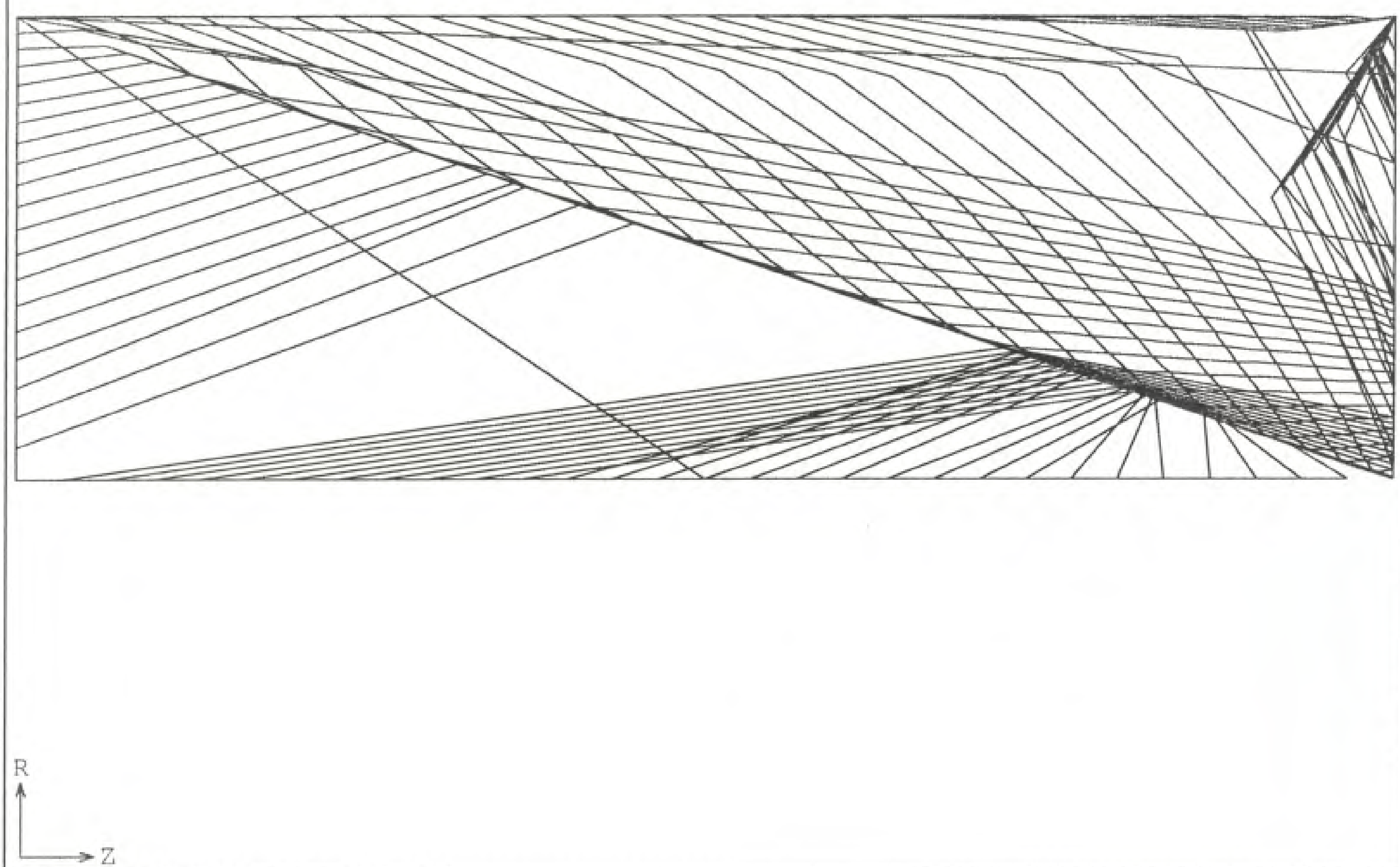

to the nature of the software, the extremely small size of the region of flow then leads to the problem that continuity is not satisfied. The above trial cases and correspondence with FDI, the company that created the software, led to the conclusion that for the software to function properly, the geometry must be such that the smaller dimension is of the order of unity. The Reynolds number would have to be held constant by varying the other parameters. As can be seen from the analytical case, the velocity distribution is not expected to be governed to a large extent by the density of the fluid or its viscosity. Therefore, the velocity is taken to be the original velocity, and the inlet velocity is thus .203 m/s . This is because the velocity is again of an order of magnitude which would facilitate smooth computation. However, it is noted that this is simply an assumed value, and that it is expected to be reasonable. A different value of the velocity could lead to changes in other parameters, and as is shown later, since the results are sensitive to the numerical value input, the exact results obtained here are for this velocity only. Having decided on the radius of the tube (a), the length (L) is determined using Eq. 4.4. As the velocity has been fixed at .203 m/s, there is a range of values for the ratio ($\rho/\mu$) which would satisfy Eq.4.3. A table of such values can be computed as shown below.

Given

$$a_2 = 1\ m \tag{4.7}$$

Eq. 4.4 gives

$$L_2 = 3\ m \tag{4.8}$$

Also, taking

$$U_2 = .203\ m/s \tag{4.9}$$

Eq. 4.5 gives

$$\rho_2 \mu_2^{-1} = \rho_1 \mu_1^{-1} (a_1 U_1 (a_2 U_2)^{-1}) \tag{4.10}$$

Substituting Eqs. 4.7 and 4.9 in 4.10 gives

$$\rho_2 \mu_2^{-1} = \rho_1 \mu_1^{-1} (.00016891) \tag{4.11}$$

Using the value calculated for $\rho\ \mu^{-1} = 5.5\ m^{-2}s$

$$\rho_2 \mu_2^{-1} = 9.2895 \times 10^{-4}\ m^{-2}\ s \tag{4.12}$$

There are no further restrictions on the possible values of density and viscosity. Thus, there exist an infinite number of possible models, all of which would satisfy dynamic similarity, and should give identical results. Some of the possible cases are shown in Table 4.2 below. However, on running a number of FIDAP cases with the values shown, it can be determined that cases up to case (5) give results which are highly dependent on mesh shape. The cause can be traced back to the finite digit arithmetic being employed by the software. For cases (1) through (5), a substantial number of the pivot points for solving the equation go below the cutoff value of $10^{-7}$, and are thus replaced by $10^{-7}$. The error decreases as the density and viscosity are reduced, and a satisfactory result is obtained by case 9. Cases after case 9 gave results in agreement with case 9. Therefore the values for this case are used as the input for the program, and increasingly finer mesh densities are used till the system limit is reached.

Table 4.2

| No. | Density | Viscosity |
|---|---|---|
| 1 | 92895 | 100000000 |
| 2 | 9289.5 | 10000000 |
| 3 | 928.95 | 1000000 |
| 4 | 92.895 | 100000 |
| 5 | 9.2895 | 10000 |
| 6 | .92895 | 1000 |
| 7 | .092895 | 100 |
| 8 | .0092895 | 10 |

| | | |
|---|---|---|
| 9 | .00092895 | 1 |
| 10 | .000092895 | .1 |
| 11 | .0000092895 | .01 |

Eq. 4.6 gives the value of the corresponding shear stress. For a corresponding value of the shear strain rate

$$s_2 = s_1 (a_1 a_2^{-1}). \quad (4.13)$$

which gives

$$s_2 = s_1 (.00016891) \quad (4.14)$$

For the strain rate in the finite element case which would be equivalent to the break rate in the analytical case,

$$s_2 = 4.22 \times 10^{-3} \quad (4.15)$$

## 4.2 FIDAP Program

A sample copy of the program used is attached as Appendix II-B. The parameters varied are the fluid properties of density and viscosity, as well as the mesh size and the mesh generation algorithm. All these are varied using the same program by commenting/uncommenting the appropriate lines.

### 4.2.1 Geometry and Meshing

The program generates an axi-symmetric two dimensional representation of the cylinder. The region is mapped using one of the two meshing algorithms, "mapping" and "paving." Mapping generates more regular meshes, and thus is suitable mainly for regular geometries like the one under consideration. For irregular geometries, paved meshes are used. Both approaches are used to determine the sensitivity of the solution to the mesh shape. Figs. 4.2 and 4.3 show the mesh shapes for the two algorithms.

### 4.2.2 Boundary Conditions

The boundary conditions are the same as that used in the analytical case, namely that at the inlet, axial velocity is .203 m/s while the radial velocity is zero. At the walls, all velocity conditions are assumed to be zero because of no slip conditions. At the centerline, radial velocity is zero because of symmetry.

## 4.3 Solution

FIGURE 4.2: MAPPED MESH

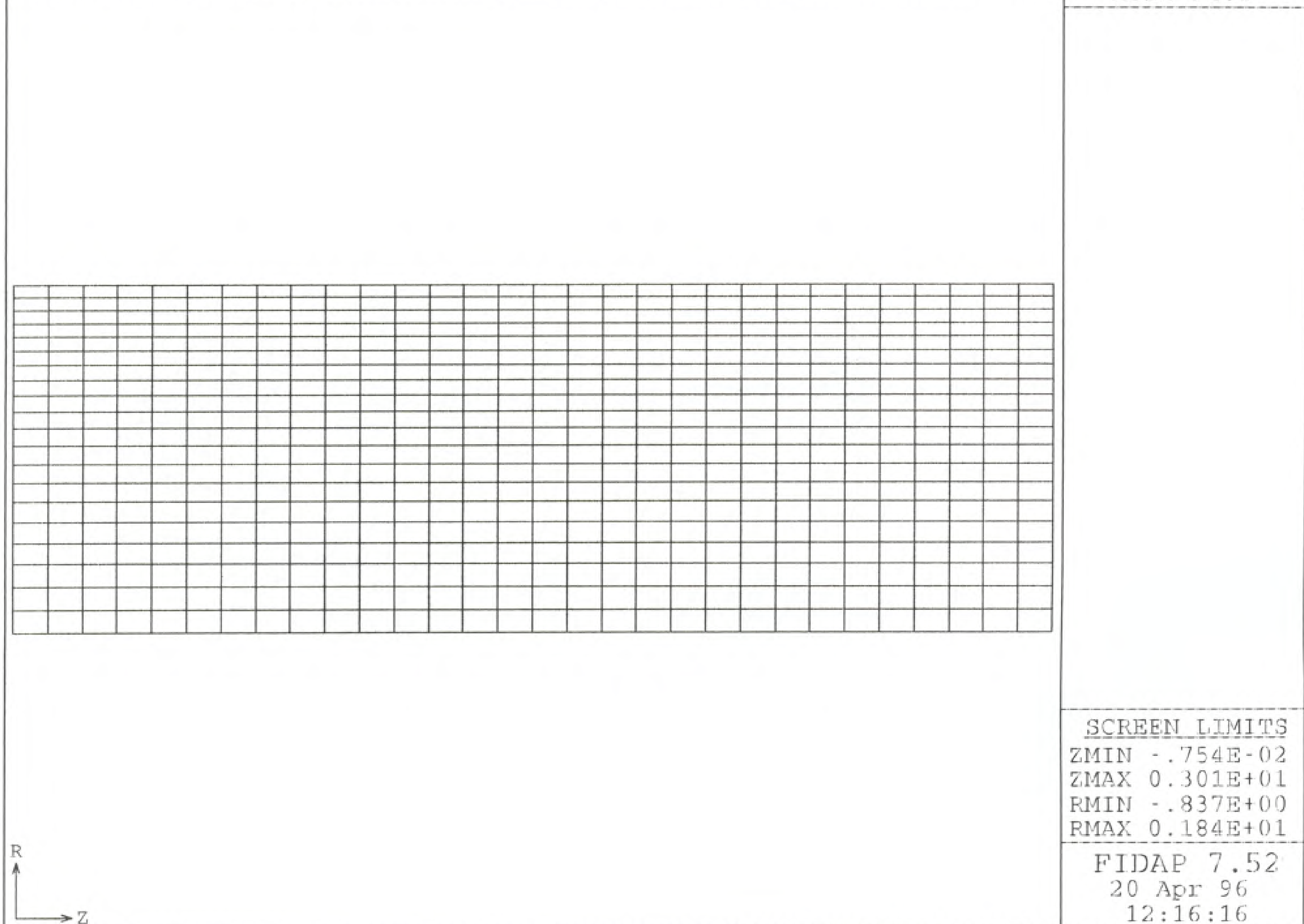

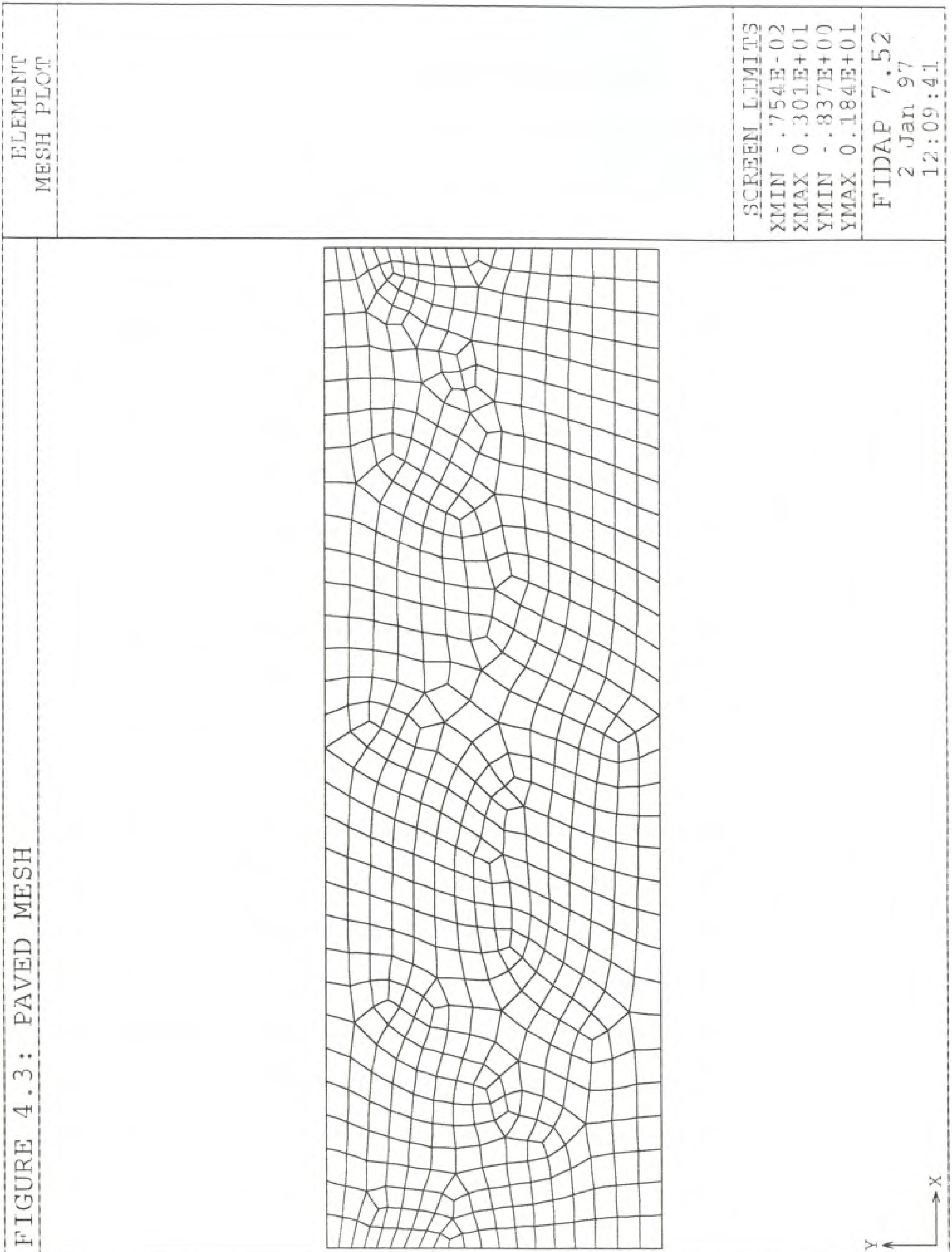


FIGURE 4.3: PAVED MESH

The case is studied for steady state laminar incompressible flow of a Newtonian fluid. As continuity violation is one of the problems encountered, and the pressure penalty method of analysis involves satisfying an approximate continuity equation only, a mixed pressure approach is used instead of the default pressure penalty method.

## 4.4 Results

The shear rates and velocity distributions are plotted in Figs. 4.4 to 4.18 along with the corresponding meshed regions for the three mesh densities. For comparison, velocity, and shear rates scaled to the analytical case have been tabulated (Tables 4.3- 4.4) and graphed at selected points along with the analytical results (Figs. 4.19 - 4.45). The results show that the mesh density is sufficient, as three varying densities converge to the same solution.

### 4.4.1 Velocity

Figure 4.5 is a velocity vector plot corresponding to the mesh density of Figure 4.4. The plot is axisymmetric about the lower edge, which is the axis of the tube. The inlet is recognized by the inward pointing arrows of uniform length.The direction of the arrows near the inlet clearly indicate the relatively complex velocity distribution pattern in the entrance region, as compared to the distribution downstream of the inlet, at a distance of the order of the radius of the tube. The fluid, impinges on the inlet at a uniform velocity of .203 m/s, and comes to rest at the discontinuity created by the walls due to the no-slip condition for viscous fluids. Thus, to maintain continuity, the fluid,

TABLE 4.3
VELOCITY DISTRIBUTION

| x/a | r/a | Analytical u/U | Analytical v/U | FIDAP u/U | FIDAP v/U |
|---|---|---|---|---|---|
| 0.1 | 0.1 | 1.04022 | -0.01866 | 1.04567 | -0.04250 |
| 0.2 | 0.1 | 1.13838 | -0.02916 | 1.15816 | -0.06699 |
| 0.3 | 0.1 | 1.26318 | -0.06499 | 1.30257 | -0.07543 |
| 0.4 | 0.1 | 1.39029 | -0.06178 | 1.4508 | -0.07217 |
| 0.5 | 0.1 | 1.50442 | -0.05302 | 1.58454 | -0.06219 |
| 0.6 | 0.1 | 1.59843 | -0.04228 | 1.69503 | -0.04969 |
| 0.7 | 0.1 | 1.6711 | -0.03187 | 1.78052 | -0.03747 |
| 0.8 | 0.1 | 1.72454 | -0.02297 | 1.84333 | -0.02698 |
| 0.9 | 0.1 | 1.76228 | -0.01595 | 1.88762 | -0.0187 |
| 0.1 | 0.2 | 1.04067 | -0.07493 | 1.04648 | -0.08557 |
| 0.2 | 0.2 | 1.13845 | -0.11574 | 1.1594 | -0.13367 |
| 0.3 | 0.2 | 1.26023 | -0.12777 | 1.30146 | -0.14887 |
| 0.4 | 0.2 | 1.38142 | -0.12007 | 1.44389 | -0.14074 |
| 0.5 | 0.2 | 1.48871 | -0.10191 | 1.56929 | -0.11988 |
| 0.6 | 0.2 | 1.57337 | -0.08046 | 1.6705 | -0.09477 |
| 0.7 | 0.2 | 1.63828 | -0.06012 | 1.74716 | -0.07079 |
| 0.8 | 0.2 | 1.68521 | -0.04302 | 1.80248 | -0.05056 |
| 0.9 | 0.2 | 1.71789 | -0.02970 | 1.84088 | -0.03481 |
| 0.1 | 0.3 | 1.04149 | -0.11295 | 1.04803 | -0.12983 |
| 0.2 | 0.3 | 1.13837 | -0.17151 | 1.16159 | -0.19951 |
| 0.3 | 0.3 | 1.25426 | -0.18560 | 1.29893 | -0.21778 |
| 0.4 | 0.3 | 1.36452 | -0.17089 | 1.43045 | -0.20155 |
| 0.5 | 0.3 | 1.45699 | -0.14228 | 1.54093 | -0.16820 |
| 0.6 | 0.3 | 1.52846 | -0.11042 | 1.62621 | -0.13055 |
| 0.7 | 0.3 | 1.58066 | -0.08132 | 1.68830 | -0.09599 |
| 0.8 | 0.3 | 1.61772 | -0.05747 | 1.73158 | -0.06765 |
| 0.9 | 0.3 | 1.64198 | -0.03927 | 1.76077 | -0.04606 |
| 0.1 | 0.4 | 1.04820 | -0.15163 | 1.05068 | -0.17616 |
| 0.2 | 0.4 | 1.13760 | -0.22382 | 1.16482 | -0.26343 |
| 0.3 | 0.4 | 1.24304 | -0.23458 | 1.29338 | -0.27832 |
| 0.4 | 0.4 | 1.33560 | -0.20928 | 1.40671 | -0.24913 |
| 0.5 | 0.4 | 1.40724 | -0.16931 | 1.49241 | -0.20158 |
| 0.6 | 0.4 | 1.45863 | -0.12819 | 1.55658 | -0.15232 |
| 0.7 | 0.4 | 1.49374 | -0.09245 | 1.59884 | -0.10951 |
| 0.8 | 0.4 | 1.51693 | -0.06425 | 1.62650 | -0.07577 |
| 0.9 | 0.4 | 1.53187 | -0.04325 | 1.64417 | -0.05081 |
| 0.1 | 0.5 | 1.04471 | -0.19095 | 1.05512 | -0.22577 |
| 0.2 | 0.5 | 1.13456 | -0.24771 | 1.16879 | -0.32284 |
| 0.3 | 0.5 | 1.22166 | -0.26861 | 1.28086 | -0.32404 |
| 0.4 | 0.5 | 1.28705 | -0.22884 | 1.36513 | -0.27601 |
| 0.5 | 0.5 | 1.33000 | -0.17795 | 1.41998 | -0.21384 |
| 0.6 | 0.5 | 1.35608 | -0.13039 | 1.45281 | -0.15588 |
| 0.7 | 0.5 | 1.37117 | -0.09159 | 1.47146 | -0.10886 |
| 0.8 | 0.5 | 1.37959 | -0.06229 | 1.48168 | -0.07360 |
| 0.9 | 0.5 | 1.38417 | -0.04123 | 1.48713 | -0.04843 |
| 0.1 | 0.6 | 1.04710 | -0.22999 | 1.06270 | -0.28022 |
| 0.2 | 0.6 | 1.12449 | -0.30044 | 1.17137 | -0.37134 |
| 0.3 | 0.6 | 1.17920 | -0.27800 | 1.25160 | -0.34372 |
| 0.4 | 0.6 | 1.21507 | -0.22206 | 1.29107 | -0.27249 |
| 0.5 | 0.6 | 1.21218 | -0.16396 | 1.30339 | -0.19923 |
| 0.6 | 0.6 | 1.21024 | -0.11537 | 1.30257 | -0.13882 |
| 0.7 | 0.6 | 1.20519 | -0.07852 | 1.29704 | -0.09364 |
| 0.8 | 0.6 | 1.19985 | -0.05208 | 1.29084 | -0.06161 |
| 0.9 | 0.6 | 1.19534 | -0.03348 | 1.28552 | -0.03967 |
| 0.1 | 0.7 | 1.04785 | -0.26867 | 1.07569 | -0.34002 |
| 0.2 | 0.7 | 1.09220 | -0.30144 | 1.16244 | -0.39223 |
| 0.3 | 0.7 | 1.09143 | -0.24913 | 1.18107 | -0.31904 |
| 0.4 | 0.7 | 1.06611 | -0.18263 | 1.15750 | -0.22884 |
| 0.5 | 0.7 | 1.03557 | -0.12659 | 1.12267 | -0.15558 |
| 0.6 | 0.7 | 1.00867 | -0.08502 | 1.09083 | -0.10287 |
| 0.7 | 0.7 | 0.98787 | -0.05587 | 1.06603 | -0.06676 |
| 0.8 | 0.7 | 0.97287 | -0.03605 | 1.04820 | -0.04265 |
| 0.9 | 0.7 | 0.96253 | -0.02287 | 1.03597 | -0.02683 |
| 0.1 | 0.8 | 1.02980 | -0.26789 | 1.09390 | -0.3939 |
| 0.2 | 0.8 | 0.98830 | -0.24200 | 1.09823 | -0.34445 |
| 0.3 | 0.8 | 0.90925 | -0.17091 | 1.01165 | -0.22897 |
| 0.4 | 0.8 | 0.83580 | -0.11297 | 0.92128 | -0.14448 |
| 0.5 | 0.8 | 0.77971 | -0.07300 | 0.85195 | -0.09050 |
| 0.6 | 0.8 | 0.74002 | -0.04669 | 0.80367 | -0.05664 |
| 0.7 | 0.8 | 0.72654 | -0.02962 | 0.77144 | -0.03536 |
| 0.8 | 0.8 | 0.69585 | -0.01857 | 0.75045 | -0.02194 |
| 0.9 | 0.8 | 0.68450 | -0.01157 | 0.73703 | -0.01347 |
| 0.1 | 0.9 | 0.84854 | -0.15532 | 1.04298 | -0.33981 |
| 0.2 | 0.9 | 0.67843 | -0.10296 | 0.81289 | -0.16777 |
| 0.3 | 0.9 | 0.55906 | -0.06064 | 0.63961 | -0.08529 |
| 0.4 | 0.9 | 0.48056 | -0.03723 | 0.53583 | -0.0471 |
| 0.5 | 0.9 | 0.43104 | -0.02173 | 0.47373 | -0.02735 |
| 0.6 | 0.9 | 0.40012 | -0.01326 | 0.43604 | -0.01631 |
| 0.7 | 0.9 | 0.38159 | -0.00874 | 0.41296 | -0.00984 |
| 0.8 | 0.9 | 0.36952 | -0.00473 | 0.39882 | -0.00594 |
| 0.9 | 0.9 | 0.36269 | -0.00305 | 0.39018 | -0.00356 |

TABLE 4.4
Shear Rate Comparison (1/s)

| x/a | r/a | Analytical | Low | Medium | High |
|---|---|---|---|---|---|
| 0.0 | 0.1 | 274.34 | 614.05 | 615.95 | 617.43 |
| 0.1 | 0.1 | 692.67 | 1837.19 | 1800.19 | 1816.23 |
| 0.2 | 0.1 | 1049.94 | 2795.16 | 2796.28 | 2789.36 |
| 0.3 | 0.1 | 1167.42 | 3112.84 | 3105.38 | 3127.11 |
| 0.4 | 0.1 | 1106.91 | 2955.01 | 2971.70 | 2982.36 |
| 0.5 | 0.1 | 947.61 | 2528.27 | 2543.78 | 2558.17 |
| 0.6 | 0.1 | 754.29 | 2007.64 | 2025.93 | 2037.24 |
| 0.7 | 0.1 | 569.42 | 1510.45 | 1528.92 | 1535.67 |
| 0.8 | 0.1 | 416.36 | 1099.11 | 1111.12 | 1118.76 |
| 0.9 | 0.1 | 311.64 | 797.29 | 808.89 | 811.97 |
| 1.0 | 0.1 | 249.47 | 605.00 | 610.62 | 614.65 |
| | | | | | |
| 0.0 | 0.2 | 553.90 | 1240.54 | 1246.23 | 1250.19 |
| 0.1 | 0.2 | 761.71 | 1979.22 | 1945.36 | 1961.28 |
| 0.2 | 0.2 | 1042.56 | 2796.28 | 2797.17 | 2790.54 |
| 0.3 | 0.2 | 1137.47 | 3027.35 | 3019.54 | 3041.68 |
| 0.4 | 0.2 | 1053.75 | 2804.57 | 2819.96 | 2831.27 |
| 0.5 | 0.2 | 885.25 | 2341.72 | 2356.58 | 2370.43 |
| 0.6 | 0.2 | 694.59 | 1821.38 | 1837.37 | 1848.97 |
| 0.7 | 0.2 | 525.17 | 1366.29 | 1382.93 | 1388.55 |
| 0.8 | 0.2 | 410.62 | 1044.17 | 1053.99 | 1060.33 |
| 0.9 | 0.2 | 372.01 | 873.84 | 882.48 | 884.85 |
| 1.0 | 0.2 | 372.02 | 823.04 | 827.54 | 830.15 |
| | | | | | |
| 0.0 | 0.3 | 845.13 | 1900.89 | 1911.08 | 1917.23 |
| 0.1 | 0.3 | 851.15 | 2194.66 | 2159.79 | 1945.83 |
| 0.2 | 0.3 | 1024.66 | 2780.06 | 2782.25 | 2775.80 |
| 0.3 | 0.3 | 1069.44 | 2858.62 | 2854.48 | 2876.03 |
| 0.4 | 0.3 | 958.26 | 2537.62 | 2545.50 | 2556.51 |
| 0.5 | 0.3 | 778.26 | 2014.68 | 2033.98 | 2045.29 |
| 0.6 | 0.3 | 600.46 | 1520.51 | 1536.38 | 1547.10 |
| 0.7 | 0.3 | 469.88 | 1180.04 | 1194.25 | 1197.86 |
| 0.8 | 0.3 | 448.75 | 1047.66 | 1053.11 | 1057.78 |
| 0.9 | 0.3 | 489.98 | 1069.39 | 1073.18 | 1075.78 |
| 1.0 | 0.3 | 538.56 | 1149.84 | 1152.68 | 1155.23 |
| | | | | | |
| 0.0 | 0.4 | 1157.55 | 2623.88 | 2639.28 | 2648.22 |
| 0.1 | 0.4 | 955.08 | 2459.30 | 2423.89 | 2448.11 |
| 0.2 | 0.4 | 985.11 | 2715.35 | 2718.73 | 2713.40 |
| 0.3 | 0.4 | 961.94 | 2567.82 | 2567.70 | 2589.37 |
| 0.4 | 0.4 | 810.06 | 2093.19 | 2112.55 | 2125.39 |
| 0.5 | 0.4 | 627.97 | 1551.65 | 1573.38 | 1581.97 |
| 0.6 | 0.4 | 498.80 | 1180.45 | 1192.47 | 1201.35 |
| 0.7 | 0.4 | 475.18 | 1107.34 | 1115.51 | 1116.04 |
| 0.8 | 0.4 | 575.86 | 1238.29 | 1240.78 | 1242.56 |
| 0.9 | 0.4 | 669.11 | 1415.49 | 1417.68 | 1419.99 |
| 1.0 | 0.4 | 741.40 | 1568.65 | 1572.55 | 1574.86 |
| | | | | | |
| 0.0 | 0.5 | 1507.14 | 3459.89 | 3483.04 | 3495.59 |
| 0.1 | 0.5 | 1046.96 | 2741.40 | 2702.68 | 2732.64 |
| 0.2 | 0.5 | 902.90 | 2536.50 | 2509.62 | 2538.63 |
| 0.3 | 0.5 | 788.10 | 2086.14 | 2094.96 | 2114.56 |
| 0.4 | 0.5 | 600.69 | 1480.91 | 1501.92 | 1515.13 |
| 0.5 | 0.5 | 483.50 | 1063.05 | 1085.61 | 1087.92 |
| 0.6 | 0.5 | 479.31 | 1093.90 | 1097.80 | 1100.82 |
| 0.7 | 0.5 | 655.21 | 1377.95 | 1379.61 | 1379.85 |
| 0.8 | 0.5 | 797.68 | 1670.12 | 1672.78 | 1674.03 |
| 0.9 | 0.5 | 902.52 | 1895.27 | 1903.62 | 1907.23 |
| 1.0 | 0.5 | 976.01 | 2066.19 | 2072.17 | 2075.54 |

TABLE 4.4 (Continued)
Shear Rate Comparison (1/s)

| x/a | r/a | Analytical | Low | Medium | High |
|---|---|---|---|---|---|
| 0.0 | 0.6 | 1923.95 | 4508.02 | 4547.39 | 4565.80 |
| 0.1 | 0.6 | 1080.47 | 2979.75 | 2931.56 | 2970.34 |
| 0.2 | 0.6 | 734.58 | 2110.47 | 2119.12 | 2122.91 |
| 0.3 | 0.6 | 520.73 | 1363.21 | 1389.85 | 1403.17 |
| 0.4 | 0.6 | 471.95 | 956.25 | 970.52 | 978.27 |
| 0.5 | 0.6 | 558.43 | 1189.86 | 1194.66 | 1190.99 |
| 0.6 | 0.6 | 792.20 | 1631.05 | 1631.28 | 1630.04 |
| 0.7 | 0.6 | 967.02 | 2012.08 | 2012.73 | 2018.47 |
| 0.8 | 0.6 | 1091.56 | 2294.30 | 2299.45 | 2302.11 |
| 0.9 | 0.6 | 1177.40 | 2491.09 | 2496.60 | 2501.98 |
| 1.0 | 0.6 | 1235.04 | 2623.53 | 2631.93 | 2637.03 |
| 0.0 | 0.7 | 2471.50 | 5988.16 | 6079.63 | 6113.26 |
| 0.1 | 0.7 | 950.45 | 2996.92 | 2919.84 | 2968.33 |
| 0.2 | 0.7 | 474.84 | 1287.49 | 1301.28 | 1314.61 |
| 0.3 | 0.7 | 593.21 | 1234.92 | 1229.65 | 1228.05 |
| 0.4 | 0.7 | 866.10 | 1766.21 | 1764.19 | 1761.77 |
| 0.5 | 0.7 | 1090.45 | 2250.67 | 2248.77 | 2250.84 |
| 0.6 | 0.7 | 1247.19 | 2609.50 | 2614.17 | 2615.77 |
| 0.7 | 0.7 | 1355.07 | 2860.04 | 2864.84 | 2871.59 |
| 0.8 | 0.7 | 1427.83 | 3029.01 | 3038.30 | 3043.99 |
| 0.9 | 0.7 | 1457.94 | 3140.37 | 3149.61 | 3157.42 |
| 1.0 | 0.7 | 1507.20 | 3212.24 | 3223.79 | 3230.89 |
| 0.0 | 0.8 | 3304.29 | 8473.86 | 8791.31 | 8906.16 |
| 0.1 | 0.8 | 649.24 | 2118.35 | 1964.60 | 1958.79 |
| 0.2 | 0.8 | 1222.78 | 2397.90 | 2240.60 | 2185.72 |
| 0.3 | 0.8 | 1562.65 | 3270.14 | 3244.27 | 3258.95 |
| 0.4 | 0.8 | 1683.61 | 3572.73 | 3590.97 | 3597.54 |
| 0.5 | 0.8 | 1732.53 | 3697.95 | 3704.40 | 3714.70 |
| 0.6 | 0.8 | 1753.06 | 3744.48 | 3759.22 | 3766.38 |
| 0.7 | 0.8 | 1765.58 | 3771.59 | 3783.49 | 3793.62 |
| 0.8 | 0.8 | 1772.54 | 3785.39 | 3799.89 | 3808.54 |
| 0.9 | 0.8 | 1775.43 | 3793.50 | 3807.23 | 3816.88 |
| 1.0 | 0.8 | 1778.42 | 3797.82 | 3812.50 | 3821.62 |
| 0.0 | 0.9 | 4779.94 | 13932.45 | 15617.19 | 16453.85 |
| 0.1 | 0.9 | 3364.38 | 5649.64 | 4576.76 | 4918.89 |
| 0.2 | 0.9 | 3200.26 | 7467.65 | 7093.54 | 7151.92 |
| 0.3 | 0.9 | 2809.10 | 6204.43 | 6387.31 | 6400.92 |
| 0.4 | 0.9 | 2530.90 | 5629.74 | 5635.37 | 5655.50 |
| 0.5 | 0.9 | 2374.78 | 5103.31 | 5133.38 | 5149.84 |
| 0.6 | 0.9 | 2203.94 | 4795.99 | 4815.82 | 4828.25 |
| 0.7 | 0.9 | 2140.99 | 4594.87 | 4614.00 | 4626.49 |
| 0.8 | 0.9 | 2098.06 | 4470.78 | 4488.96 | 4500.27 |
| 0.9 | 0.9 | 2038.74 | 4393.05 | 4410.46 | 4421.70 |
| 1.0 | 0.9 | 2040.30 | 4345.21 | 4362.50 | 4373.33 |
| 0.0 | 1.0 | 3893.60 | 68239.18 | 80813.10 | 82674.86 |
| 0.1 | 1.0 | 6891.86 | 24150.73 | 22633.24 | 23698.06 |
| 0.2 | 1.0 | 5224.62 | 13103.66 | 12245.57 | 12411.52 |
| 0.3 | 1.0 | 3720.75 | 8682.02 | 8695.99 | 8732.58 |
| 0.4 | 1.0 | 3080.82 | 6959.39 | 6967.08 | 6981.53 |
| 0.5 | 1.0 | 2837.50 | 5983.60 | 6015.10 | 6034.99 |
| 0.6 | 1.0 | 2466.10 | 5460.19 | 5479.13 | 5495.06 |
| 0.7 | 1.0 | 2399.19 | 5142.56 | 5164.11 | 5178.38 |
| 0.8 | 1.0 | 2357.91 | 4958.08 | 4764.61 | 4990.65 |
| 0.9 | 1.0 | 2215.52 | 4847.43 | 4866.73 | 4879.28 |
| 1.0 | 1.0 | 2262.43 | 4782.90 | 4801.79 | 4813.92 |

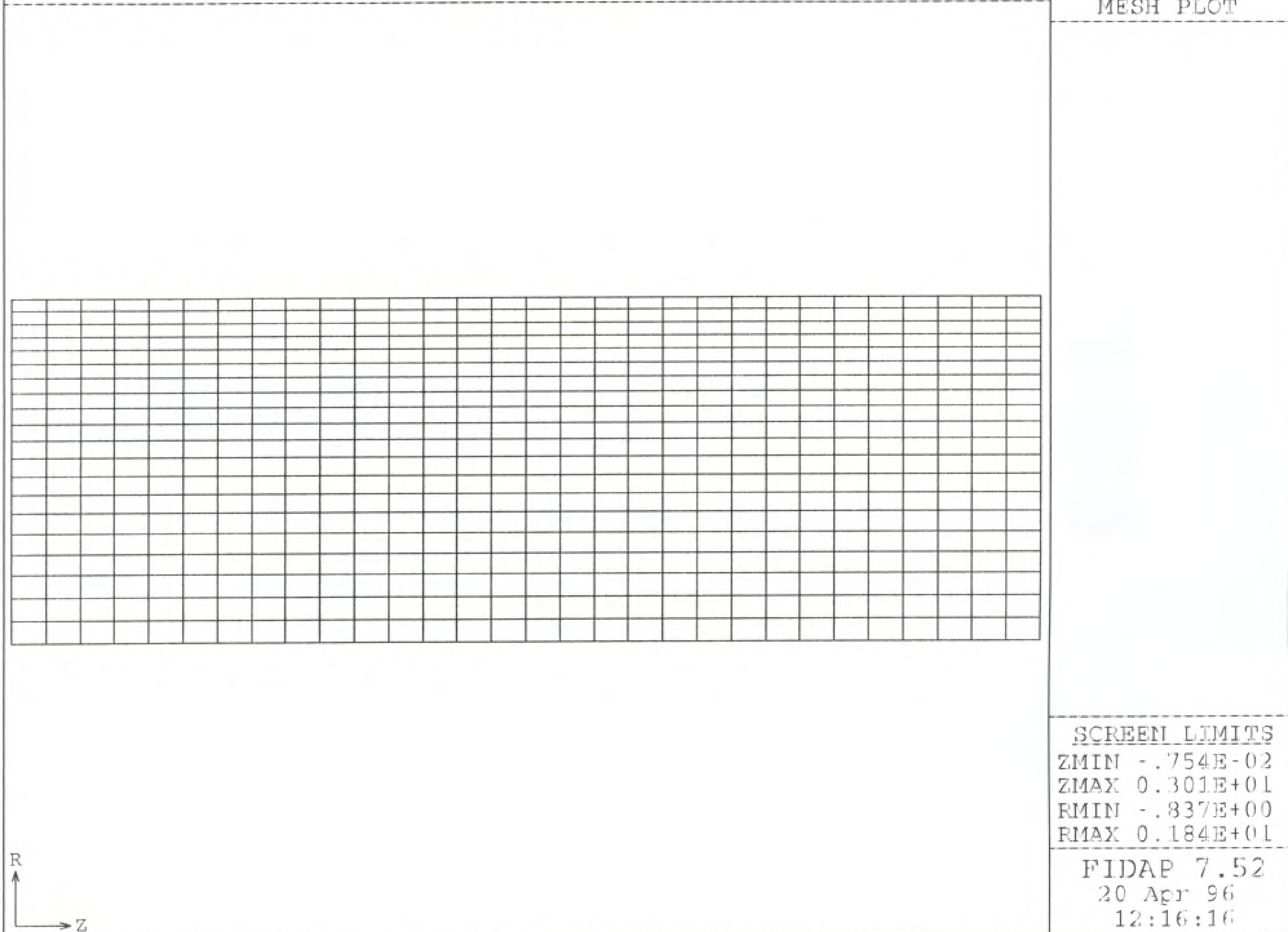


FIGURE 4.4: LOW MESH DENSITY, MESH

FIGURE 4.5: LOW MESH DENSITY, VELOCITY VECTOR

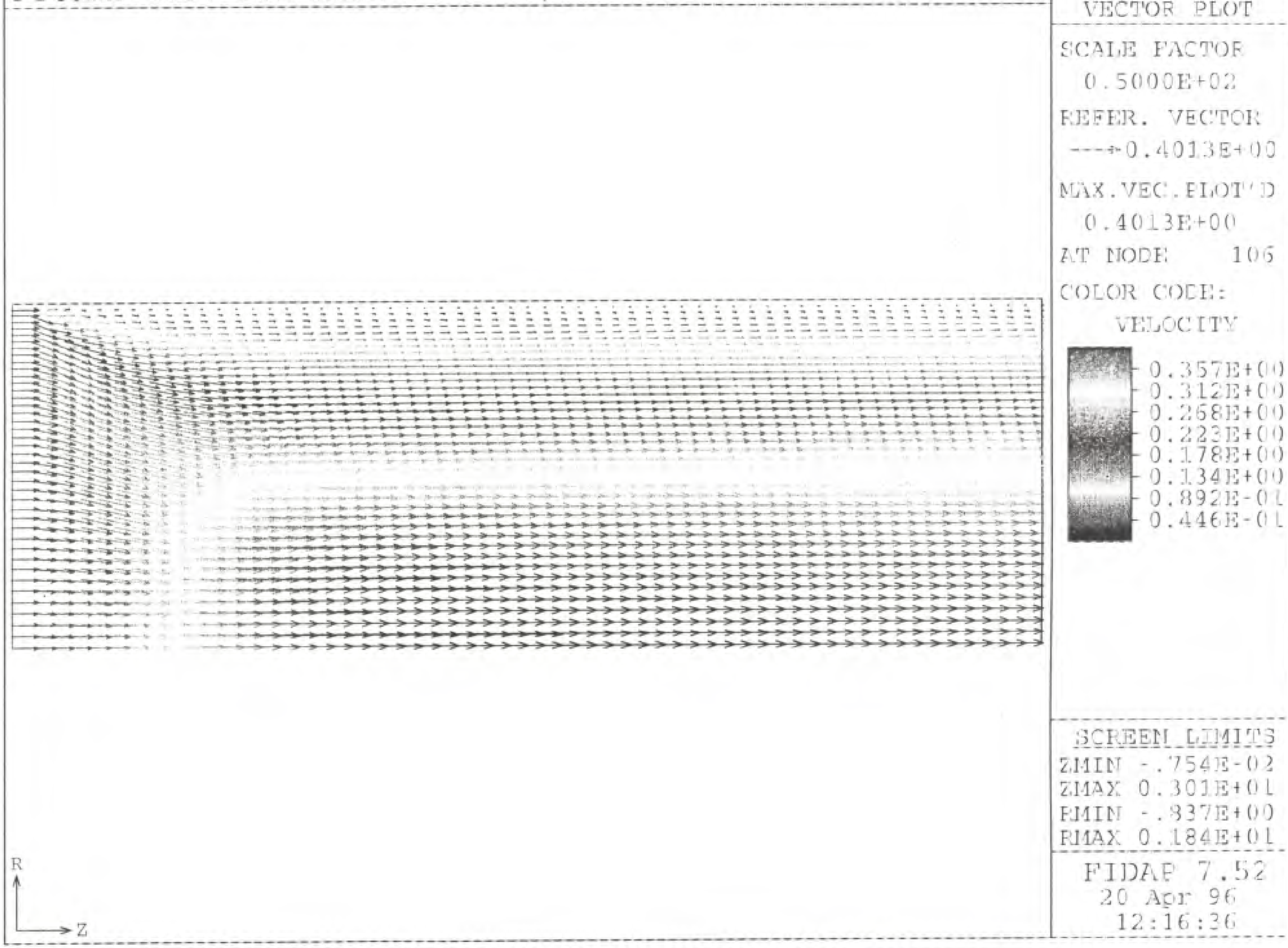

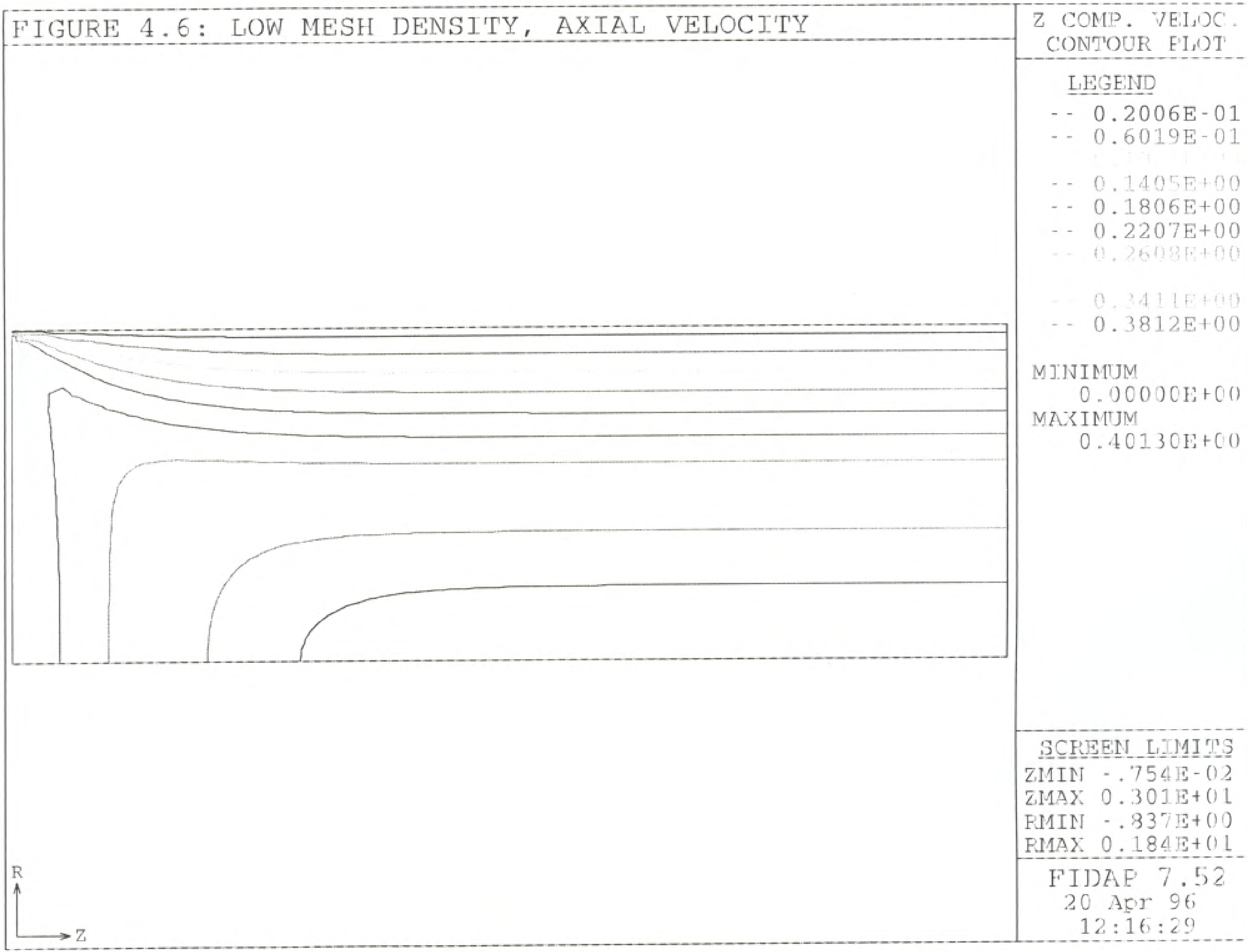


FIGURE 4.6: LOW MESH DENSITY, AXIAL VELOCITY

FIGURE 4.7: LOW MESH DENSITY, RADIAL VELOCITY

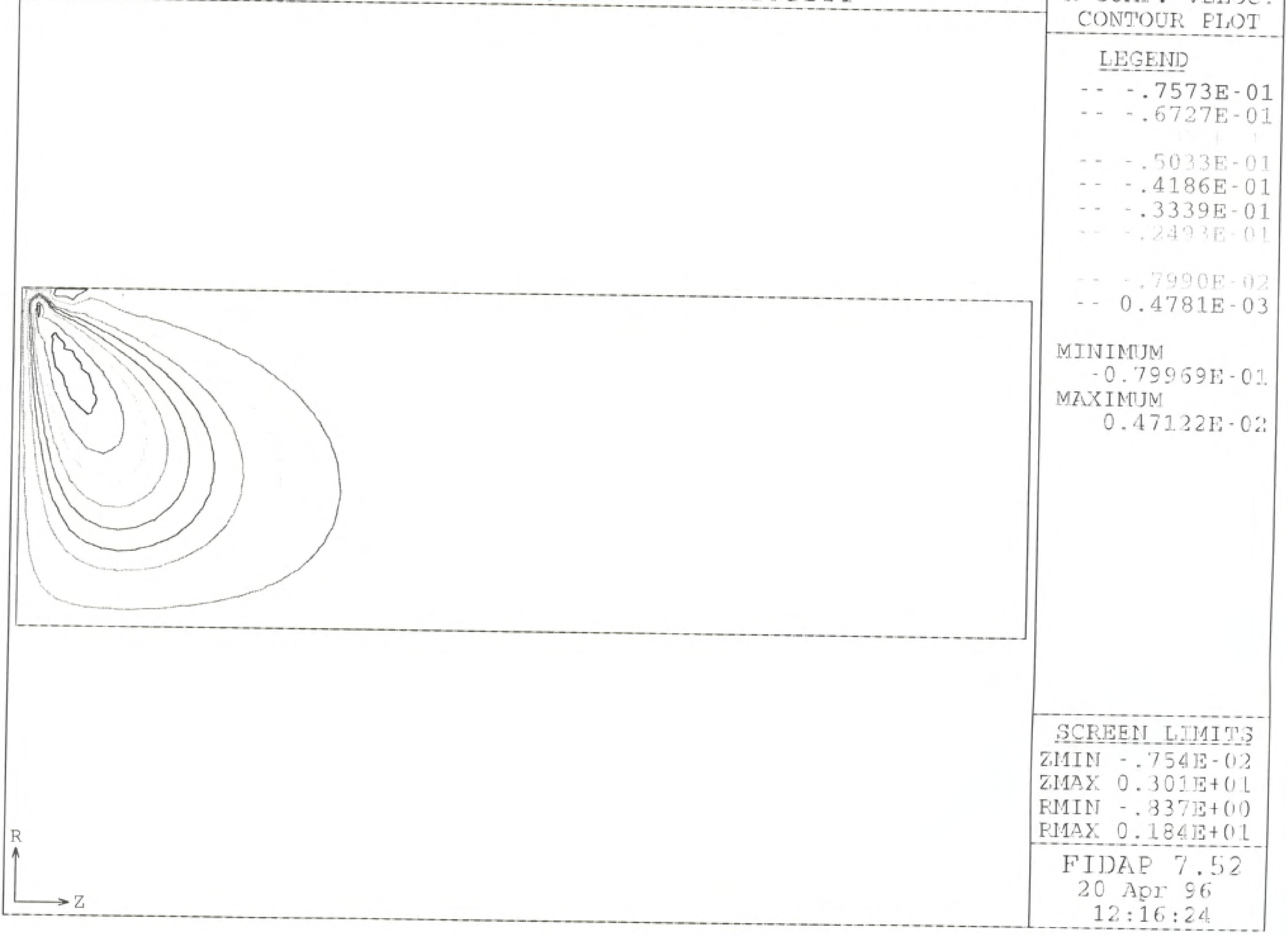

FIGURE 4.8: LOW MESH DENSITY, SHEAR STRAIN RATE

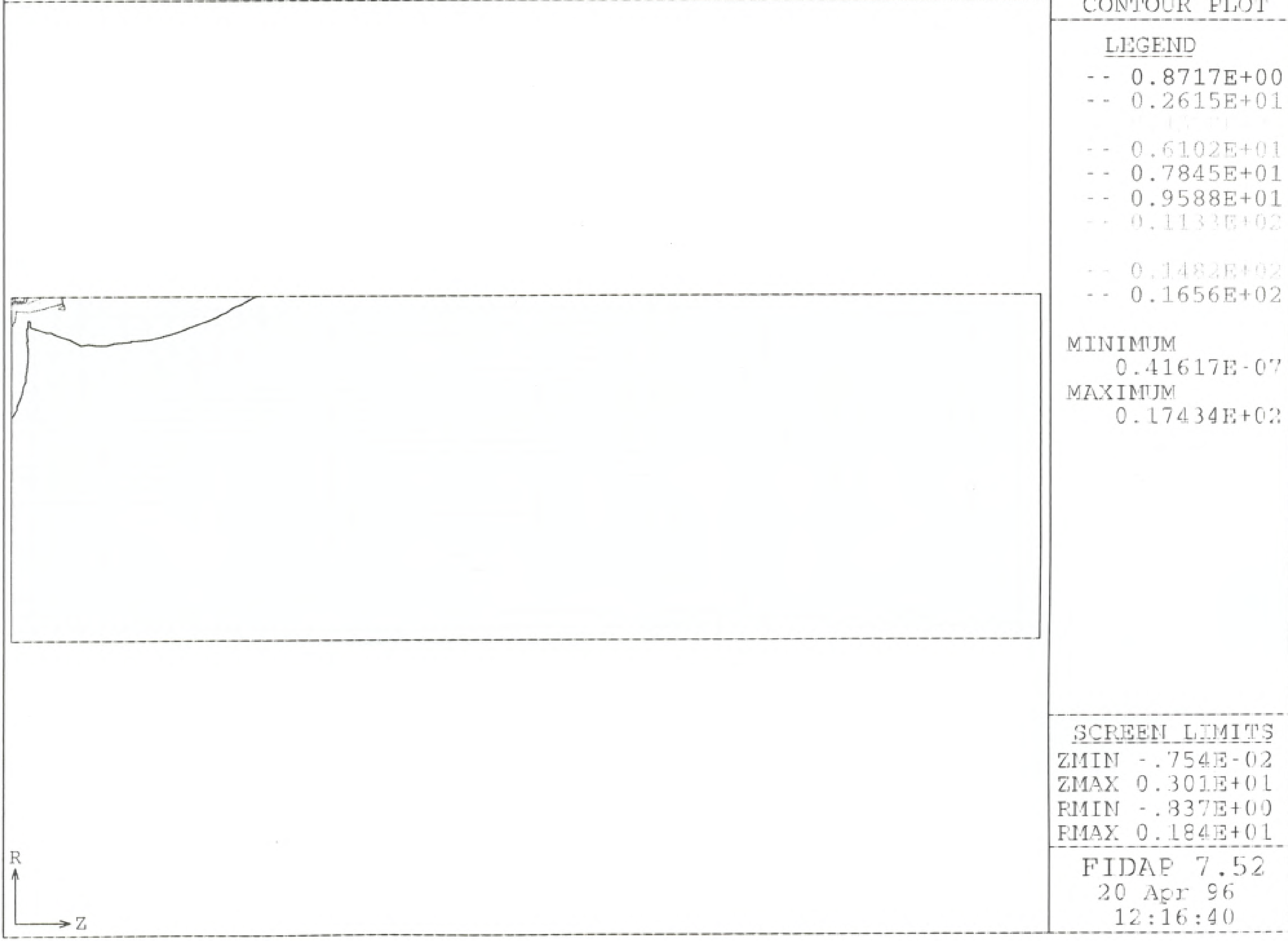

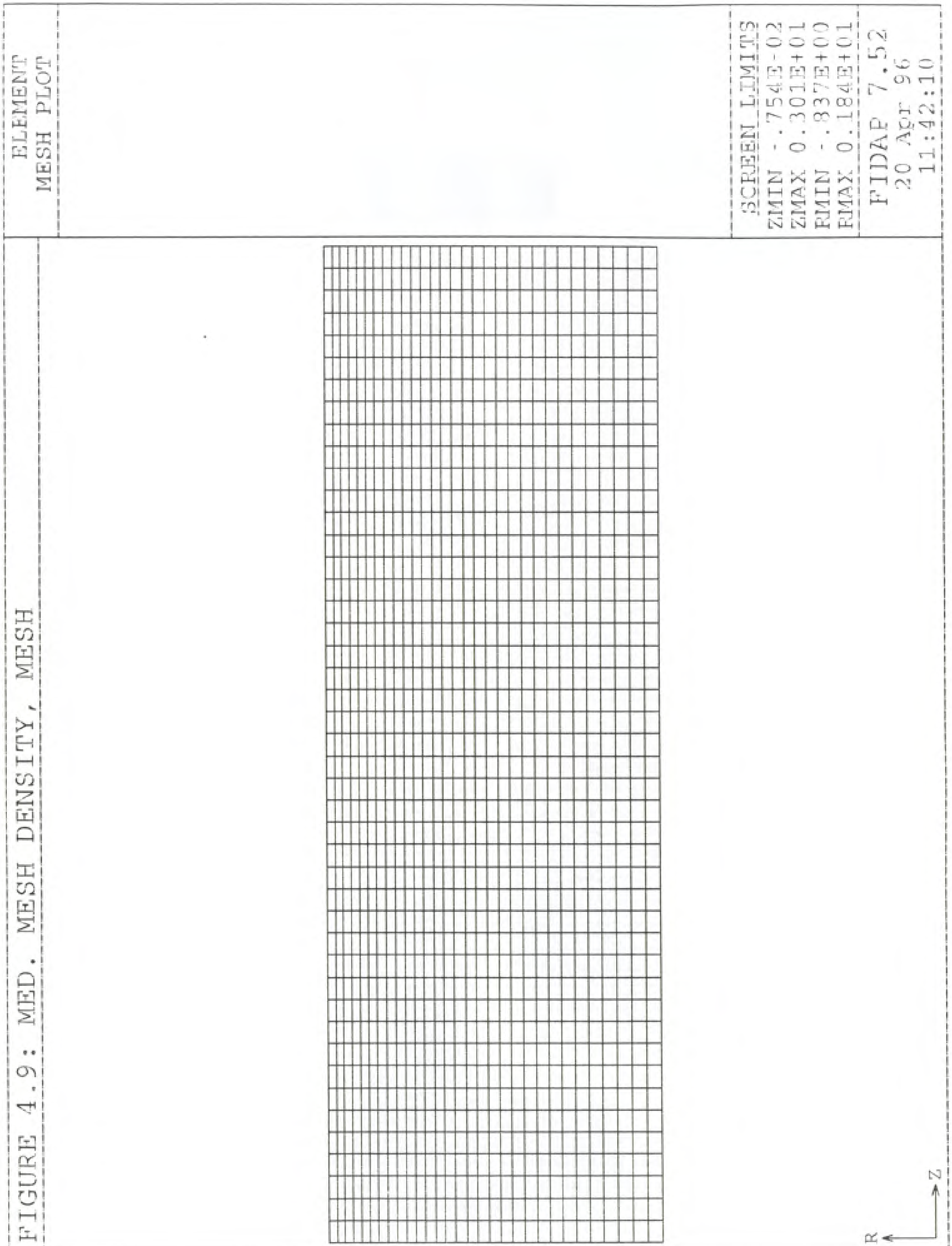


FIGURE 4.9: MED. MESH DENSITY, MESH

FIGURE 4.10: MED. MESH DENSITY, VELOCITY VECTOR

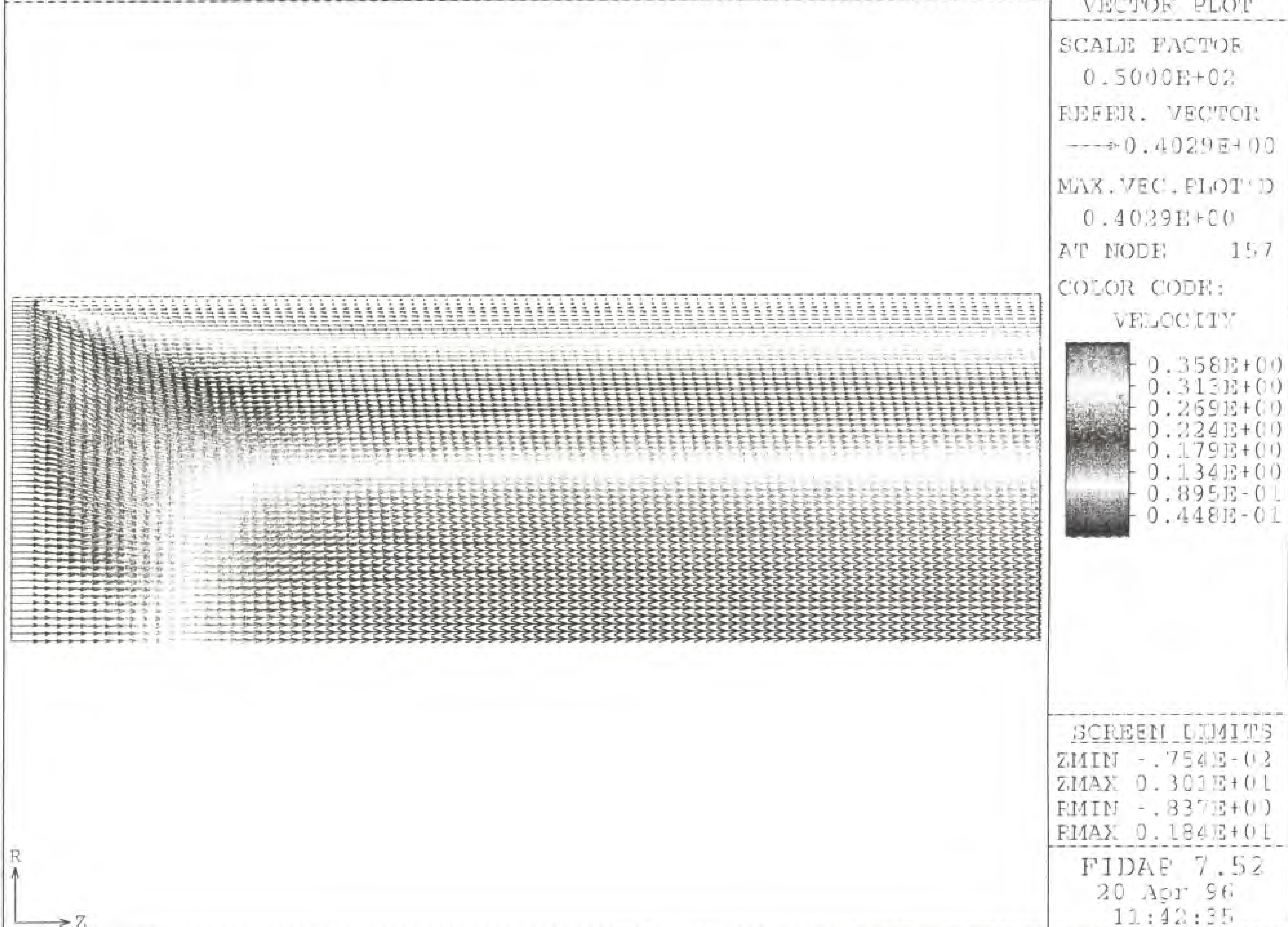

FIGURE 4.11: MED. MESH DENSITY, AXIAL VELOCITY

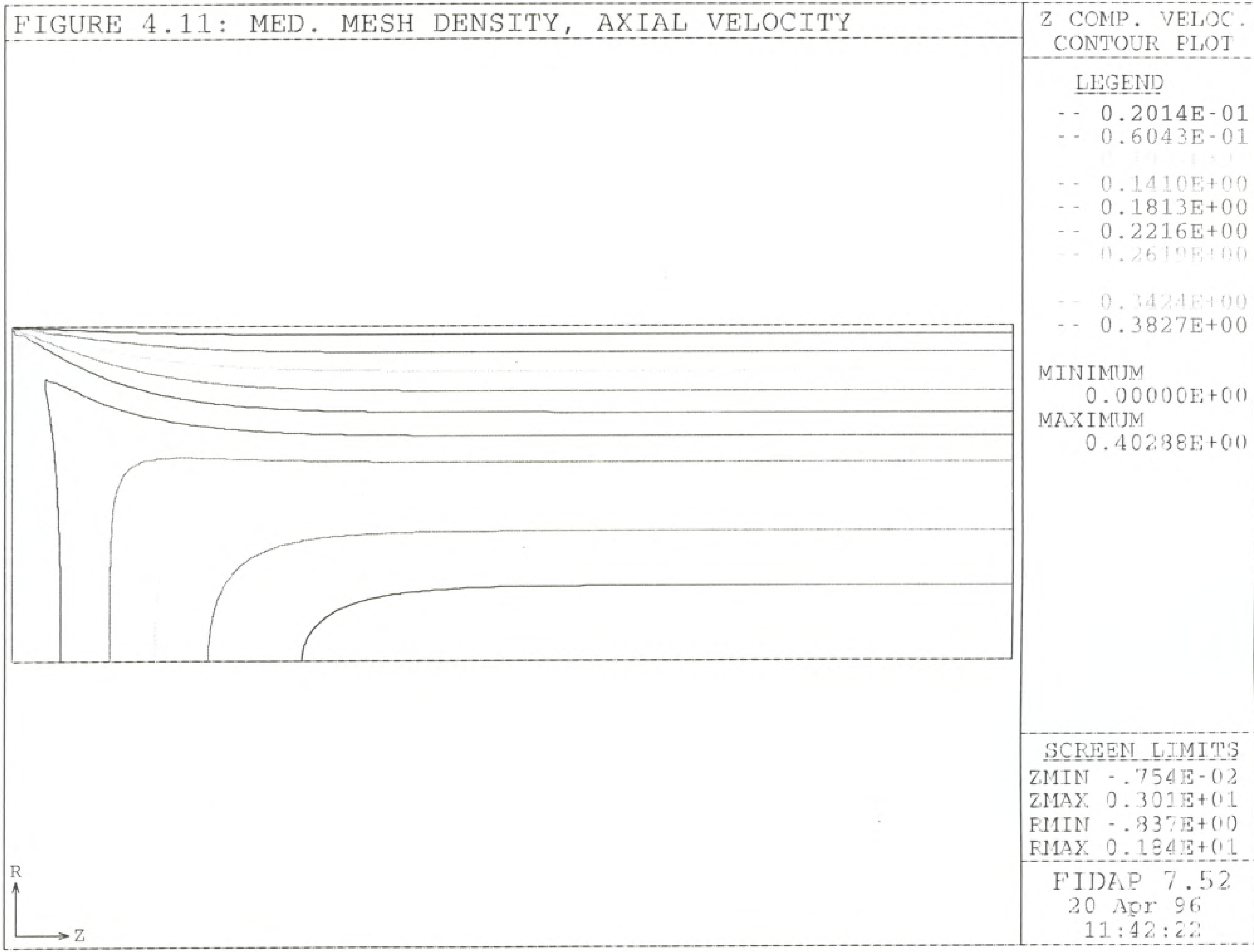

FIGURE 4.12: MED. MESH DENSITY, RADIAL VELOCITY

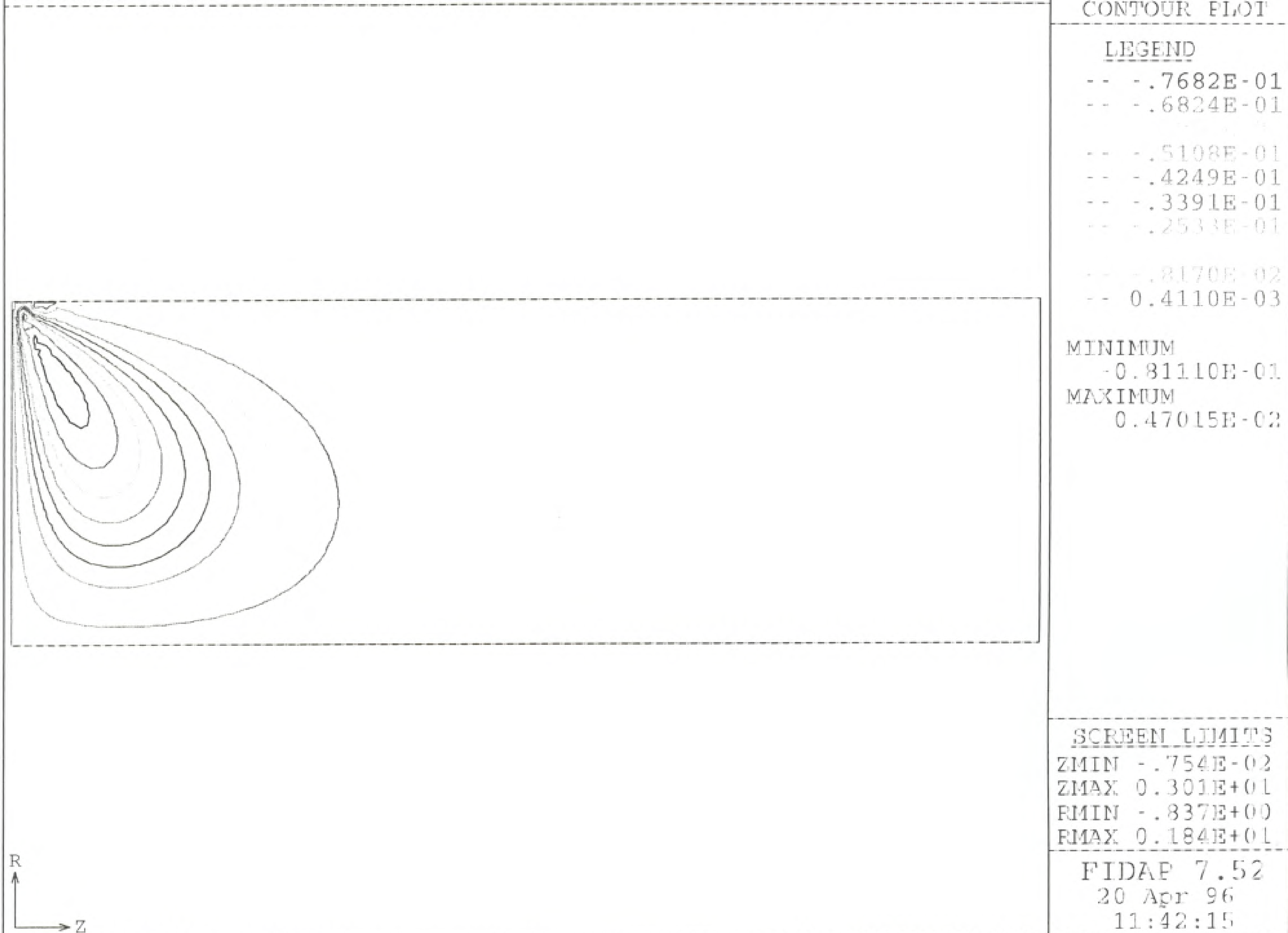

FIGURE 4.13: MED. MESH DENSITY, SHEAR STRAIN RATE


SHEAR RATE
CONTOUR PLOT

LEGEND

-- 0.1311E+01
-- 0.3933E+01
-- 0.9177E+01
-- 0.1180E+02
-- 0.1442E+02
-- 0.1704E+02
-- 0.2229E+02
-- 0.2491E+02

MINIMUM
0.12392E-07
MAXIMUM
0.26221E+02

SCREEN LIMITS
ZMIN -.754E-02
ZMAX 0.301E+01
RMIN -.337E+00
RMAX 0.184E+01

FIDAP 7.52
20 Apr 96
11:42:35

FIGURE 4.14: HIGH MESH DENSITY, MESH

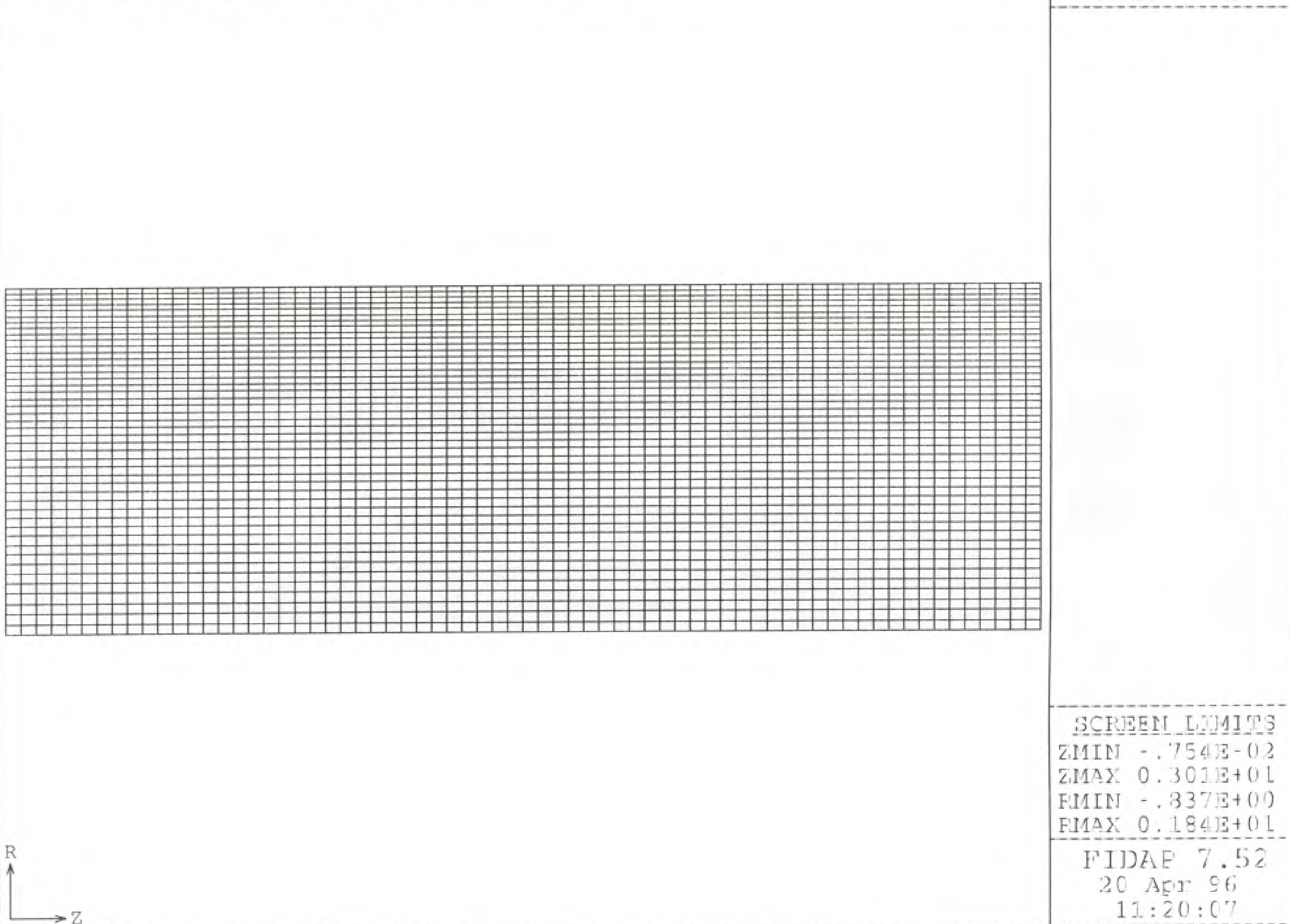

FIGURE 4.15: HI MESH DENSITY, VELOCITY VECTOR

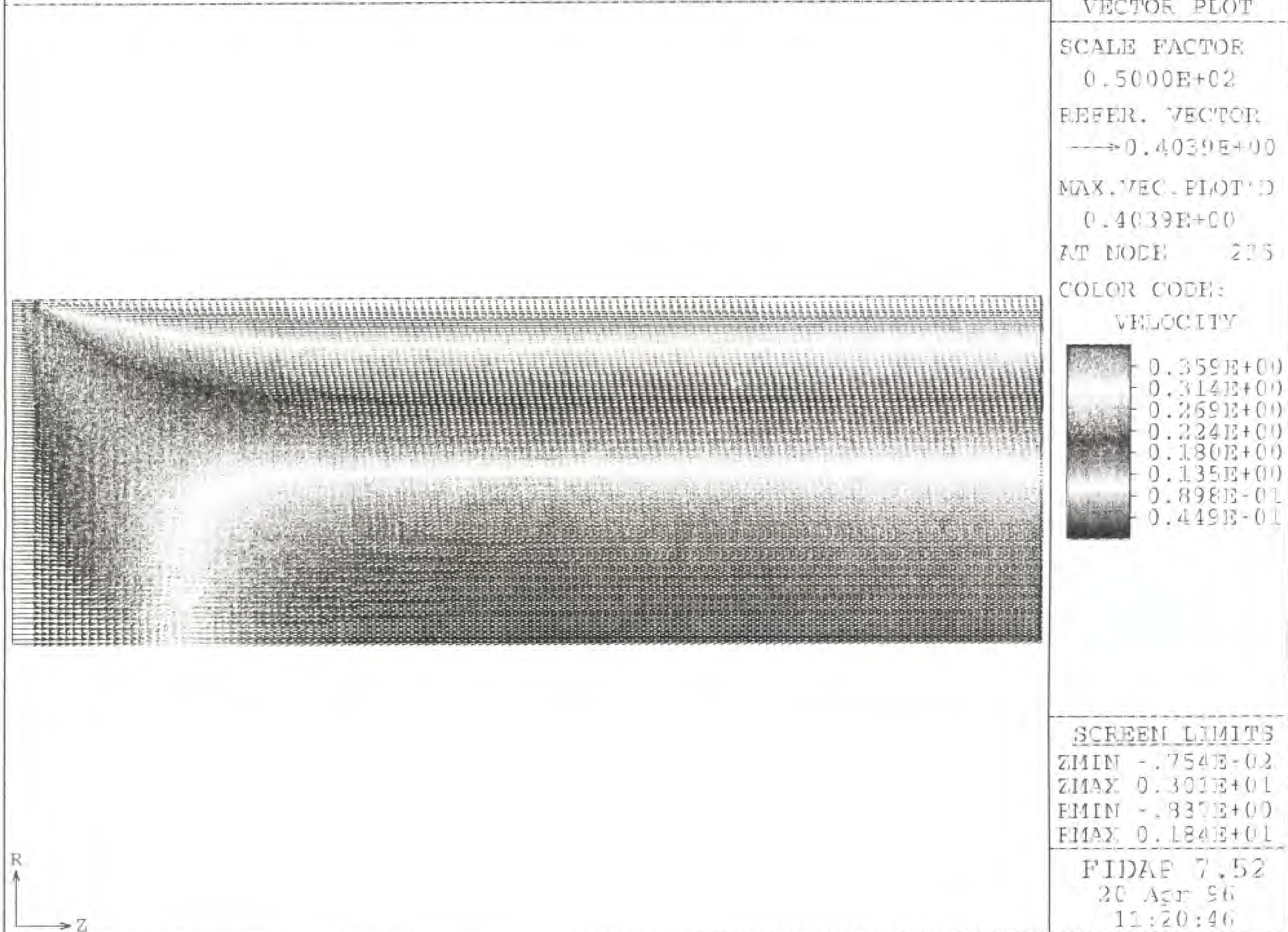

FIGURE 4.16: HIGH MESH DENSITY, AXIAL VELOCITY

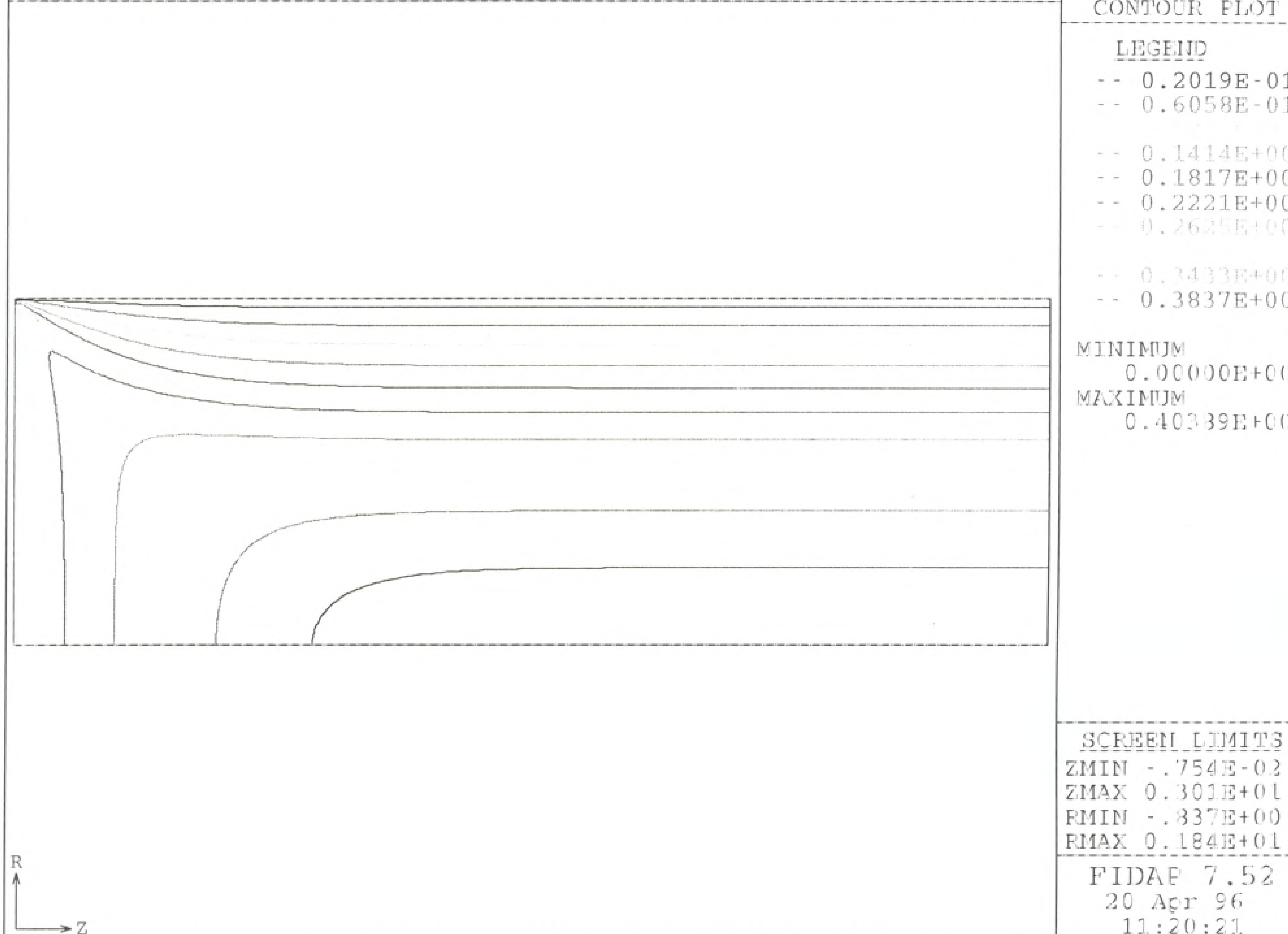

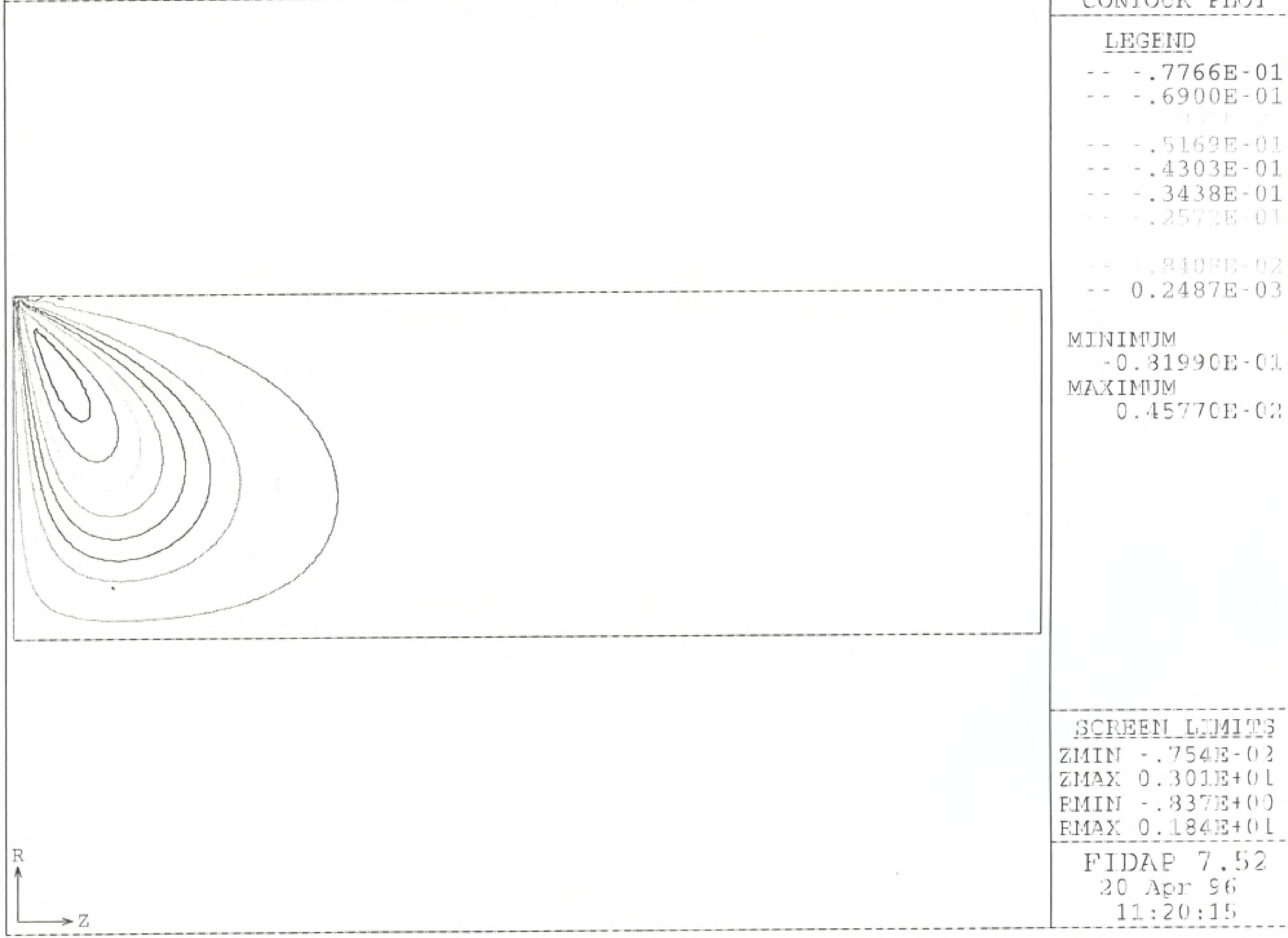


FIGURE 4.17: HI MESH DENSITY, RADIAL VELOCITY

FIGURE 4.18: HIGH MESH DENSITY, SHEAR STRAIN RATE

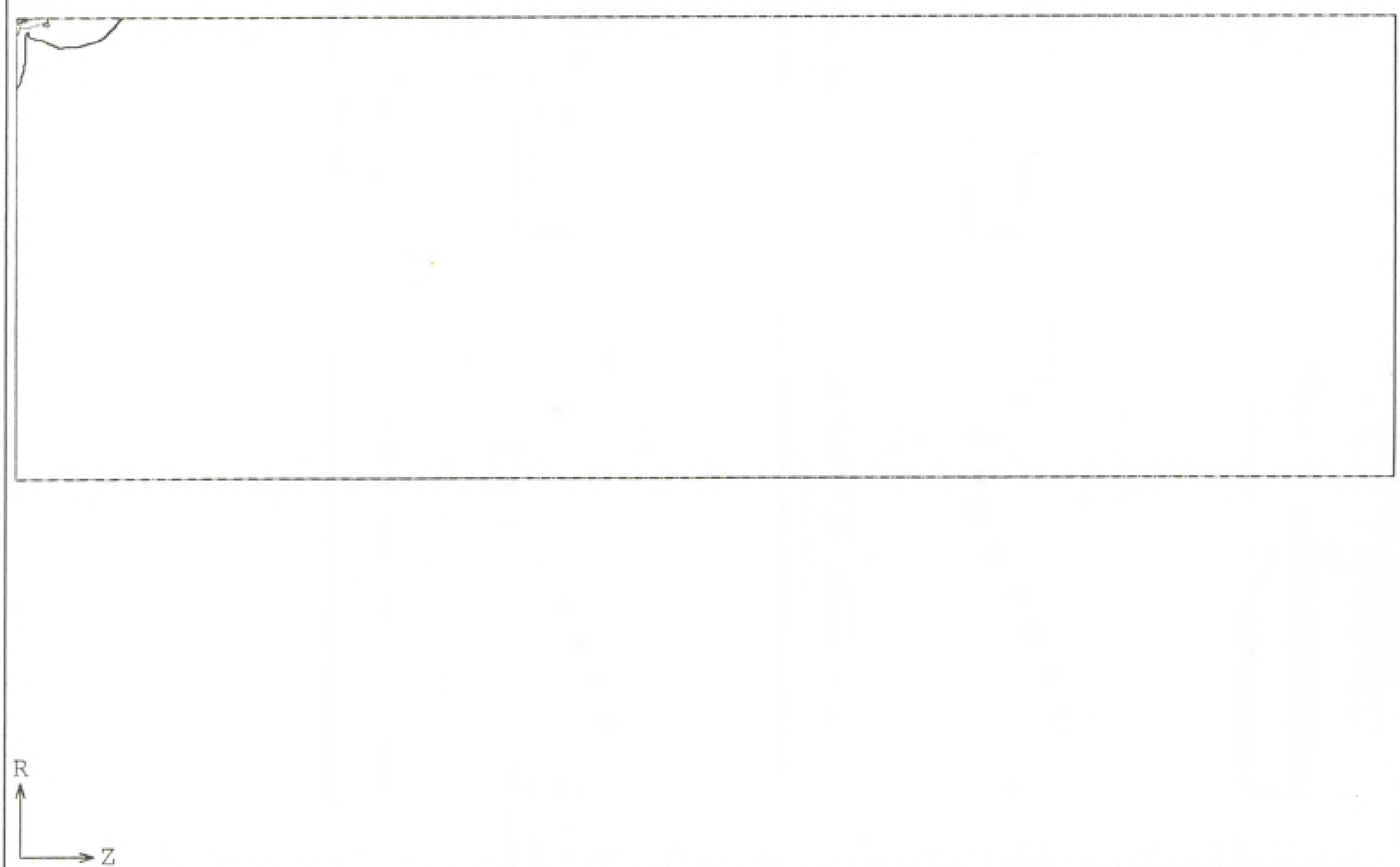

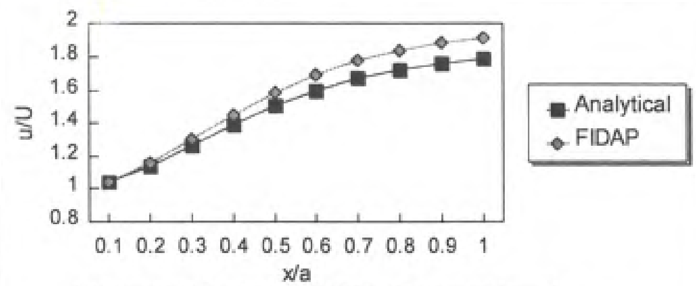


Figure 4.19 : Axial Velocity Comparison
at r/a = 0.1

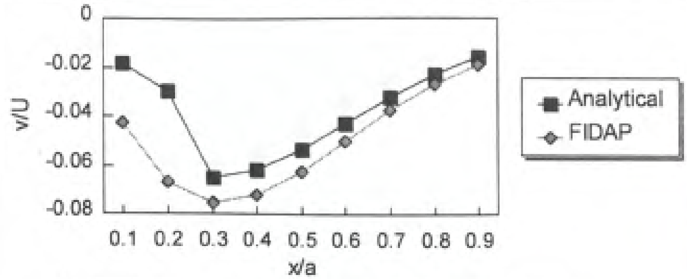


Figure 4.20 : Radial Velocity Comparison
at r/a= 0.1

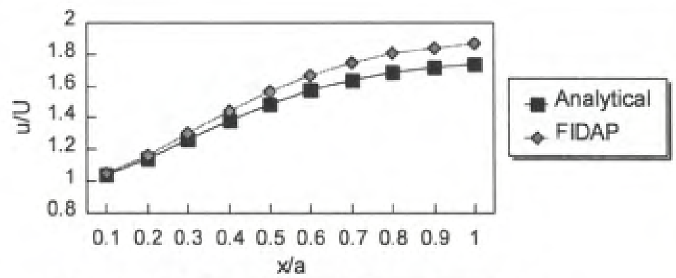


Figure 4.21 Axial Velocity Comparison
at r/a = 0.2

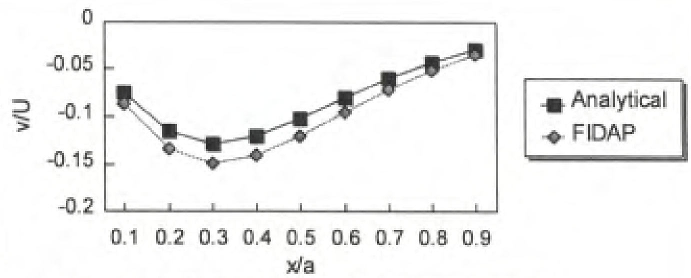


Figure 4.22 : Radial Velocity Comparison
at r/a = 0.2

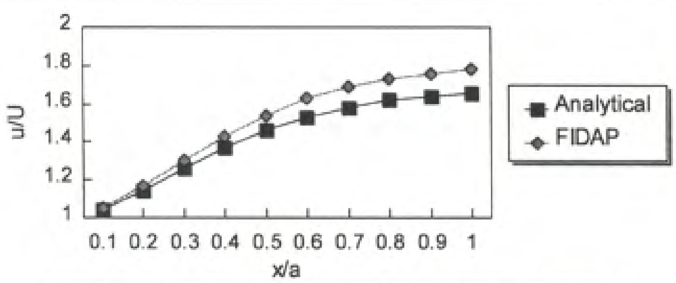


Figure 4.23 : Axial Velocity Comparison
at r/a = 0.3

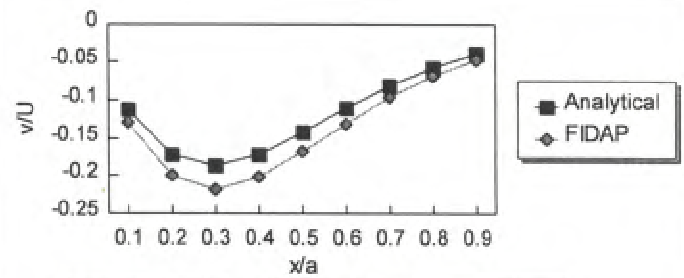


Figure 4.24 : Radial Velocity Comparison
at r/a = 0.3

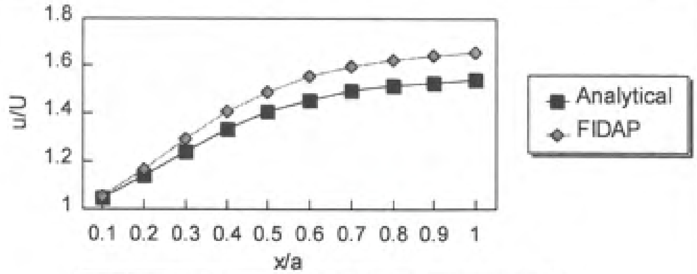


Figure 4.25: Axial Velocity Comparison
at r/a = 0.4

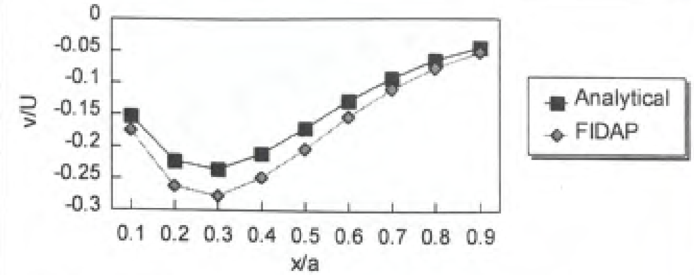


Figure 4.26 : Radial Velocity Comparison
at r/a = 0.4

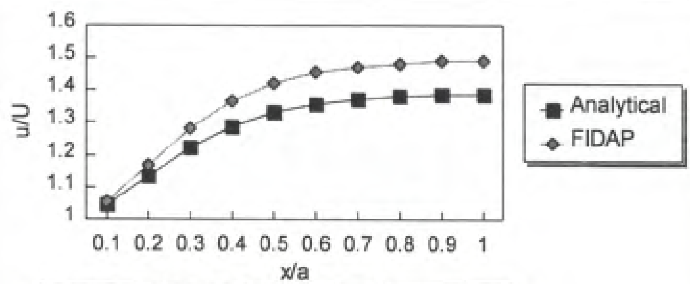


Figure 4.27: Axial Velocity Comparison
at r/a =0.5

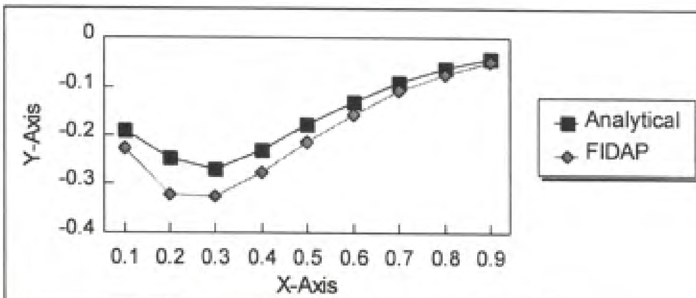


Figure 4.28 : Radial Velocity Comparison
at r/a = 0.5

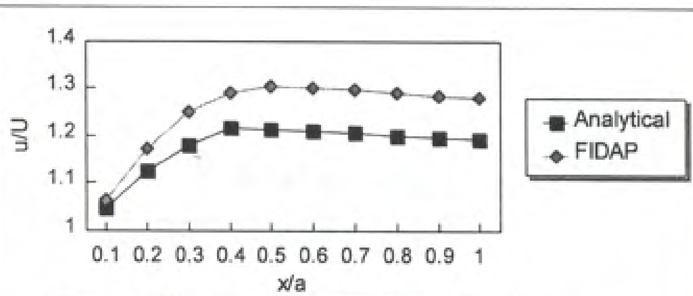


Figure 4.29 : Axial Velocity Comparison
at r/a = 0.6

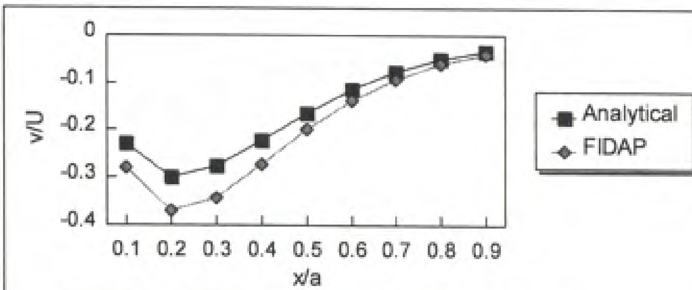


Figure 4.30: Radial Velocity Comparison
at r/a = 0.6

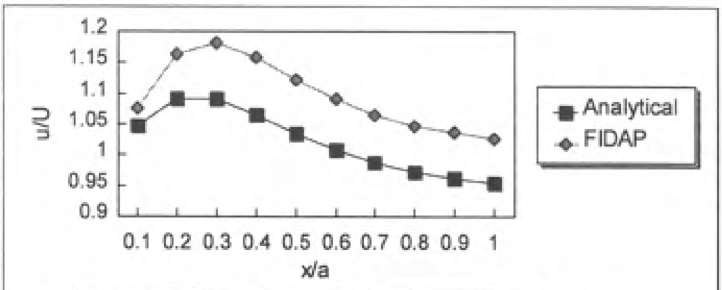


Figure 4.31 : Axial Velocity Comparison at r/a = 0.7

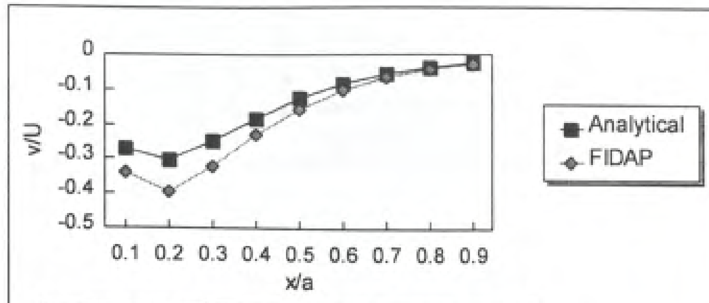


Figure 4.32 Radial Velocity Comparison at r/a = 0.7

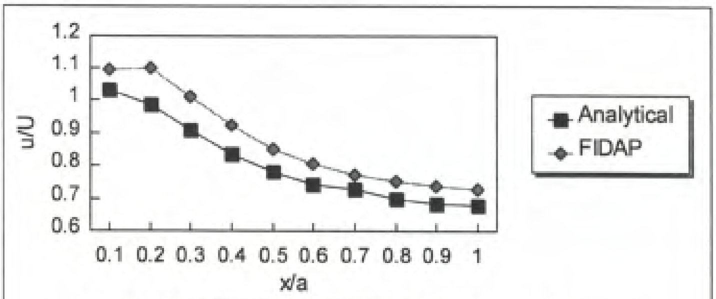


Figure 4.33 : Axial Velocity Comparison at r/a = 0.8

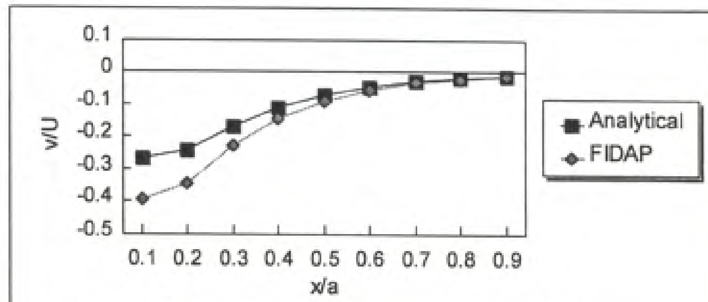


Figure 4.34 : Radial Velocity Comparison at r/a = 0.8

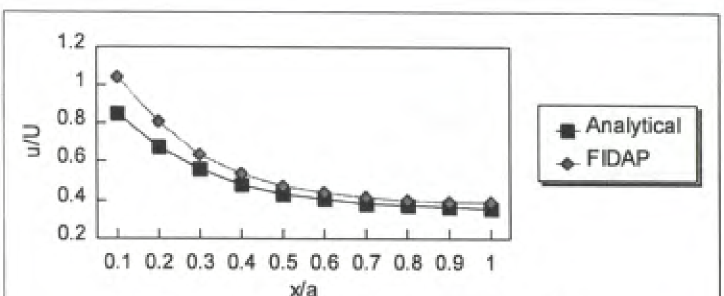


Figure 4.35: Axial Velocity Comparison at r/a = 0.9

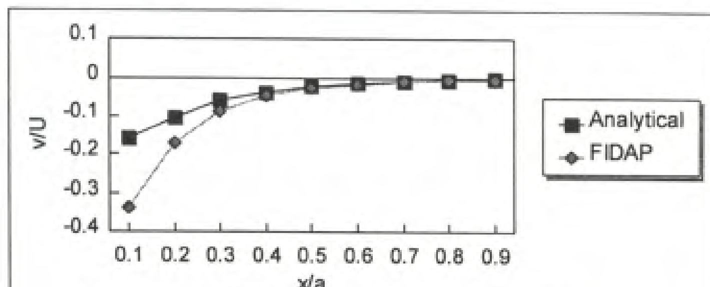


Figure 4.36: Radial Velocity Comparison at r/a = 0.9

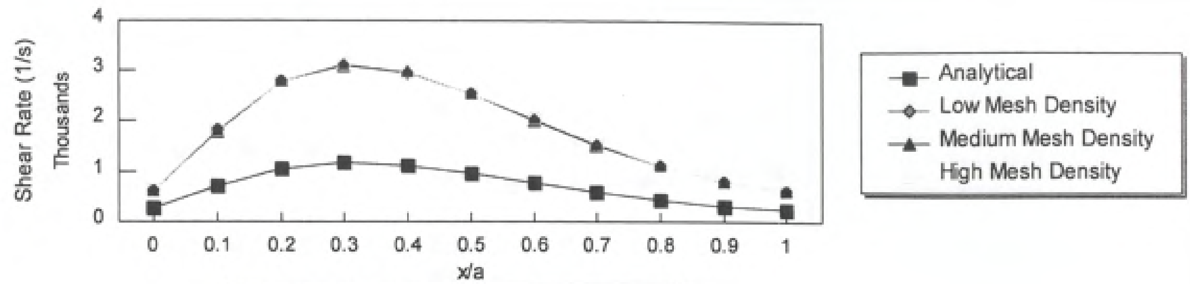


Figure 4.37 : Strain Rate Comparison
at r/a = 0.1

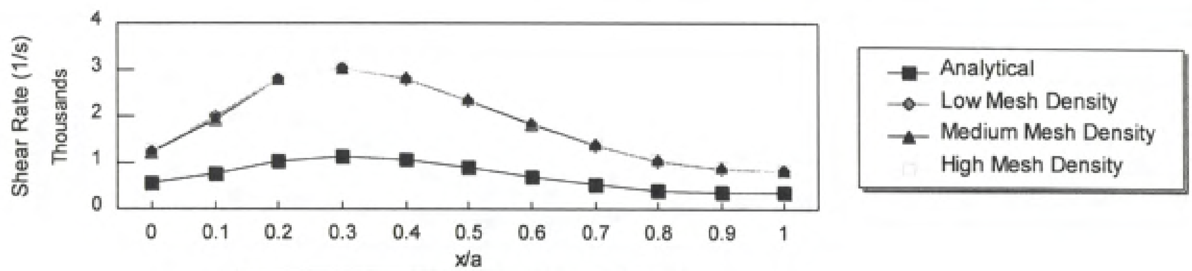


Figure 4.38: Strain Rate Comparison
at r/a = 0.2

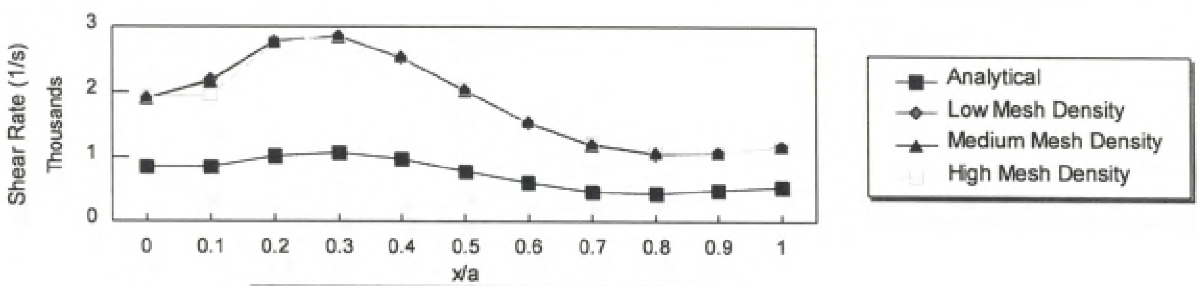


Figure 4.39 : Strain Rate Comparison
at r/a = 0.3

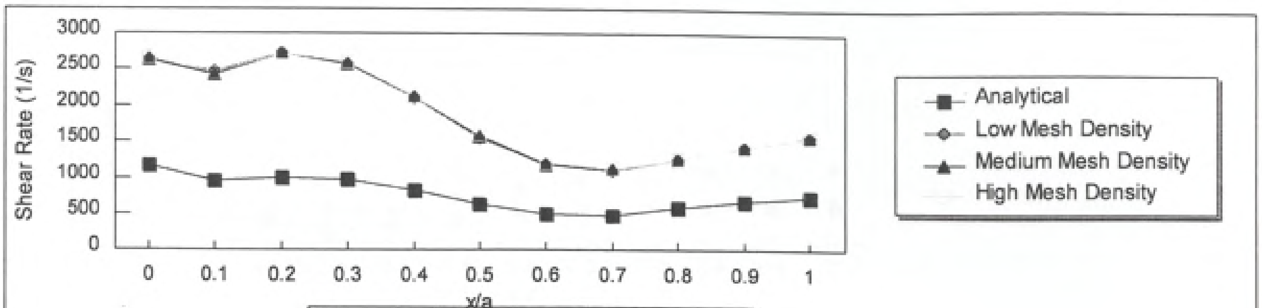


Figure 4.40: Strain Rate Comparison
at r/a = 0.4

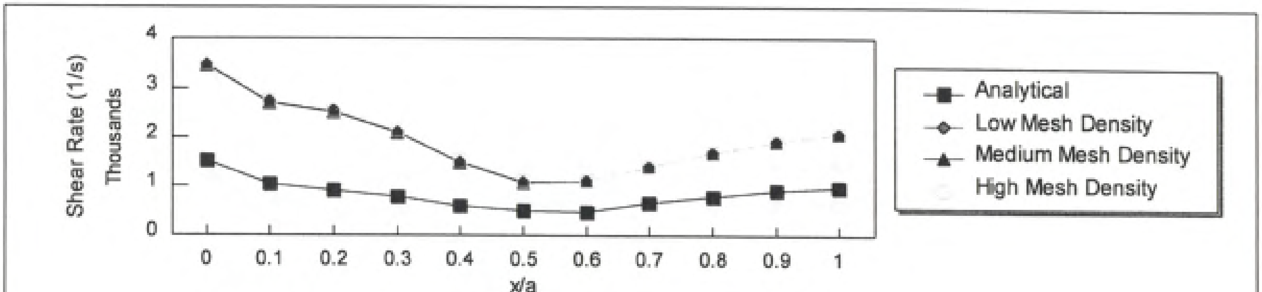


FIgure 4.41 : Strain Rate Comparison
at r/a = 0.5

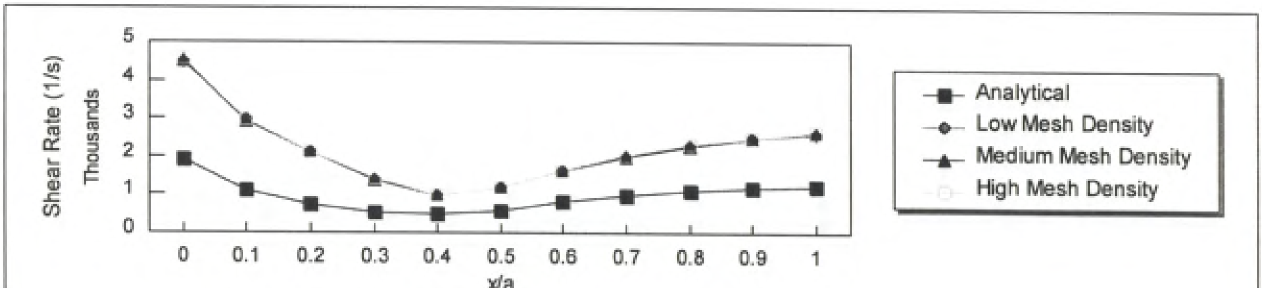


Figure 4.42 : Strain Rate Comparison
at r/a = 0.6

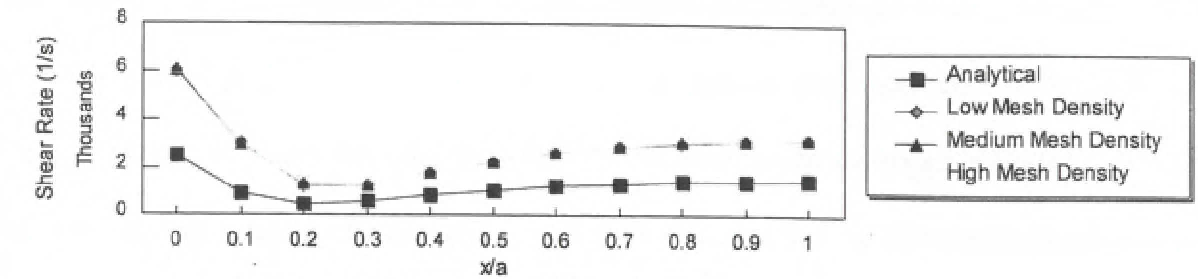


Figure 4.43 : Strain Rate Comparison
at r/a = 0.7

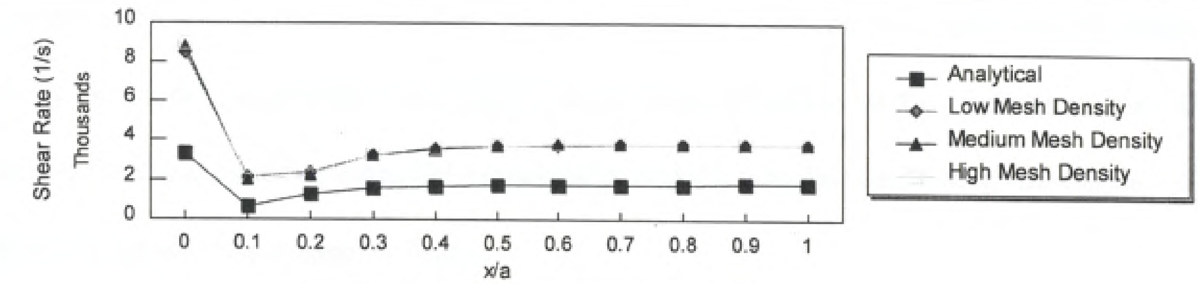


Figure 4.44 : Strain Rate Comparison
at r/a = 0.8

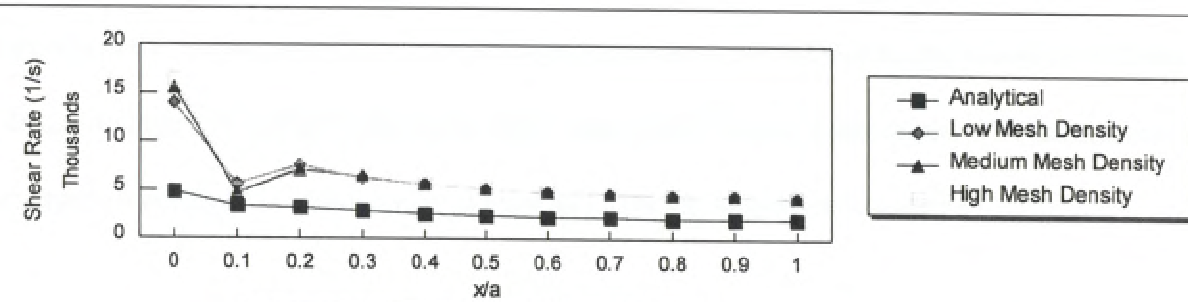


Figure 4.45 : Strain Rate Comparison
at r/a = 0.9

in addition to axial flow, is seen trying to move inwards away from the walls, Tabulated values (Table 4.3) and graphs indicate that the radial velocity reaches about one third of the axial inlet velocity. This region where the radial velocity is significant can be observed in Figure 4.7, which plots radial velocity contours for the region. It is quite apparent that the flow settles down towards the outlet, which confirms the analytical observation that for all practical purposes, a tube with length three times the radius can be considered infinite. Figure 4.6, the countour plot for axial velocity can be seen to confirm the same, i.e., the presence of an entrance region with a complex velocity distribution, extending to the order of one to one and a half times the tube radius. After this distance, the contours become parallel to each other and the tube axis, indicating that the flow has settled to a steady state Poiseuille flow.

A look at the corresponding plots for higher mesh densities indicates that but for minor variations in the values, and the vector plots getting more crowded due to the increased number of nodes, the pattern is virtually the same. This, along with values from Table 4.3 confirm that the convergence achieved is satisfactory, at least as far as the velocity is concerned.

Figures 4.19 to 4.36 compare the axial and radial velocity components obtained using the analytical solution and those obtained for the highest mesh density using FIDAP. The abscissa (x/a) is the ratio of the axial distance from the inlet (x) to the radius of the tube (a), while the ordinate (u/U, v/U) is the ratio of the relevant axial (u) or radial (v) velocity component to the uniform inlet velocity (U). In each graph, the radial distance from the axis is kept constant.

Figures 4.19, 4.21, and 4.23, the plots of the axial velocities at lower radii (r/a = .1, .2, .3 respectively) indicate that the correlation between the analytical solution and the FIDAP results is quite good, particularly near the inlet. FIDAP does tend to overpredict the axial component a bit. The correlation is seen to get worse for r/a = .7 (Figure 4.31). The value of r/a = 0.7 is seen to be a transition region as far as the shapes of the curves are concerned, and the finite element solution does not seem to be capable of handling this transition accurately. However, the maximum error even here is still about 10%. For points farther away from the axis, at r/a = .8 (Figure 4.33) and r/a = 0.9 (Figure 4.35), the correlation is seen to improve, however the correlation is better away from the inlet for r/a =0.9 than near the inlet as for smaller radii. This could be because of the discontinuity in the problem at the inlet due to the wall.

The plots for radial velocity components show that the correlation is not good at the inlet for r/a = 0.1 (Figure 4.20), as also for r/a = 0.9 (Figure 4.36). Besides, convergence is better in all cases downstream, away from the inlet as compared to the inlet. The code also overpredicts the magnitudes of the radial velocity components at all points. The curves for FIDAP are below the curves for analytical solutions as the values are all negative, i.e. inwards, towards the axis. Relative accuracy is not as good near the inlet for radial velocity components obtained using FIDAP as compared to the accuracy achieved for axial components.

The higher velocities would indicate that the parameter of interest, the shear strain rates, would tend to be higher in the FIDAP solutions, as compared to analytical solutions.

### 4.4.2 Shear Strain Rate

Figure 4.8 is the countour plot for shear strain rate obtained for the lowest density FIDAP solution. The maximum is concentrated near the inlet at the wall, as can be expected, due to the discontiuity at that point. It can be seen however that increasing the mesh density (Figures 4.13 and 4.18) concentrates the region of high strain rates closer and closer to the wall at the inlet, while the value of the maxima shoots up without converging. This is simply because in such a numerical solution, a discontinuity, when averaged over a coarser mesh, would appear smeared out over the larger area, but on refining the mesh, would approach the threoretical singularity. In this respect, it is to be noted that the analytical solution of Lew and Fung (1969) also breaks down at the walls. Any exact solution would have to incorporate the nonlinearities inherent in the region at the wall at the inlet. However, this does not prohibit comparison of the results away from the wall, i.e. in the bulk of the flow volume. It is this bulk region which is of interest as it controls the deposition of the solder paste on the board.

Figures 4.37 to 4.45 plot the strain rates obtained using the three mesh densities of FIDAP against the rates obtained using the analytical solution. All the curves show strikingly similar characteristics. The most important result as far as convergence of the numerical solution is concerned is that the three FIDAP curves are virtually indistinguishable. The only deviation found is again at the wall at the inlet. Thus, the convergence is excellent for the three mesh densities for the shear strain rate.

However, comparison with the analytical curves shows that even though the plots are in excellent agreement as far as the shape is concerned, the peaks in the finite element result are two to three times the values obtained from analytical solutions. As expected, the deviation is the worst near the wall at the inlet, a region of discontinuity, where the velocity goes suddenly from the inlet velocity to zero. Therefore, the results should be compared only slightly away from the wall, especially at the inlet. Away from the wall at the inlet, the characteristics of all the curves can be explained as those of the analytical curves in Chapter 3, since the shapes are identical. However, the discrepency in the values is quite large.

The apparent discrepancy in the shear rate over the bulk of the volume would seem quite large in view of the fact that the velocity curves do not show a similar deviation for the two cases. We can see that the velocity curves are slightly steeper for the numerical case as compared to the analytical one, even though the difference is not substantial. This leads to a higher strain rate. Besides, getting the shear rate from the velocity curve involves numerical differentiation in the finite element model. To show the error that numerical differentiation causes, the exact velocity points calculated by Lew & Fung (1969) are taken, and shear rate components are obtained using a finite difference scheme. The program used is listed in Appendix (II-C). As the results (Figs 4.46 - 4.54) show, such a scheme of approximating the derivative at a point as the average slope over the interval between neighboring points introduces an extremely large error in the pattern for lower radii. In fact, the sum of the main diagonal which should be zero if the flow were to be incompressible would seem to vary quite a bit from that number. The agreement is better for intermediate radii, and again seems to deviate when the radius is increased. So, numerical differentiation seems to be a little

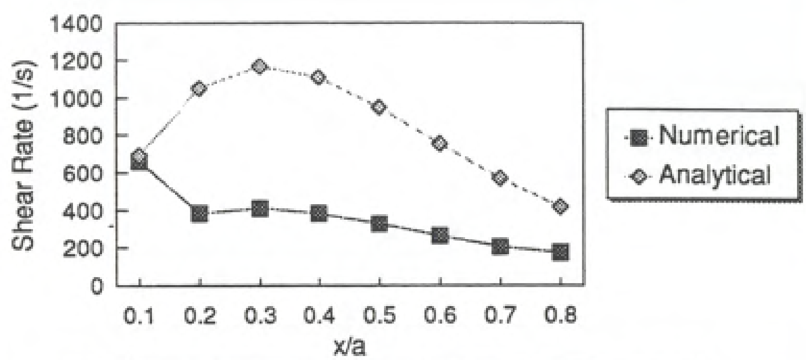


Figure 4.46 : Numerical Differentiation Error
at r/a =0.1

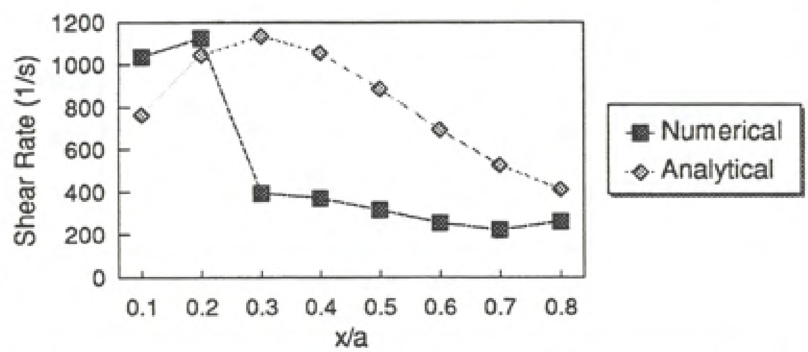


Figure 4.47: Numerical Differentiation Error
at r/a = 0.2

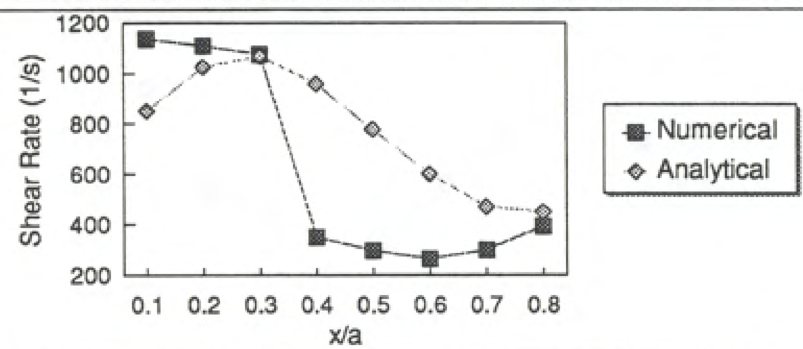


Figure 4.48 : Numerical Differentiation Error
at r/a = 0.3

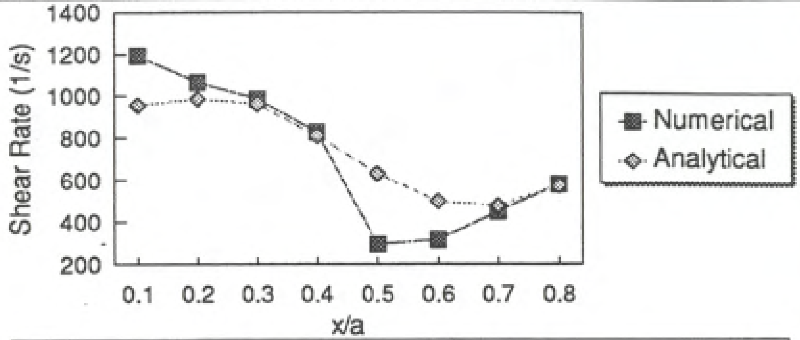


Figure 4.49 : Numerical Differentiation Error
at r/a =0.4

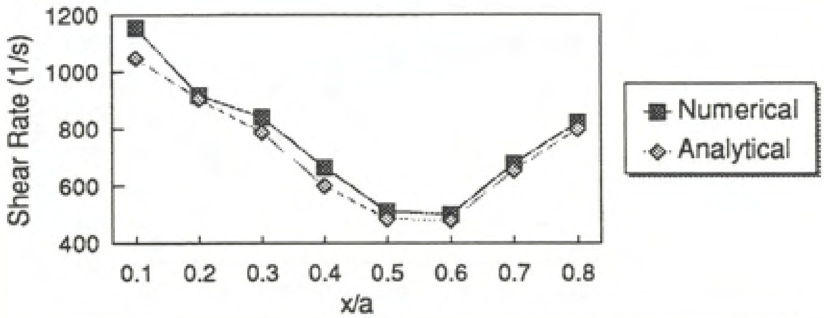


Figure 4.50 : Numerical Differentiation Error
at r/a =0.5

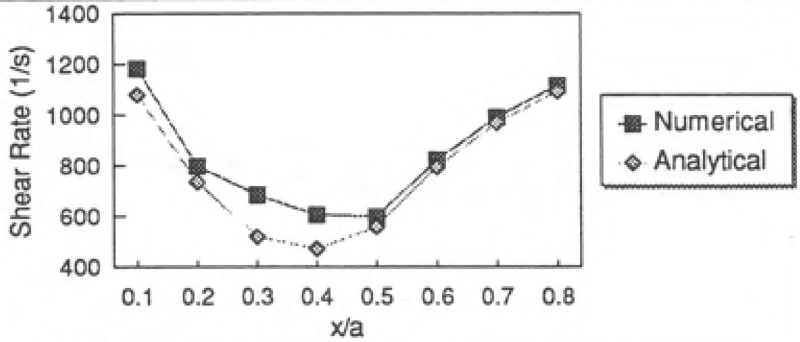


Figure 4.51 : Numerical Differentiation Error
at r /a =0.6

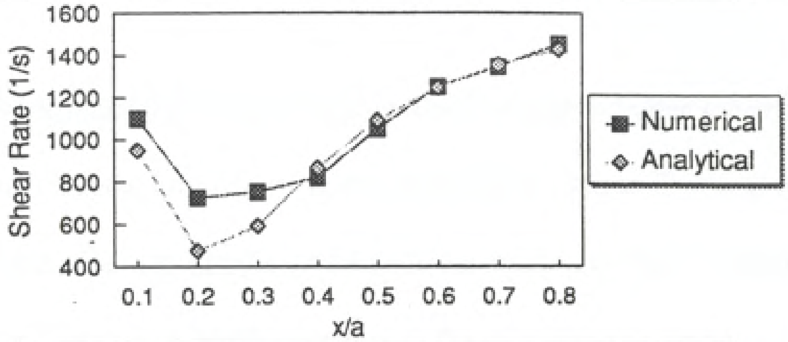


Figure 4.52 : Numerical Differentiation Error
at r/a =0.7

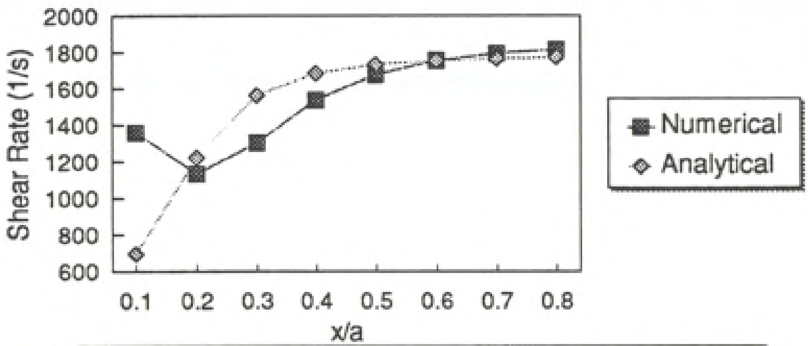


Figure 4.53: Numerical Differentiation Error
at r/a =0.8

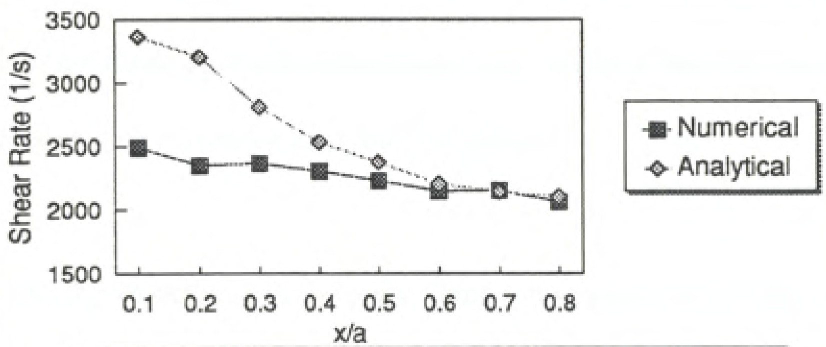


Figure 4.54 : Numerical Differentiation Error
at r/a =0.9

tricky. As the FIDAP results show a velocity which is slightly different, the shear rate can be expected to vary as is observed.

Thus it can be expected that though the program should use a better scheme to carry out the shear rate calculations than the crude finite difference scheme used to illustrate the point, a slight deviation in velocity would lead to a larger deviation in the shear rate. This would further emphasize the point that since the shear rate is highly sensitive to the velocity field, approximations regarding the velocity field could drastically affect the shear rates obtained. Thus it is suggested that models based on break rate of solder paste use the best available velocity field. In particular, use of a different geometry for solving the problem is not recommended.

## 4.5 Conclusions

A number of important conclusions can be drawn from the above observations, both regarding the validity of a model of paste printing based on steady state uniform entry of a Newtonian fluid into a circular aperture, and regarding the ability of the finite element solution to predict results for cases with no known analytical solutions.

It is seen that the velocity plots show excellent convergence for FIDAP, as also accuracy relative to the analytical solution. The velocity field in the entrance region has a large radial component of velocity, and no indication of a boundary layer. Thus, the radial component cannot be ignored in the entrance region. It would seem safe to use finite elements in the form used here in order to determine velocities in other cases, especially if the velocity field is not overly complicated.

The strain rate fields, being obtained by differentiation of the velocity fields, are extremely sensitive to the latter. Thus any geometric approximation, which implies different velocity distribution, is not recommended for evaluation of shear rates in fluid flows. Numerical differentiation can lead to gross errors, and as can be observed, convergence of a numerical solution, by taking more substeps, or a higher mesh density, is no guarantee of the accuracy of the solution.

It is further seen that even though the shear strain rate curves do not match in value for FIDAP and the analytical solution, both consistently predict a much higher strain rate than the break strain rate for solder paste. Thus, it would not be possible to delineate a substantial volume of the paste below the break stress limit.

Finally, the stress rates obtained using creep flow approximations would still seem to be distinctly higher than the inviscid core predicted by the boundary layer theory. As the boundary layer model does seem to give some results in agreement with the experiments, it is worthwhile to study the huge difference in the shear rates predicted. A satisfactory resolution can be obtained if it is noted that the core in the boundary layer model is not actually inviscid. Even though the velocity is assumed to be solely axial, an approximation which would seem to violate continuity, but could still be a valid approximation, the velocity is a function of the axial distance (x) from the inlet. In such a case, the general strain rate matrix would have non-zero components, as also non-zero eigenvalues.

A simple MAPLE program for including the effect of the variation in the axial velocity with axial distance downstream of the inlet shows that even the boundary layer model would give shear strain rates higher than the breaking rate all over the volume. The results from these calculations have not been presented here.

# CHAPTER 5

# FINITE ELEMENT ANALYSIS FOR FLOW THROUGH RECTANGULAR SLOTS

Rectangular apertures are among the more popular geometries used in solder paste printing. Entry flow of a highly viscous fluid at conditions of very low Reynold's number for rectangular apertures would therefore be of interest. As it is not feasible to carry out an analytical solution for this problem, a finite element model is created to determine the velocities and strain rates in the region. The methodology applied to the analysis of flow through a circular aperture is extended to the rectangular aperture. A FIDAP program is written for the case and is executed. The results obtained are discussed. Dimensions used are the same as used for sample calculations in the previous model (Sahay et. al., 1995), so as to facilitate direct comparison of results.

## 5.1 Problem Definition

The aim is to study the entry flow of fluid into a rectangular aperture for the conditions noted below. The inlet of the aperture is a rectangle $2.032 \times 10^{-4}$ m long and $1.016 \times 10^{-3}$ m wide, while the depth is $1.524 \times 10^{-4}$ m. At the inlet, the normal component of the velocity is .203 m/s, and the transverse component is zero (Fig. 5.1). The fluid has a density of 5500 kg/m$^3$ and a viscosity of 1000 Ns/m$^2$ . As in the previous chapters, although the numbers are unwieldy, they are reported exactly as input into the code, so as to assure repeatability. The output from the code has been found to be sensitive to the actual numerical values input.

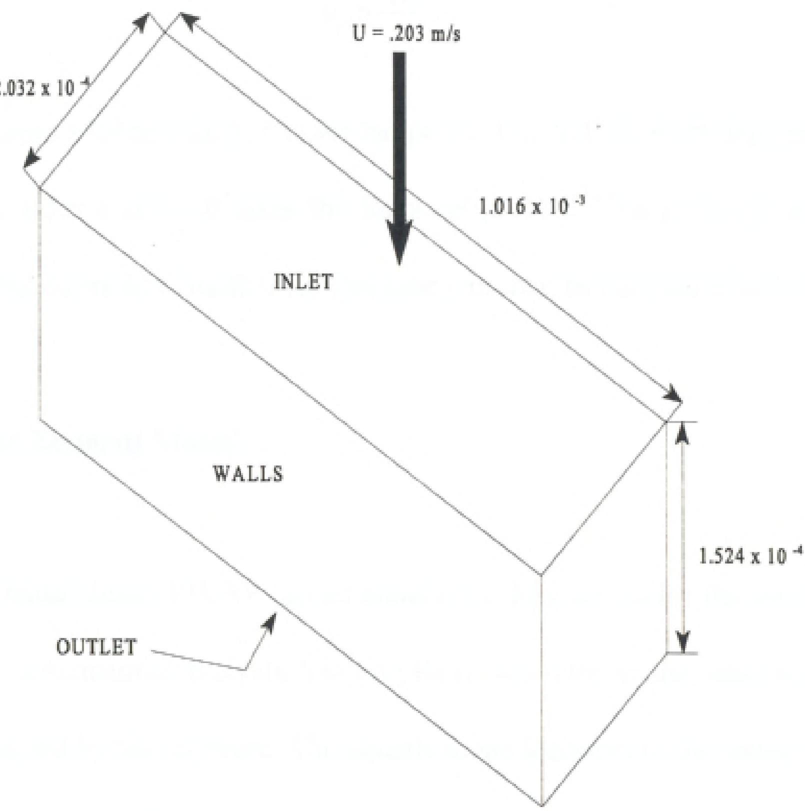


Figure 5.1 : Schematic of flow for Rectangular Apertures

The Reynolds number for the flow is calculated based on the concept of equivalent hydraulic diameter, which is defined as

$$D_h = \frac{4A}{P} \qquad (5.1)$$

where A is the cross sectional area, P is wetted perimeter, and $D_h$ is the equivalent diameter. For a rectangle with sides a and b it takes the form $2ab(a+b)^{-1}$. This gives the equivalent radius as .00016891 m. The Reynold's number for this case can then be calculated to be Re = $3.77 \times 10^{-4}$

## 5.2 Finite Element Model

As for circular ducts, FIDAP cannot handle the dimensions for this problem. So the model is scaled using dimensional analysis, keeping Reynolds number the same and using parameters which can be handled by the software. The equations are identical to the ones obtained for circular ducts, with the exception that one more parameter, another ratio of lengths, is formed. This is because there are three length dimensions in the rectangular case as opposed to two in the cylindrical case, and so two ratios need to be kept constant to ensure geometric similarity.

After taking into consideration the problems of maintaining dynamic similarity, while using numbers that FIDAP can handle, the best results are obtained for an inlet which is 2.032 m long, 10.16 m wide, with a corresponding slot depth of 1.524 m. The inlet velocity has a normal component of .203 m/s, while the transverse component is zero. The fluid density for the case is

.0000000055 kg/m$^3$ and the viscosity .0001 Ns/m$^2$. The Reynolds number is maintained at 3.77 x 10$^{-4}$. This is accordance with observations for the circular case, where the geometric dimensions have to be of the order unity in order to obtain accurate solutions. The fluid density is not expected to play a major role in the determination of the velocity or strain rate fields for the given Reynolds number, and hence its order of magnitude is not of prime importance.

The case still has some pivots which are replaced by 10$^{-7}$ as they are smaller than that, but the number is not large enough relative to the total number of nodes to expect problems with the solution. Since the ratio of lengths in this case is 1/10000, the corresponding break shear rate using Eq. 4.13 would be 2.5 x 10$^{-3}$/s.

## 5.3 FIDAP Program

A copy of the program is attached (Appendix III). The parameters varied were fluid parameters within the constraint of dynamic similarity, so as to get the best possible solution, i.e. one where the least number of pivots have to be replaced during solution.

### 5.3.1 Meshing

The problem is a three dimensional one, and so one of the governing constraints for meshing would be system limitations. Mesh density was increased till the system ran out of memory. Results from lower mesh densities indicate an acceptable level of convergence. Since unlike the two dimensional case, paving is not an option for three dimensional cases, only a mapped mesh is feasible. The highest mesh density used is shown in Fig 5.2.

### 5.3.2 Boundary Conditions

At the inlet, the normal velocity component is .203 m/s, while the transverse component is zero. At the walls, all velocity components are zero.

## 5.4 Solution

As for a circular duct, the case is studied for steady state laminar flow of an incompressible Newtonian fluid, with mixed pressure approach

## 5.5 Results.

Figs. 5.3 to 5.38 give the velocity distributions on various sections, while Figs. 5.39 - 5.75 give the shear rate distributions on selected surfaces and sections. In the plots, the inlet is at the top surface. Three kinds of sections are taken, namely "short sections", which are parallel to the shorter walls, "long sections" which are parallel to the longer walls, and "downstream sections" which are parallel to the inlet and give an indication of the flow conditions at various planes downstream. Due to the three dimensional nature of the problem, the amount of data is extremely large, and is presented here in this form for reference. It would not be practical to go into each plot in detail, and hence the general trends observed are discussed, keeping in mind the prime objectives of the work, viz. determination of the shear strain rates, and whether a feasible model could be created based on the same for paste release. Assumptions to be tested are modeling the process as a steady state incompressible Newtonian flow, and the approximation of the rectangular geometry by a circular one.

In this case, of course, there are no analytical solutions or experimental results available for direct comparison, and thus internal consistency in the form of continuity being satisfied by the velocity field, and relatively low number of pivots being replaced serve as guidelines as to the correctness of the solution.

### 5.5.1 Velocity

Figure 5.3, the velocity vector plot for a short section at the center shows the presence of substantial transverse components near the inlet. Figures 5.4-5.12 for the long sections show a similar trend. The velocity pattern can be seen to be different from the circular case. Figures 5.13-5.38 for the downstream sections show that the velocity shows a significant transverse component nearly all across the slot for some distance downstream, but then settles down quite soon. The arrows would not give a direct quantitative estimate as the visible length depends on the angle of view. The view chosen is for overall clarity.

FIGURE 5.2: MESH PLOT

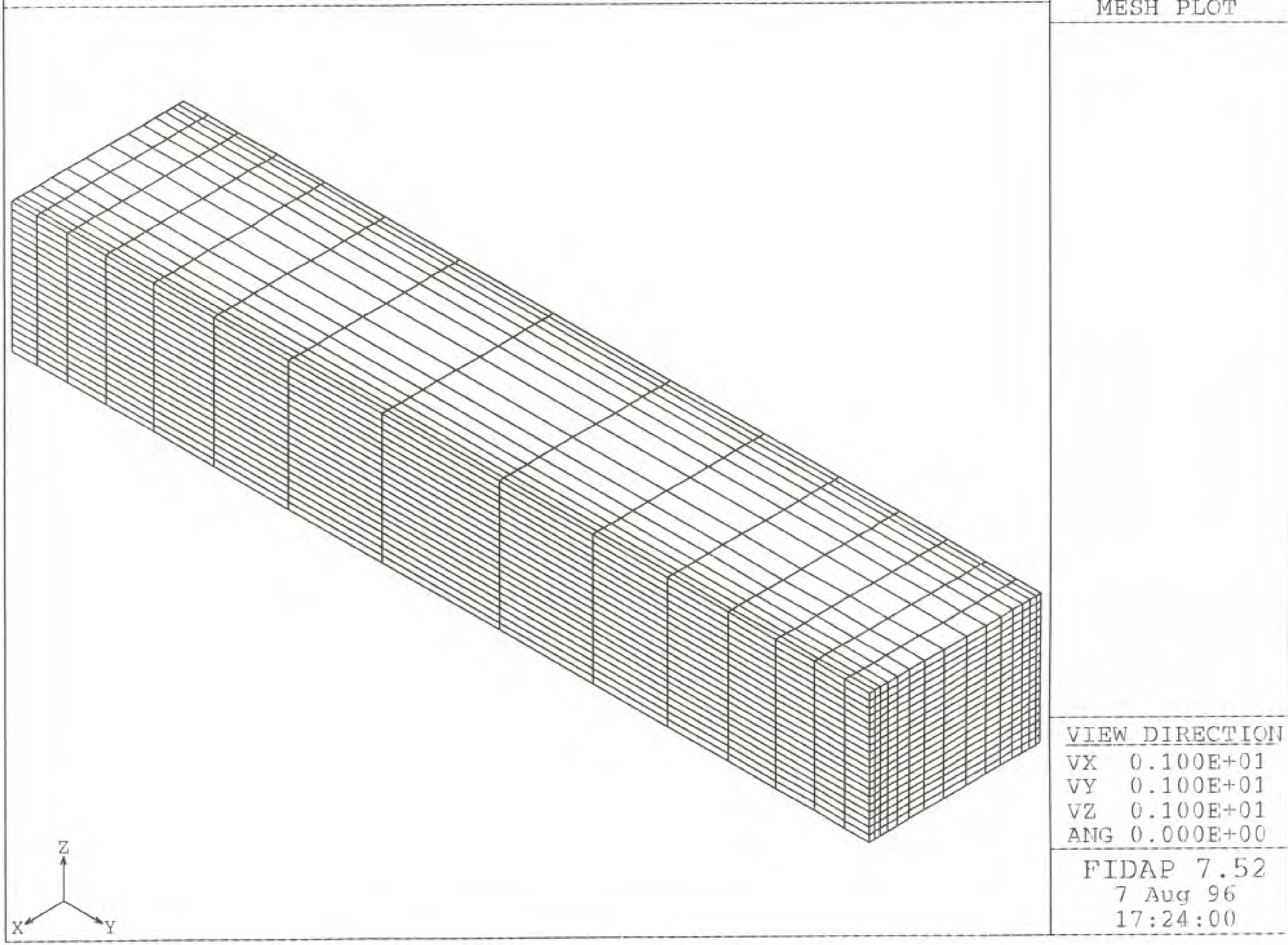

FIGURE 5.3: VELOCITY PLOT, SHORT SECTION

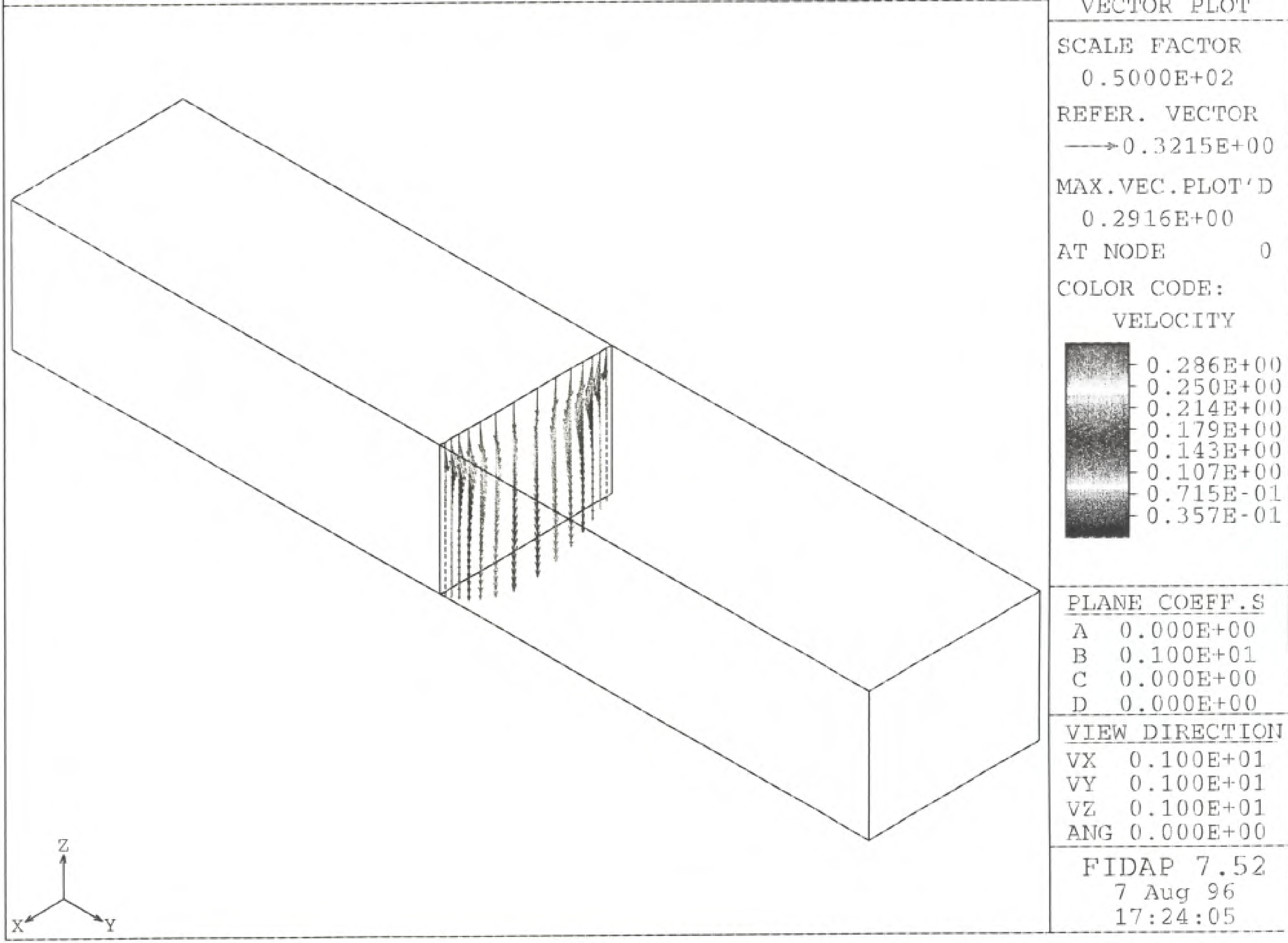

FIGURE 5.4: VELOCITY PLOT, LONG SECTION 1

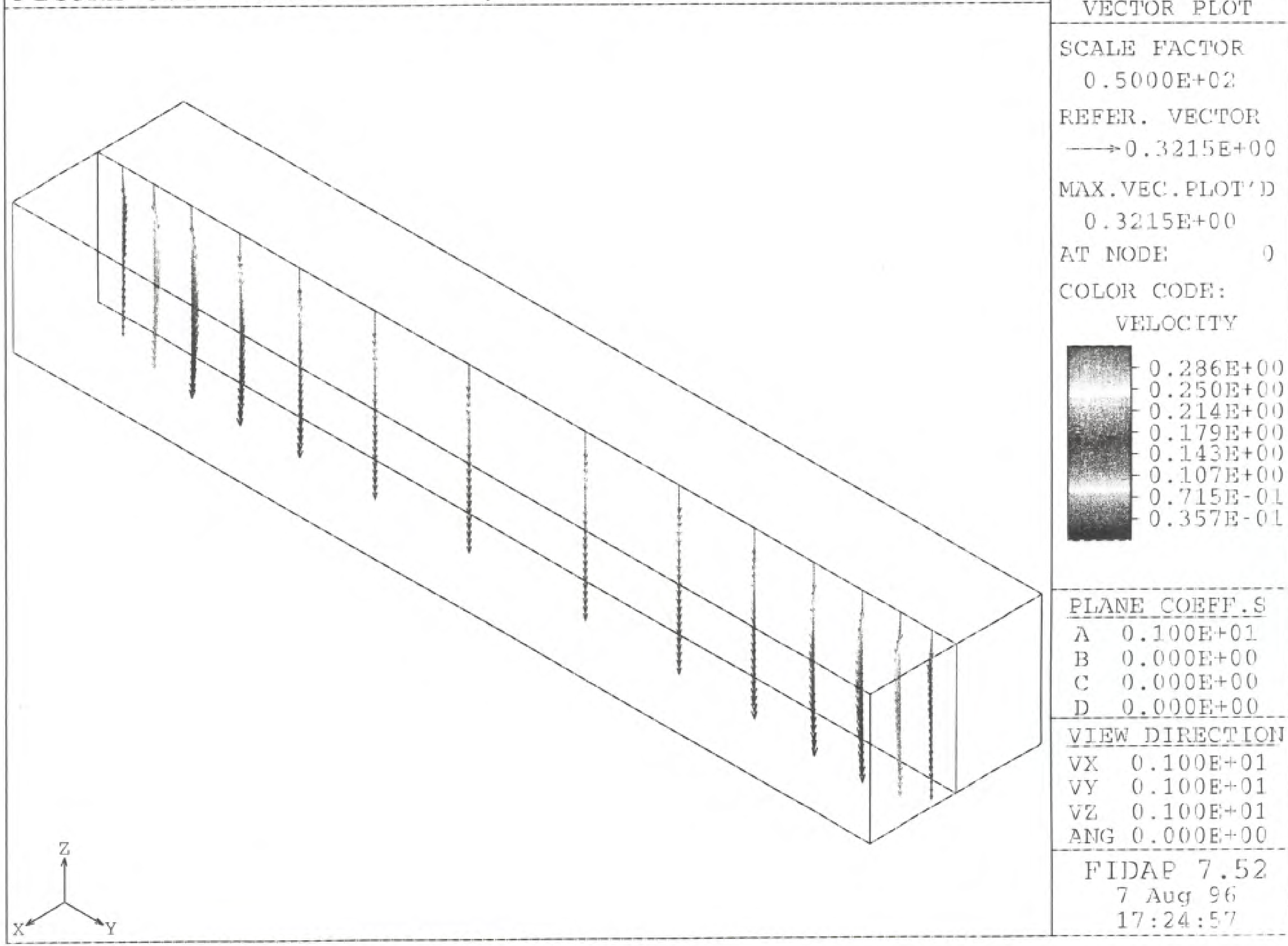

FIGURE 5.5: VELOCITY PLOT, LONG SECTION 2

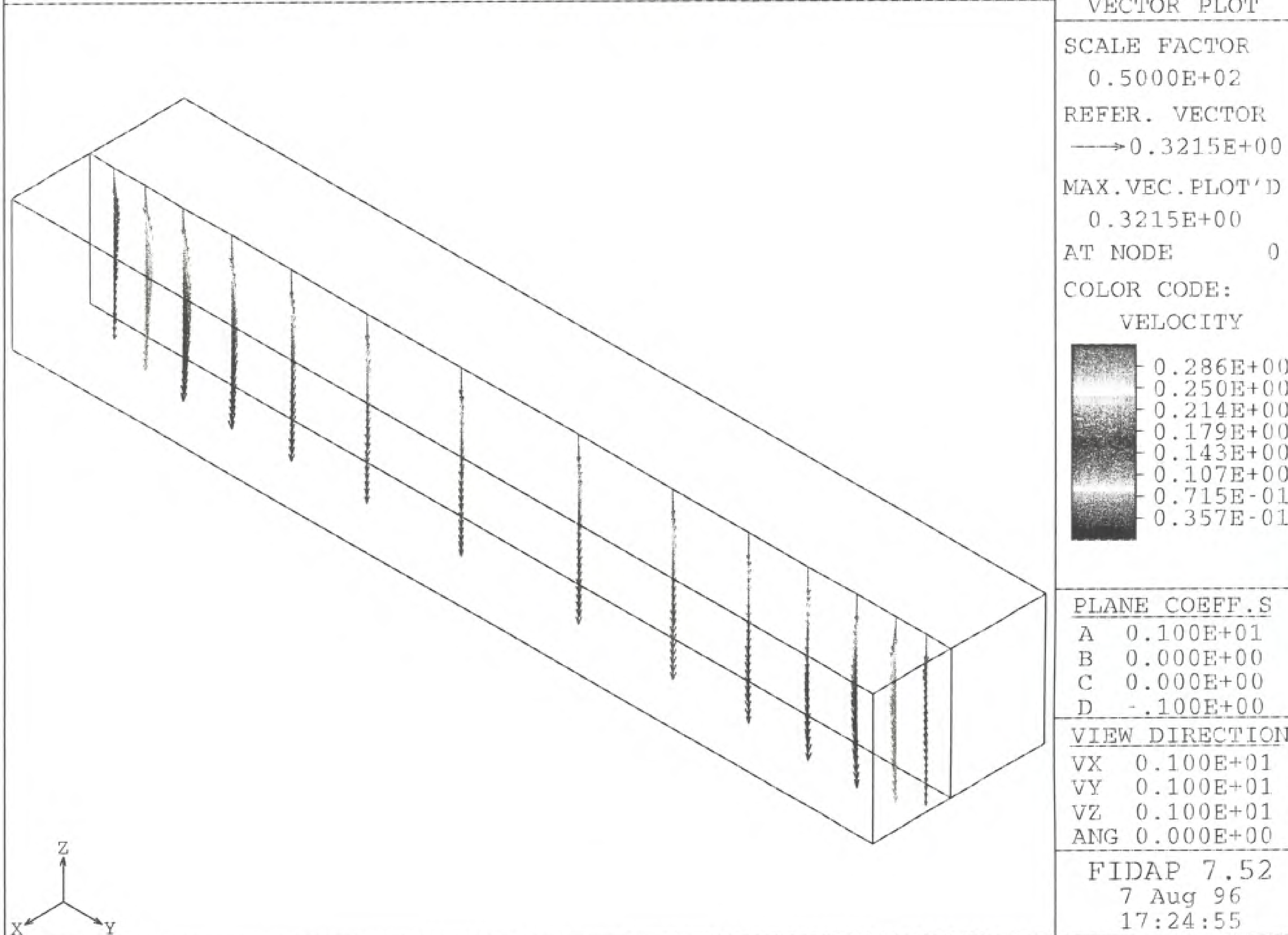

FIGURE 5.6: VELOCITY PLOT, LONG SECTION 3

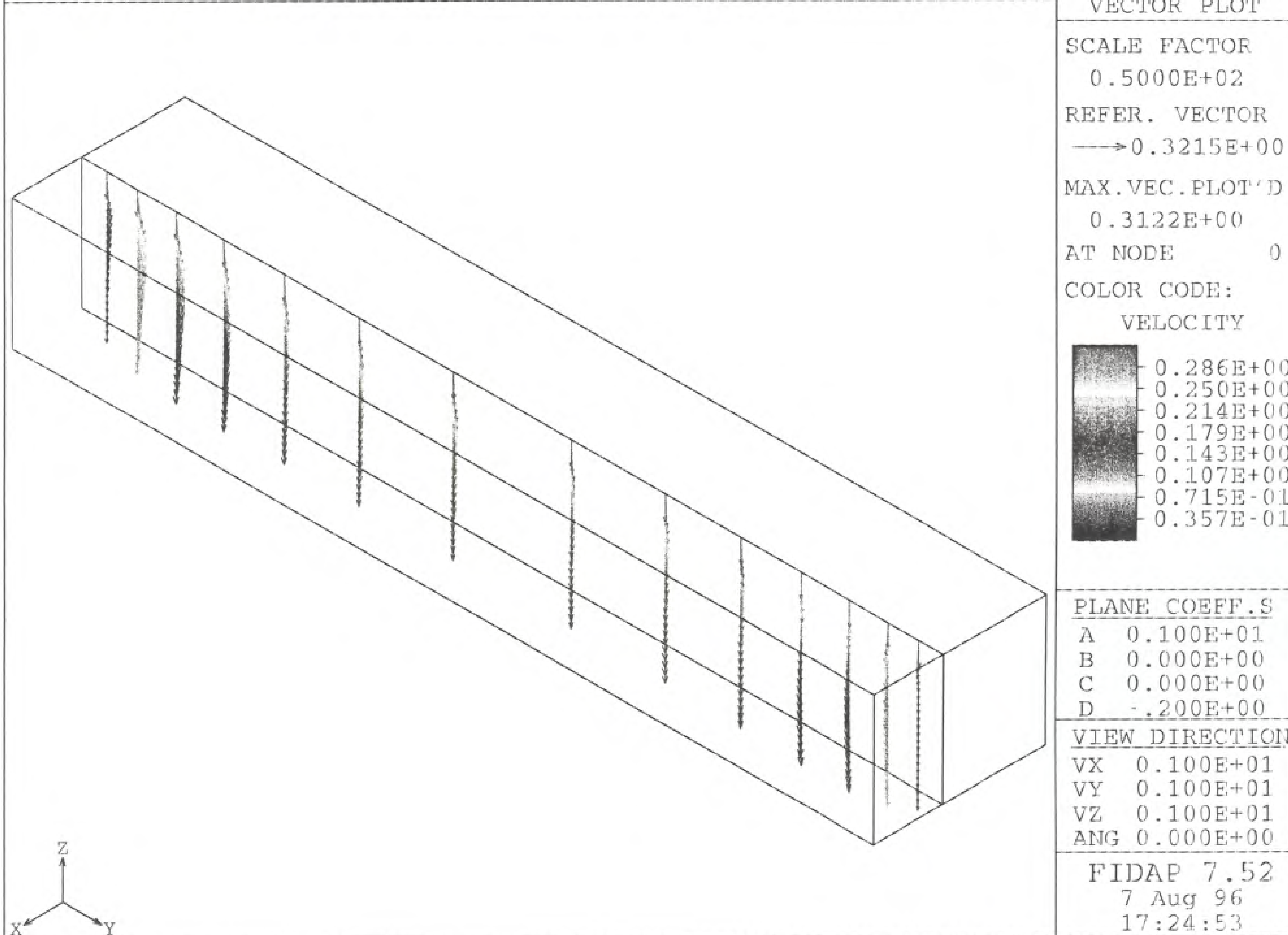

FIGURE 5.7: VELOCITY PLOT, LONG SECTION 4

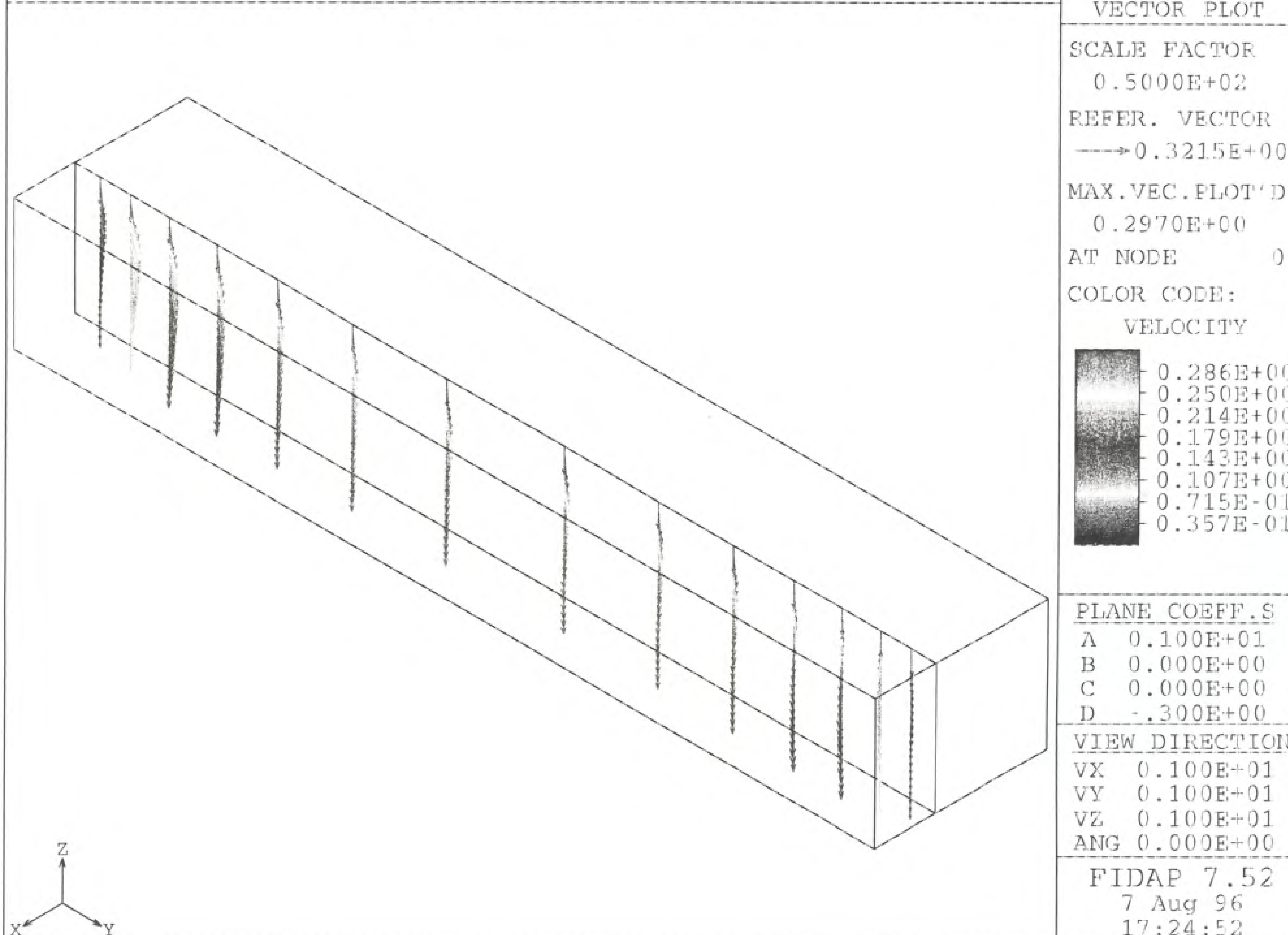

FIGURE 5.8: VELOCITY PLOT, LONG SECTION 5

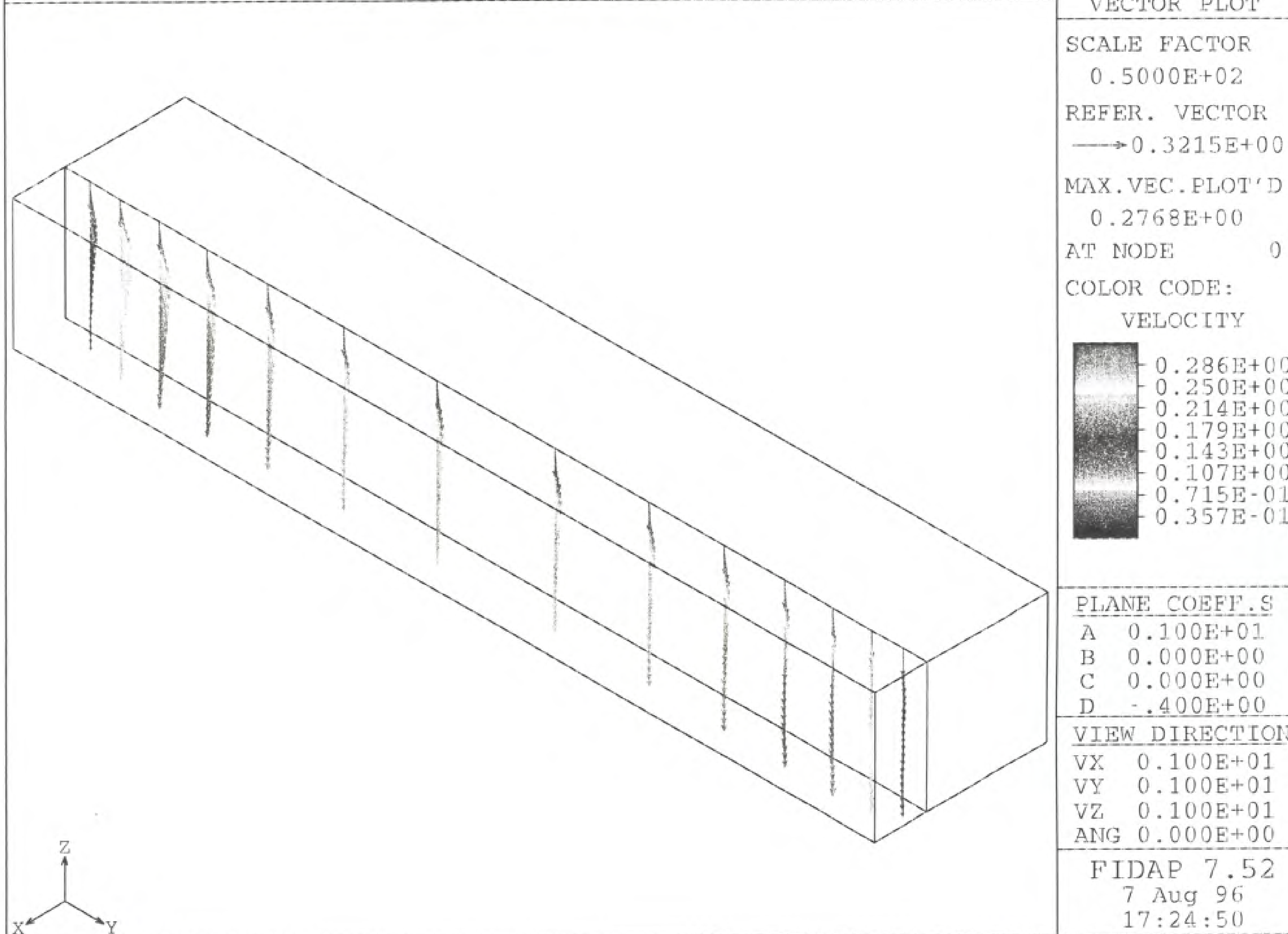

FIGURE 5.9: VELOCITY PLOT, LONG SECTION 6

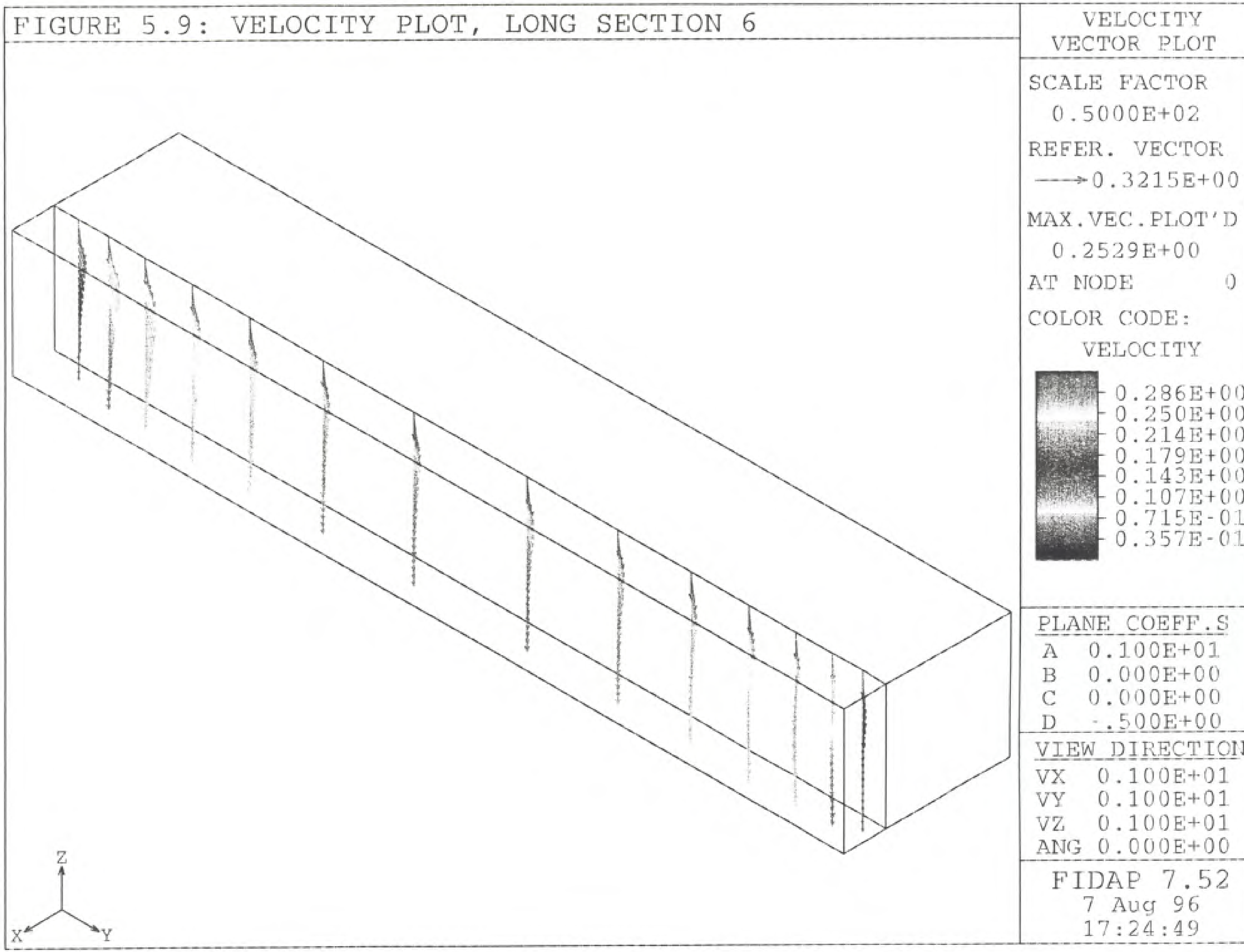

FIGURE 5.10: VELOCITY PLOT, LONG SECTION 7

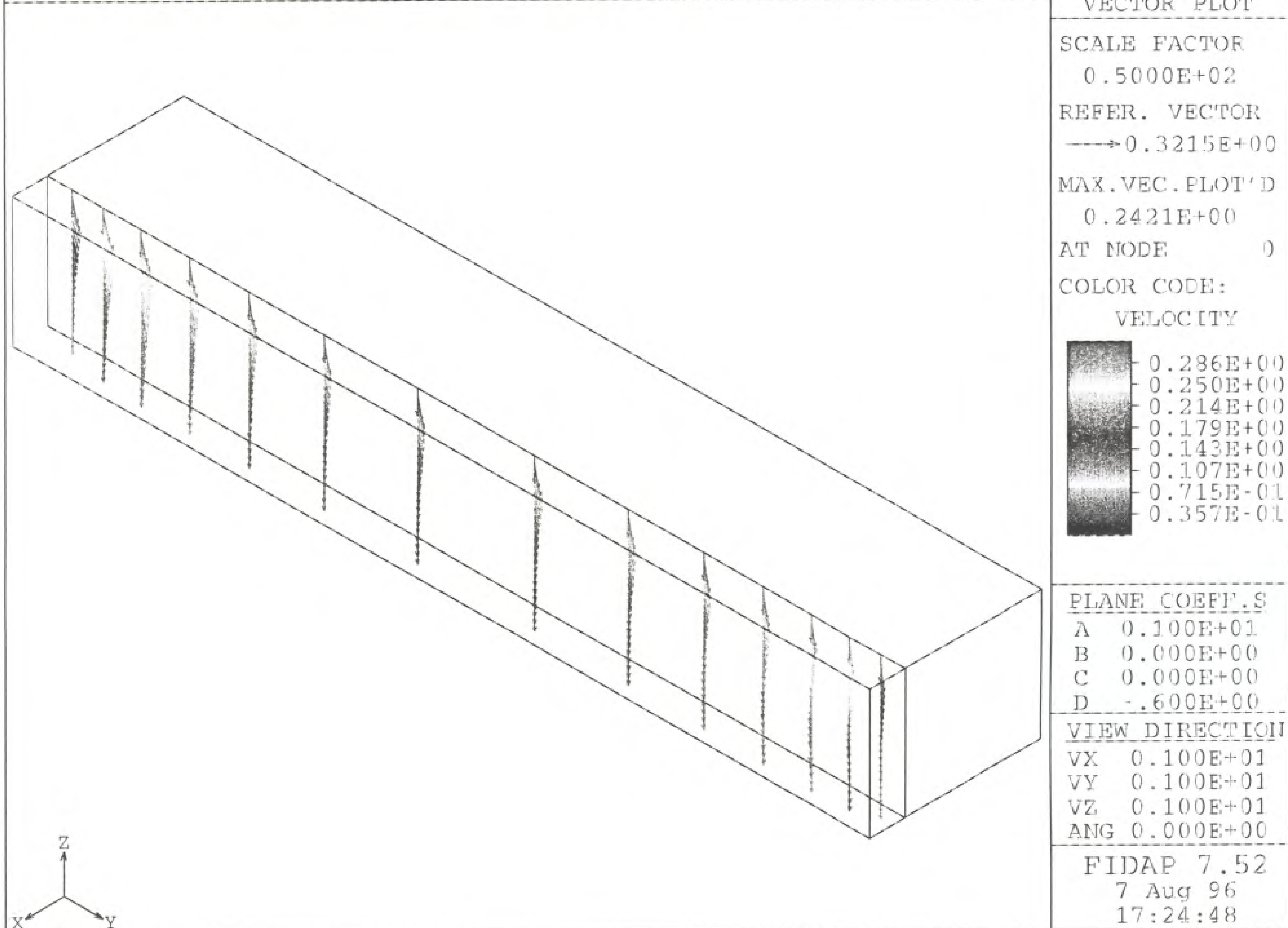

FIGURE 5.11: VELOCITY PLOT, LONG SECTION 8

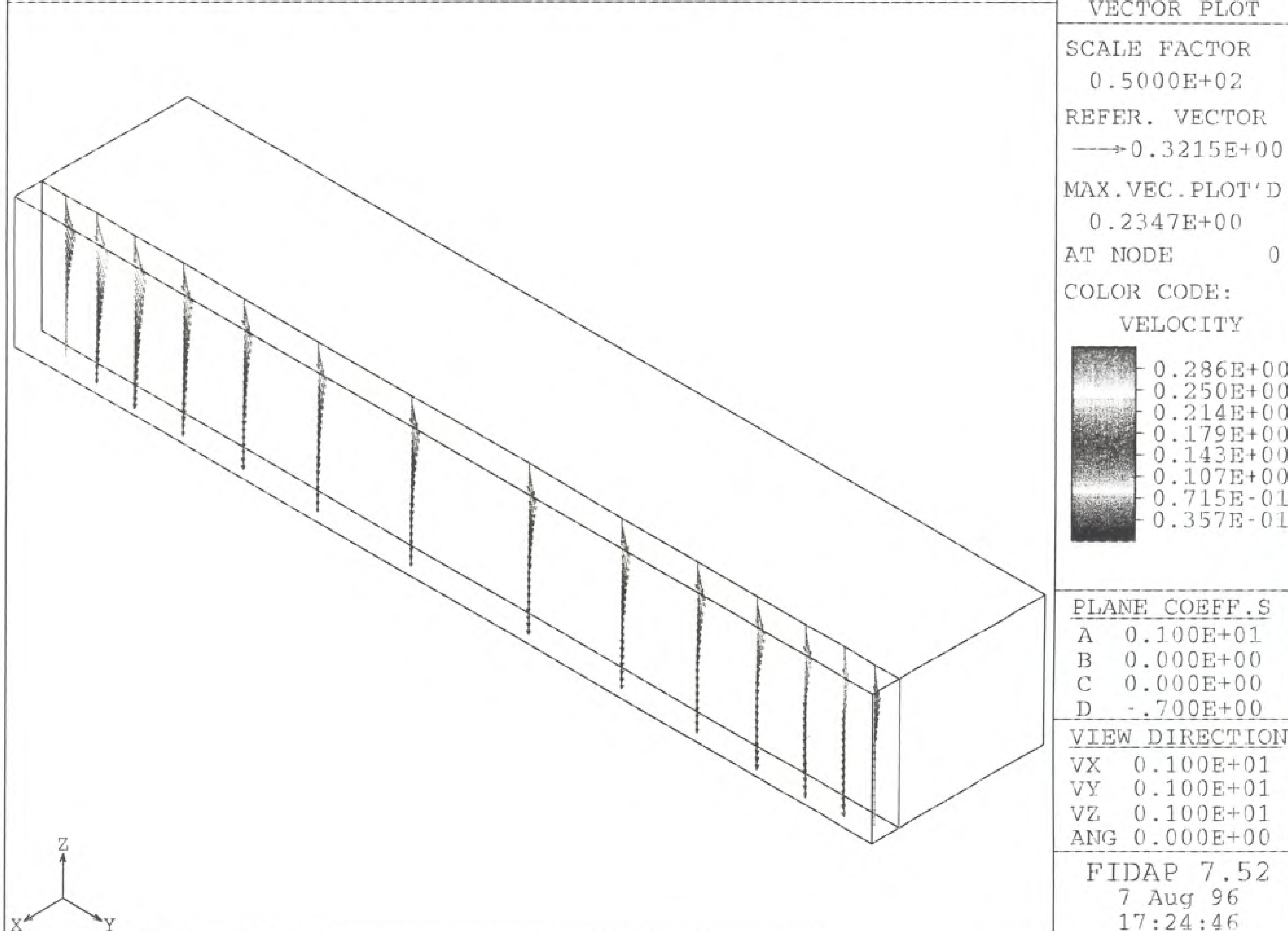

FIGURE 5.12: VELOCITY PLOT, LONG SECTION 9

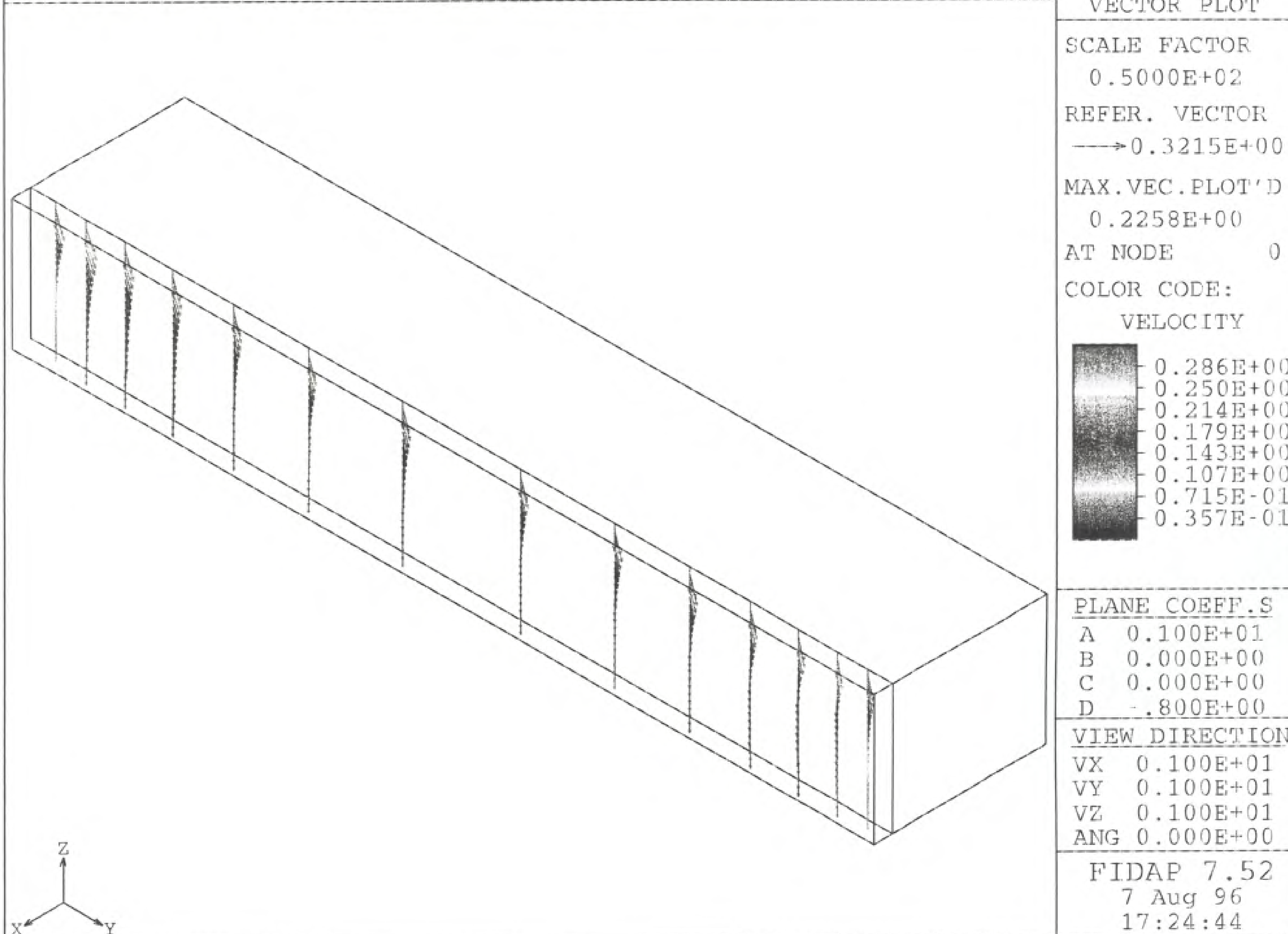

FIGURE 5.13: VELOCITY PLOT, LONG SECTION 10

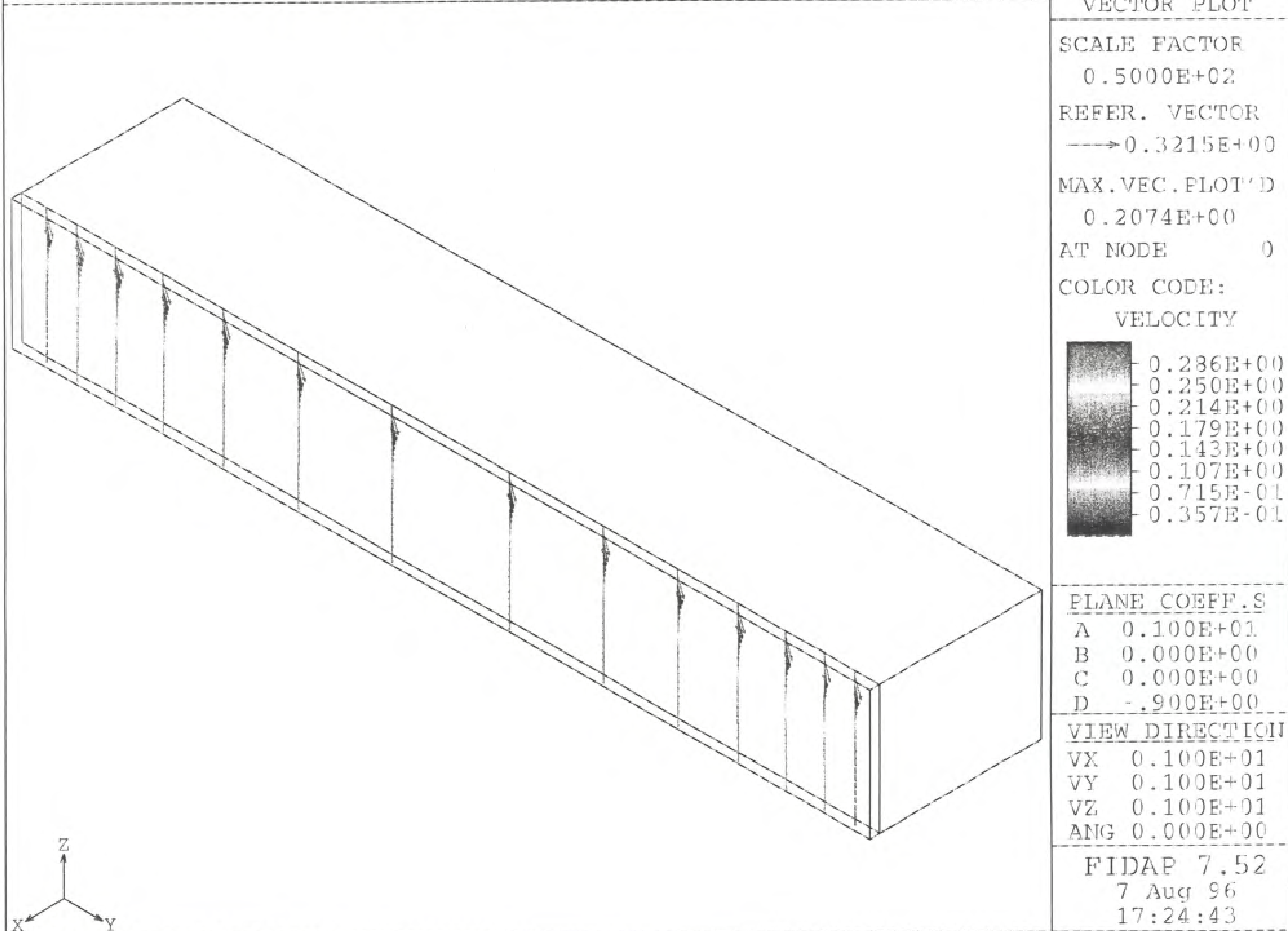

FIGURE 5.14: VELOCITY PLOT, LONG SECTION 11

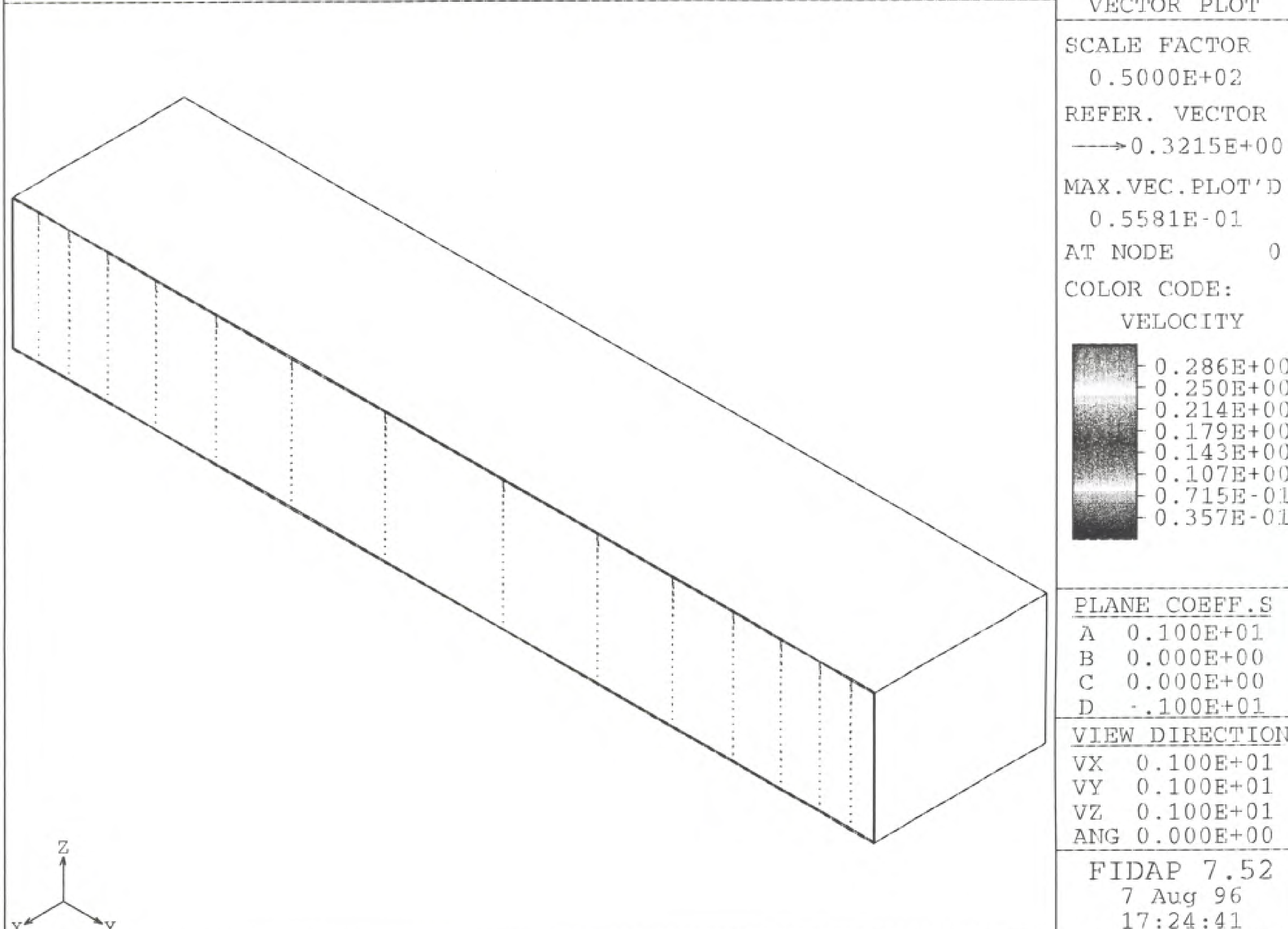

FIGURE 5.15: VELOCITY PLOT, DOWNSTREAM SECTION 1

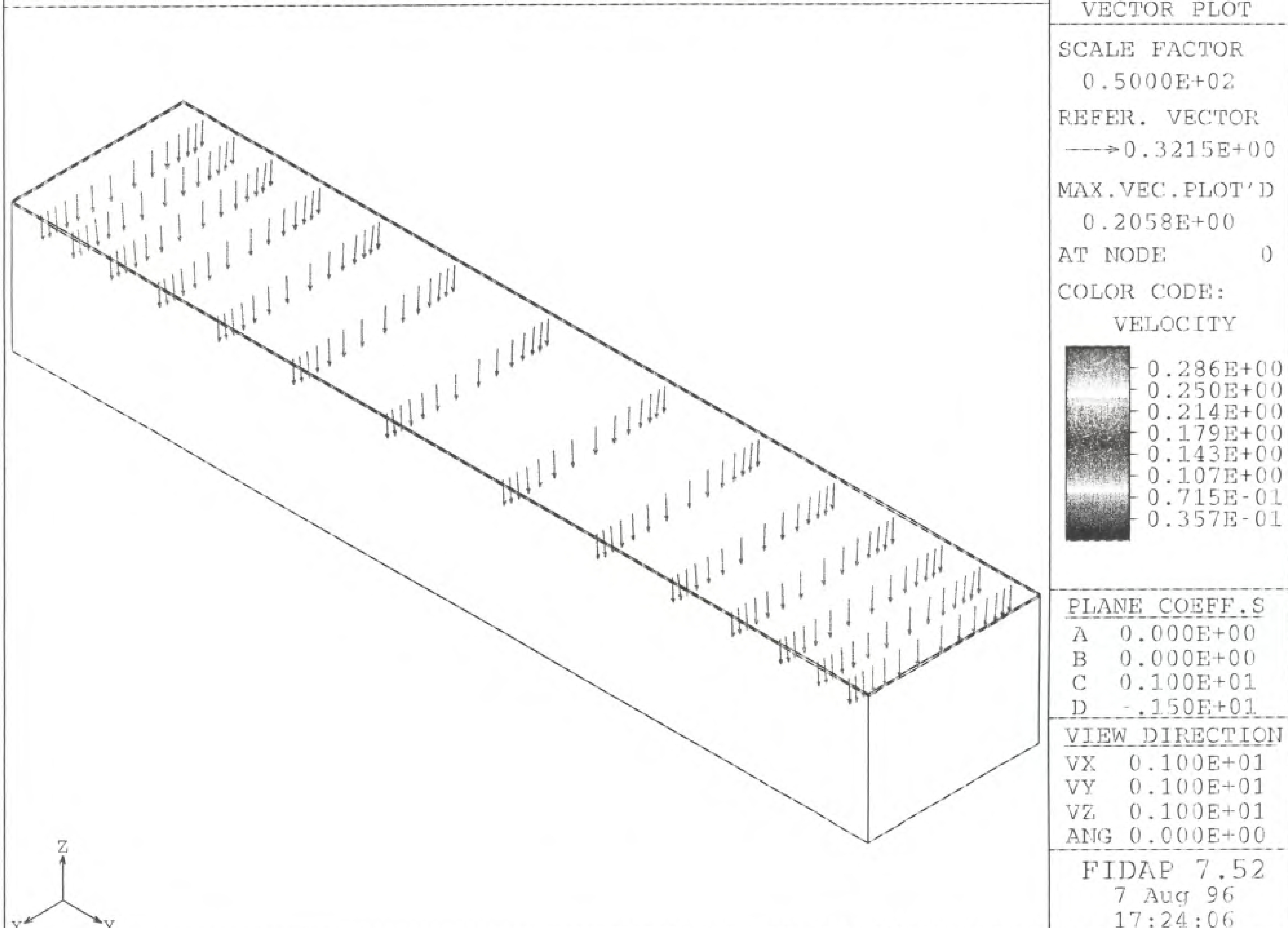

FIGURE 5.16: VELOCITY PLOT, DOWNSTREAM SECTION 2

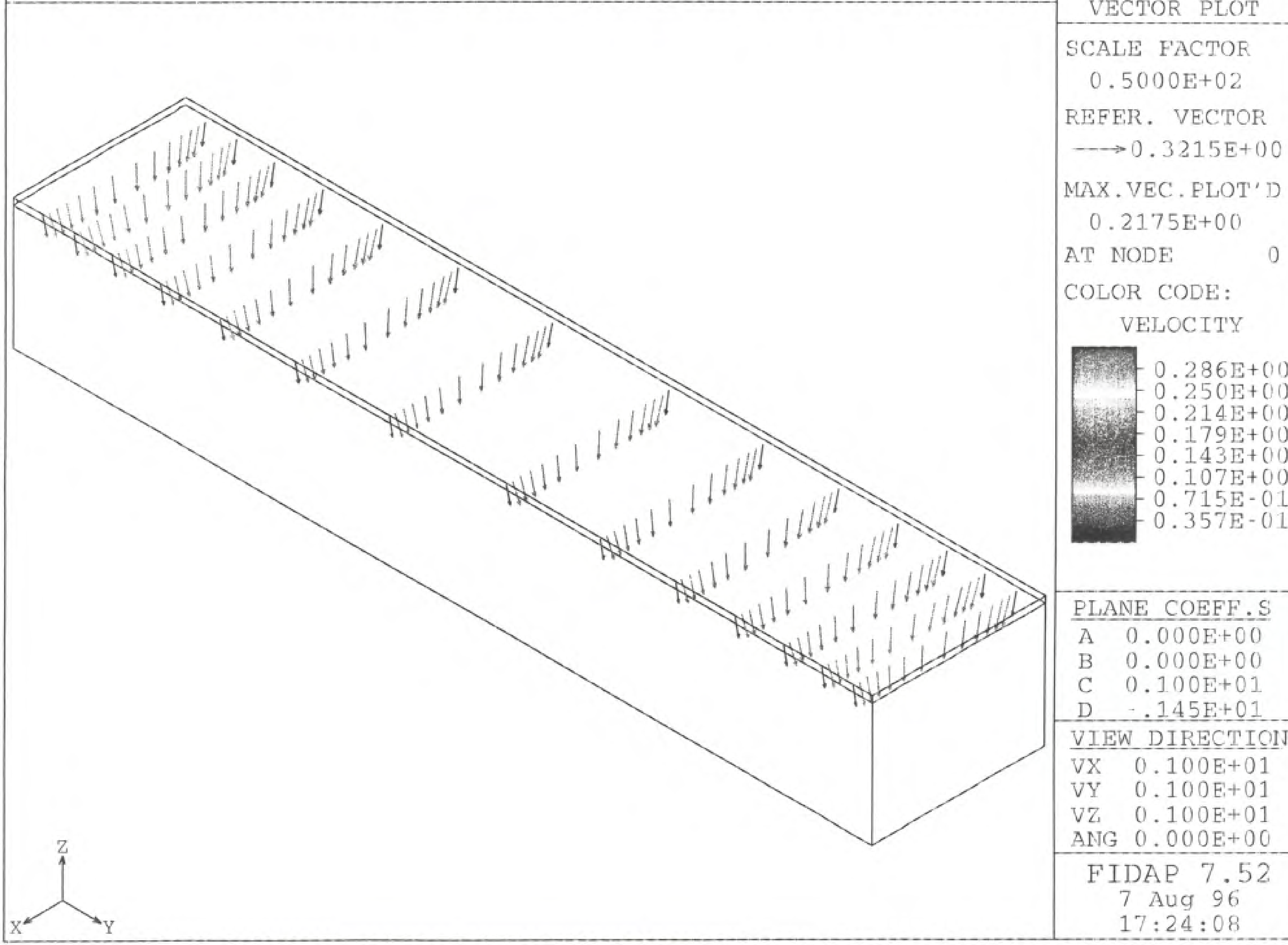

FIGURE 5.17: VELOCITY PLOT, DOWNSTREAM SECTION 3

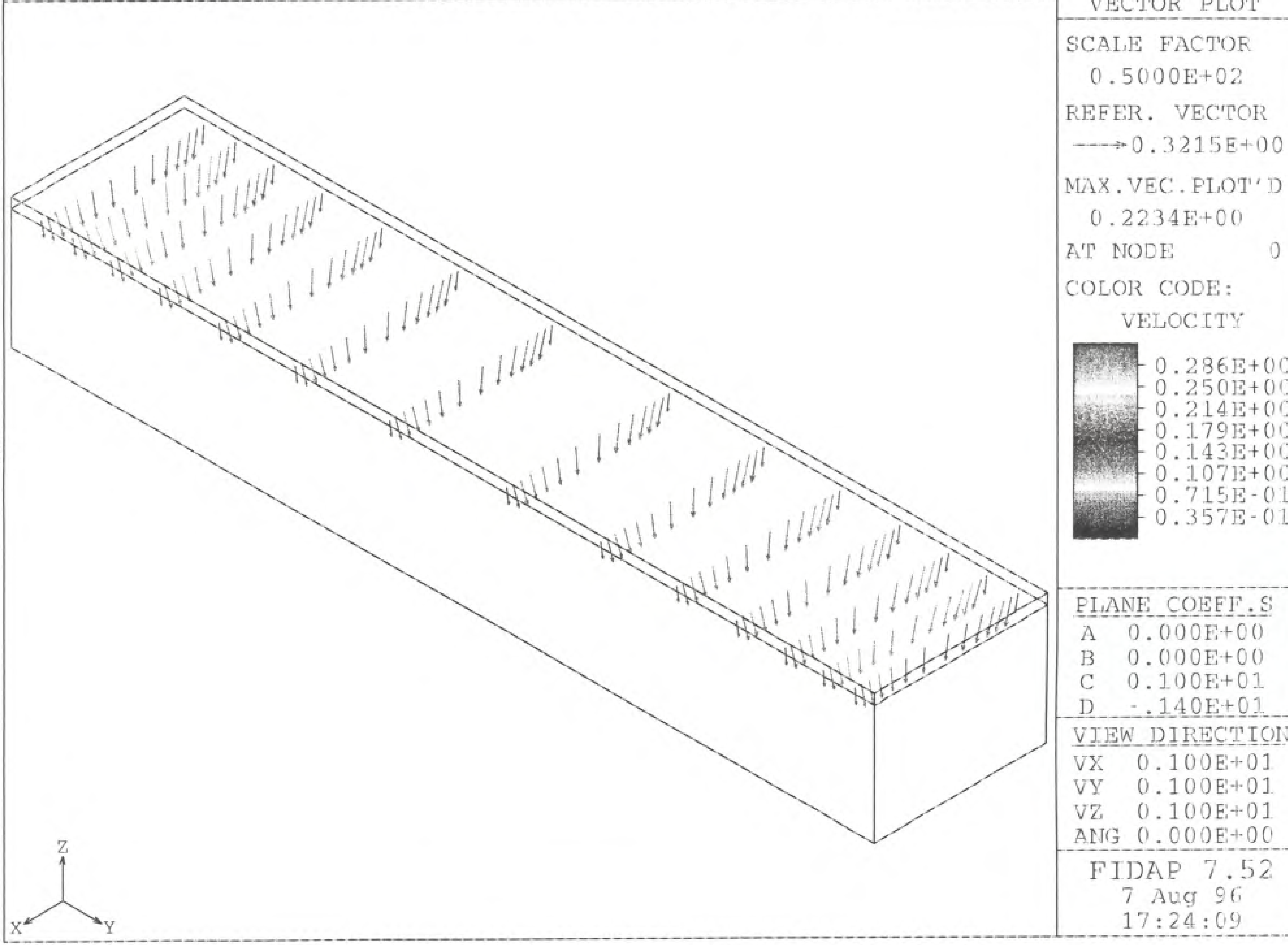

FIGURE 5.18: VELOCITY PLOT, DOWNSTREAM SECTION 4

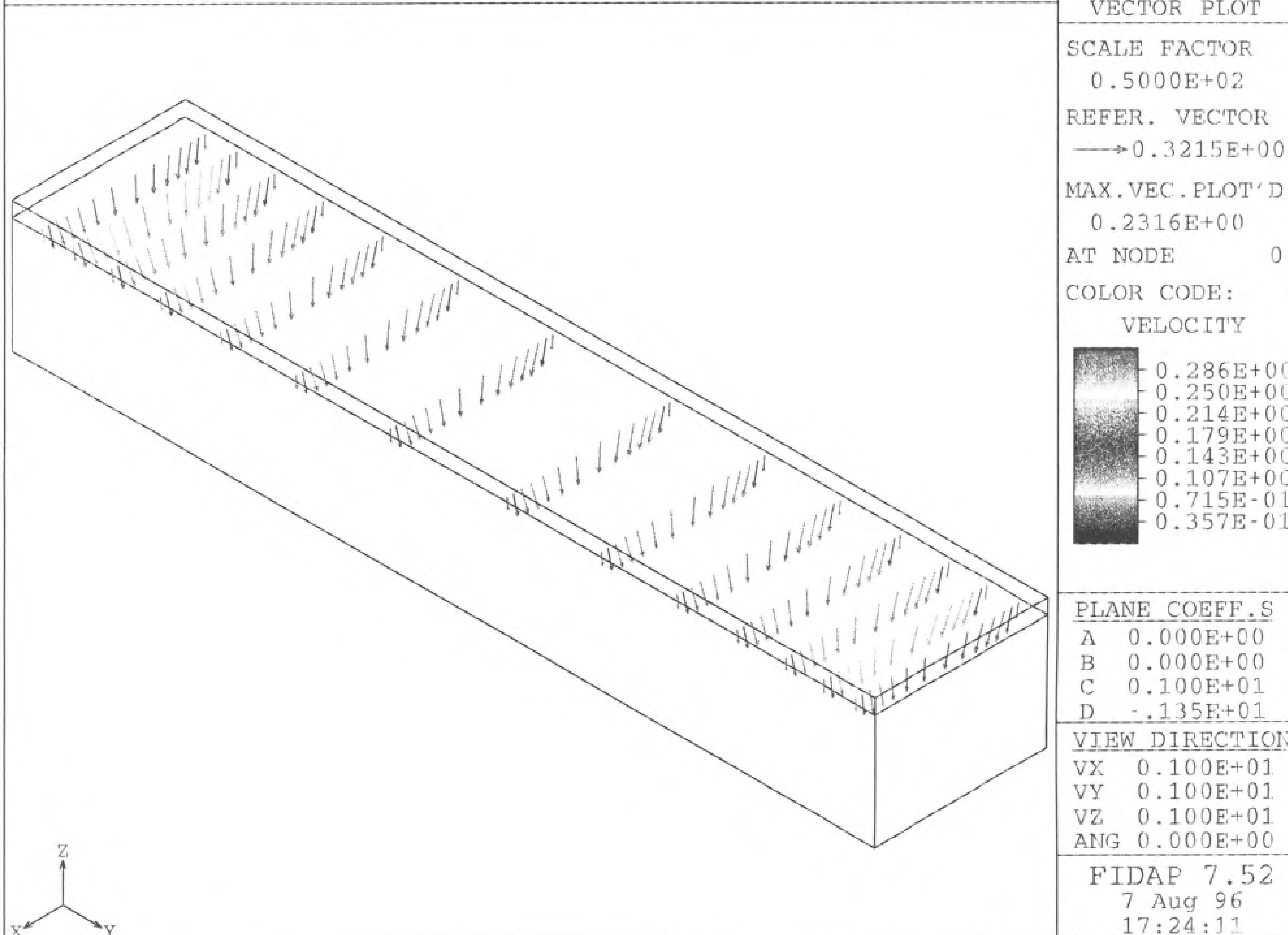

FIGURE 5.19: VELOCITY PLOT, DOWNSTREAM SECTION 5

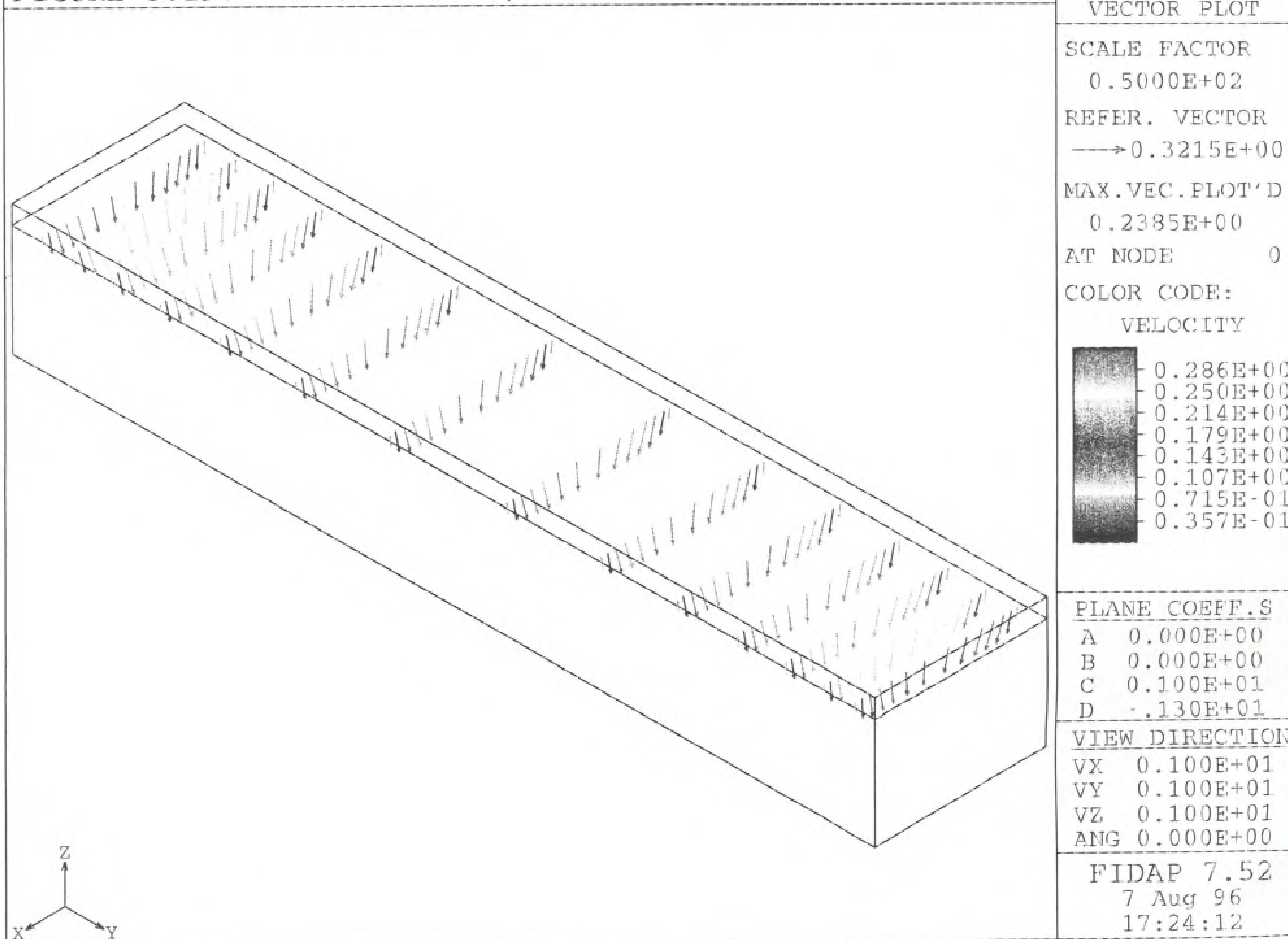

FIGURE 5.20: VELOCITY PLOT, DOWNSTREAM SECTION 6

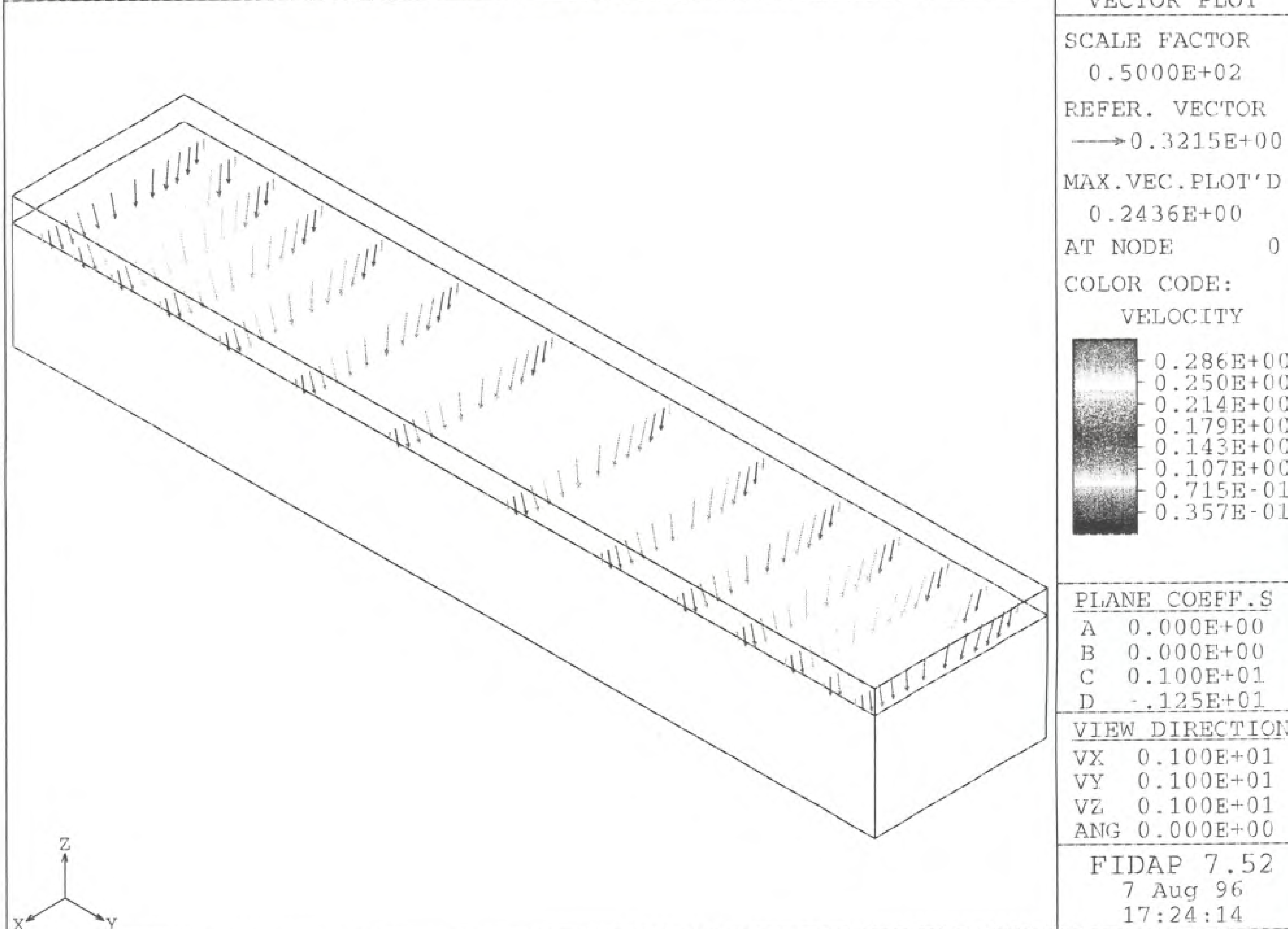

FIGURE 5.21: VELOCITY PLOT, DOWNSTREAM SECTION 7

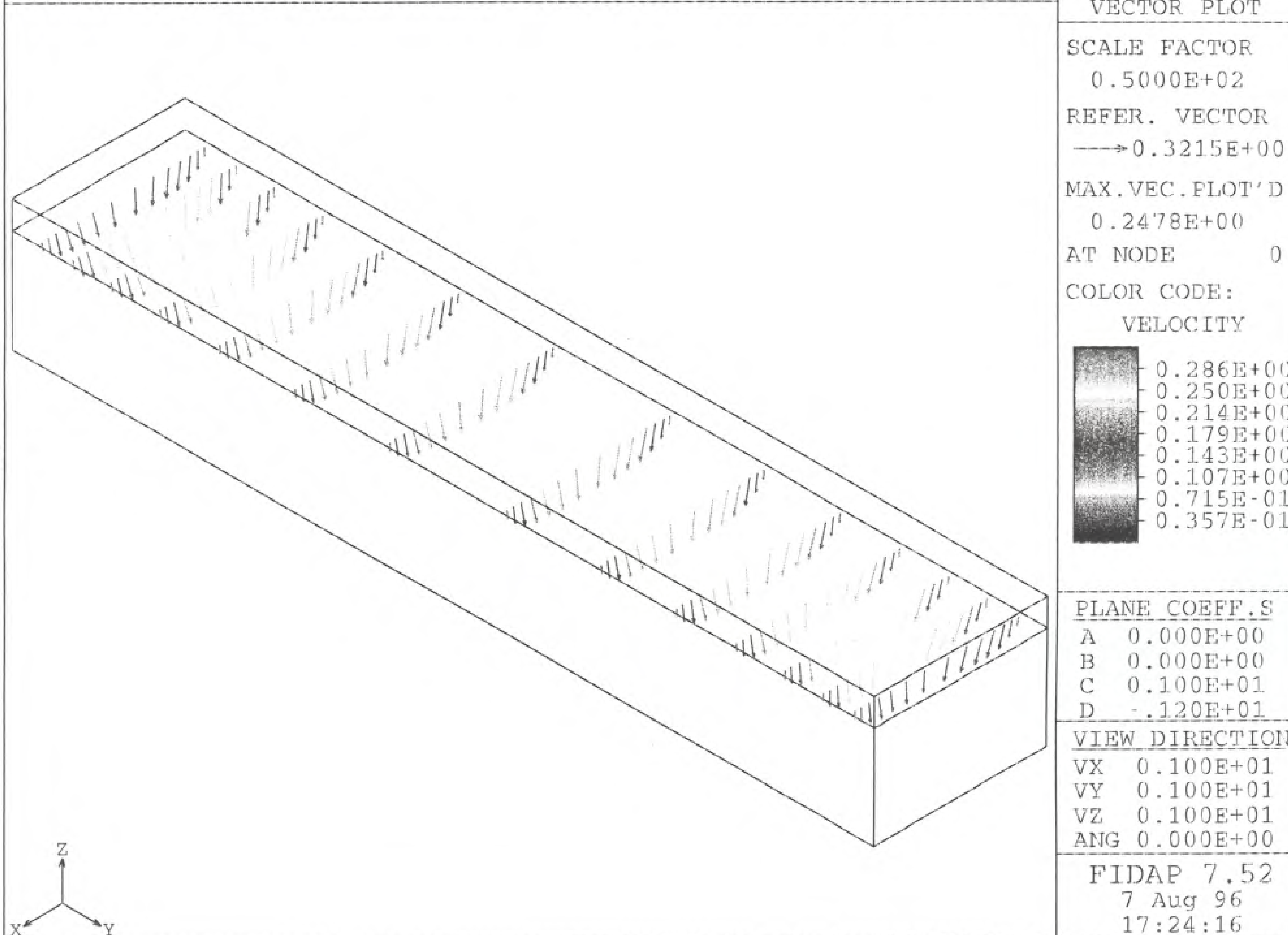

FIGURE 5.22: VELOCITY PLOT, DOWNSTREAM SECTION 8

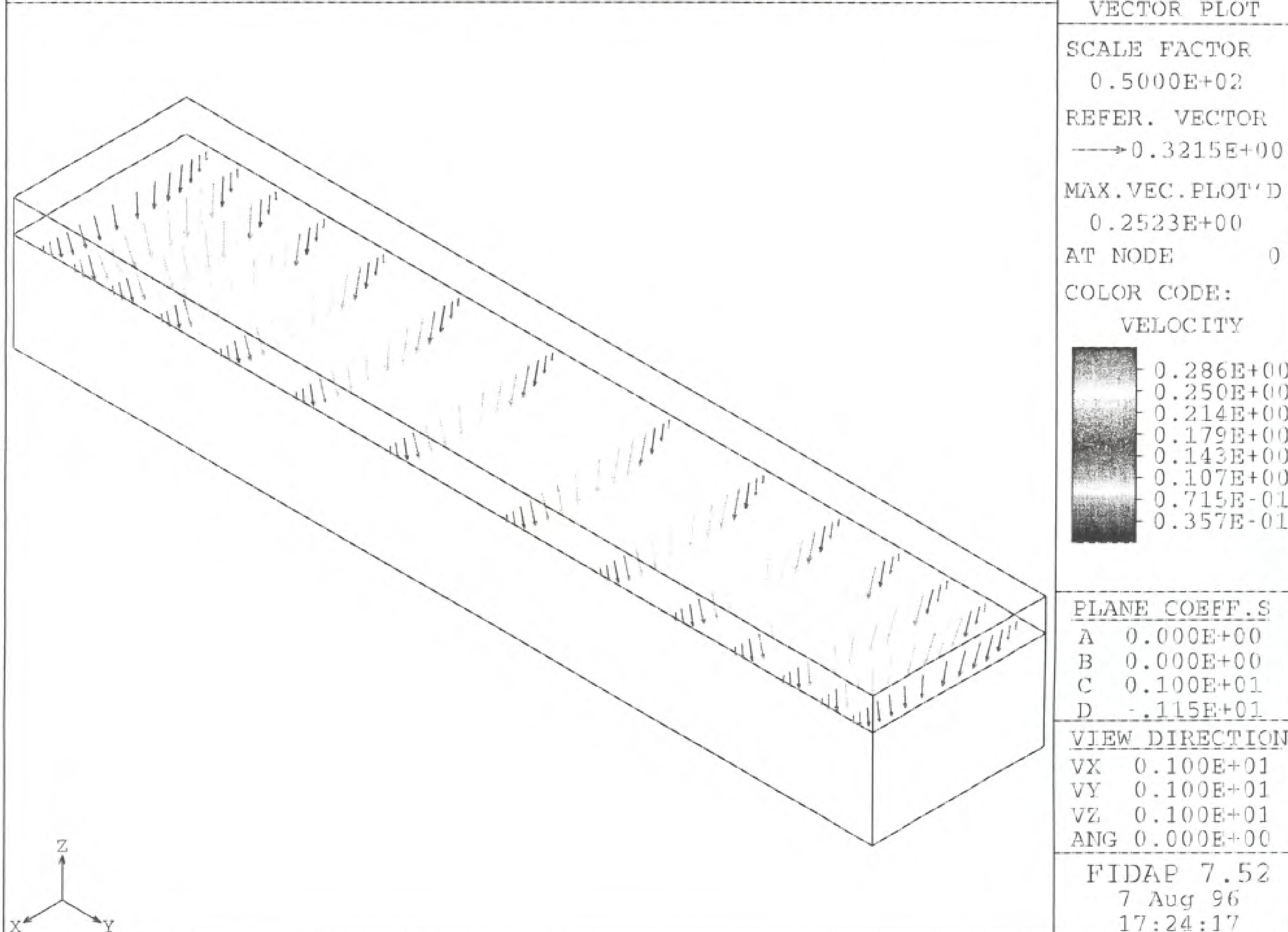

FIGURE 5.23: VELOCITY PLOT, DOWNSTREAM SECTION 9

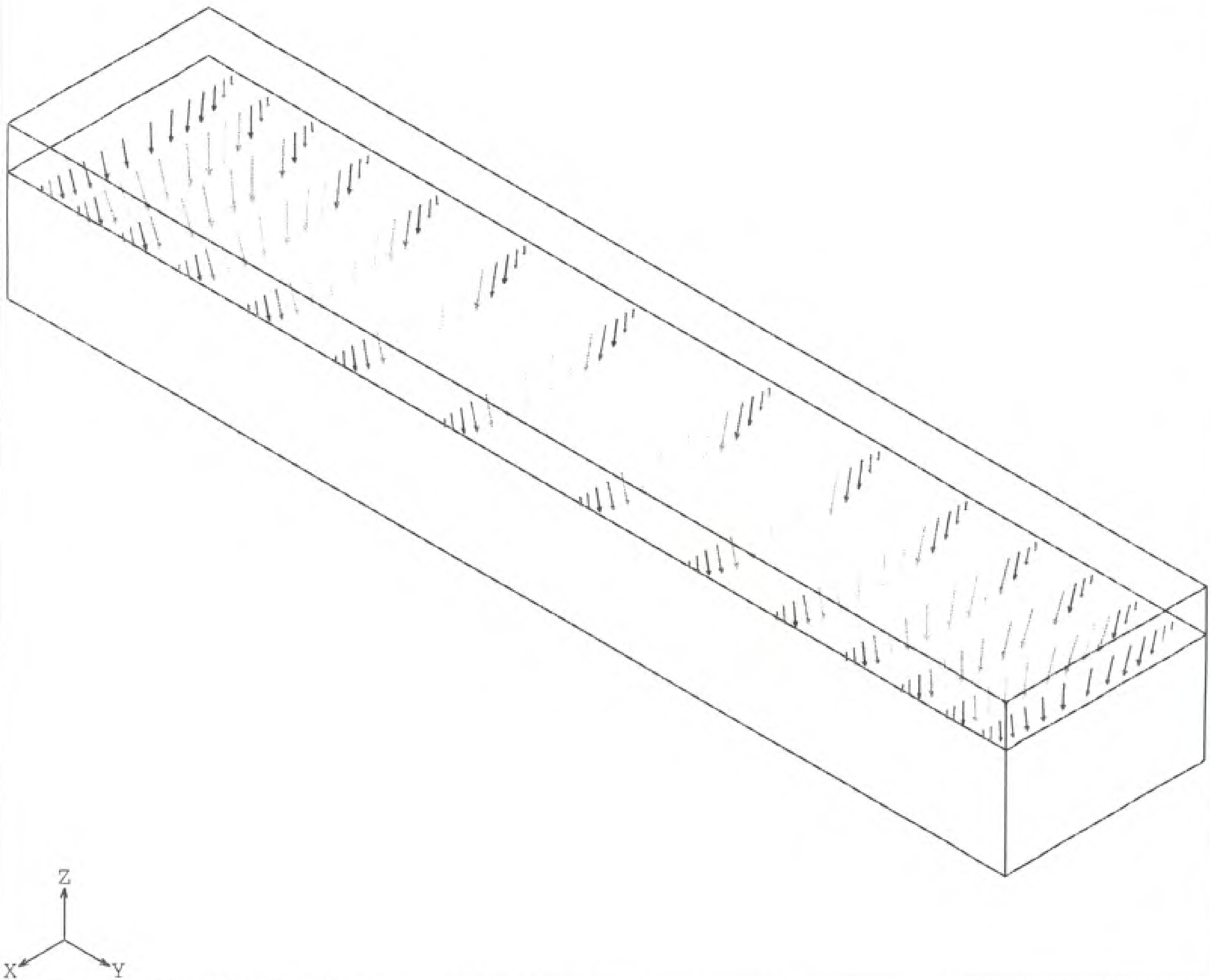


VELOCITY VECTOR PLOT

SCALE FACTOR 0.5000E+02

REFER. VECTOR ⟶ 0.3215E+00

MAX.VEC.PLOT'D 0.2583E+00

AT NODE 0

COLOR CODE: VELOCITY

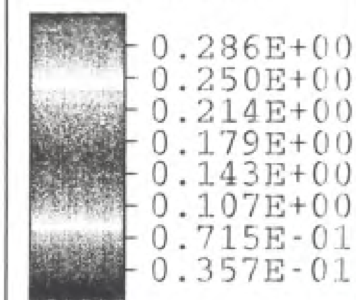


PLANE COEFF.S

| | |
|---|---|
| A | 0.000E+00 |
| B | 0.000E+00 |
| C | 0.100E+01 |
| D | -.110E+01 |

VIEW DIRECTION

| | |
|---|---|
| VX | 0.100E+01 |
| VY | 0.100E+01 |
| VZ | 0.100E+01 |
| ANG | 0.000E+00 |

FIDAP 7.52
7 Aug 96
17:24:19

FIGURE 5.24: VELOCITY PLOT, DOWNSTREAM SECTION 10

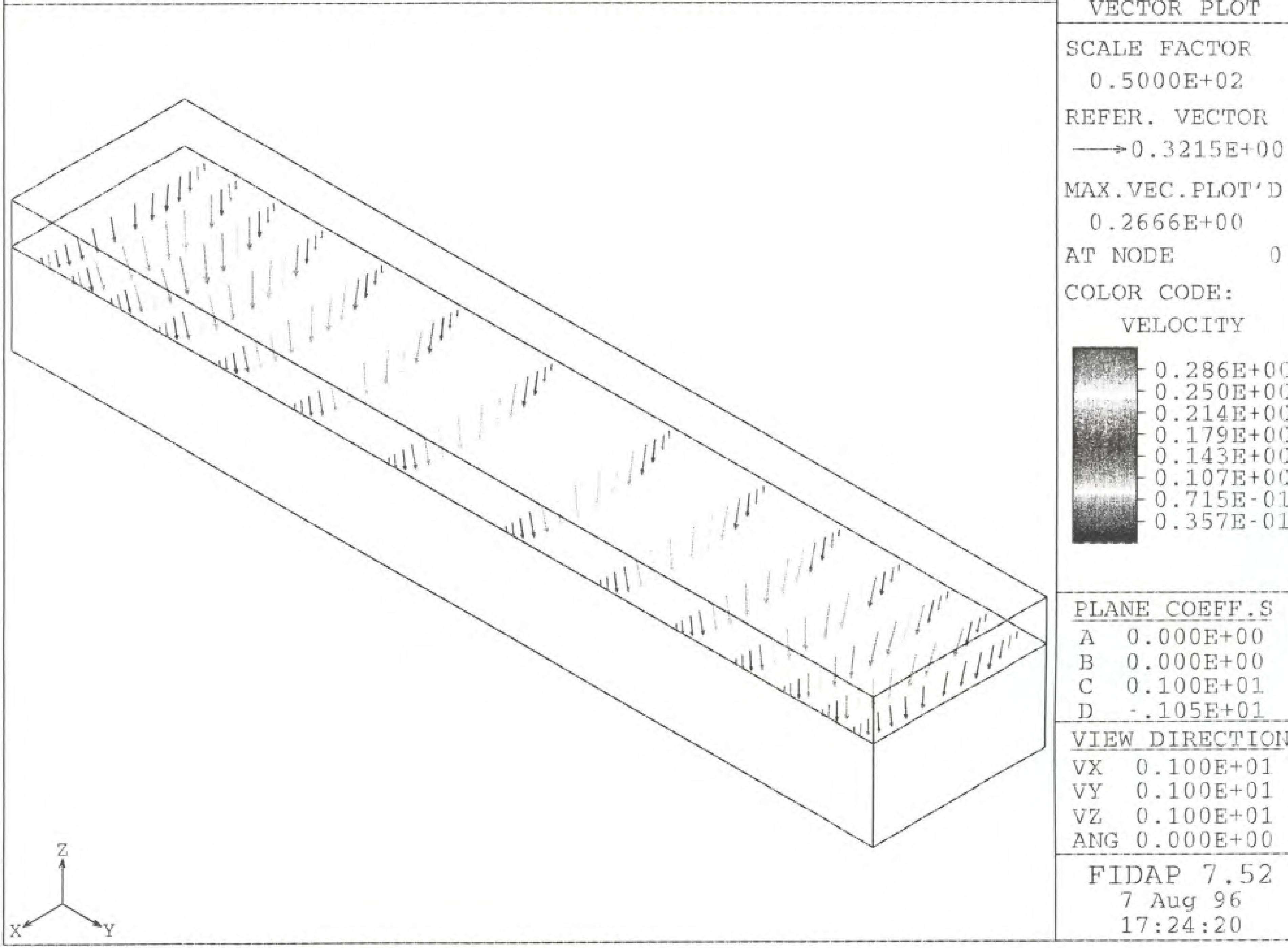

FIGURE 5.25: VELOCITY PLOT, DOWNSTREAM SECTION 11

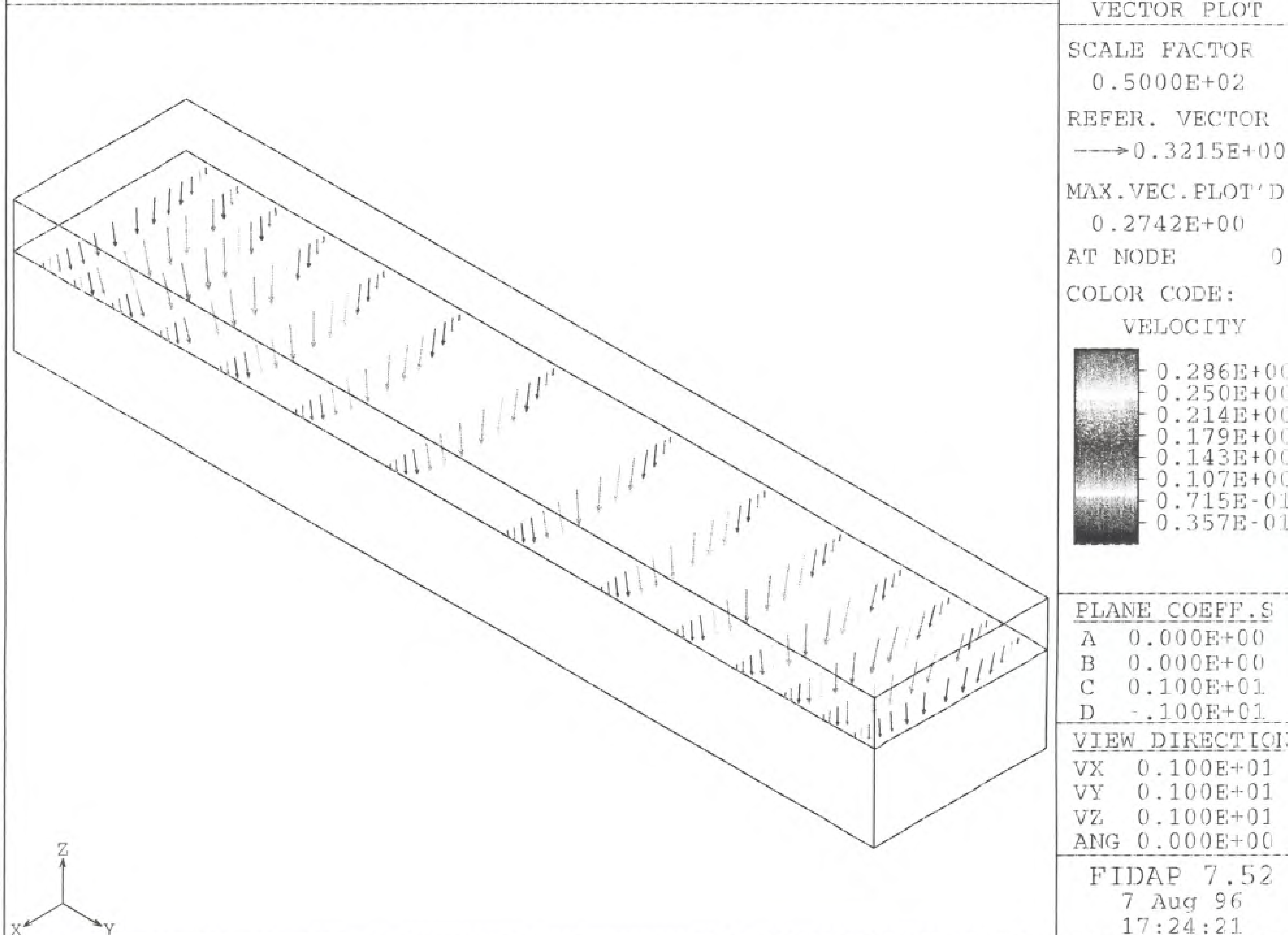

FIGURE 5.26: VELOCITY PLOT, DOWNSTREAM SECTION 12

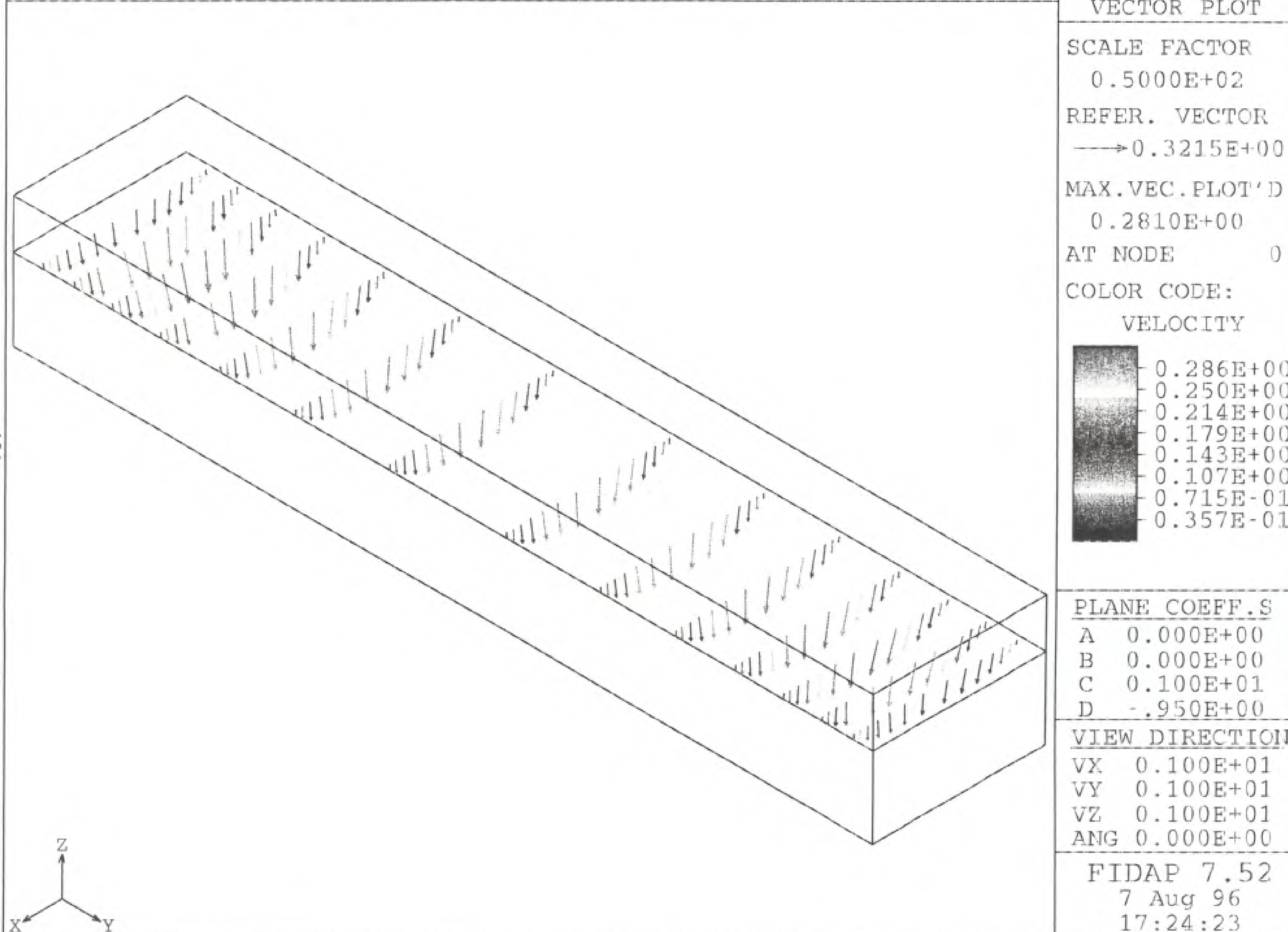

FIGURE 5.27: VELOCITY PLOT, DOWNSTREAM SECTION 13

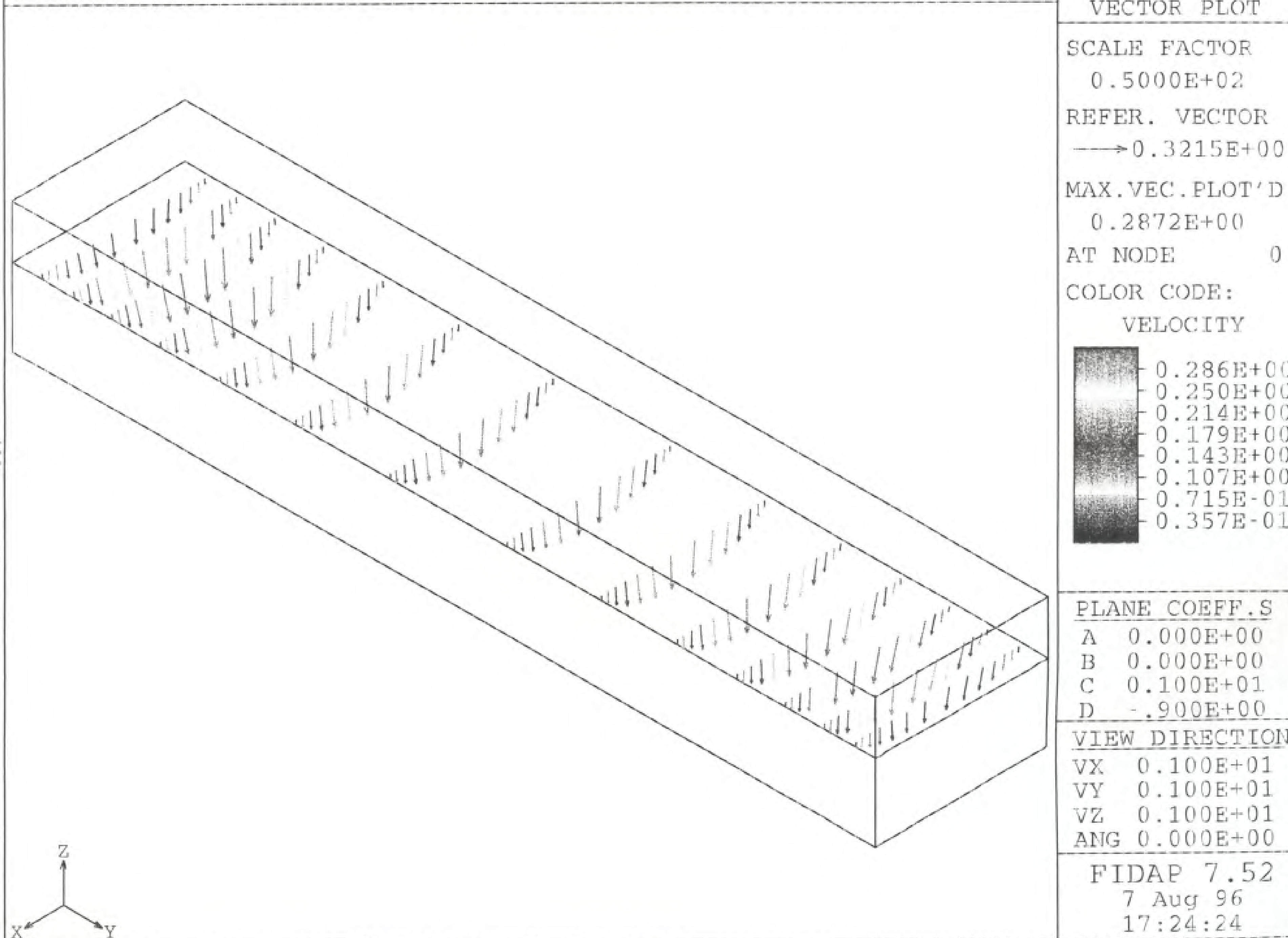

FIGURE 5.28: VELOCITY PLOT, DOWNSTREAM SECTION 14

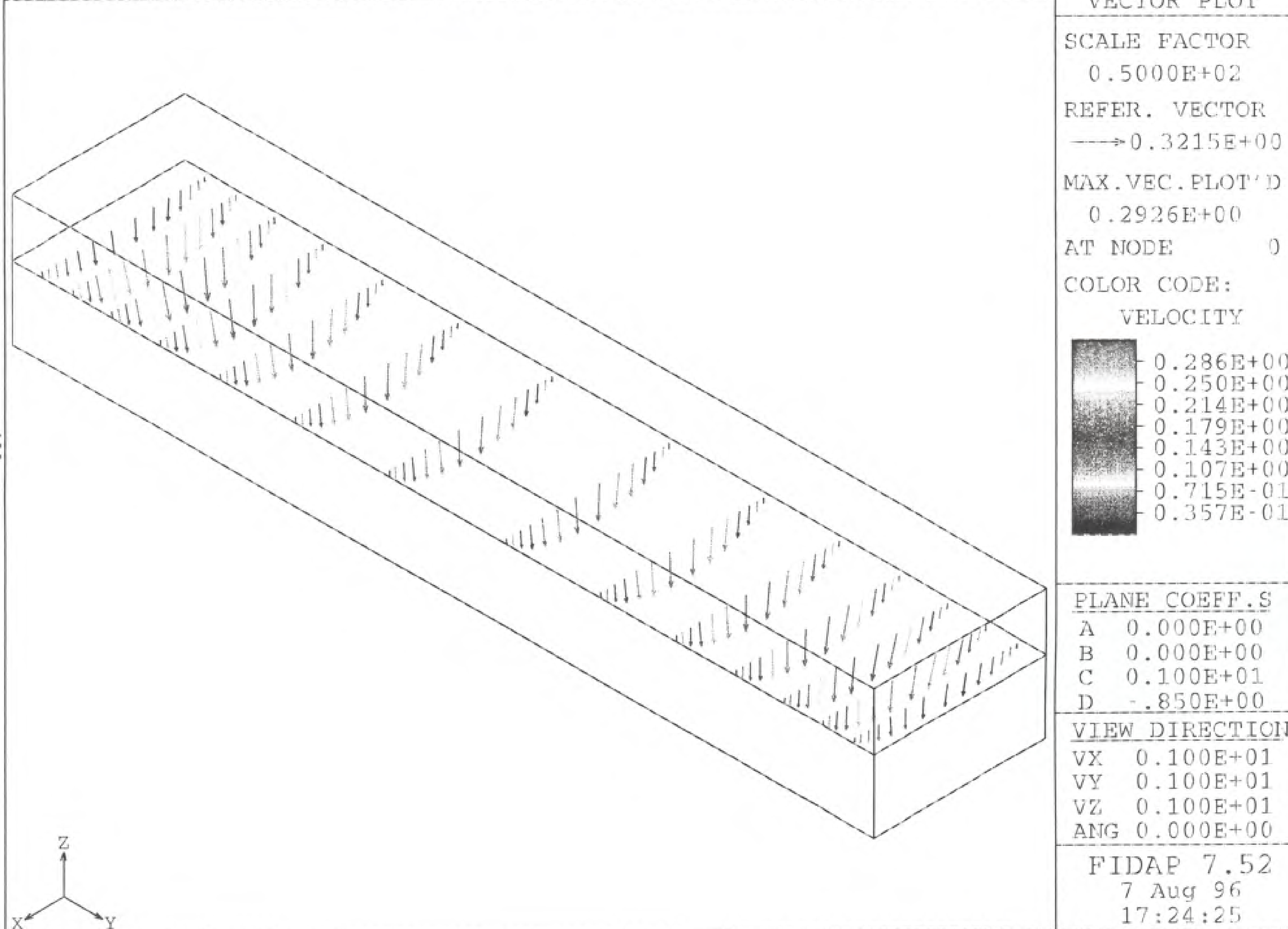

FIGURE 5.29: VELOCITY PLOT, DOWNSTREAM SECTION 15

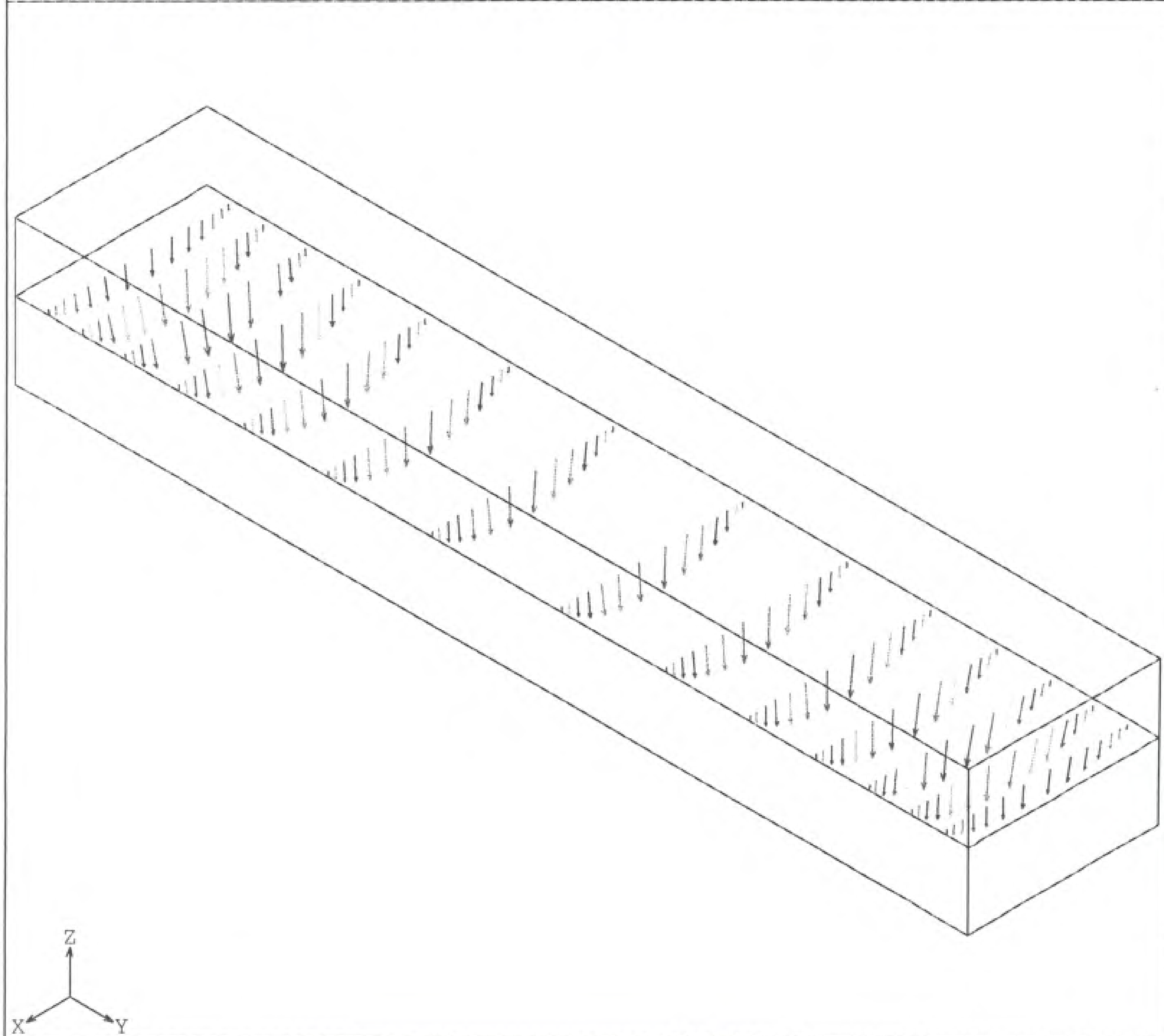


VELOCITY
VECTOR PLOT

SCALE FACTOR
0.5000E+02
REFER. VECTOR
——→0.3215E+00
MAX.VEC.PLOT'D
0.2971E+00
AT NODE 0
COLOR CODE:
VELOCITY

0.286E+00
0.250E+00
0.214E+00
0.179E+00
0.143E+00
0.107E+00
0.715E-01
0.357E-01

PLANE COEFF.S

A 0.000E+00
B 0.000E+00
C 0.100E+01
D -.800E+00

VIEW DIRECTION

VX 0.100E+01
VY 0.100E+01
VZ 0.100E+01
ANG 0.000E+00

FIDAP 7.52
7 Aug 96
17:24:27

FIGURE 5.30: VELOCITY PLOT, DOWNSTREAM SECTION 16

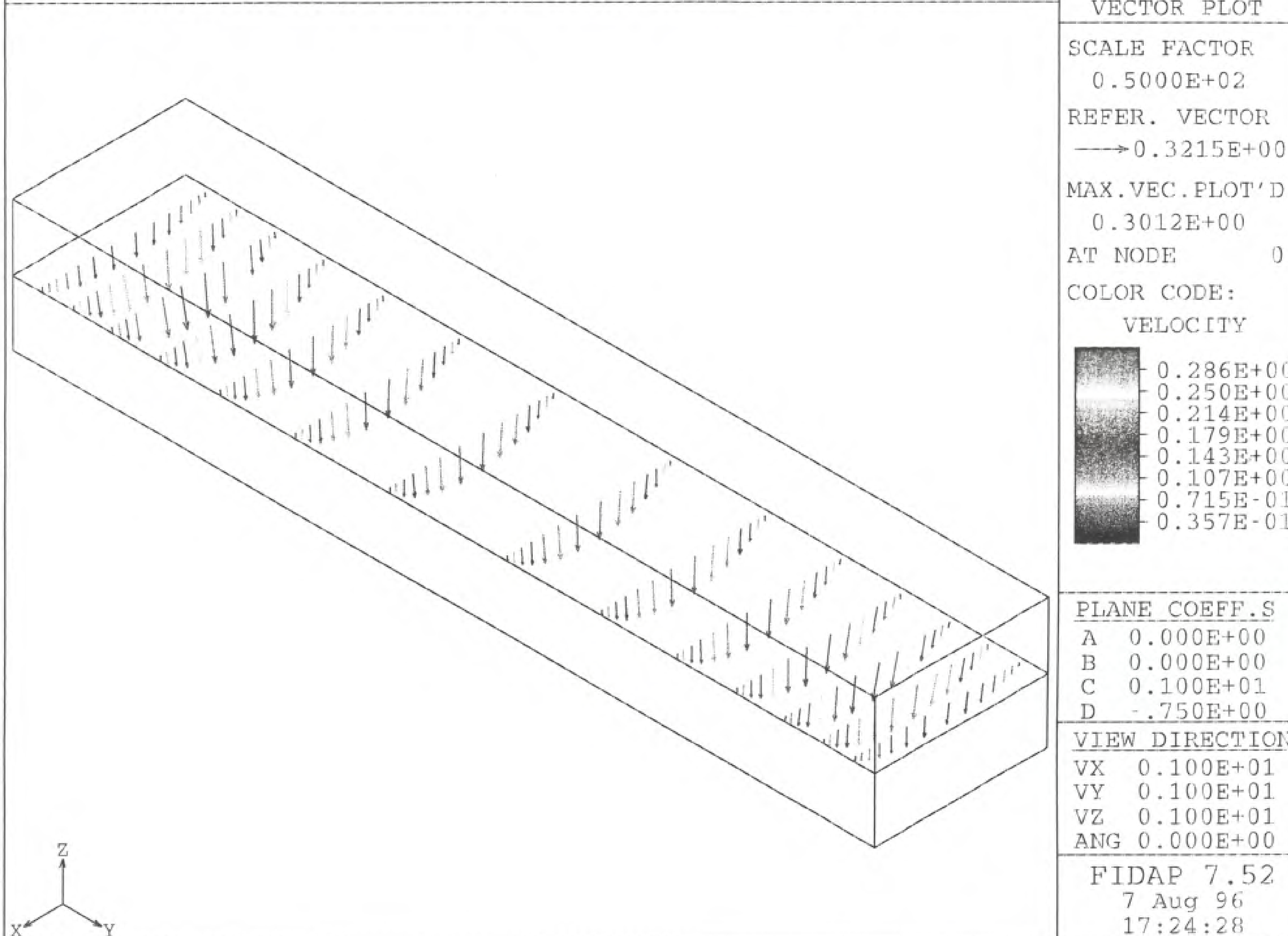

FIGURE 5.31: VELOCITY PLOT, DOWNSTREAM SECTION 17

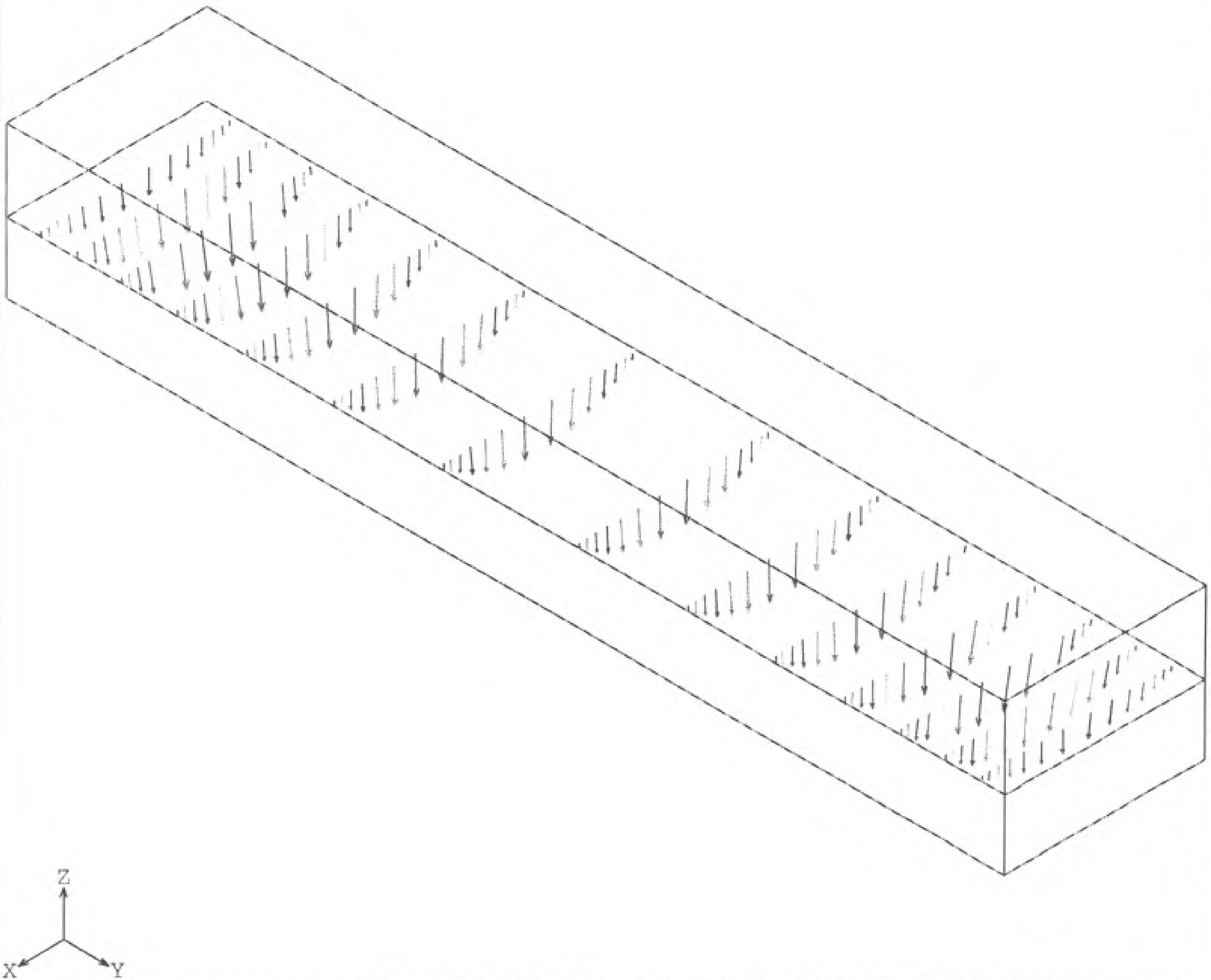


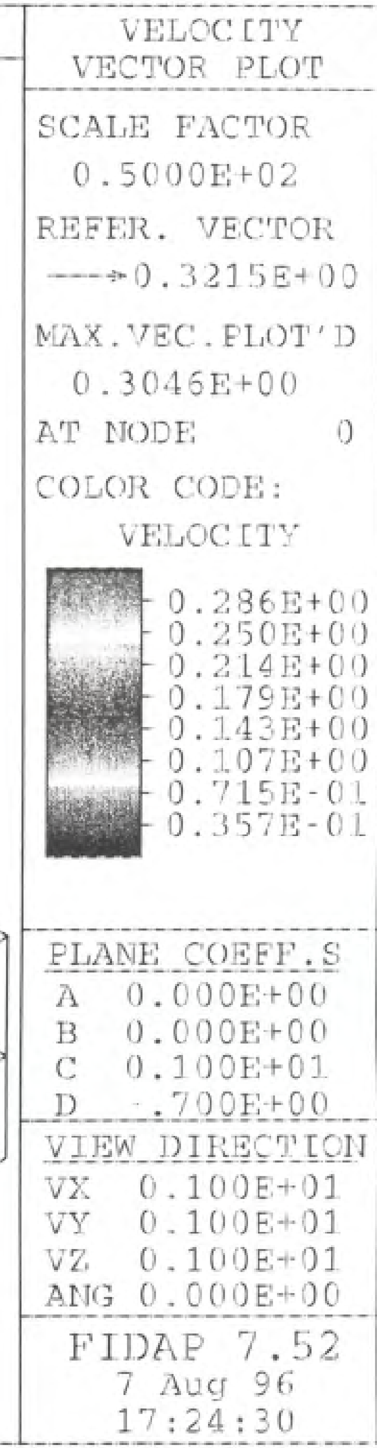

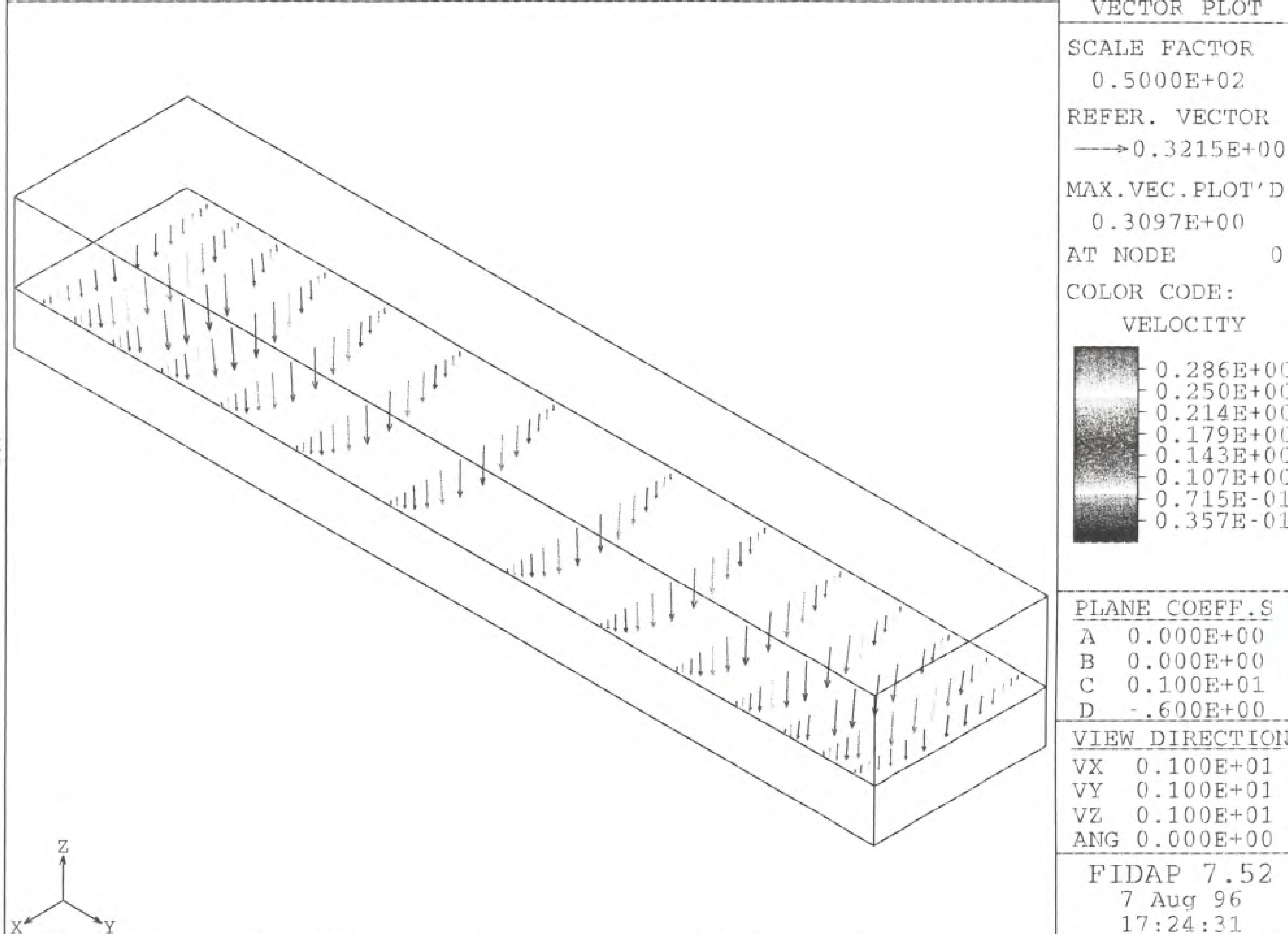


FIGURE 5.32: VELOCITY PLOT, DOWNSTREAM SECTION 18

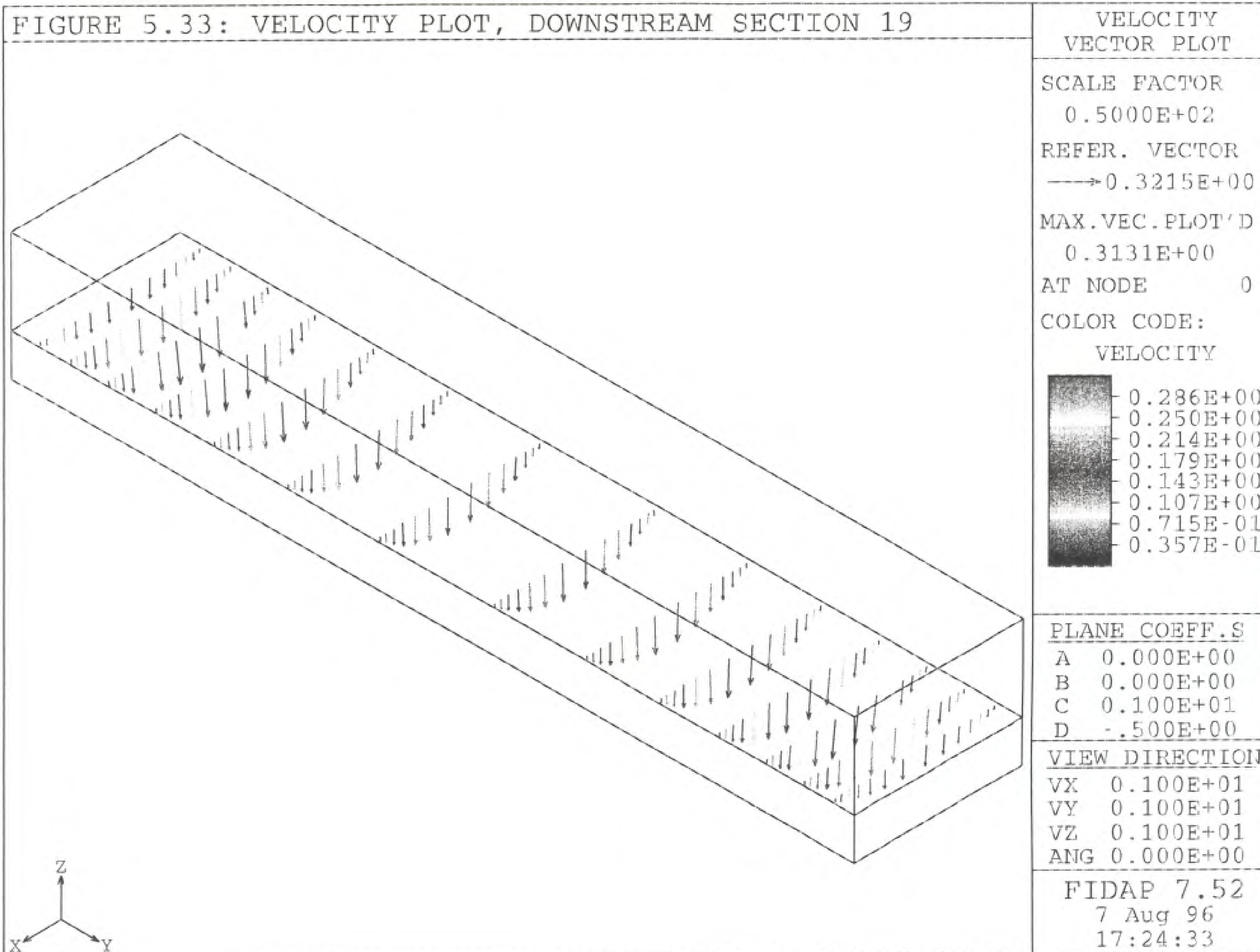

FIGURE 5.33: VELOCITY PLOT, DOWNSTREAM SECTION 19
VELOCITY
VECTOR PLOT
SCALE FACTOR
0.5000E+02
REFER. VECTOR
0.3215E+00
MAX.VEC.PLOT'D
0.3131E+00
AT NODE 0
COLOR CODE:
VELOCITY
0.286E+00
0.250E+00
0.214E+00
0.179E+00
0.143E+00
0.107E+00
0.715E-01
0.357E-01
PLANE COEFF.S
A 0.000E+00
B 0.000E+00
C 0.100E+01
D -.500E+00
VIEW DIRECTION
VX 0.100E+01
VY 0.100E+01
VZ 0.100E+01
ANG 0.000E+00
FIDAP 7.52
7 Aug 96
17:24:33
Z
X
Y

FIGURE 5.34: VELOCITY PLOT, DOWNSTREAM SECTION 20

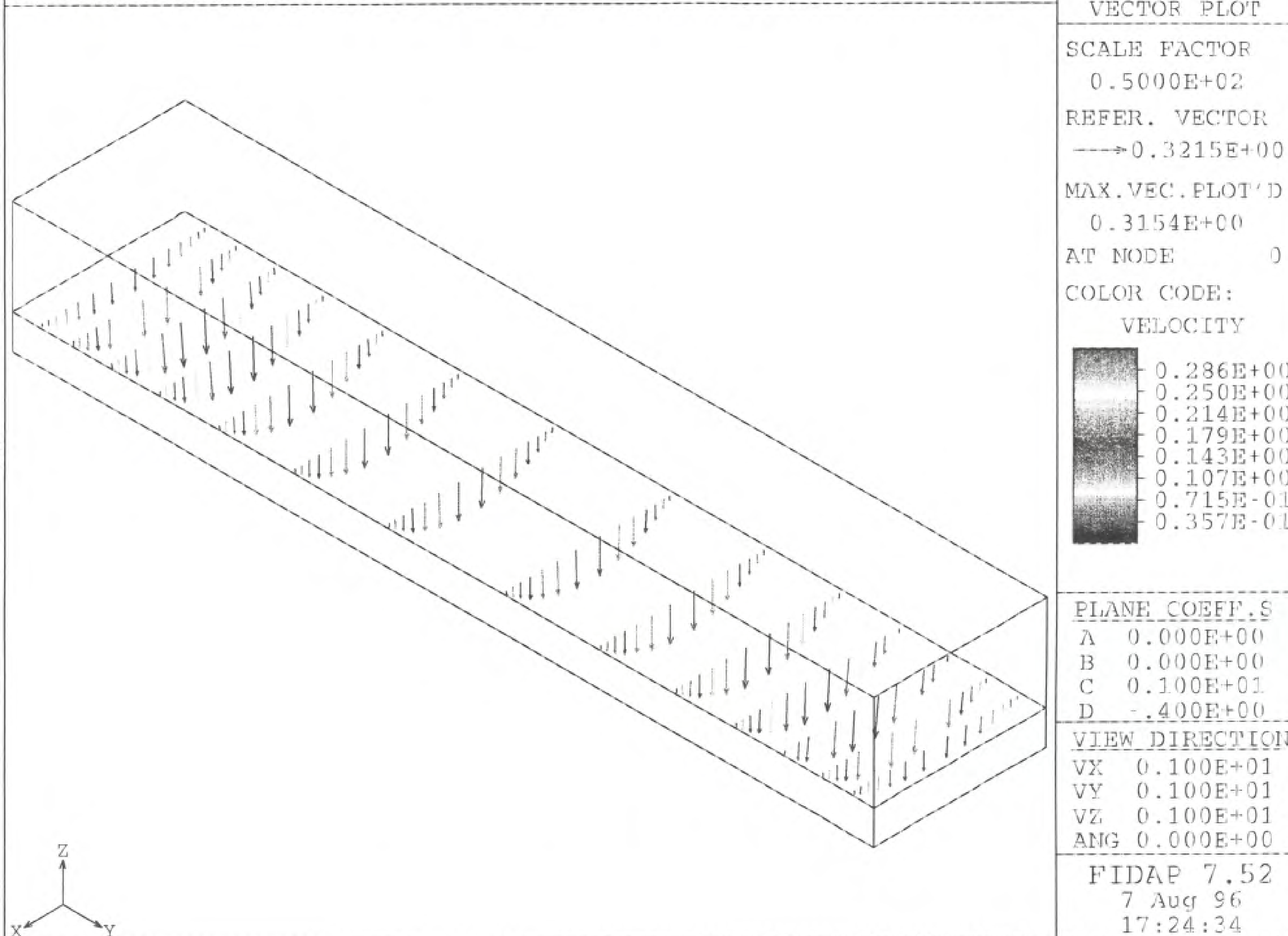

FIGURE 5.35: VELOCITY PLOT, DOWNSTREAM SECTION 21

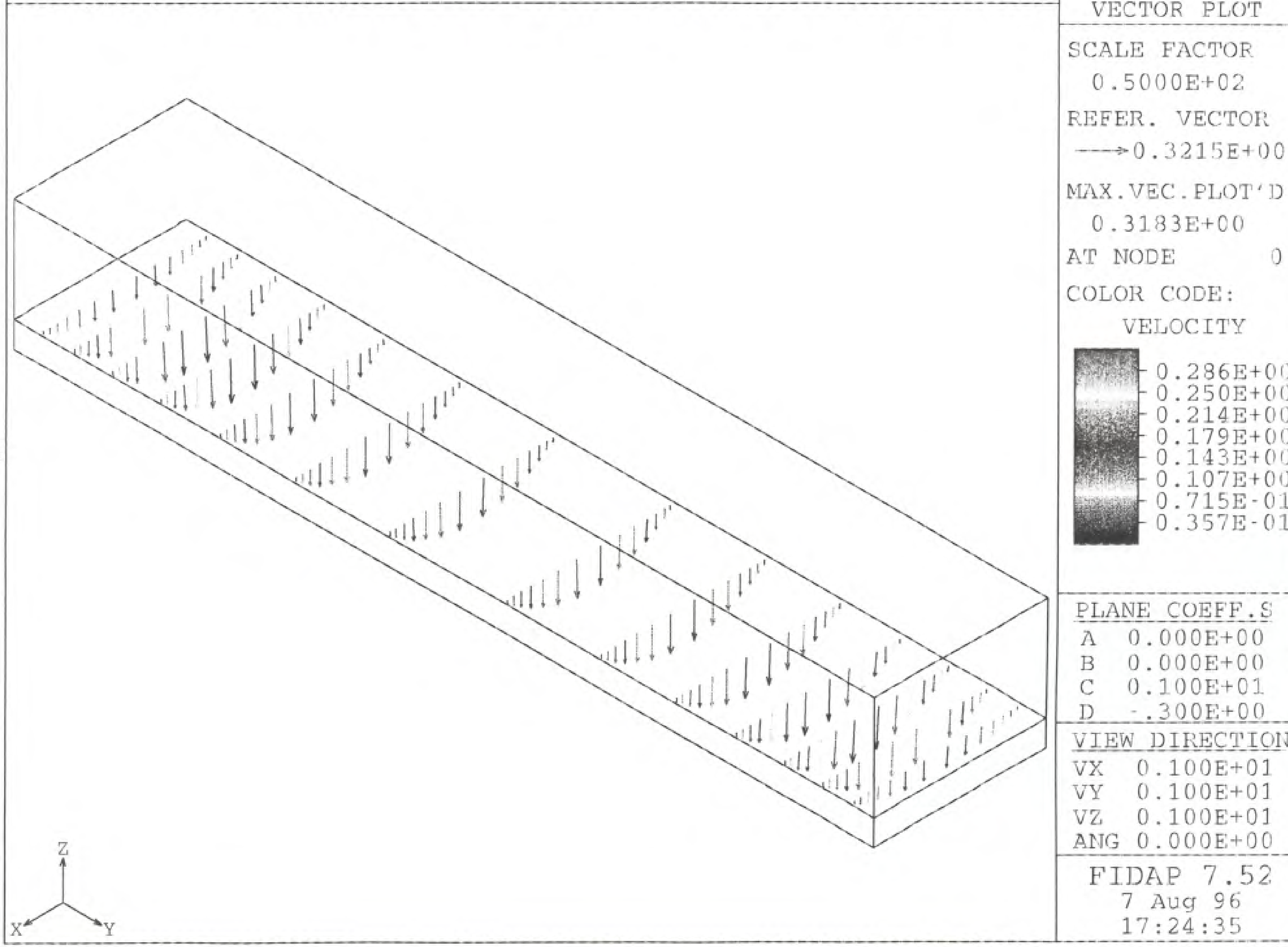

FIGURE 5.36: VELOCITY PLOT, DOWNSTREAM SECTION 22

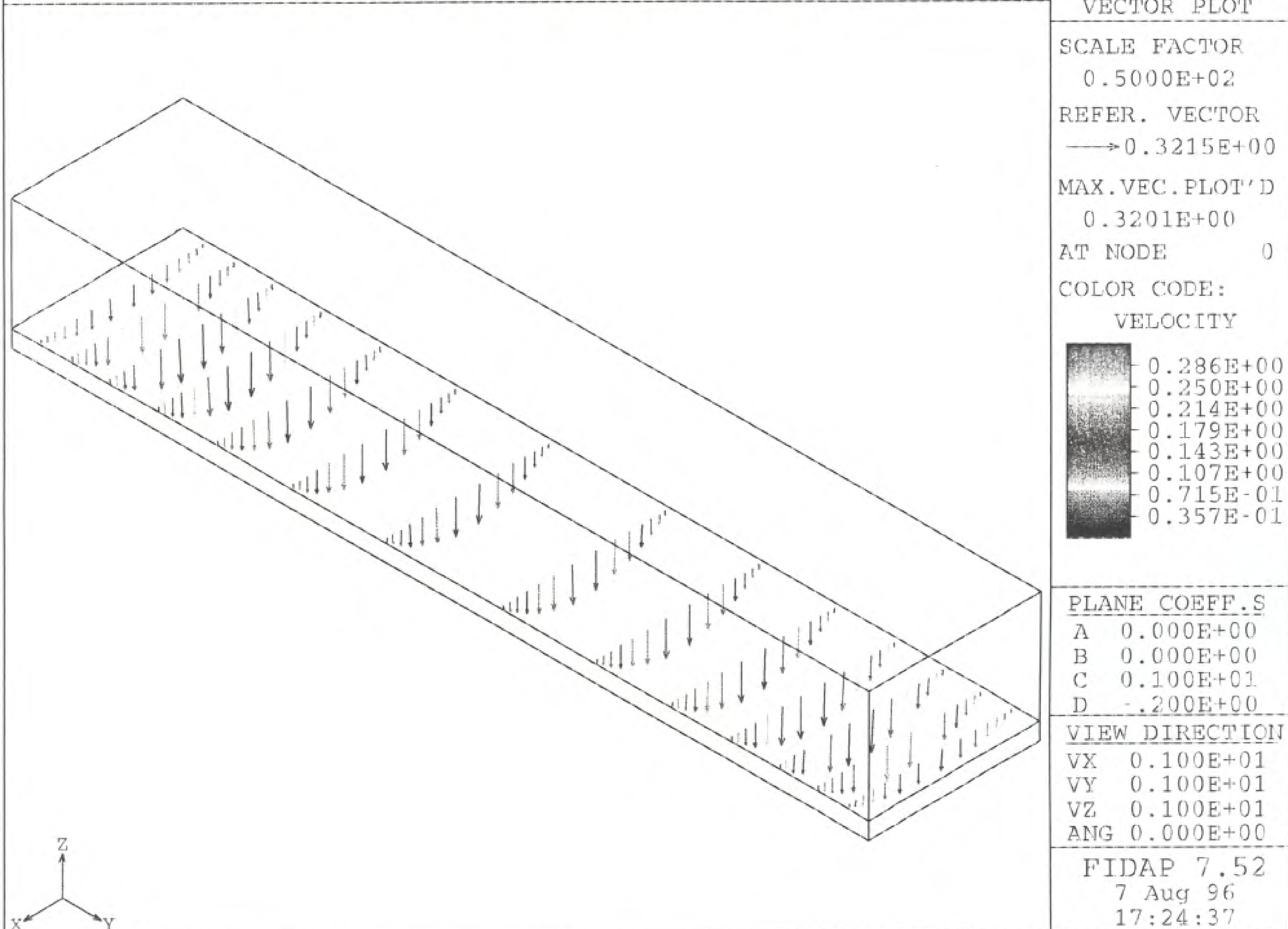

FIGURE 5.37: VELOCITY PLOT, DOWNSTREAM SECTION 23

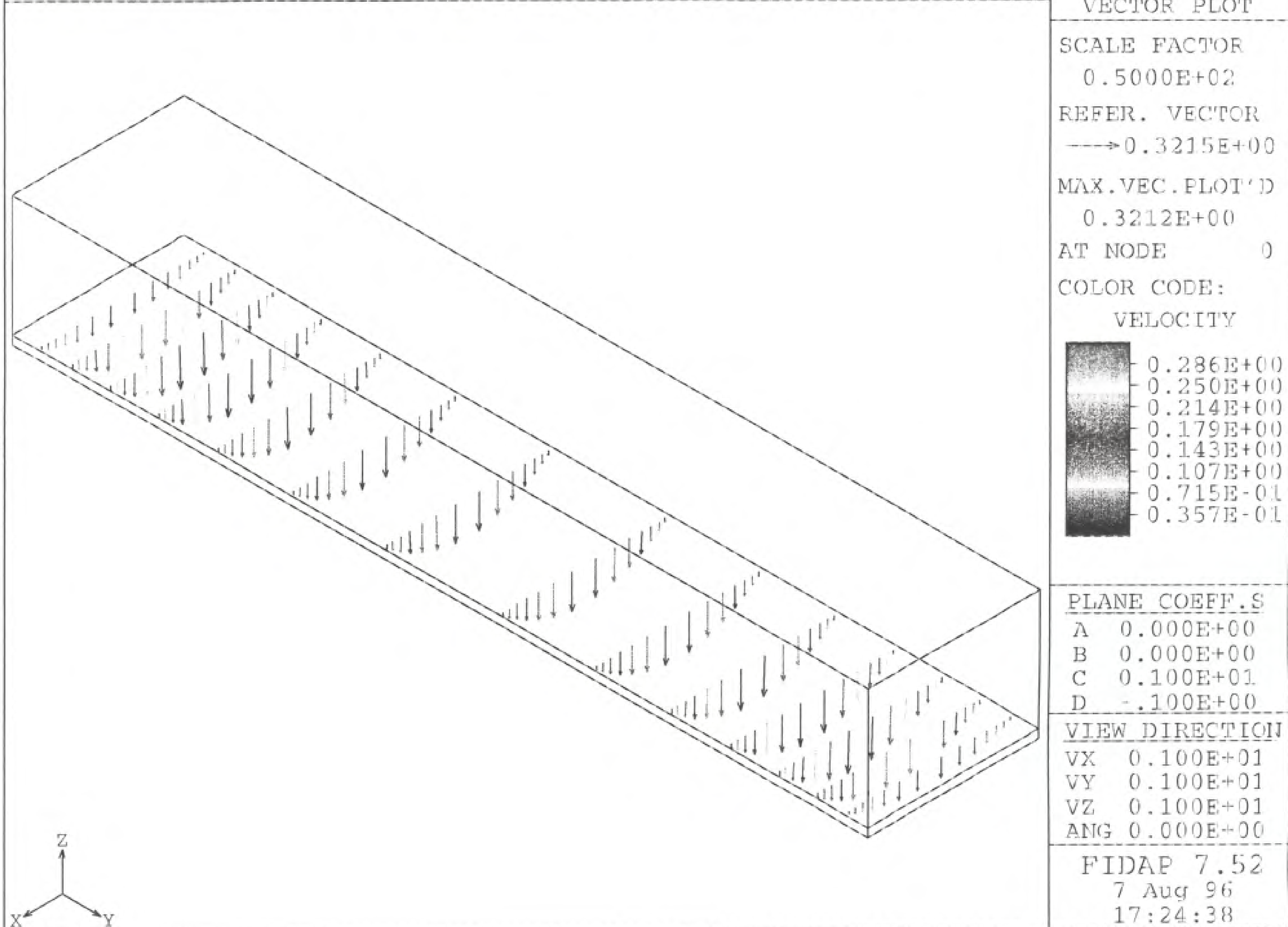

FIGURE 5.38: VELOCITY PLOT, DOWNSTREAM SECTION 24

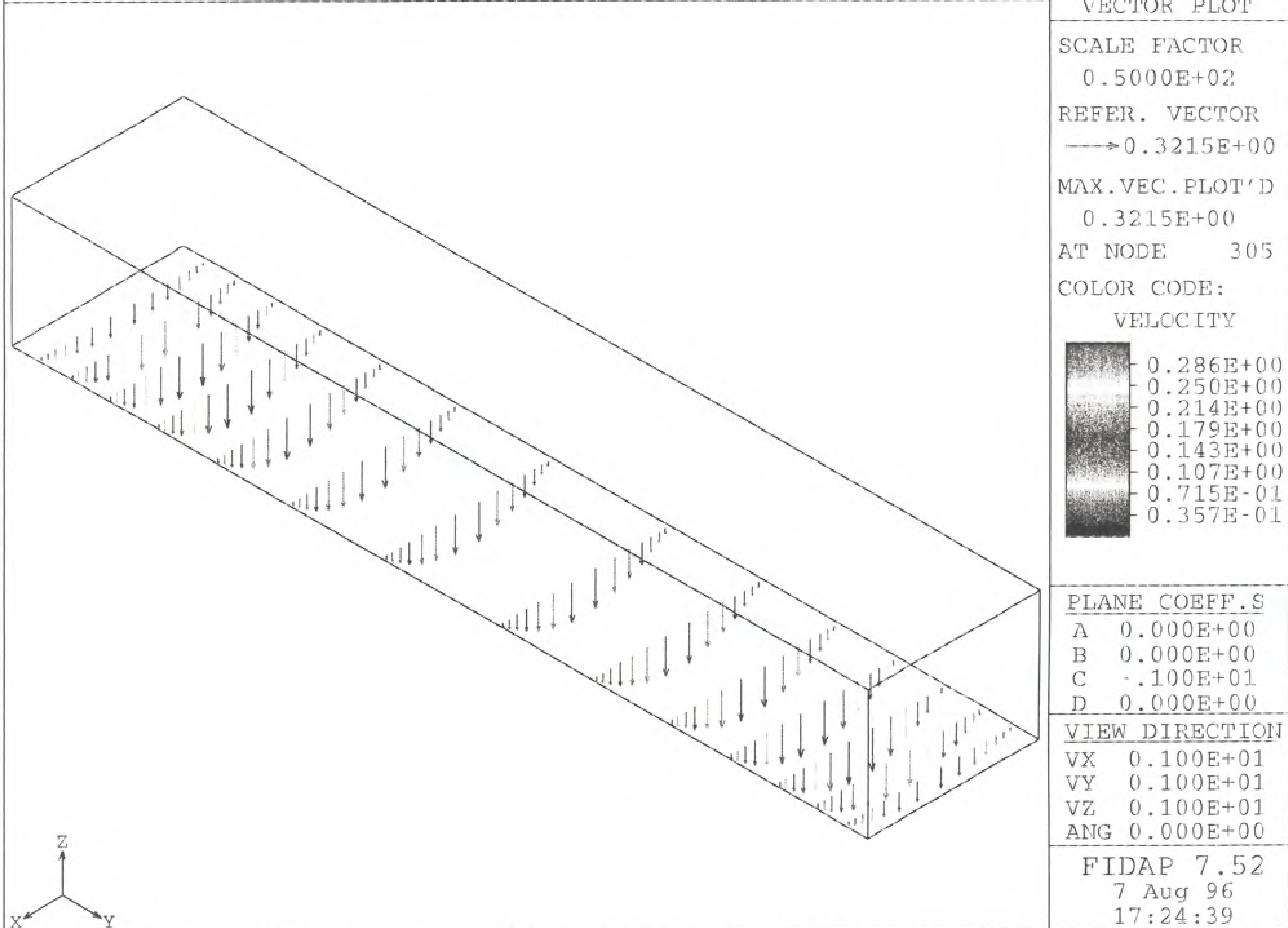

FIGURE 5.39: SHEAR STRAIN RATE ON OUTER SURFACES

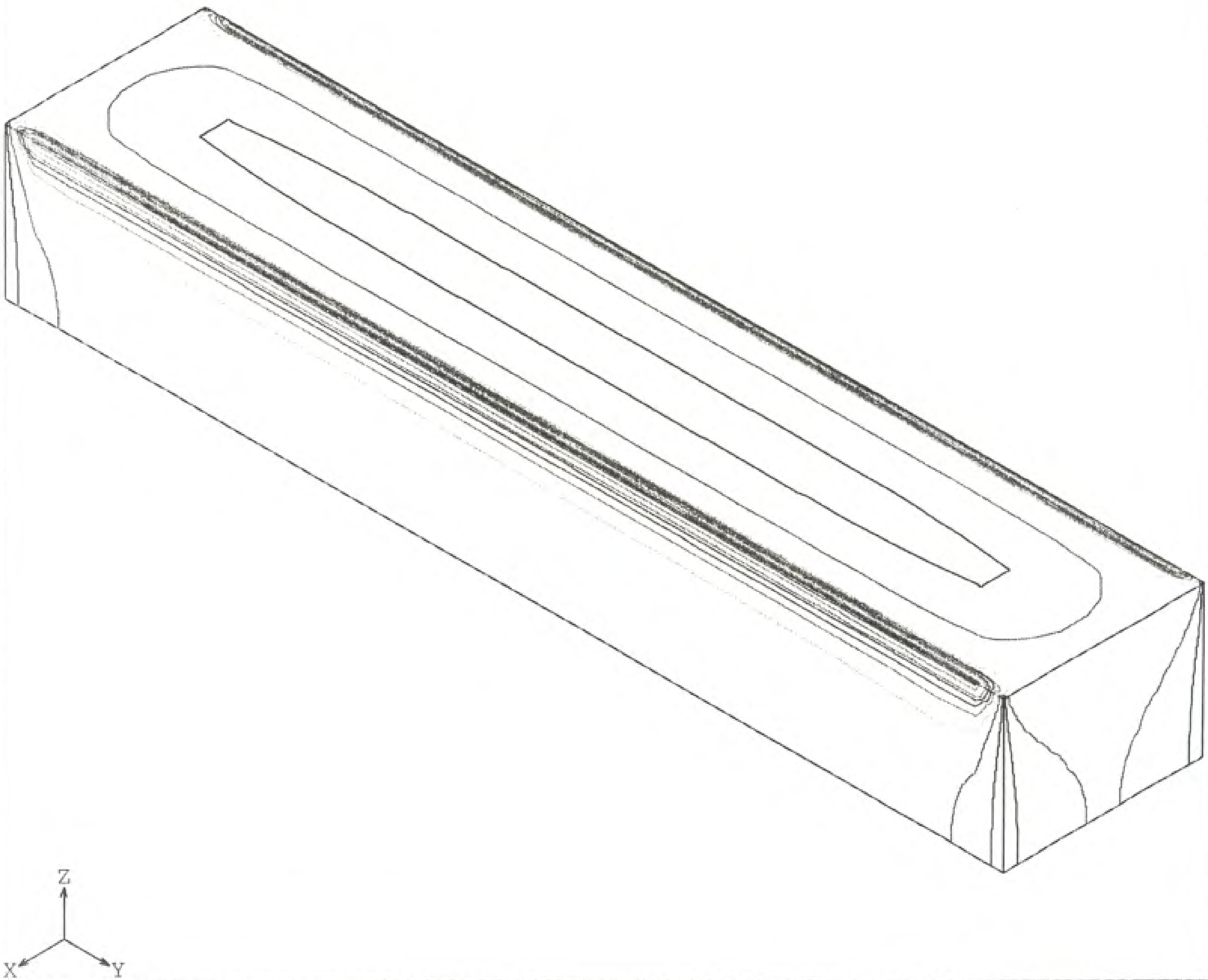

FIGURE 5.40: SHEAR STRAIN RATE, SHORT SECTION

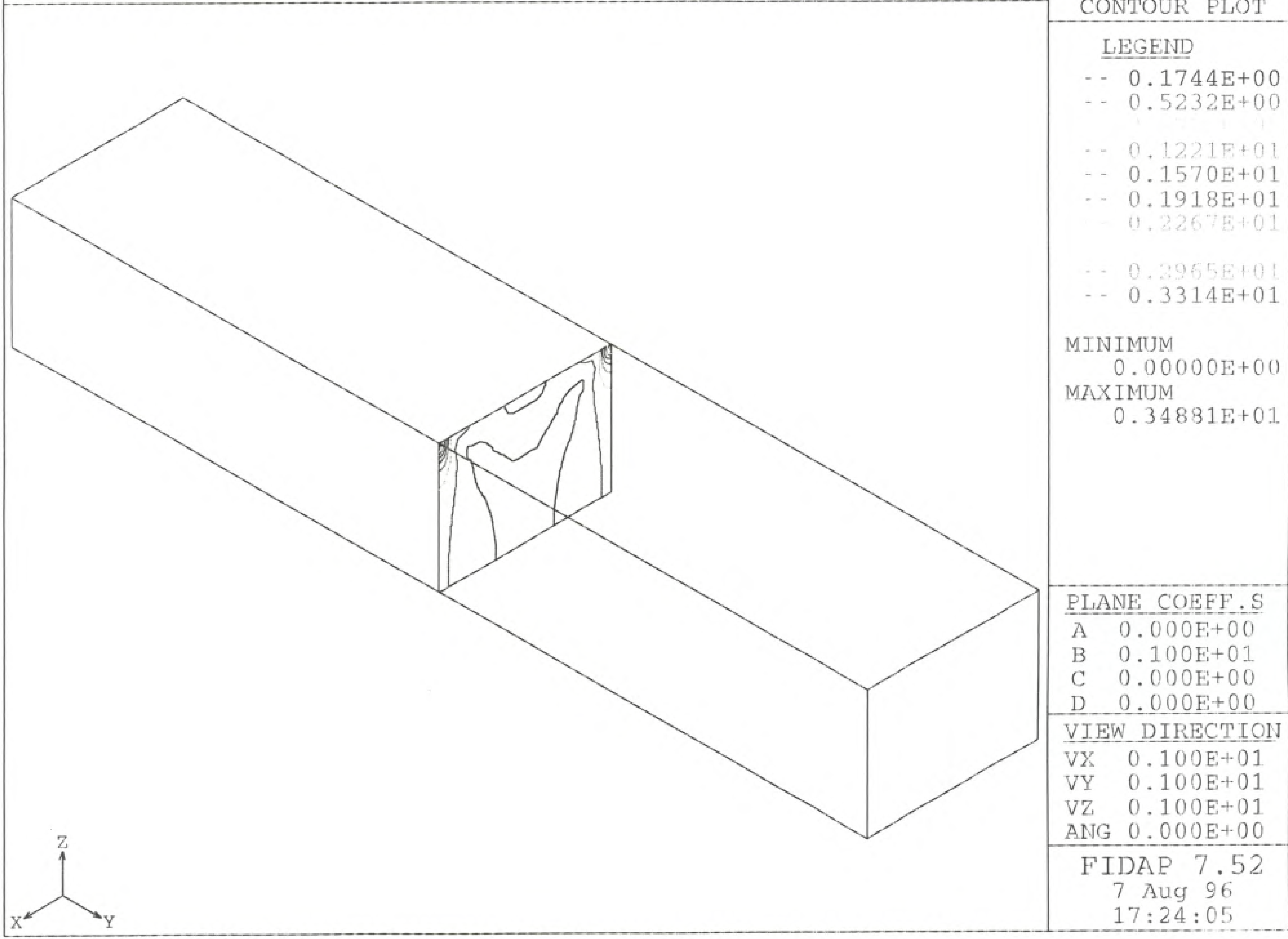

FIGURE 5.41: SHEAR STRAIN RATE, LONG SECTION 1

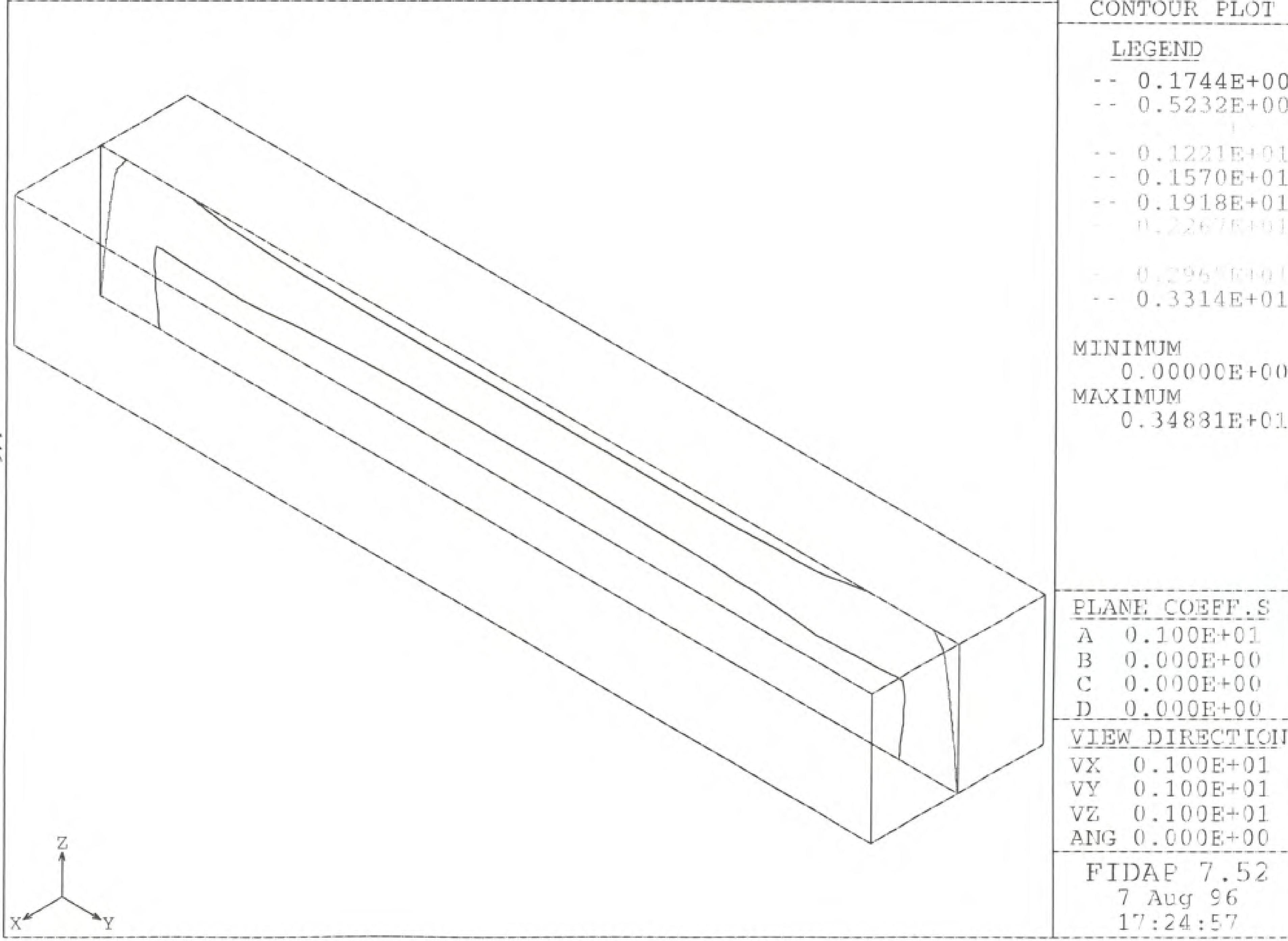

FIGURE 5.42: SHEAR STRAIN RATE, LONG SECTION 2

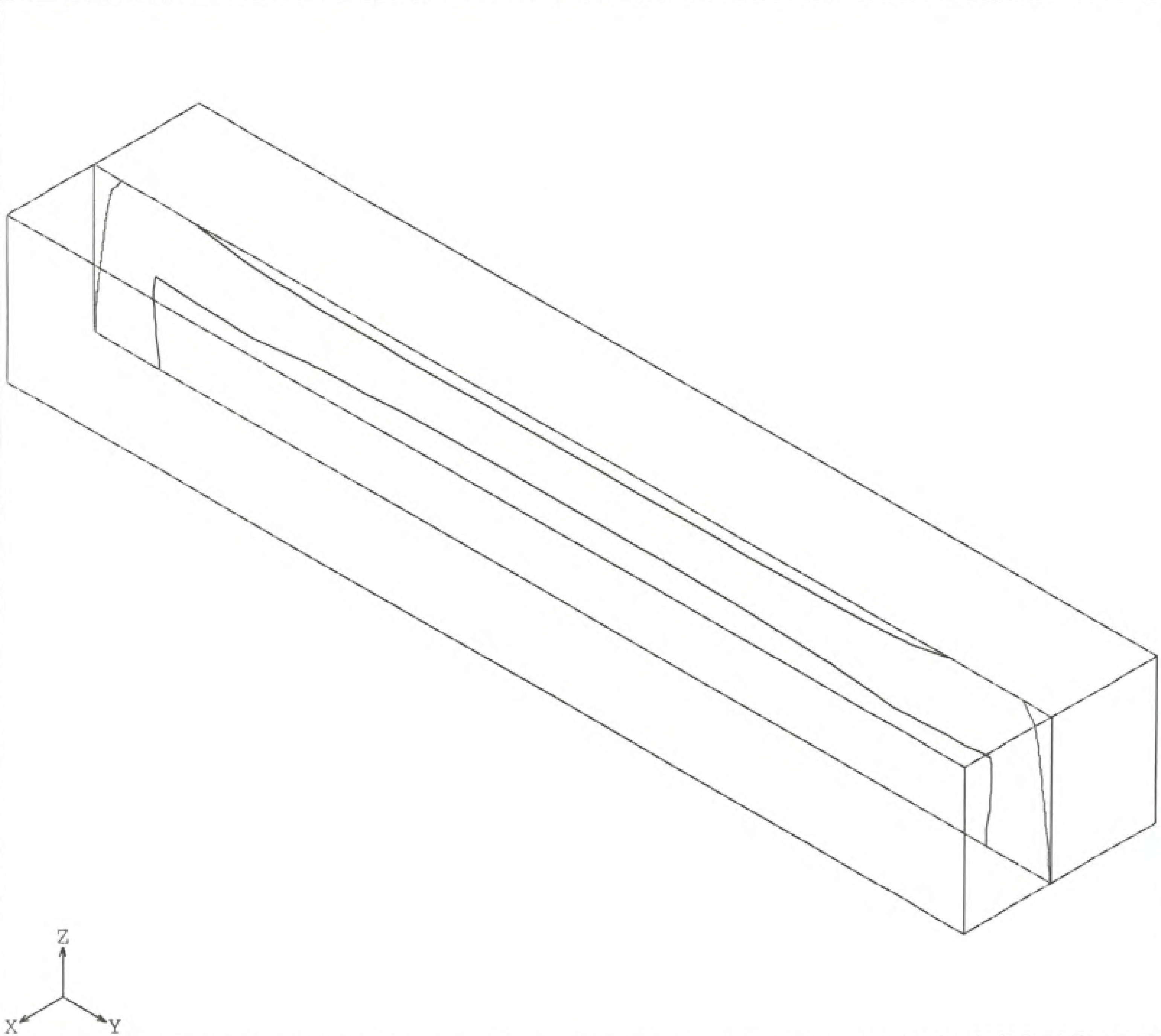

FIGURE 5.43: SHEAR STRAIN RATE, LONG SECTION 3

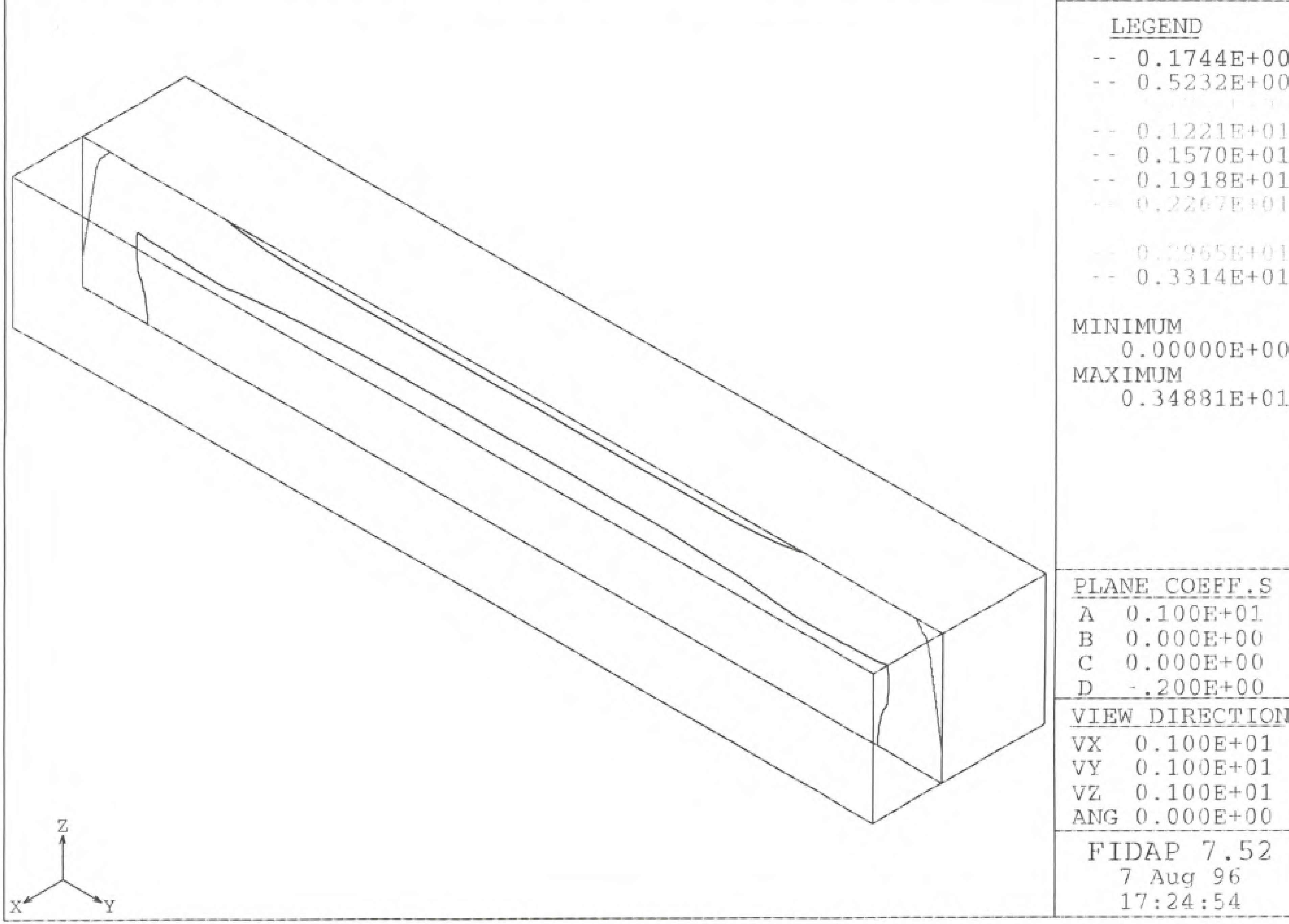

FIGURE 5.44: SHEAR STRAIN RATE, LONG SECTION 4

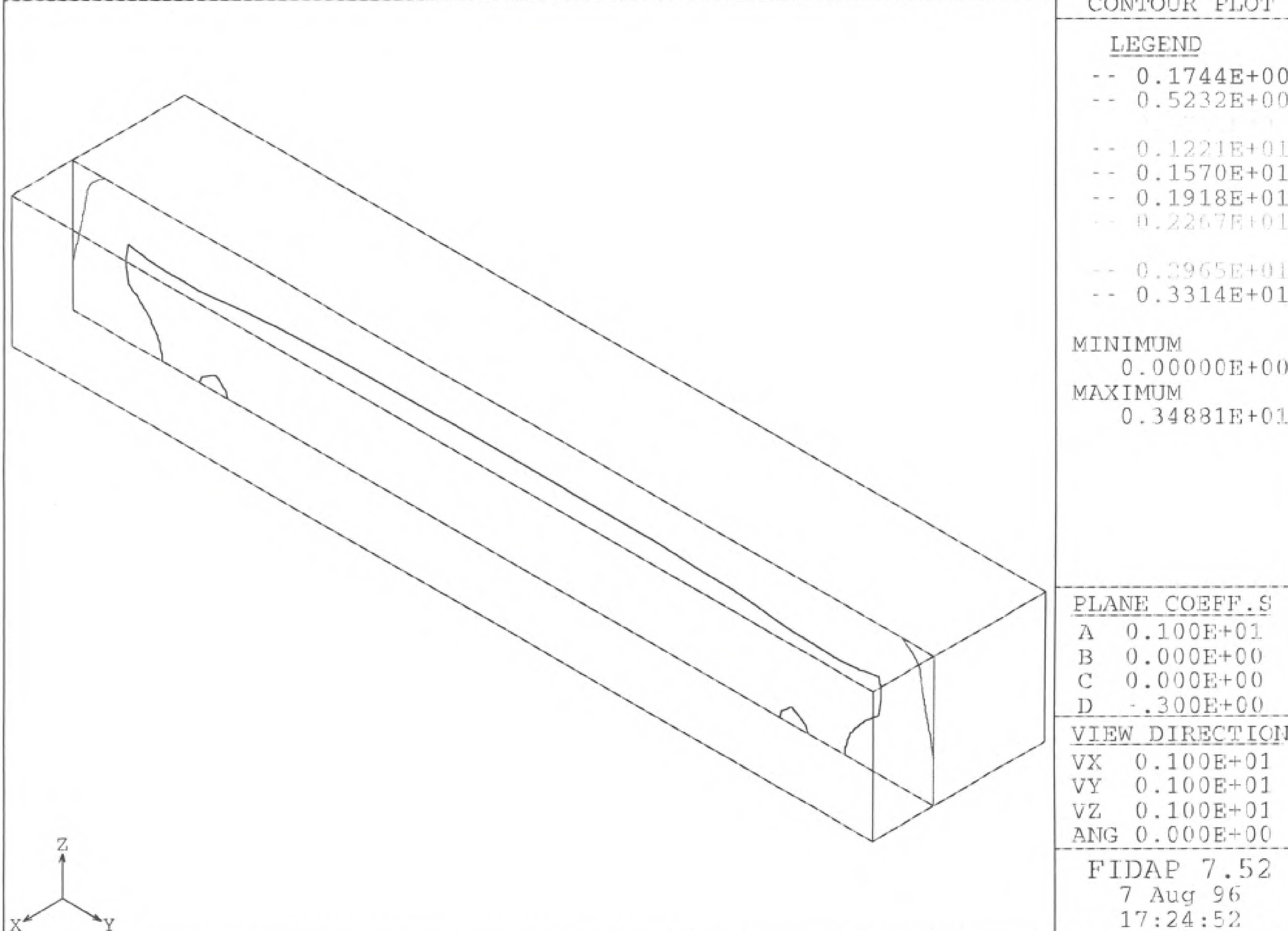

FIGURE 5.45: SHEAR STRAIN RATE, LONG SECTION 5

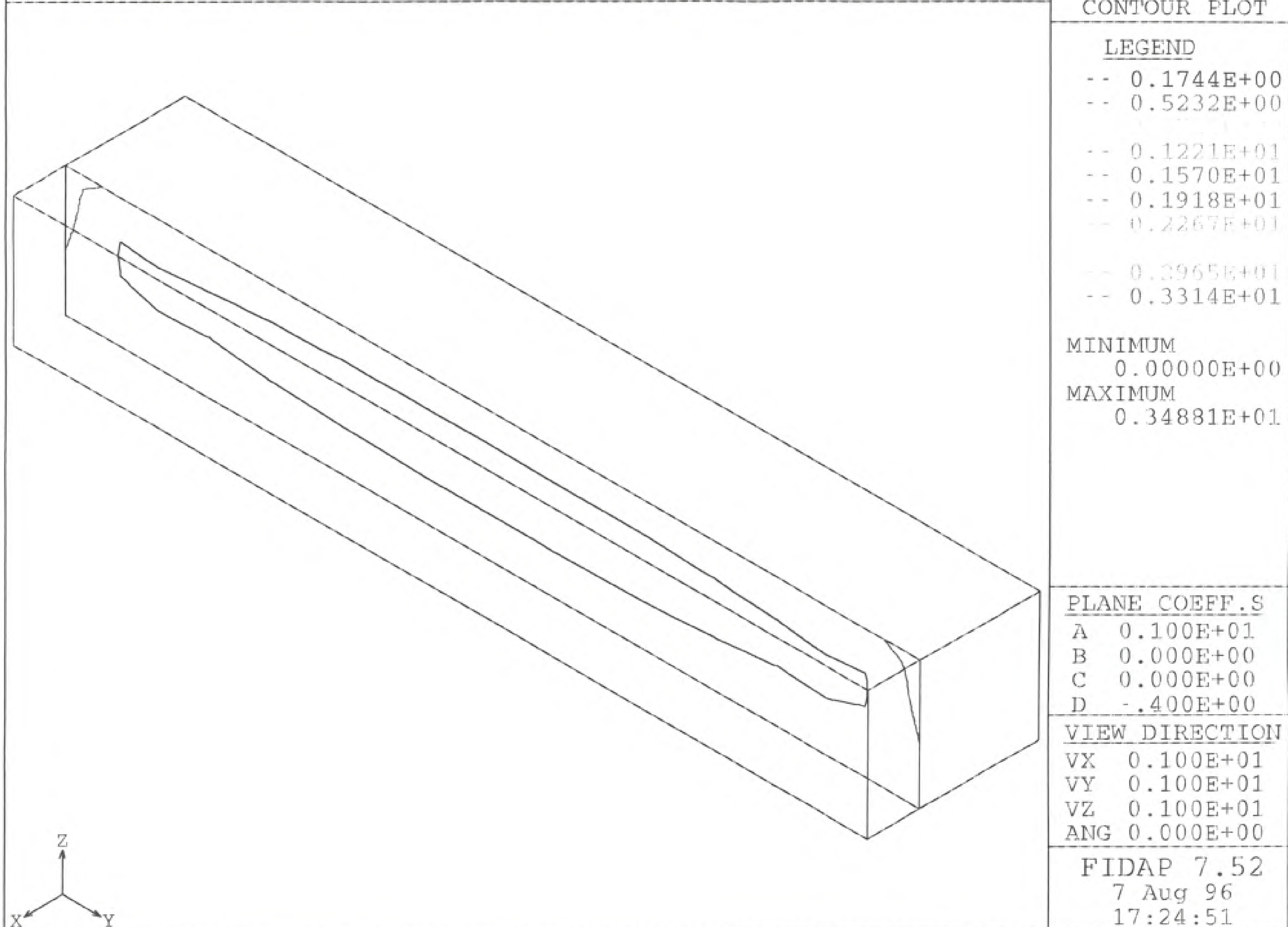

FIGURE 5.46: SHEAR STRAIN RATE, LONG SECTION 6

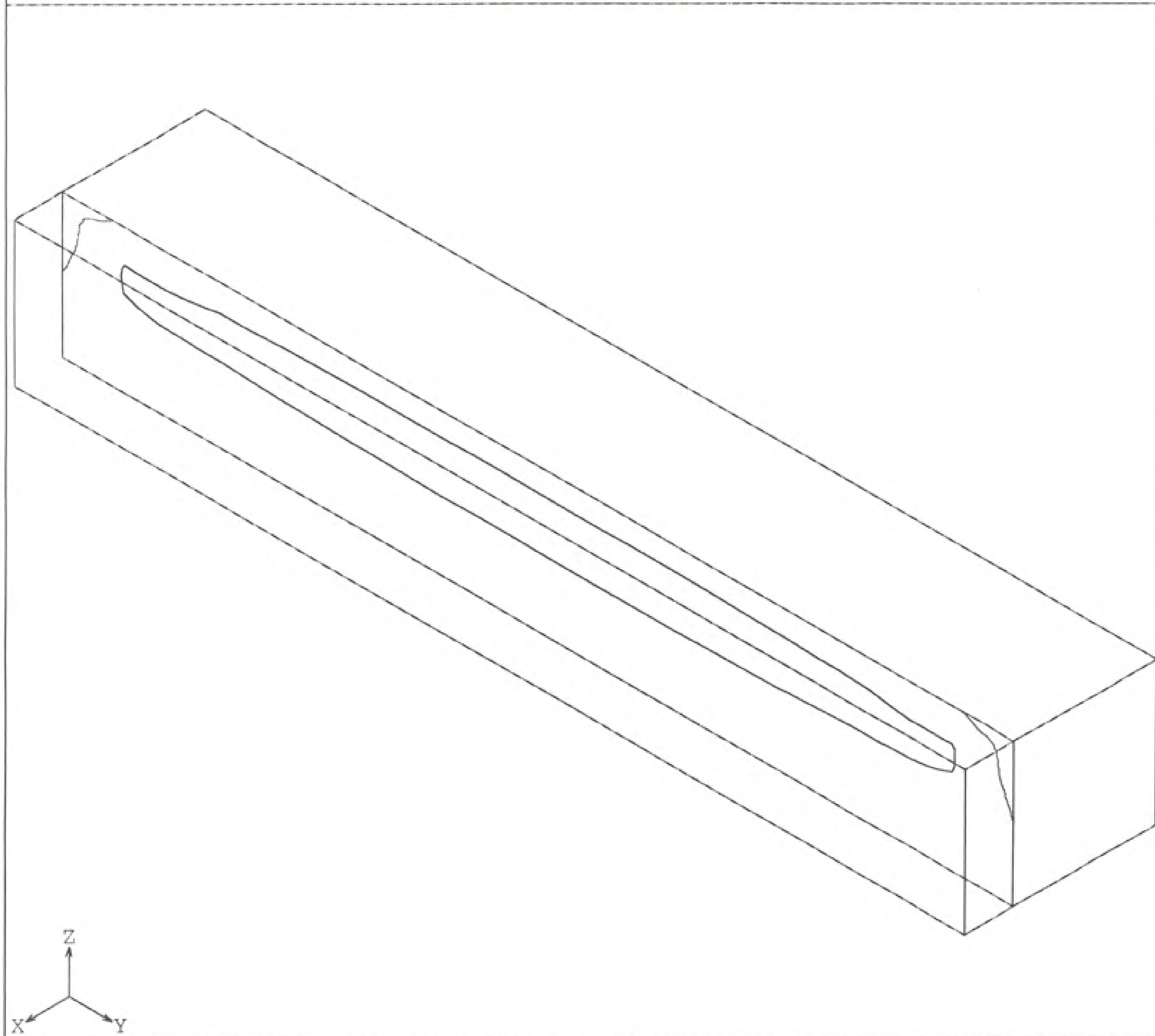


SHEAR RATE
CONTOUR PLOT

LEGEND
-- 0.1744E+00
-- 0.5232E+00
-- 0.1221E+01
-- 0.1570E+01
-- 0.1918E+01
-- 0.2267E+01
-- 0.2965E+01
-- 0.3314E+01

MINIMUM
0.00000E+00
MAXIMUM
0.34881E+01

PLANE COEFF.S
A 0.100E+01
B 0.000E+00
C 0.000E+00
D -.500E+00

VIEW DIRECTION
VX 0.100E+01
VY 0.100E+01
VZ 0.100E+01
ANG 0.000E+00

FIDAP 7.52
7 Aug 96
17:24:49

FIGURE 5.47: SHEAR STRAIN RATE, LONG SECTION 7

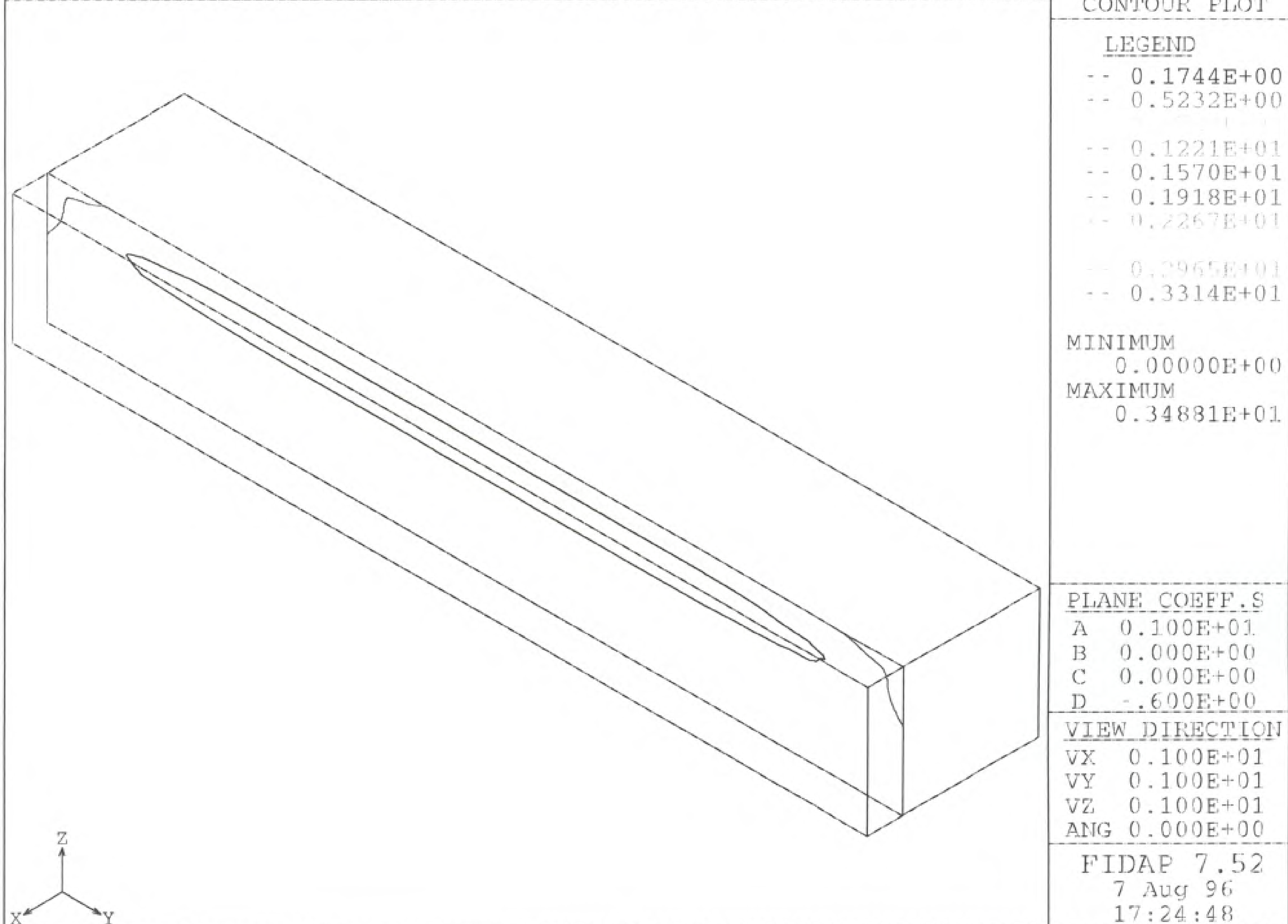

FIGURE 5.48: SHEAR STRAIN RATE, LONG SECTION 8

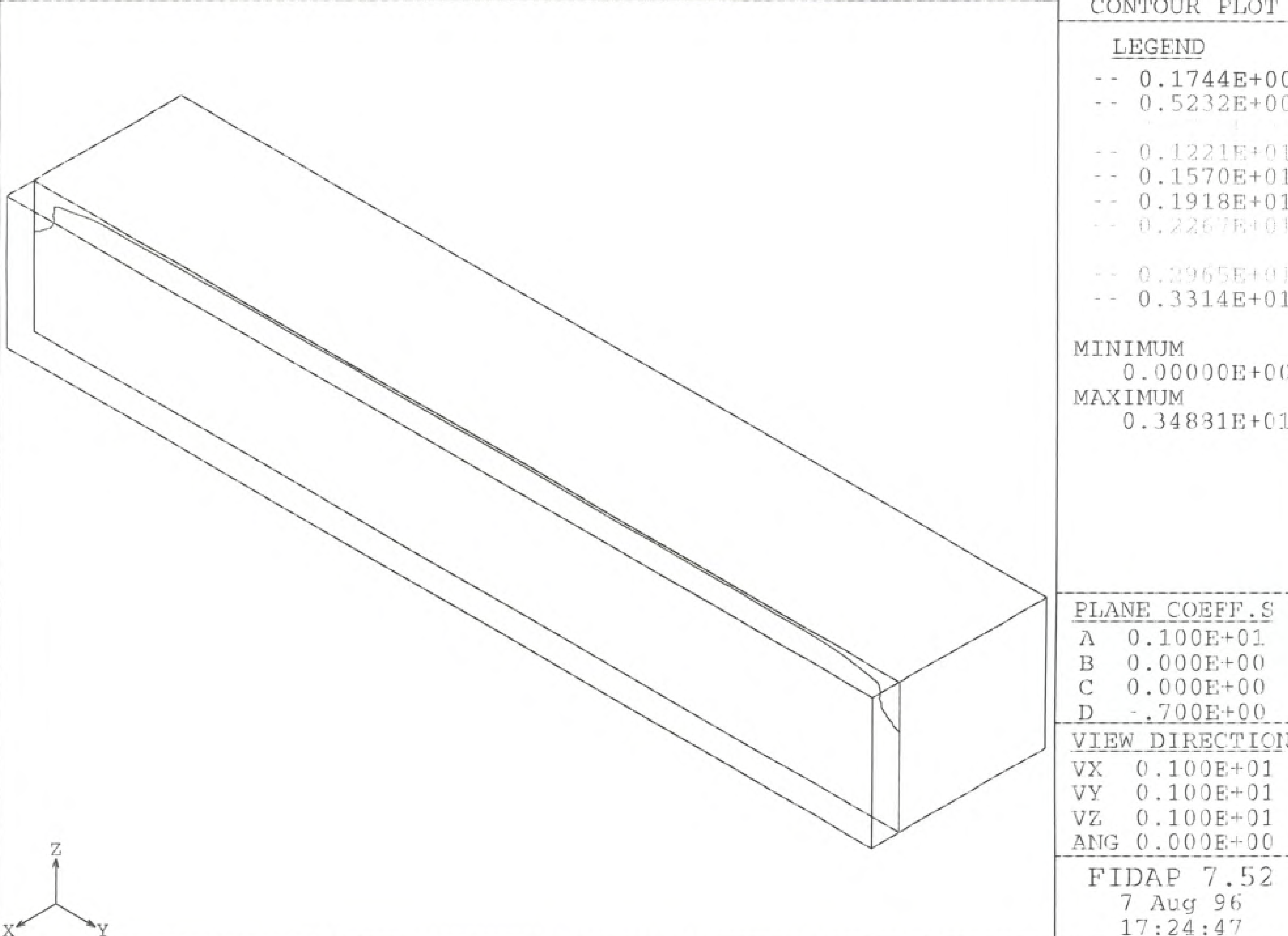

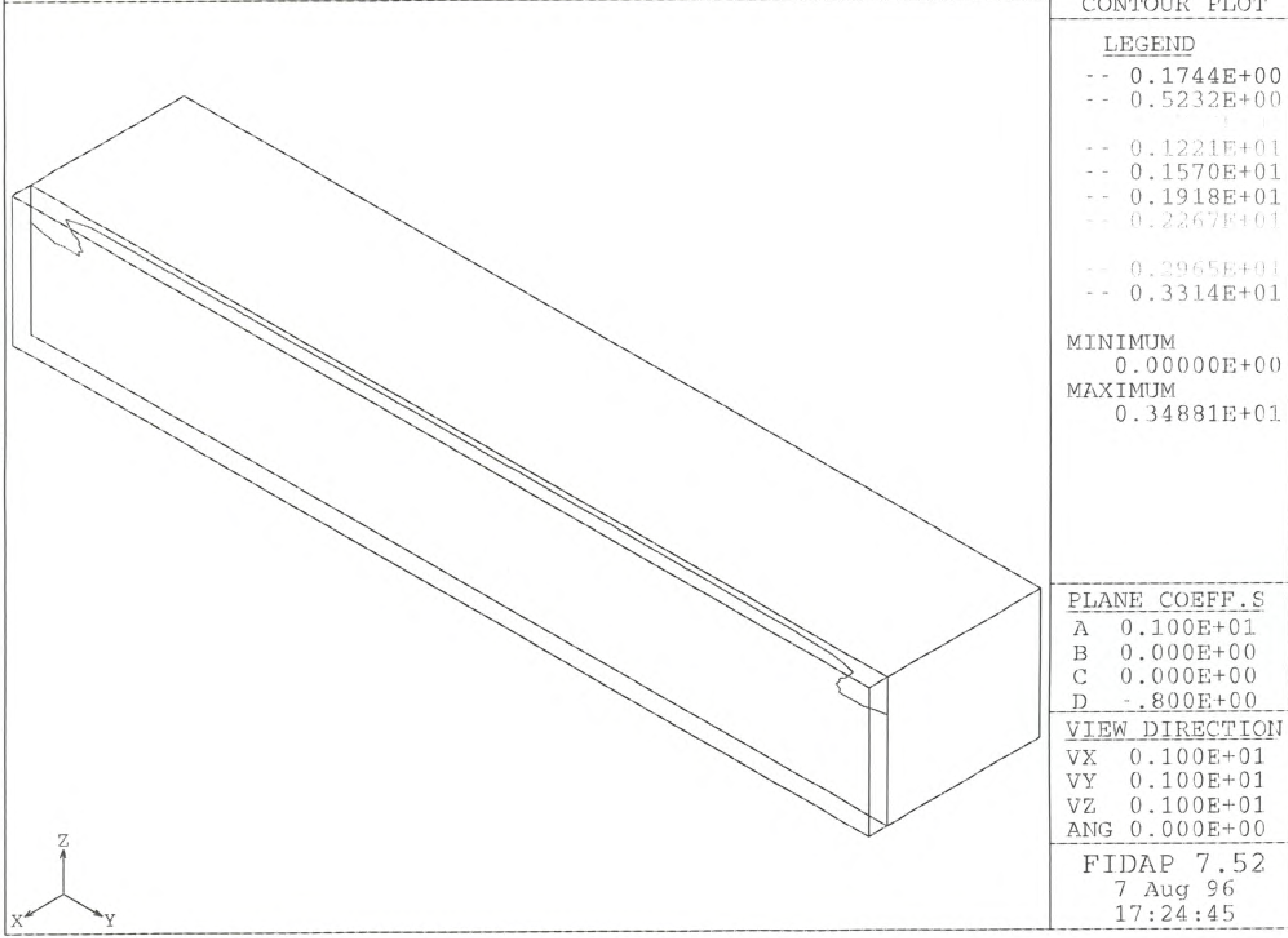


FIGURE 5.49: SHEAR STRAIN RATE, LONG SECTION 9

FIGURE 5.50: SHEAR STRAIN RATE, LONG SECTION 10

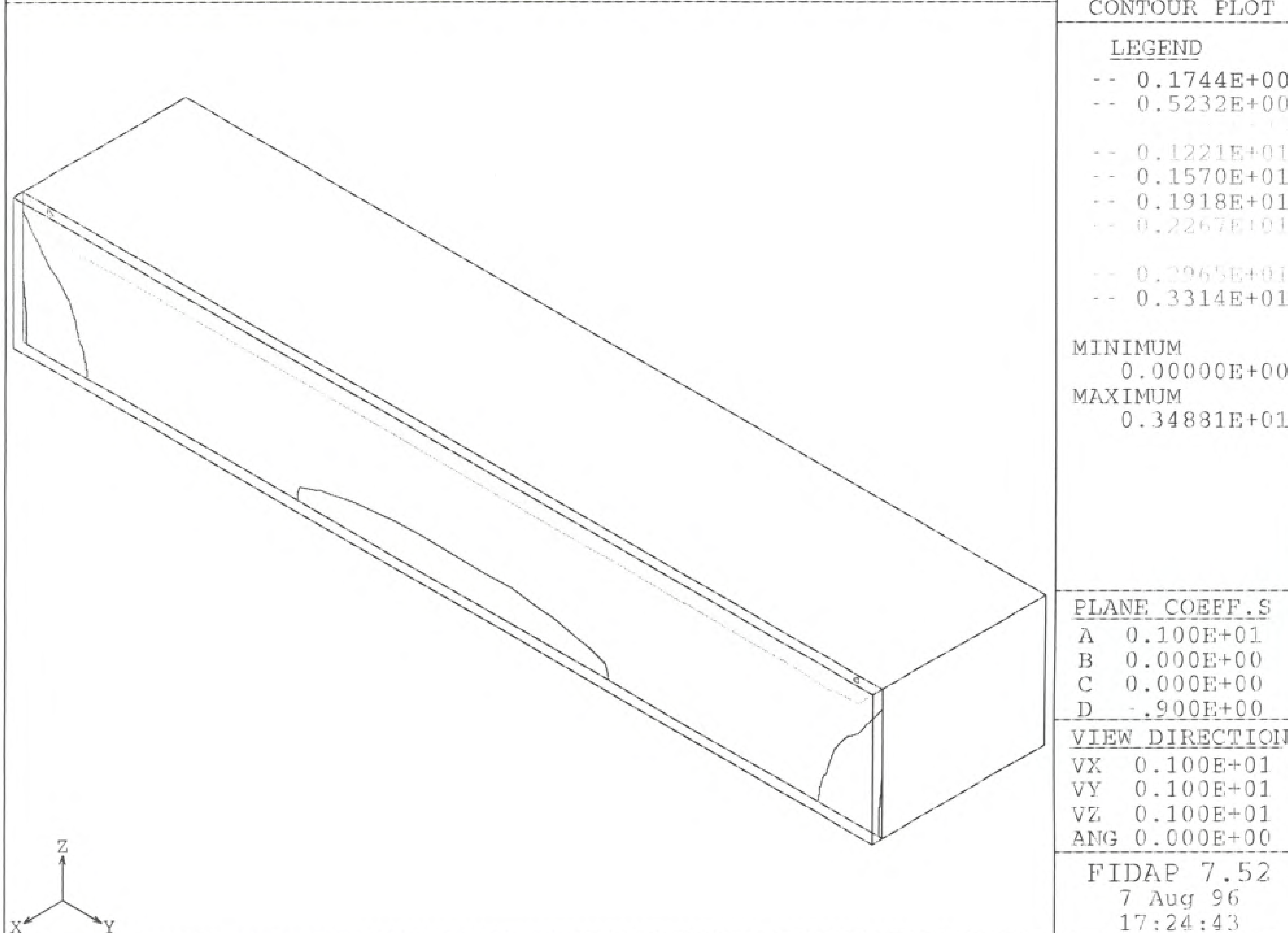

FIGURE 5.51: SHEAR STRAIN RATE, LONG SECTION 11

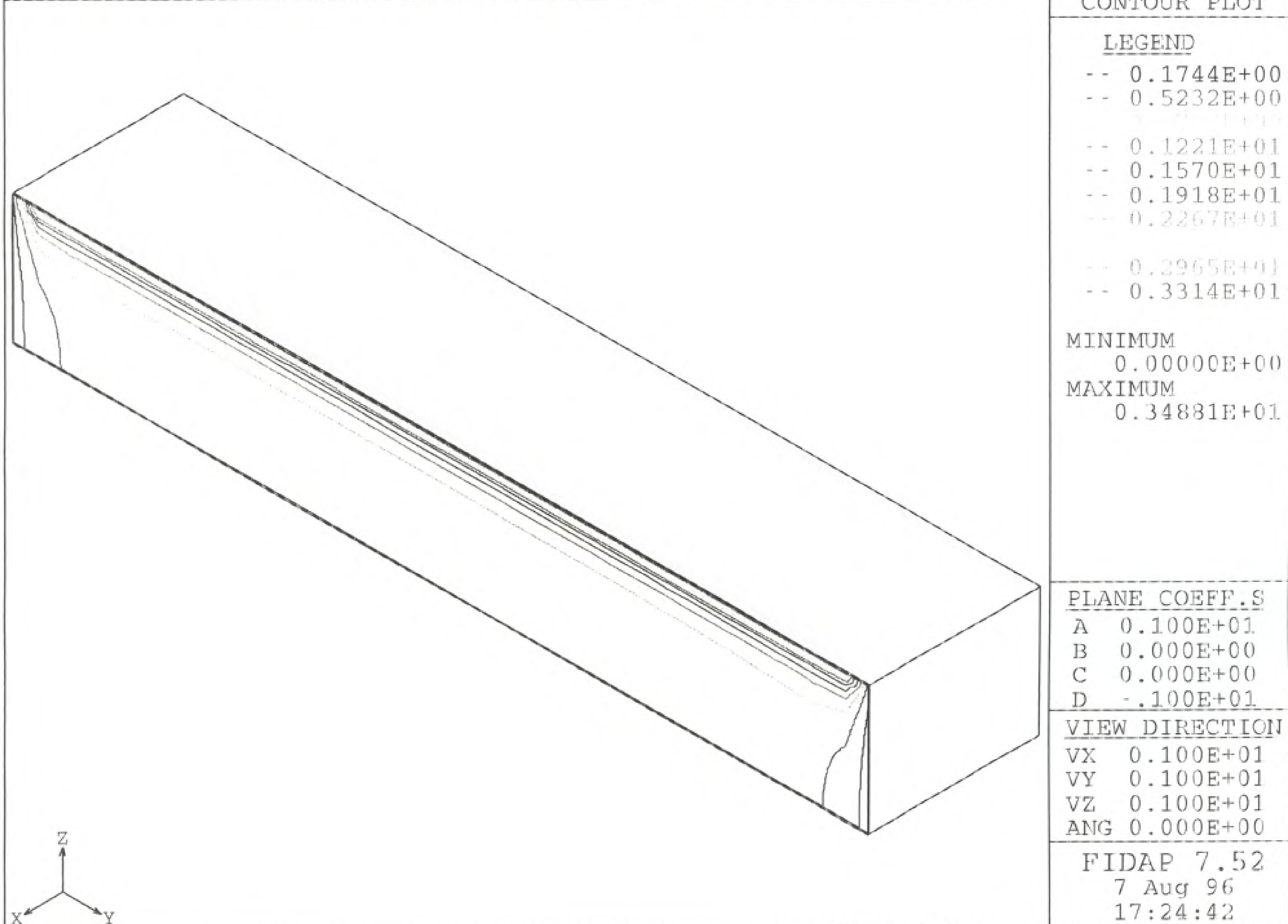

FIGURE 5.52: SHEAR STRAIN RATE, DOWNSTREAM SECTION 1

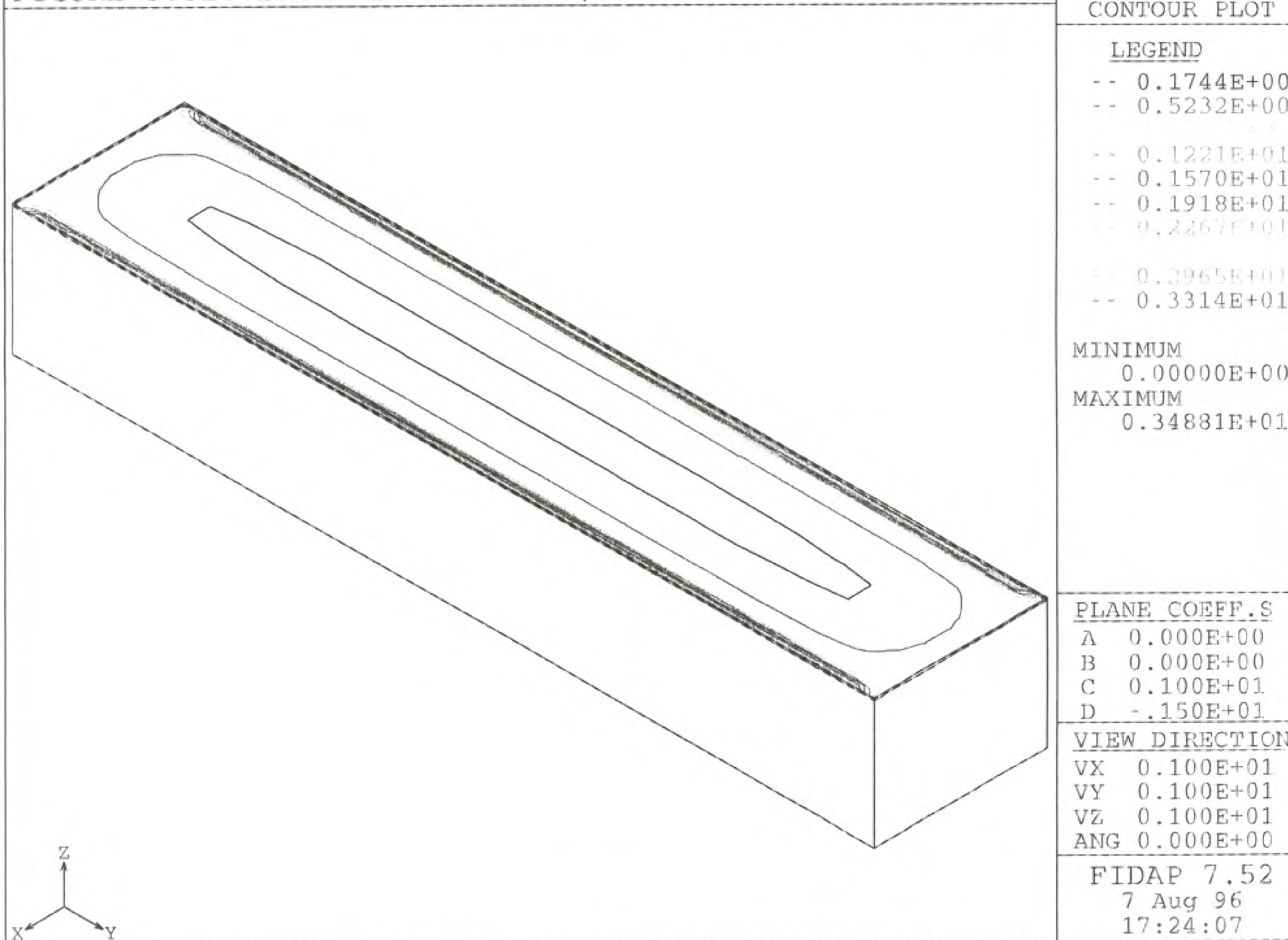

FIGURE 5.53: SHEAR STRAIN RATE, DOWNSTREAM SECTION 2

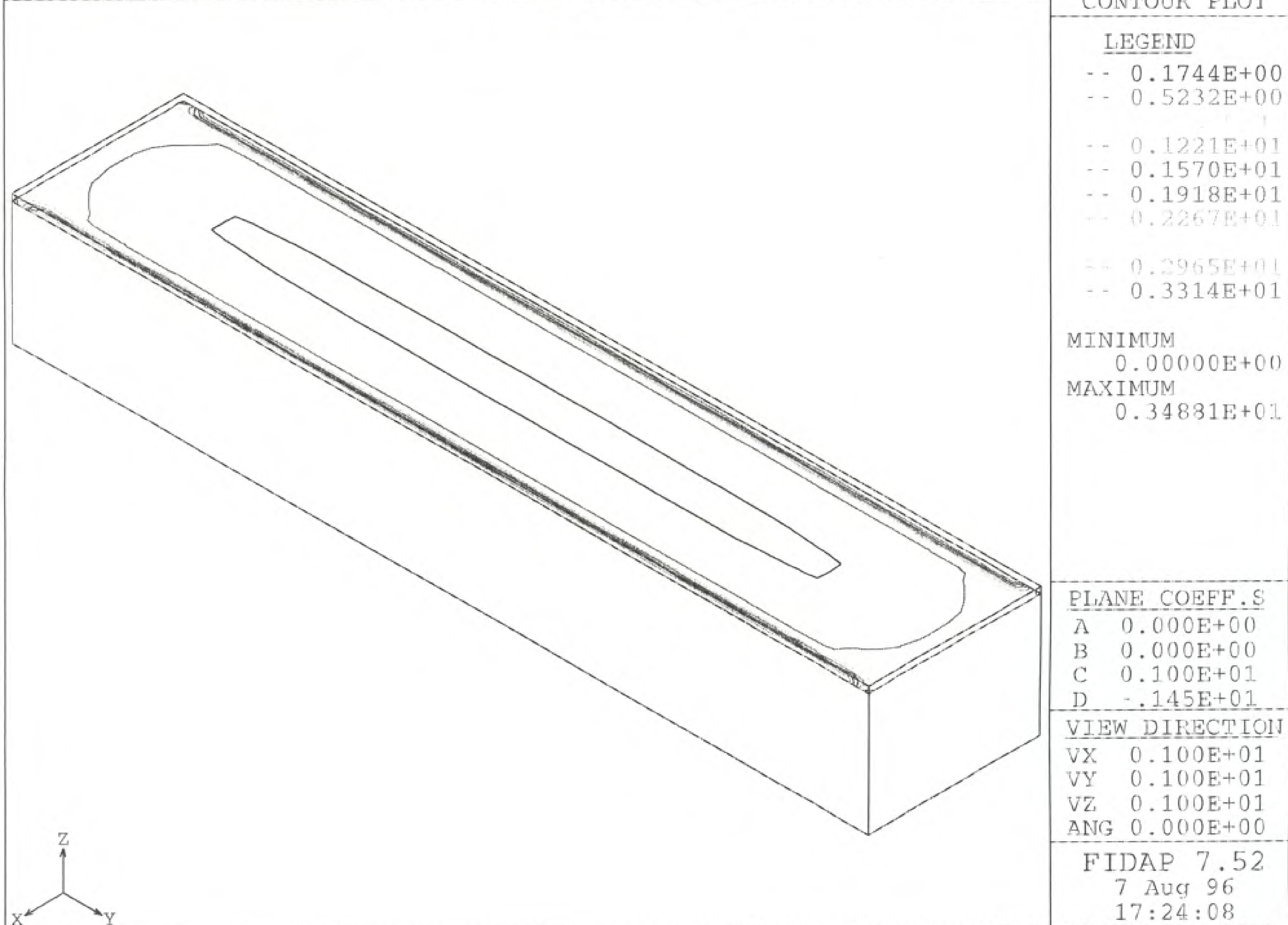

FIGURE 5.54: SHEAR STRAIN RATE, DOWNSTREAM SECTION 3

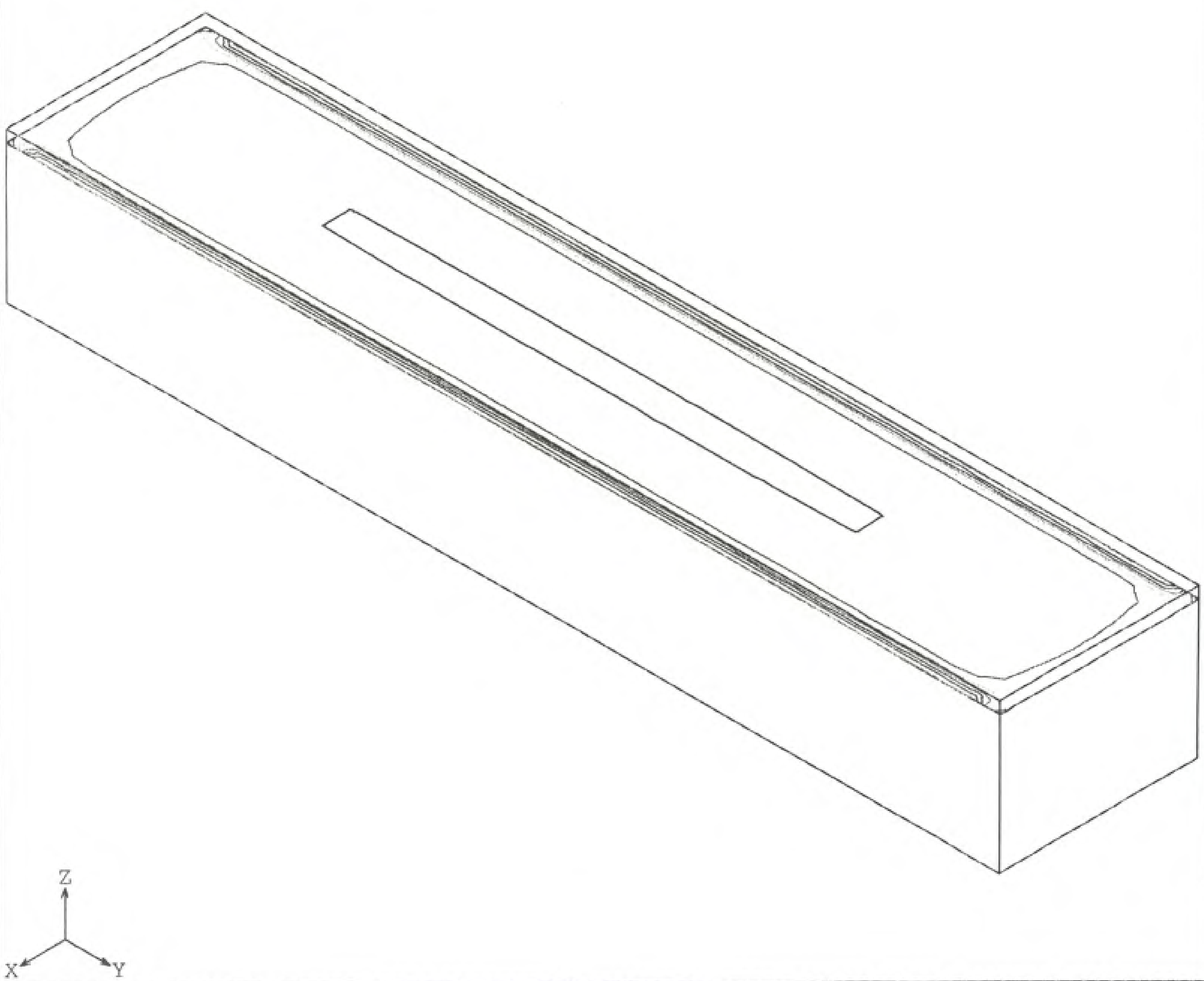

FIGURE 5.55: SHEAR STRAIN RATE, DOWNSTREAM SECTION 4

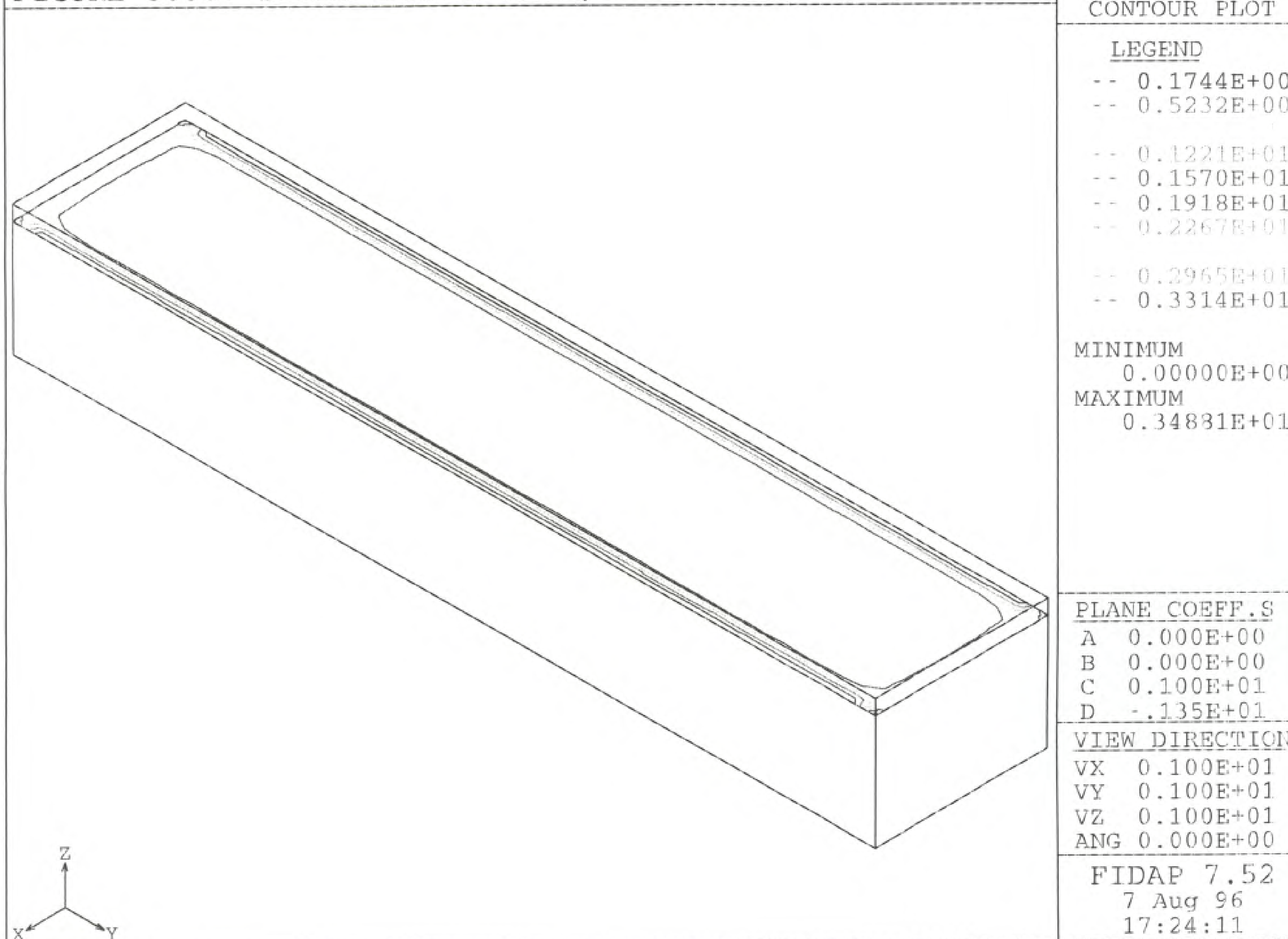

FIGURE 5.56:SHEAR STRAIN RATE, DOWNSTREAM SECTION 5

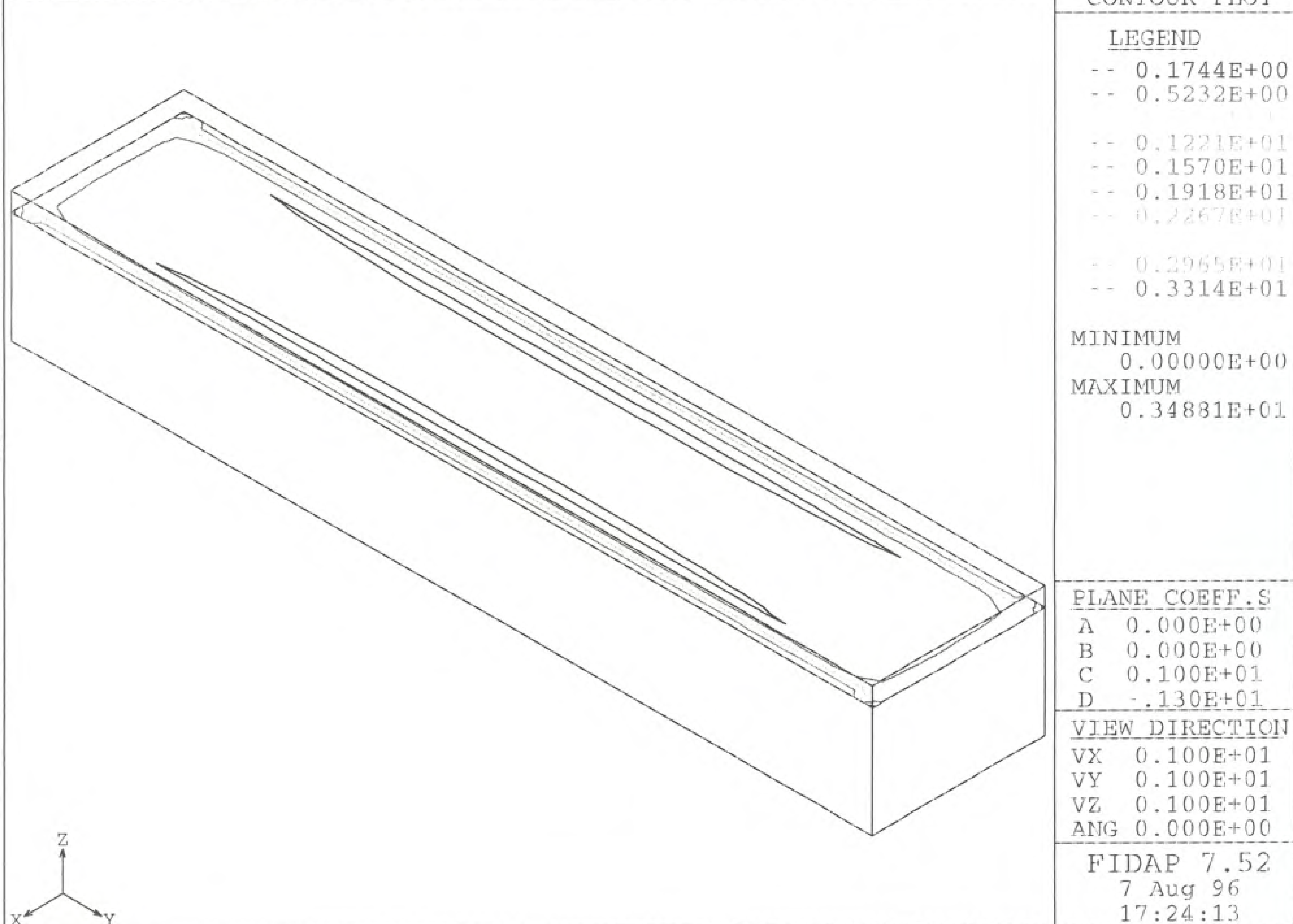

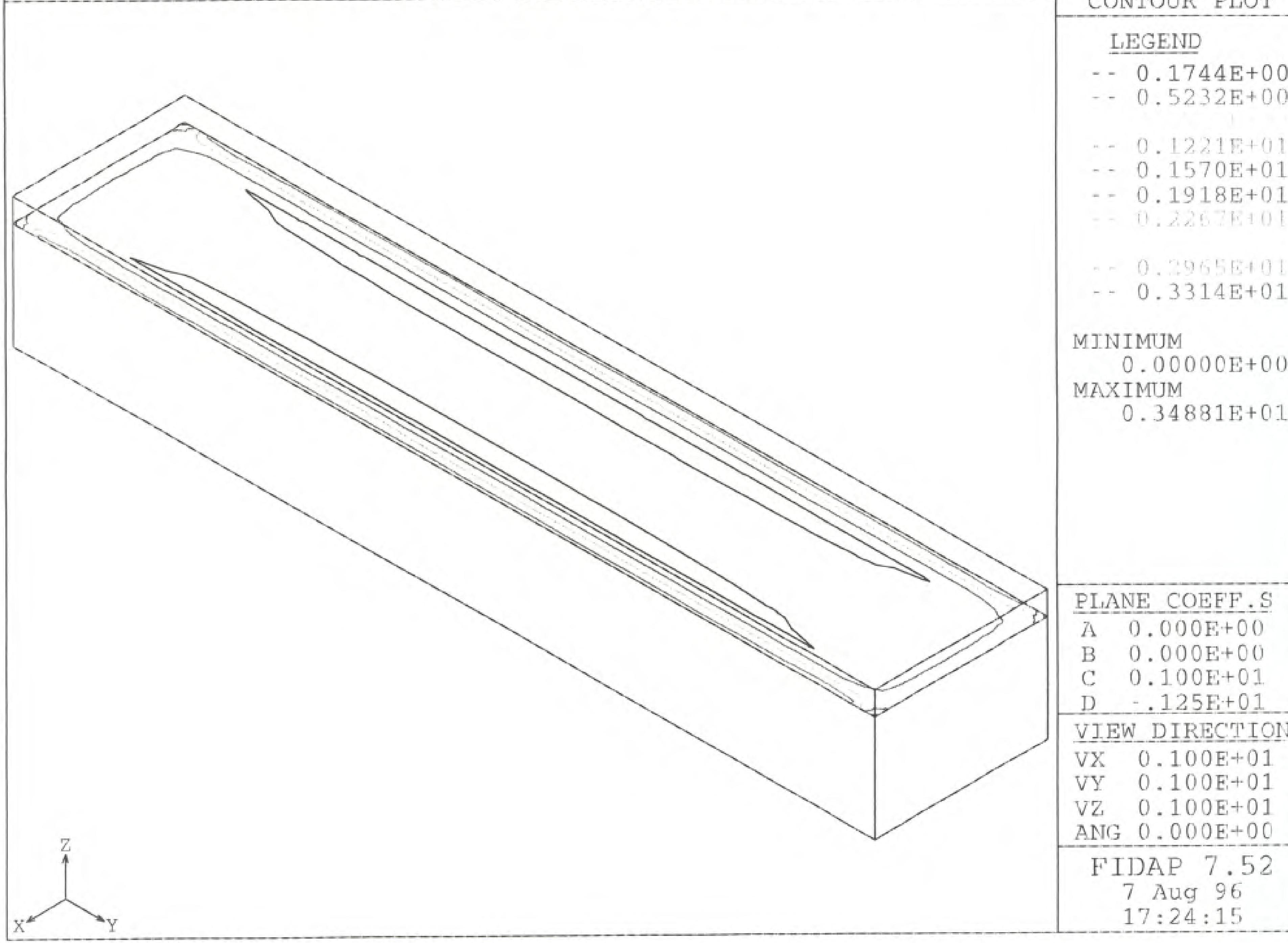


FIGURE 5.57: SHEAR STRAIN RATE, DOWNSTREAM SECTION 6

FIGURE 5.58: SHEAR STRAIN RATE, DOWNSTREAM SECTION 7

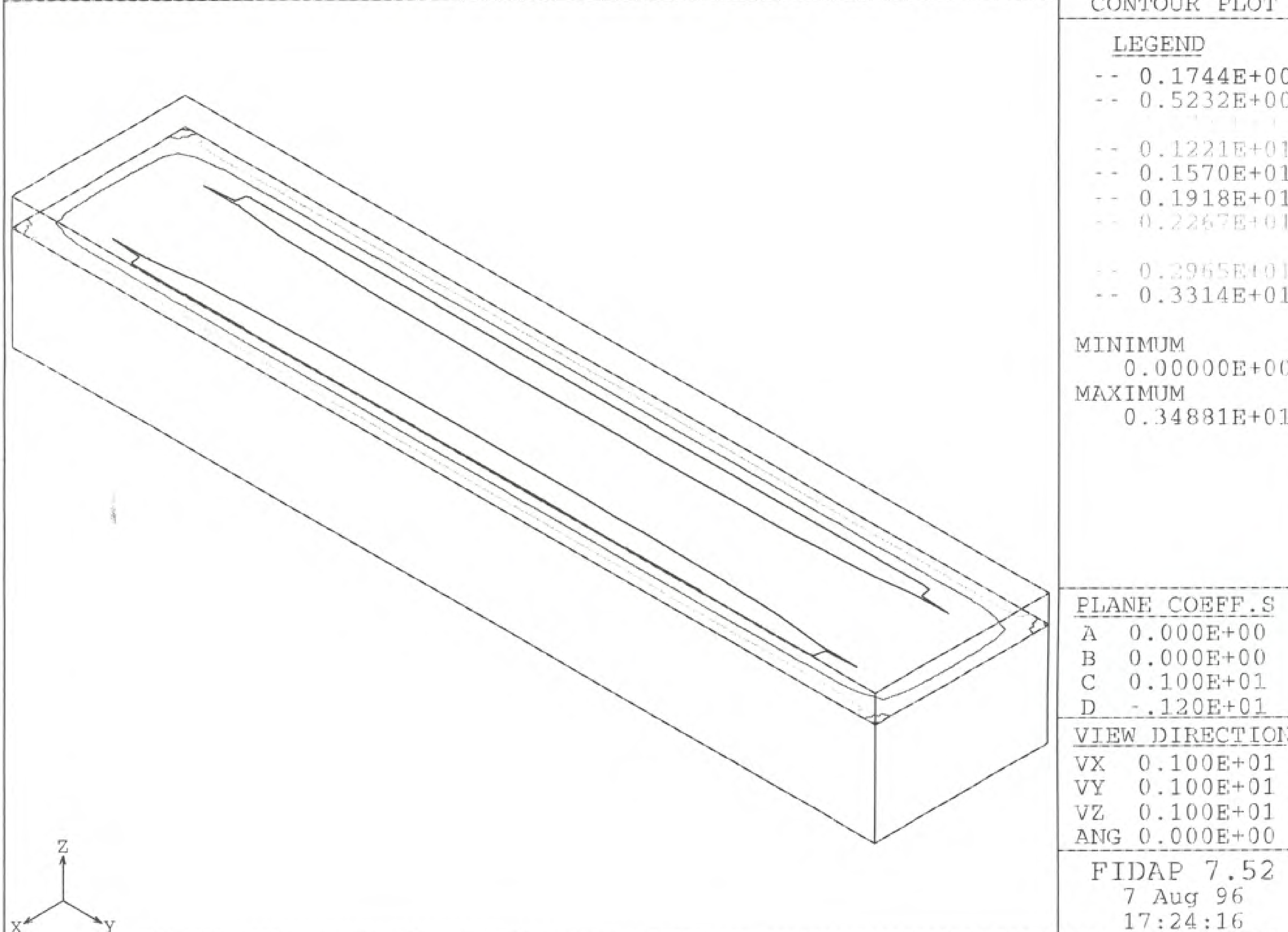

FIGURE 5.59: SHEAR STRAIN RATE, DOWNSTREAM SECTION 8

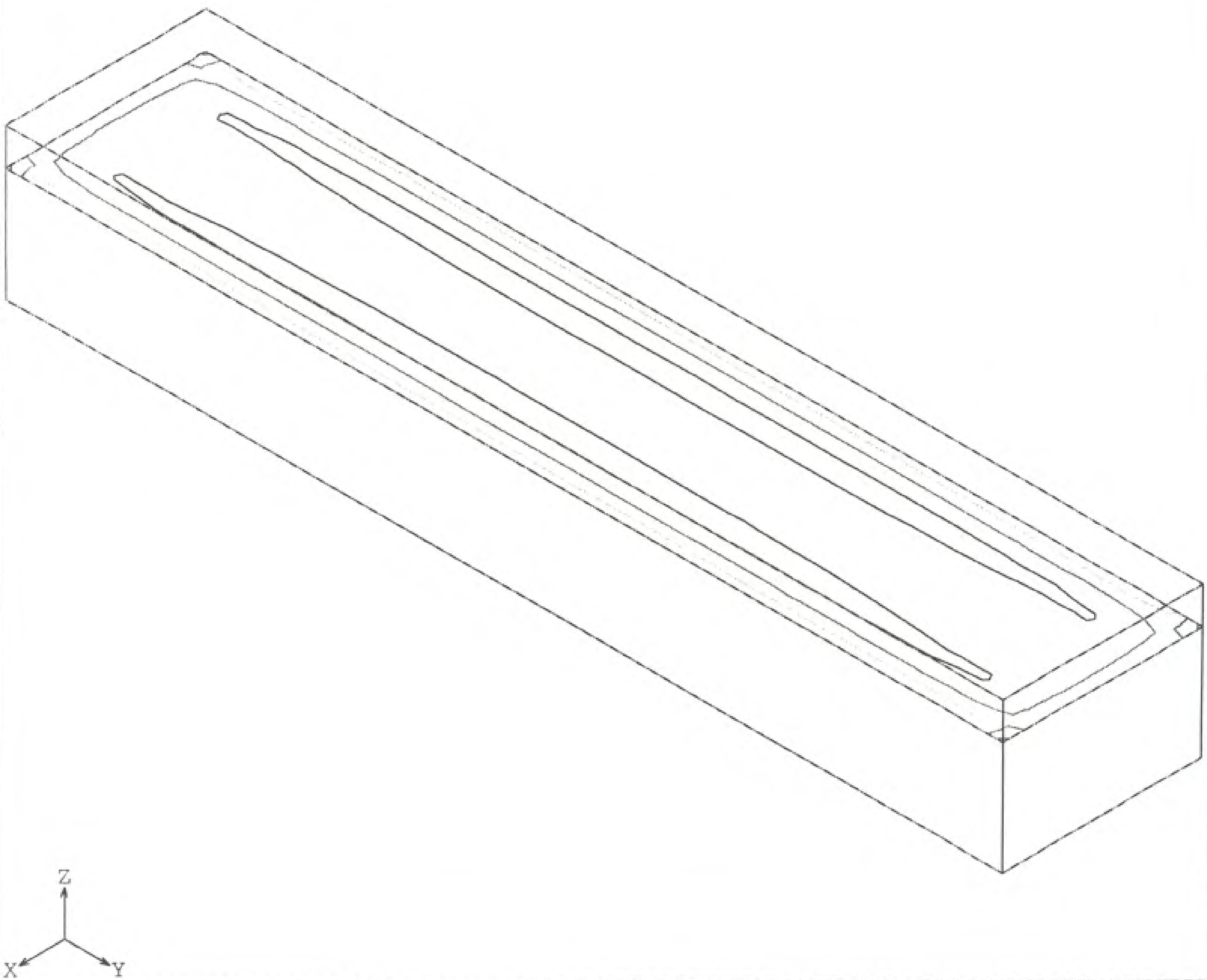


SHEAR RATE
CONTOUR PLOT

LEGEND
-- 0.1744E+00
-- 0.5232E+00

-- 0.1221E+01
-- 0.1570E+01
-- 0.1918E+01
-- 0.2267E+01

-- 0.2965E+01
-- 0.3314E+01

MINIMUM
0.00000E+00
MAXIMUM
0.34881E+01

PLANE COEFF.S
A 0.000E+00
B 0.000E+00
C 0.100E+01
D -.115E+01

VIEW DIRECTION
VX 0.100E+01
VY 0.100E+01
VZ 0.100E+01
ANG 0.000E+00

FIDAP 7.52
7 Aug 96
17:24:18

FIGURE 5.60: SHEAR STRAIN RATE, DOWNSTREAM SECTION 9

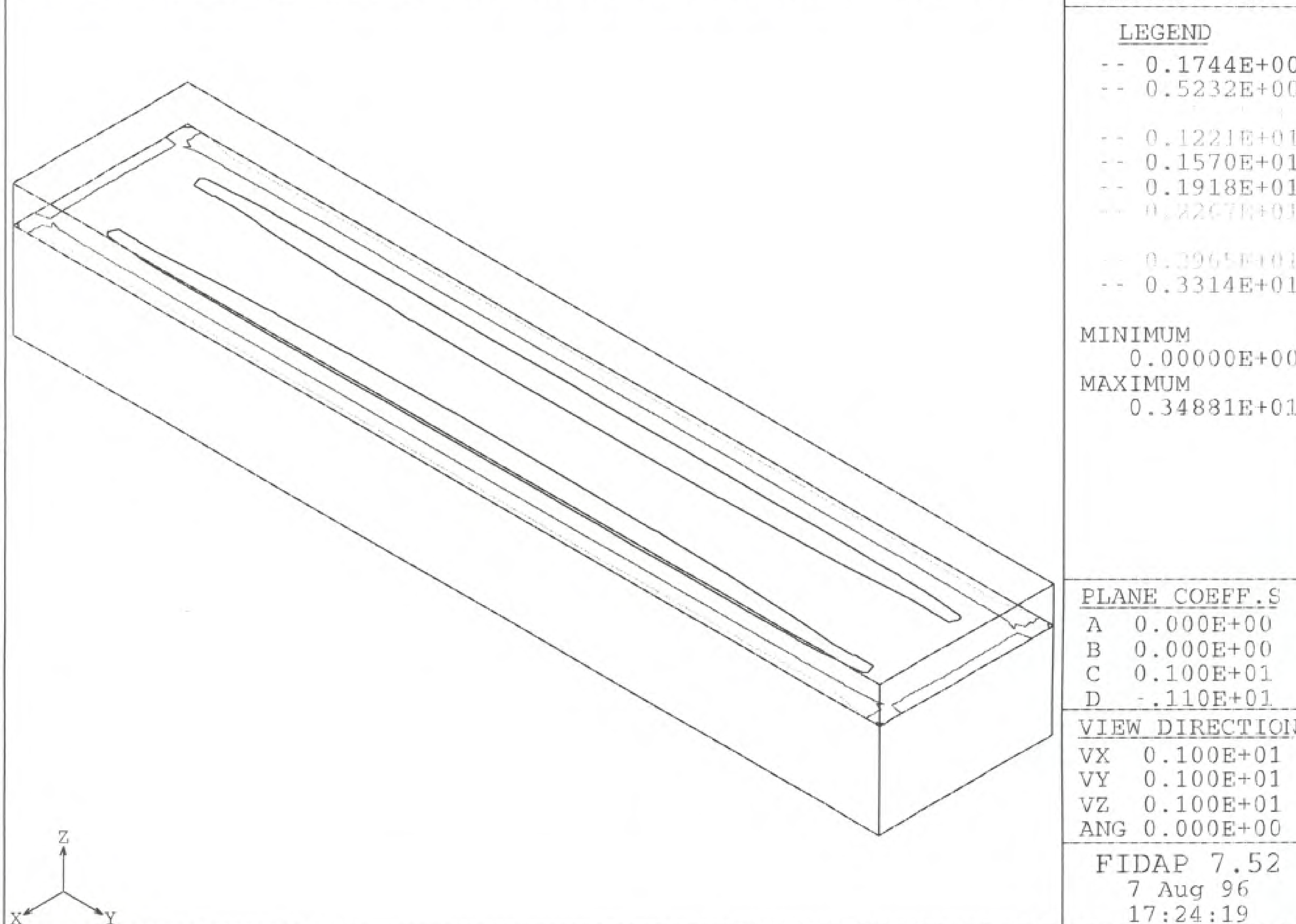

FIGURE 5.61: SHEAR STRAIN RATE, DOWNSTREAM SECTION 10

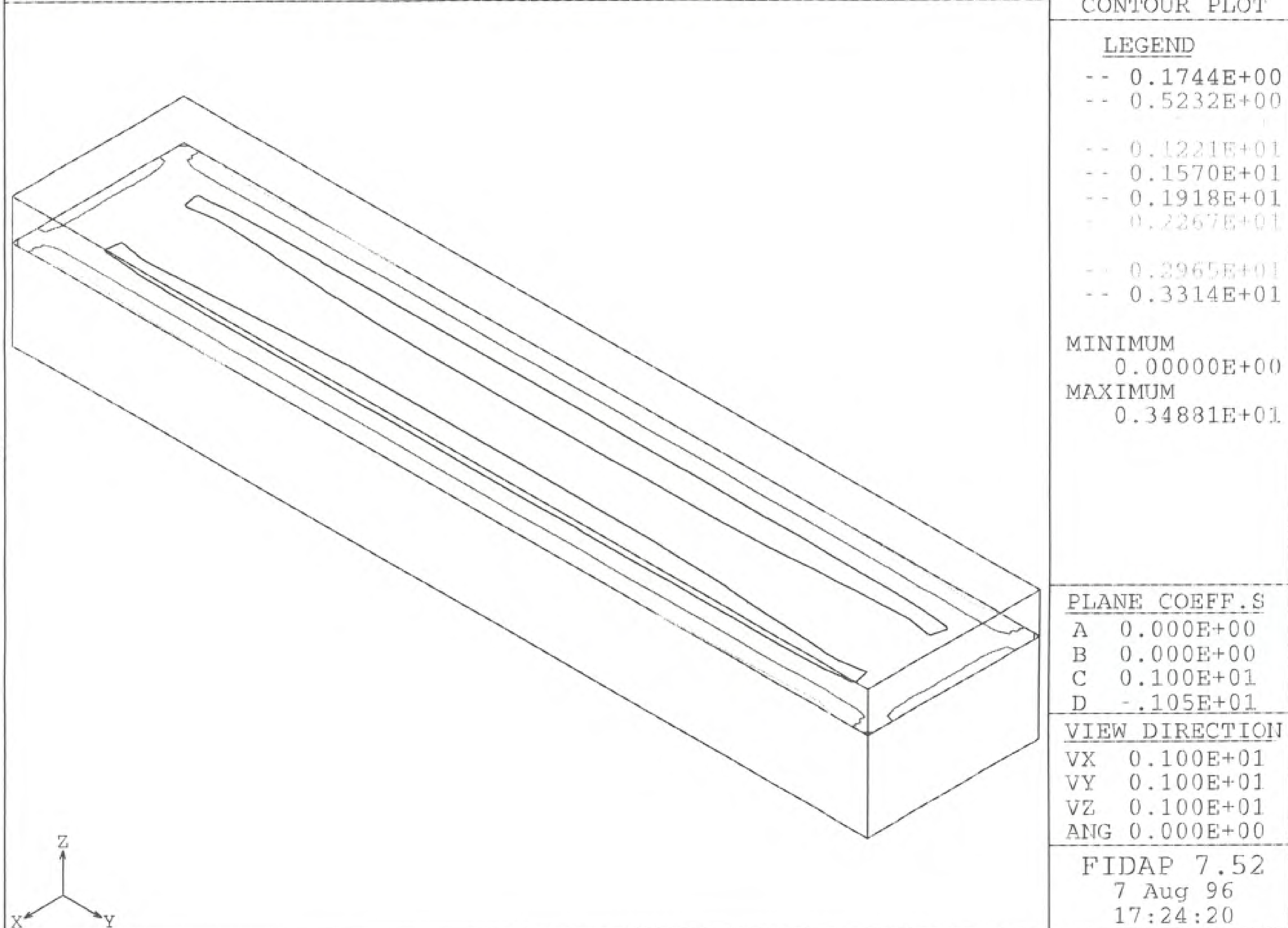

FIGURE 5.62: SHEAR STRAIN RATE, DOWNSTREAM SECTION 11

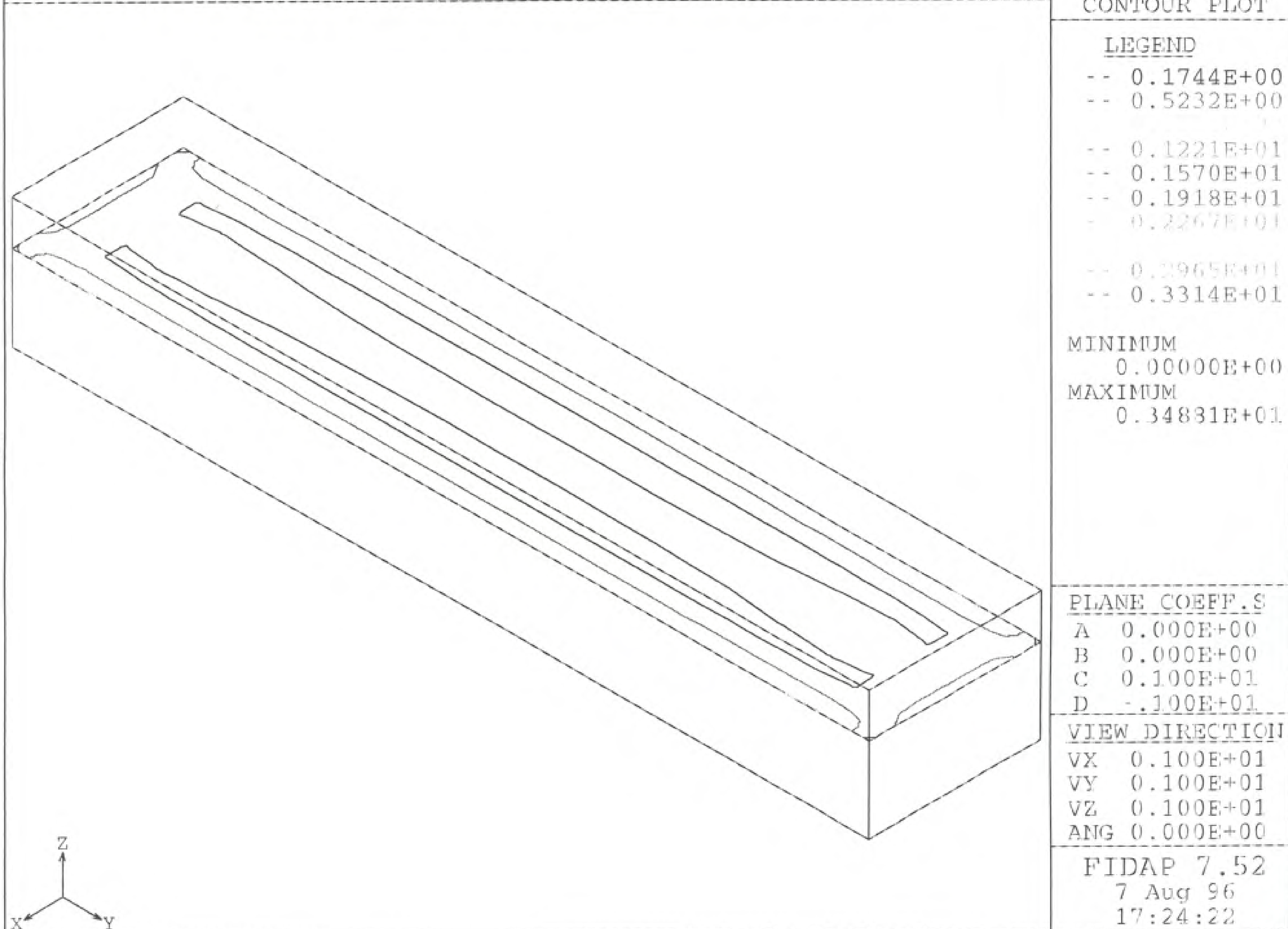

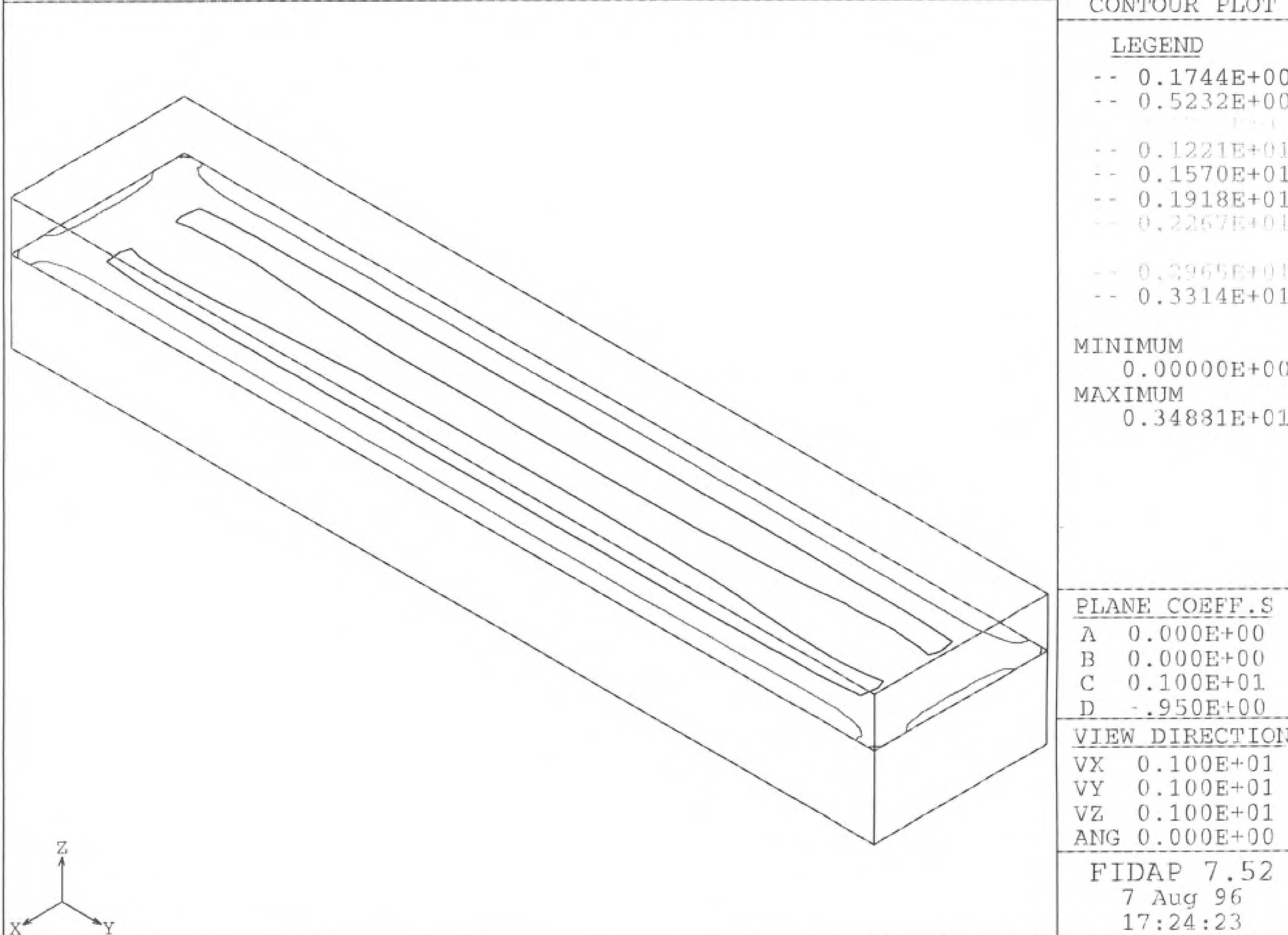


FIGURE 5.63: SHEAR STRAIN RATE, DOWNSTREAM SECTION 12

FIGURE 5.64: SHEAR STRAIN RATE, DOWNSTREAM SECTION 13

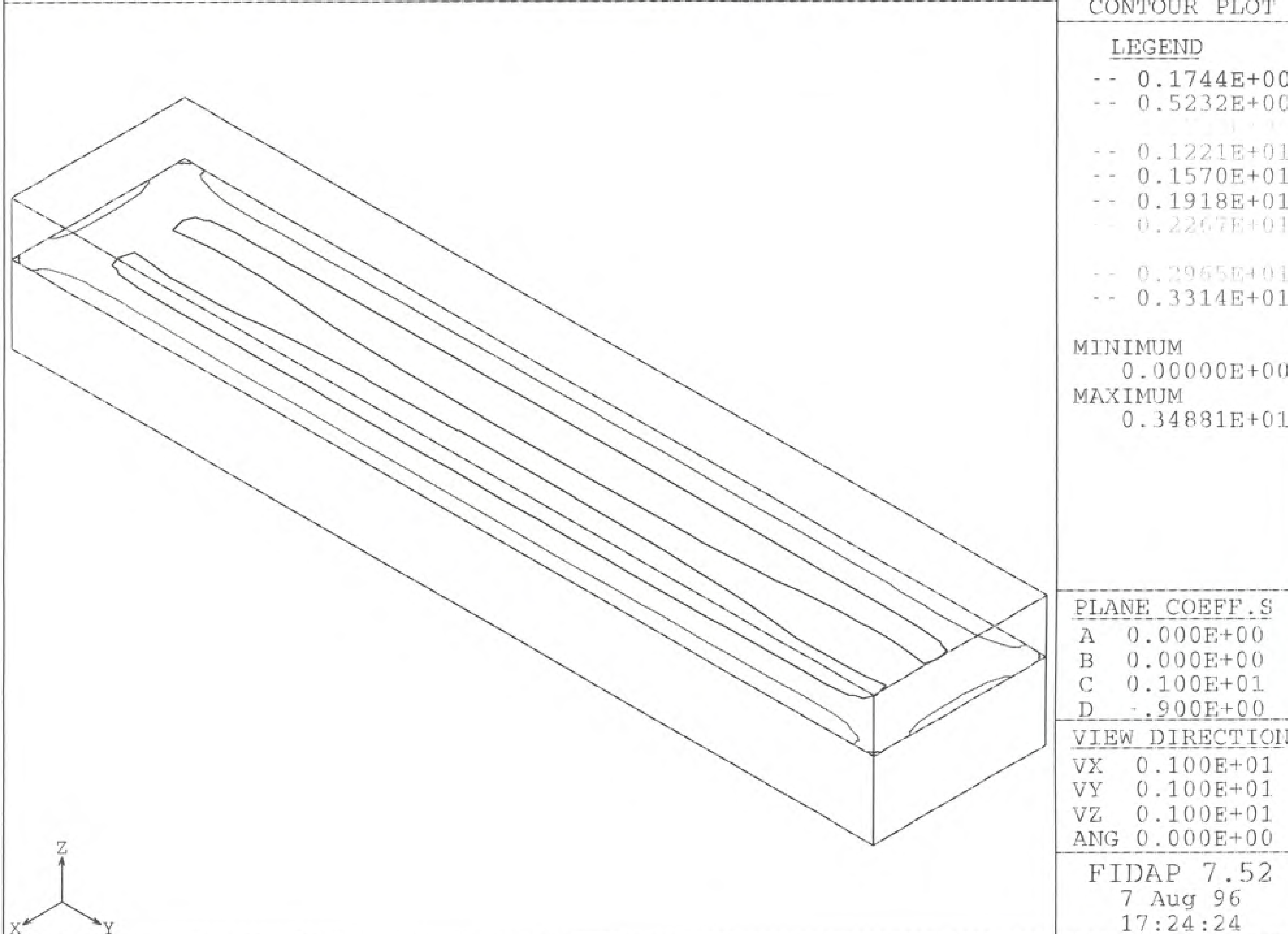

FIGURE 5.65: SHEAR STRAIN RATE, DOWNSTREAM SECTION 14

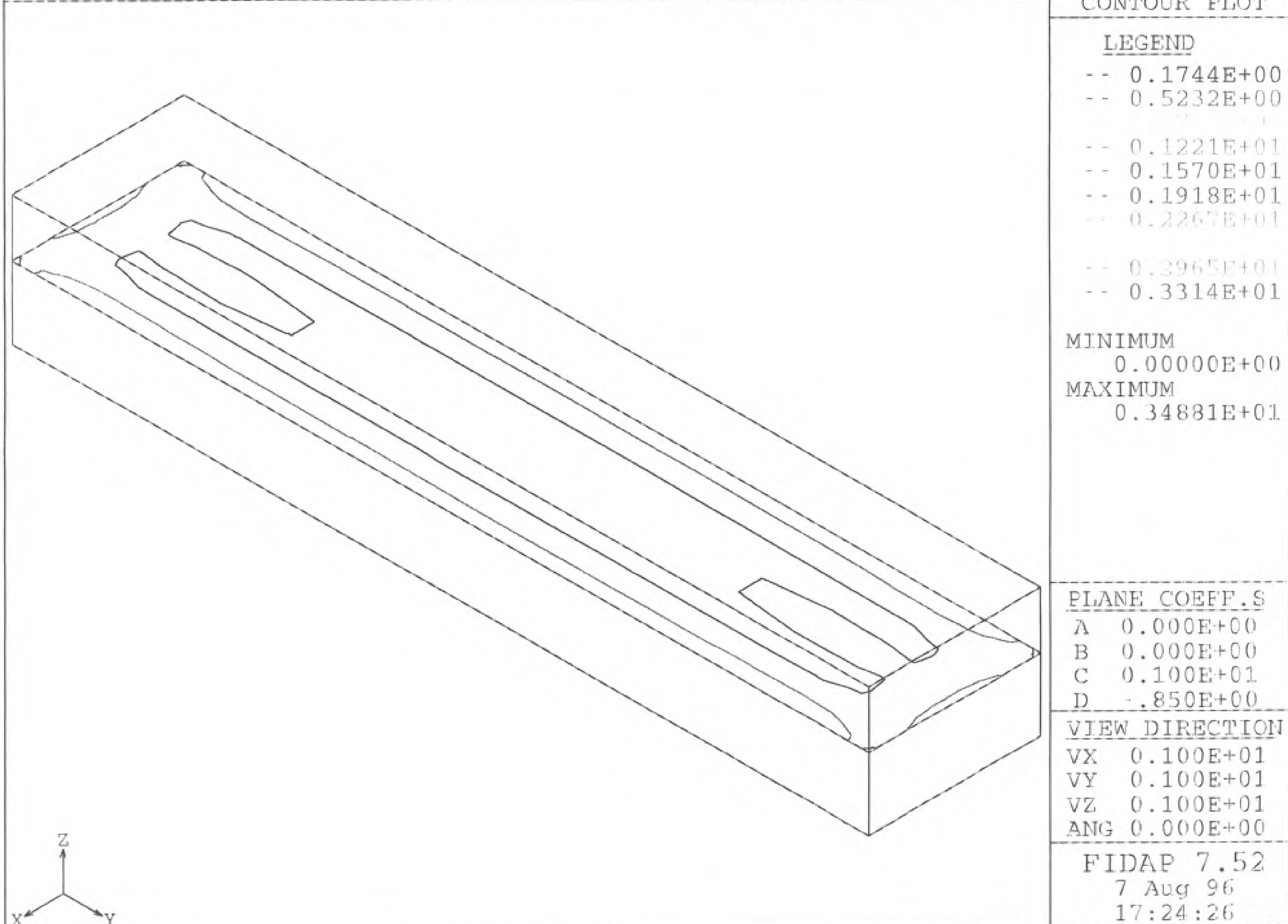

FIGURE 5.66: SHEAR STRAIN RATE, DOWNSTREAM SECTION 15

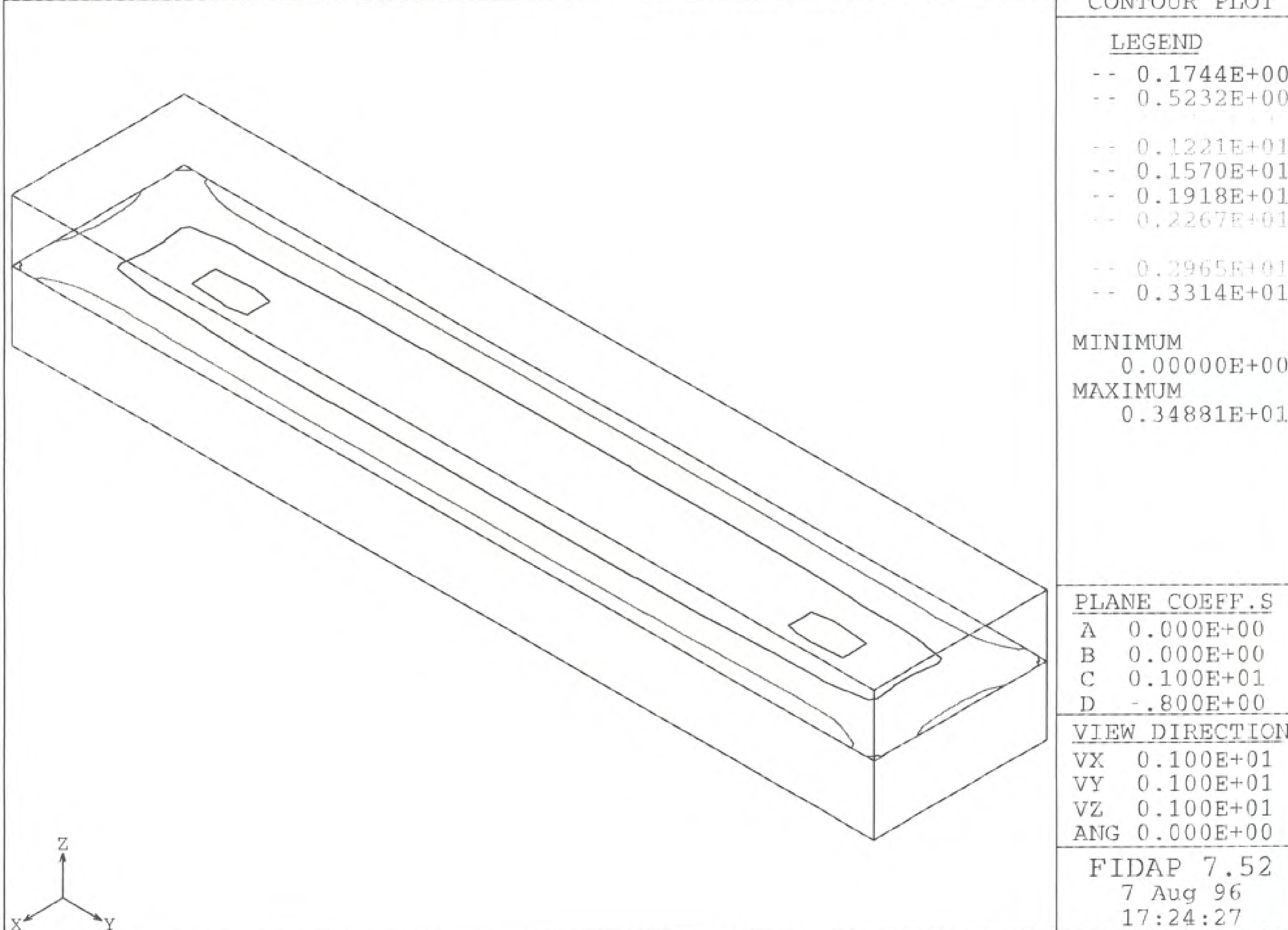

FIGURE 5.67: SHEAR STRAIN RATE, DOWNSTREAM SECTION 16

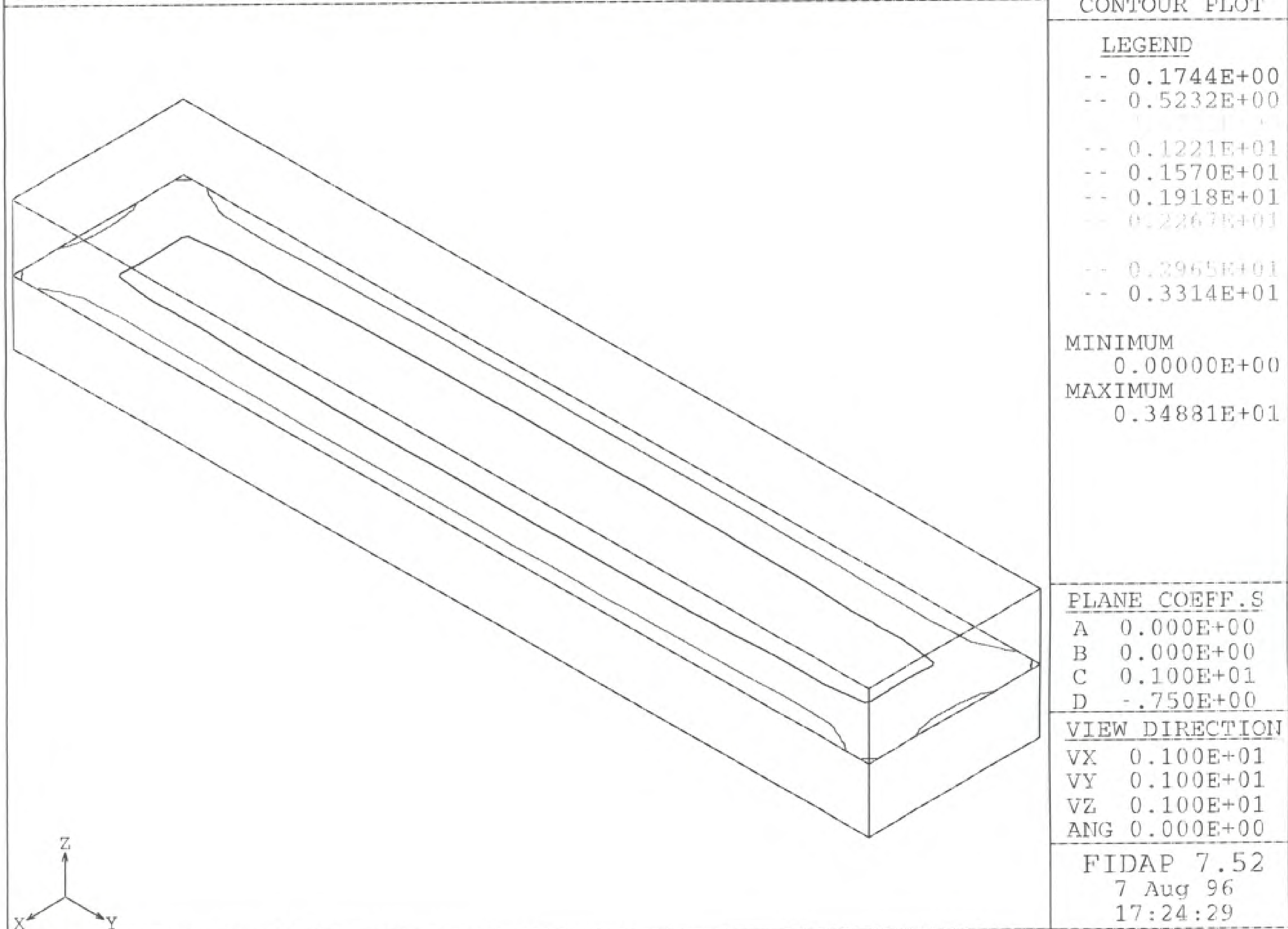

FIGURE 5.68: SHEAR STRAIN RATE, DOWNSTREAM SECTION 17

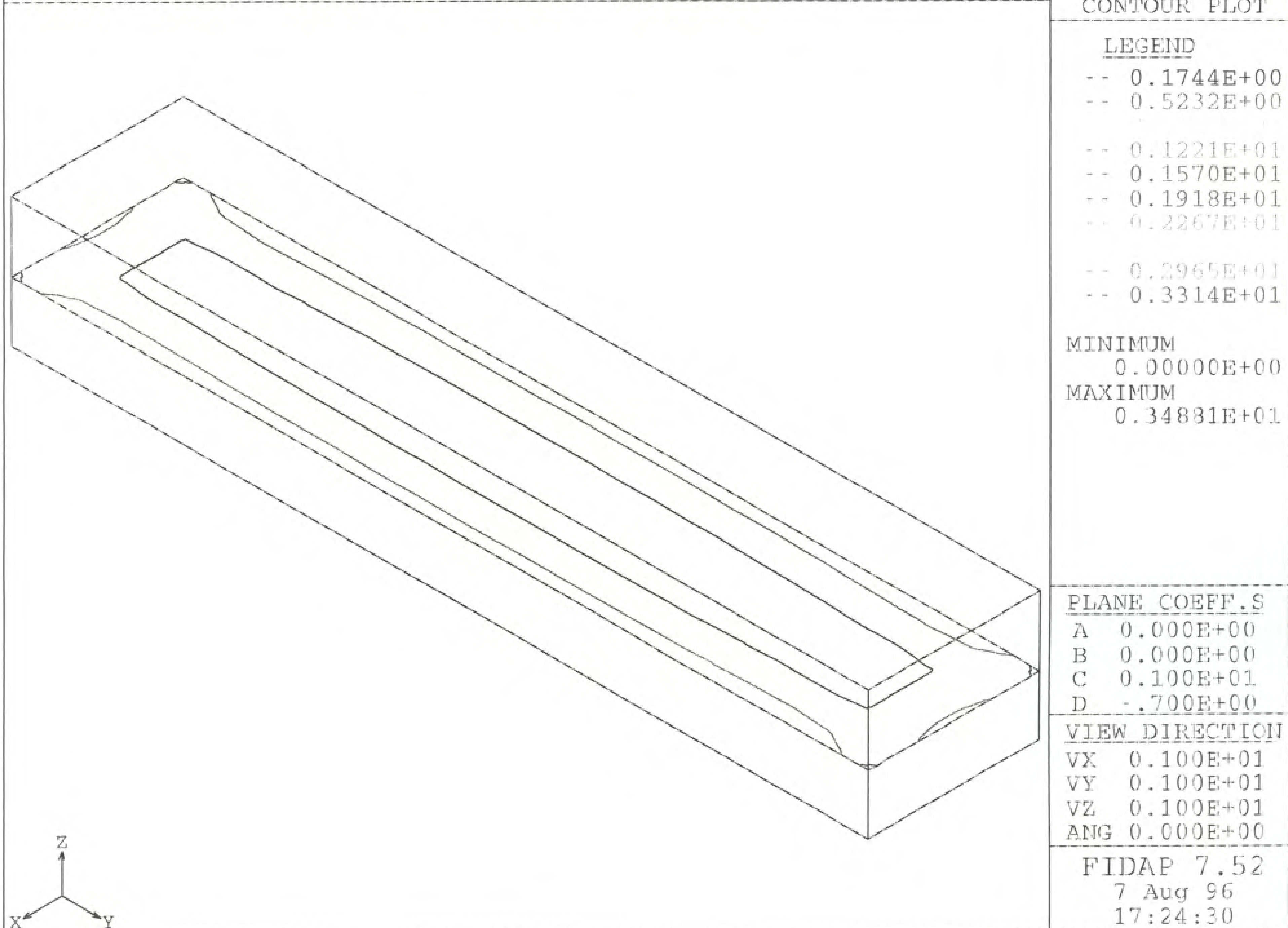

FIGURE 5.69: SHEAR STRAIN RATE, DOWNSTREAM SECTION 18

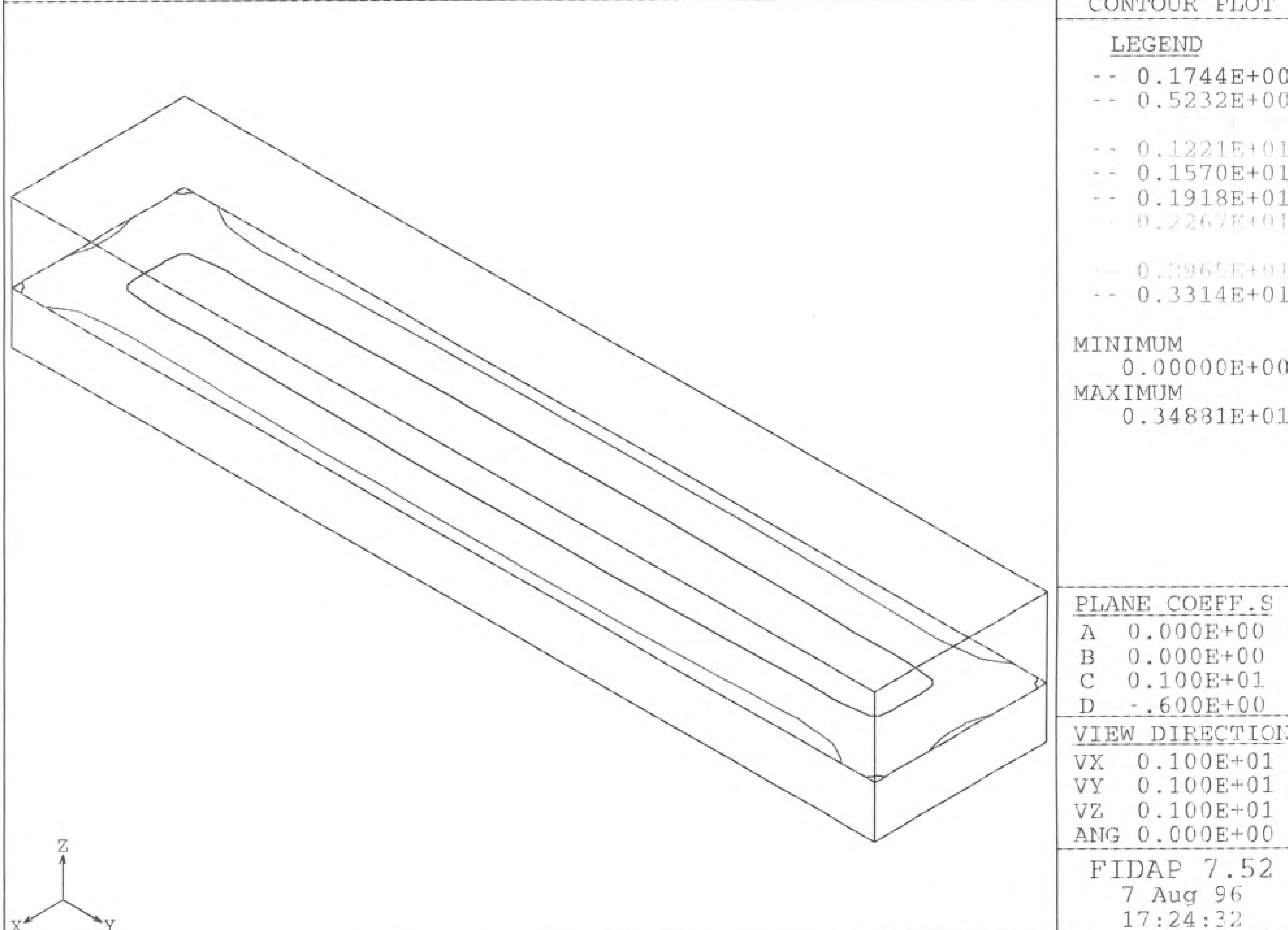

FIGURE 5.70: SHEAR STRAIN RATE, DOWNSTREAM SECTION 19

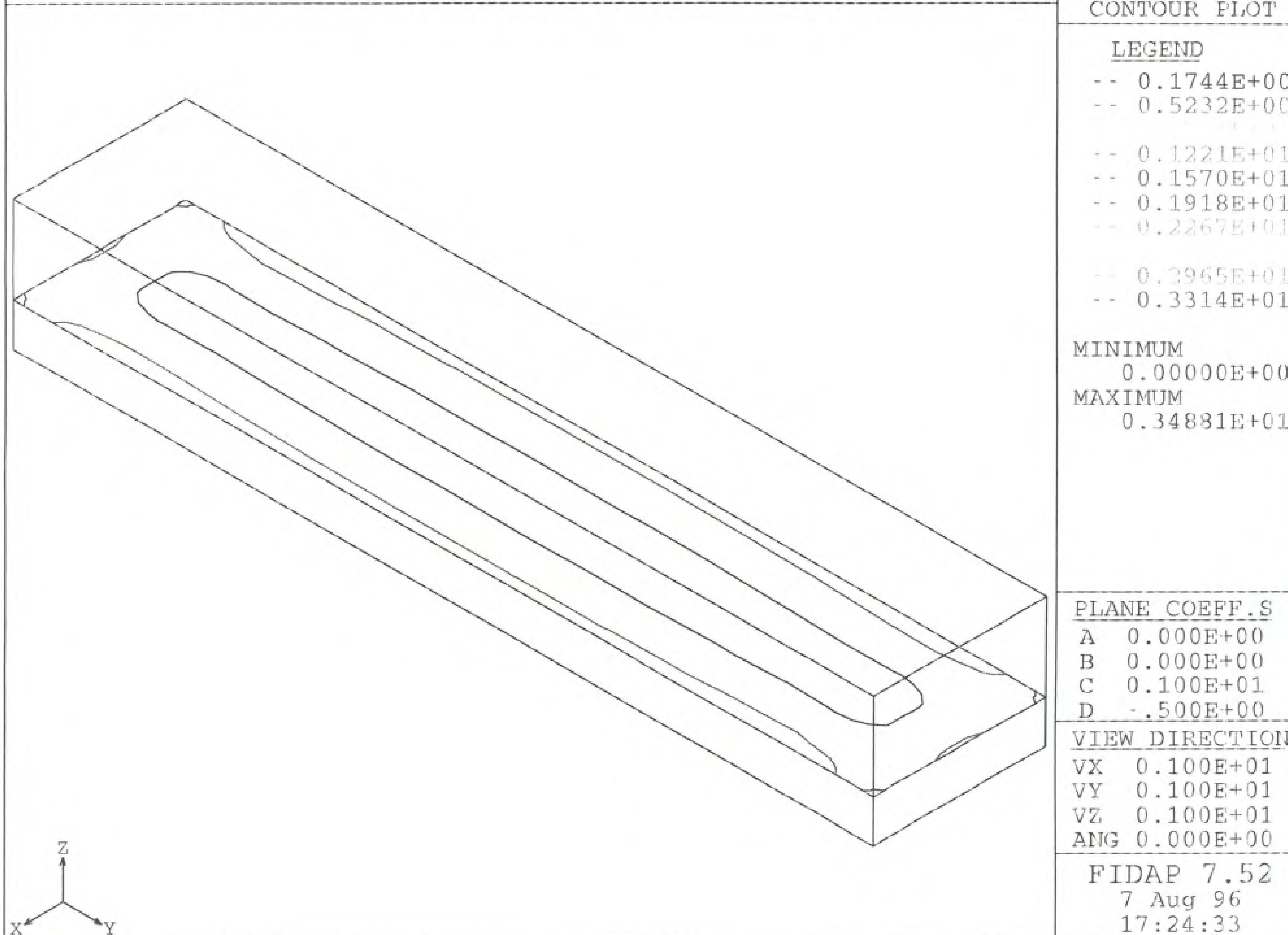

FIGURE 5.71: SHEAR STRAIN RATE, DOWNSTREAM SECTION 20

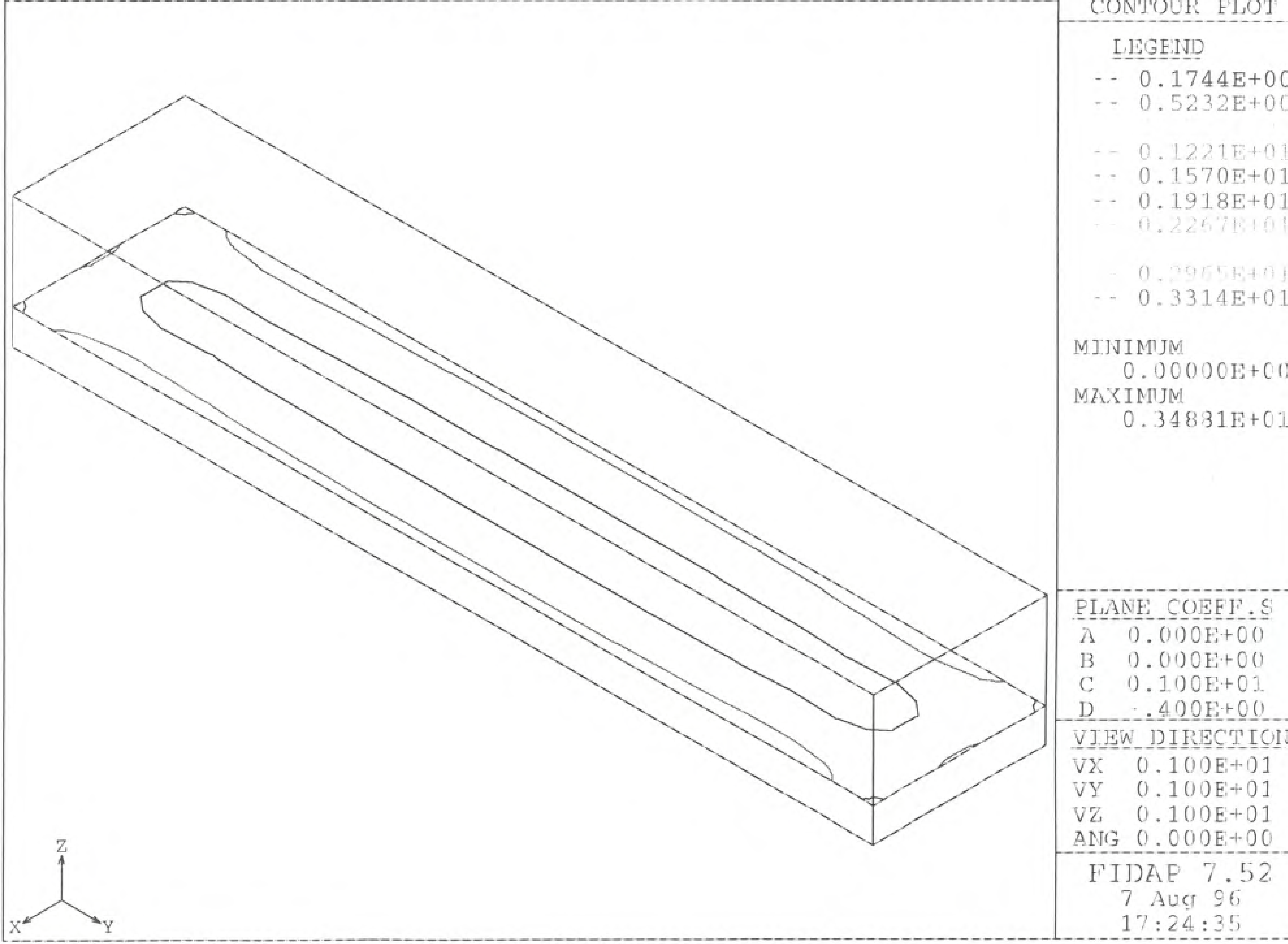

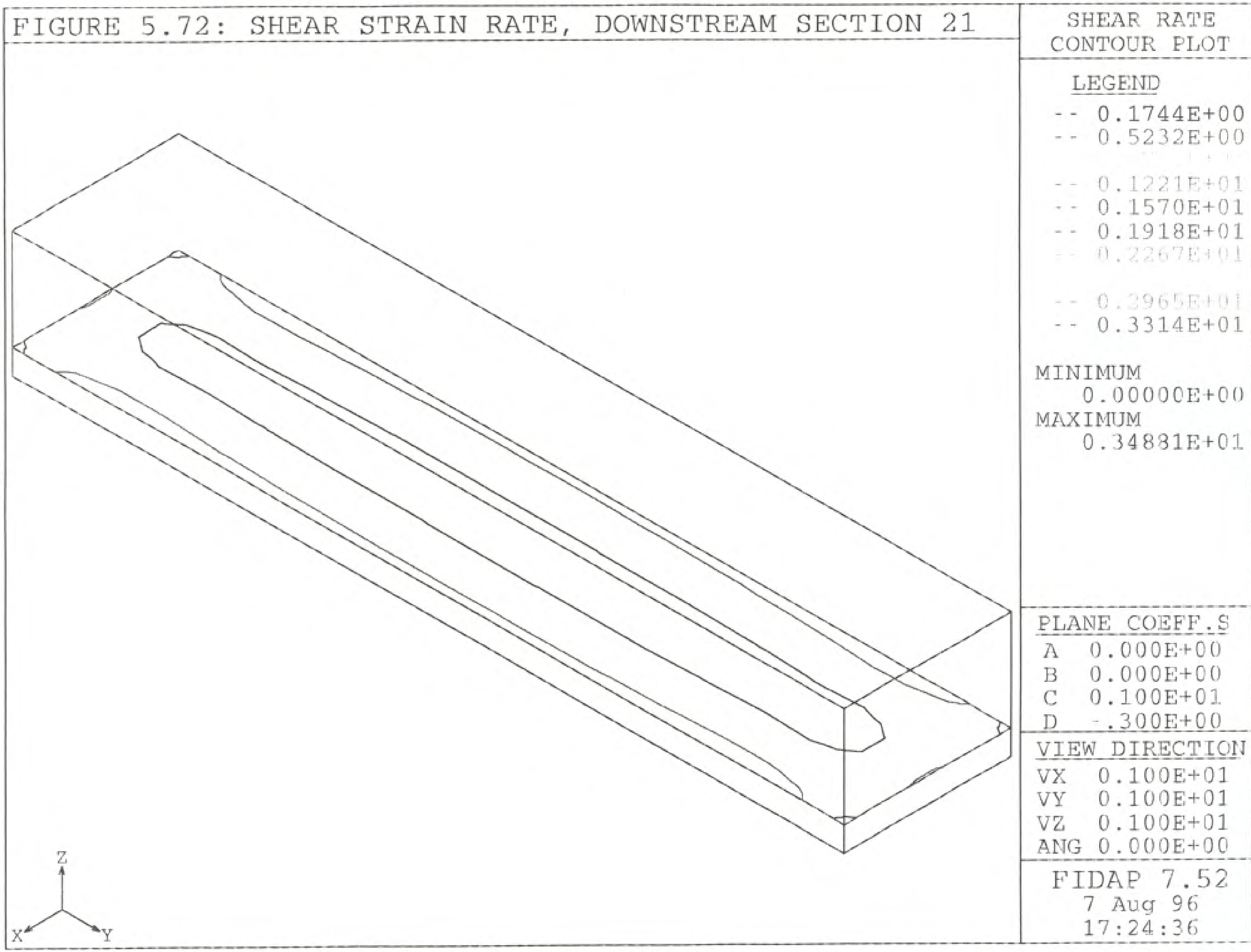


FIGURE 5.72: SHEAR STRAIN RATE, DOWNSTREAM SECTION 21

FIGURE 5.73: SHEAR STRAIN RATE, DOWNSTREAM SECTION 22

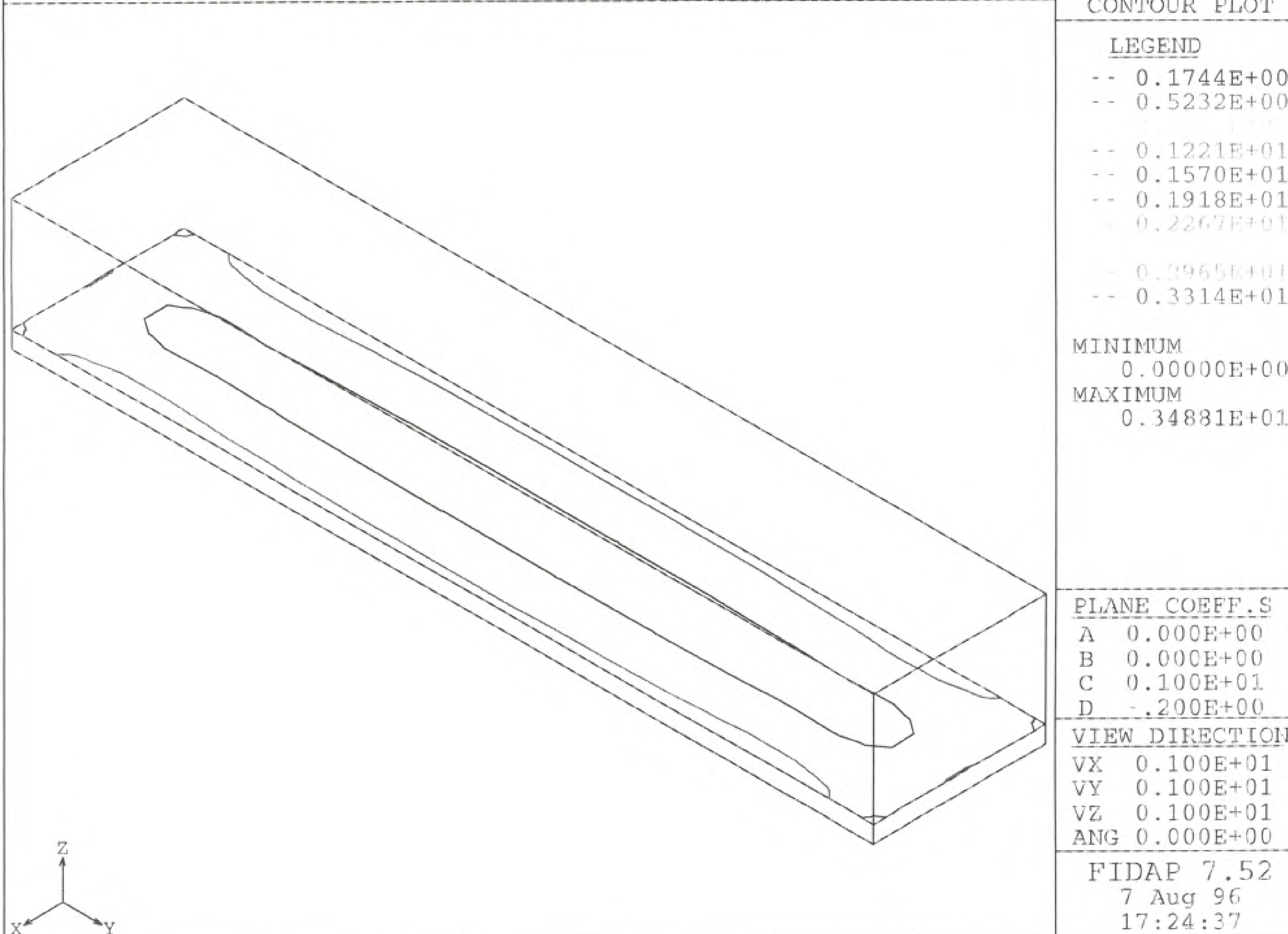

FIGURE 5.74: SHEAR STRAIN RATE, DOWNSTREAM SECTION 23

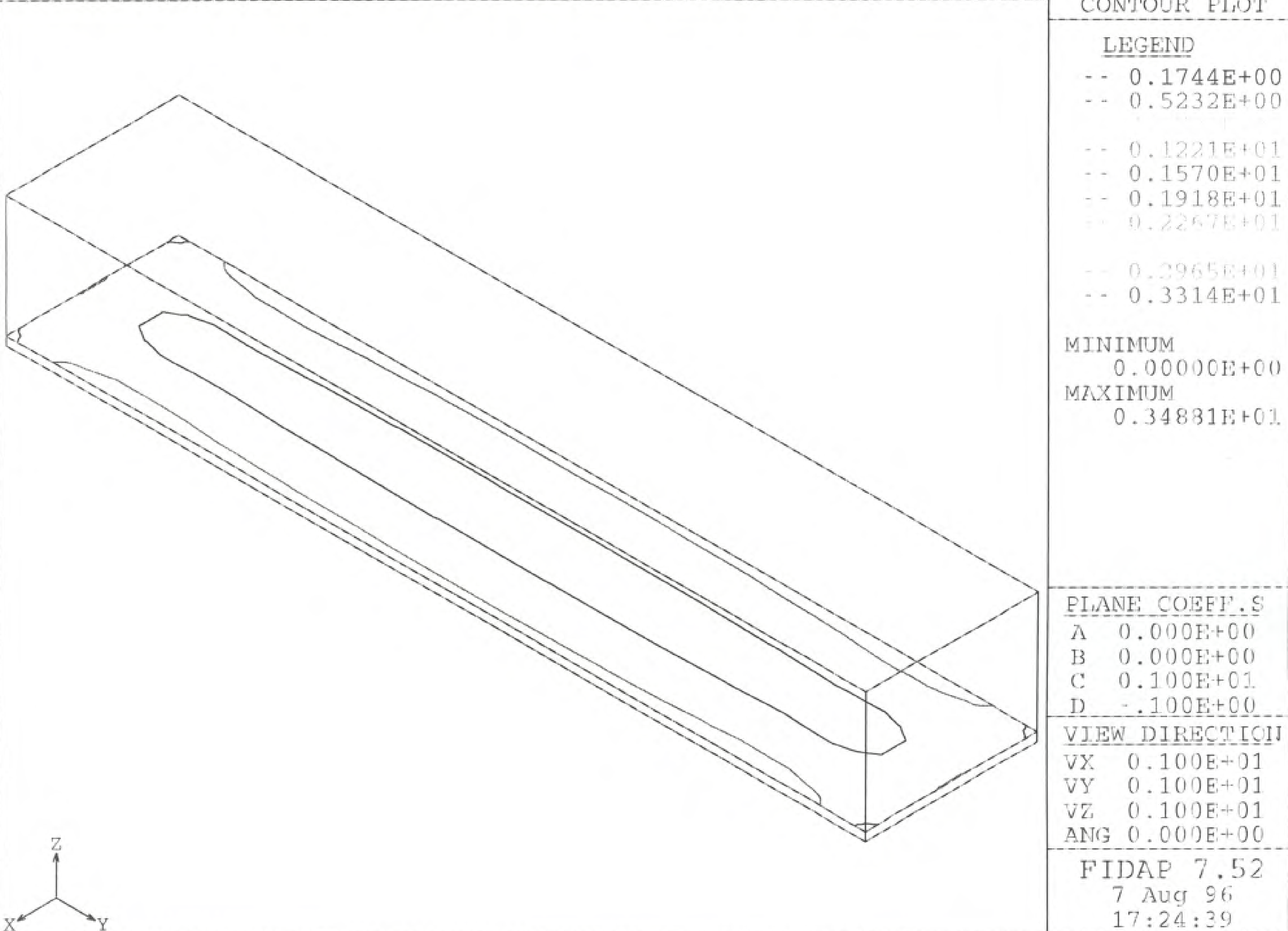

FIGURE 5.75: SHEAR STRAIN RATE, DOWNSTREAM SECTION 24

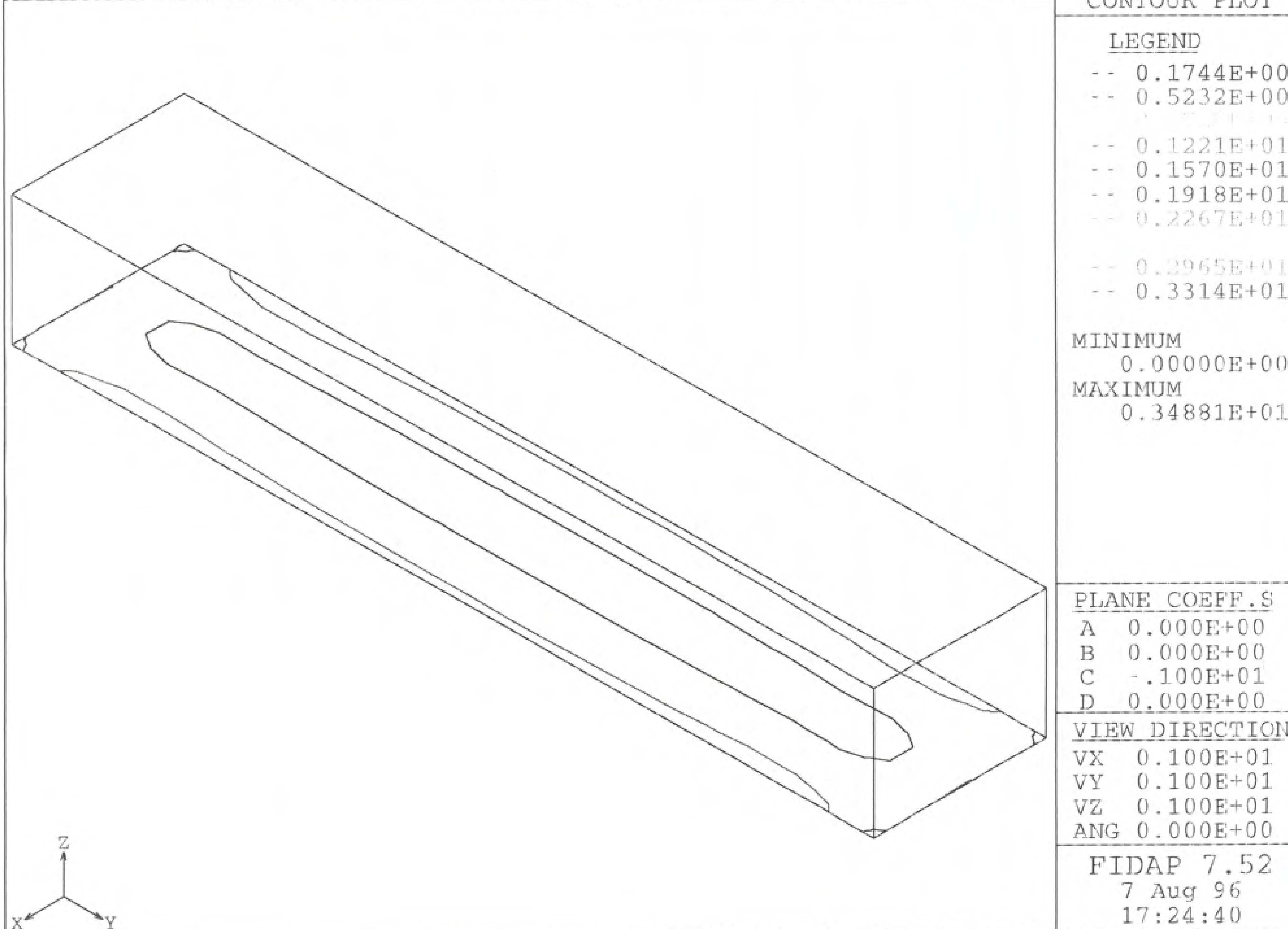

### 5.5.2 Shear Strain Rate

Figure 5.39 plots the shear strain rate over the outer surfaces. The maxima are seen to be on the longer edge at the inlet, due to the discontinuity. There are smaller local maxima on the shorter edges. A possible explanation could be that the fluid is not as constrained at the shorter edges, as at the longer ones, which form the boundaries of a narrower gap. Another point to be considered is that results at discontinuities are not very accurate, and the magnitude of the shear rates simply keeps increasing with mesh density. On the inlet itself, the shear strain rate increases from inside out. On the walls the shear strain rate decreases downstream, as also going from corners to the center of the wall. An interesting observation is the formation of a region of low shear rate near the corner, which increases in size on going downstream. The pattern can be seen to be distinct from the case for a circular tube.

Figure 5.40 shows the shear strain rate to be maximum at the inlet at the outer edge. The value here could be higher than the actual due to the discontinuity at this point. This was observed in the case of circular apertures. The pattern shows that the shear rate does not decrease uniformly inwards in the entrance region but shows a fork like pattern. The shear rate is quite low at the center at the inlet, and then increases in the entrance region, and then starts to decrease. Shear strain rate plots might give a better visual estimate of the entrance length than velocity vectors, whose small changes in length and directions from a given view angle are difficult to notice.

Figures 5.41-5.51 confirm the same observations from a different viewpoint. The pattern is complex in the entrance region, with the fork seen in Figure 5.40 creating regions of lower stress upstream of regions of higher stress in some planes. A new observation is the development of a region of low stress near the center of the long walls as the flow proceeds downstream.

The effects of the entrance region are also visible in the "downstream section" plots, where the contours are monotonically decreasing inwards at the inlet, develop the "fork" as two distinct regions of lower stress lying between the axis and the walls. These regions finally grow and combine to return the pattern to a monotonic one, except for the local effects at the corners.

The shear strain rate does fall below the break rate, right next to the corners downstream. However the volume enclosed in the region is almost negligible, and thus is of no consequence in modeling the process of paste release. The rate is higher than the break rate over the bulk of the volume, at least in the region considered. The region of flow encountered in the paste printing process, i.e. the depth of the stencil is such that the flow region is within the entrance region. Thus, the depth considered here is sufficient for modeling the process.

## 5.6 Conclusions

The results for velocity and shear strain rate distributions obtained in the previous sections indicate that there is an entrance region for the rectangular slot where transverse velocity components cannot be ignored. The shear strain rate patterns are quite complex due to the presence of these components in the entrance region. The pattern is quite different from that obtained for circular apertures. Hence, geometric simplifications are not recommended. The value of the shear strain rate exceeds the break rate nearly all over the volume. Hence, it is not feasible to further develop the model of paste release, as a steady state incompressible uniform entry flow of a Newtonian fluid, even if creep flow assumptions are used instead of boundary layer theory.

## CHAPTER 6

## CONCLUSIONS

The aim of the thesis is to determine if the model proposed by Sahay et. al. (1995) could be used with minor modifications if more appropriate approximations were to be used for calculating the velocity distribution and the shear stresses during solder paste release. Hence, a steady state analysis was carried out for a Newtonian fluid using creep flow assumptions for circular and rectangular apertures. Velocity and shear rate distributions were studied analytically and numerically for cylindrical slots, for the given flow conditions. An equivalent rectangular slot was studied using numerical techniques.

### 6.1 Model for Solder Paste Release

The present study indicates, that for steady state flow of a Newtonian fluid for the given magnitude of Reynolds number ( $\sim 10^{-4}$ ), the shear stress exceeds the breaking stress of solder paste nearly all over the volume. Hence, in its present form, the model is not able to predict the volume deposited as per the mechanism set forth by Sahay et. al. (1995). Radial or transverse velocity components play a significant role in determining the stress distribution. Besides, geometry simplifications for the problem are not recommended as the shear strain rate is very sensitive to the velocity distribution.

However, the mechanism proposed by Sahay et. al., (1995) does seem to be correct in the fundamental assumption that the paste breaks off at regions where the shear stress exceeds the break stress. It is suggested for future work that the simplifications made in the present work for a direct comparison with the previous work be replaced by others, so as to determine ones which are most appropriate, and to get a more realistic value of the stresses in the actual process of paste printing. Specifically, certain additional characteristics of the solder paste like shear thinning, Bingham-plastic behaviour, as well as the transient nature of the process and the finite region of flow should be further investigated in addition to the properties of tack strength and viscosity which are considered here.

## 6.2 Application of Finite Element Method to Fluids

It is observed that numerical methods have to be applied with care to fluids problems. Although the finite element method and software is growing rapidly for fluids applications, it is not as well developed as that for solid mechanics. The velocity correlations between numerical and analytical solutions is found to be good, while the shear strain rate correlations are not quite satisfactory. Errors resulting in totally unacceptable results do not terminate the program outright, and results should be checked carefully. The input values for this particular thesis are arbitrary in part, as dimensional analysis cannot determine the values fully. The errors noticed in the software for certain input values did serve as a guide towards possible values to be input, but the final data used still involved some degree of arbitrariness. Extreme caution is to be used for interpreting results near discontinuities. Finally, like in any numerical scheme, convergence is no guarantee of accuracy.

## APPENDIX I

```
# **********
# *                    PROGRAM IDENTIFICATION
# **********
# *        Computes the strain components based on the formulas obtained by Lew & Fung
# *
# **********
# *                    VARIABLE IDENTIFICATION
# **********
# *a             - Radius of tube
# * h#           - Intermediate terms in calculation of constants
# *m             - Index for inner loop
# *n             - Index for outer loop
# *r             - Radial position
# *s11           - Strain (r-r)
# *s22           - Strain (phi-phi)
# *s33           - Strain (x-x)
# *s12           - Strain (r-phi)
# *s13           - Strain (r-x)
# *s23           - Strain (phi-x)
# *u             - Axial velocity
# *ur            - du/dr
# *ux            - du/dx
# *u0            - Dimensionless axial velocity
# *v             - Radial velocity
# *vr            - dv/dr
# *vx            - dv/dx
# *v0            - Dimensionless radial velocity
# *x             - Axial position
# *N             - Arbitrary "large" no., length of tube = a*N
# *U             - Inlet axial velocity
# *k(1)-k(19)   - First 19 zeroes of Bessel first kind order zero
# *p#(index)    - Int. terms for radial calculations  (inner loop)
# *t#(index)    - Int. terms for axial calculations (inner loop)
# *A(1)-A(19) - 19 coefficients for 19 terms of series considered
# *P#(index)    - Int. terms for radial calculations (outer loop)
# *T#(Index)    - Int. terms for axial calculations (outer loop)
# *
# **********
# *                    INITIALIZATION BLOCK
# **********
#==================================================================
```

```
> a:=.00016891:
> N:=3:
> U:=.203:
#-------------------------------------------------------------------------------------------------------------------
--
> A(1):=-.41213:
> A(2):=.29508:
> A(3):=.23089:
> A(4):=.17204:
> A(5):=.12982:
> A(6):=.09896:
> A(7):=.07565:
> A(8):=.05760:
> A(9):=.04316:
> A(10):=.03219:
> A(11):=.02332:
> A(12):=.01638:
> A(13):=.01104:
> A(14):=.00704:
> A(15):=.00416:
> A(16):=.00221:
> A(17):=.00099:
> A(18):=.00033:
> A(19):=.00006:
#-------------------------------------------------------------------------------------------------------------------
--
> k(1):=2.4048:
> k(2):=5.5201:
> k(3):=8.6537:
> k(4):=11.7915:
> k(5):=14.9309:
> k(6):=18.0711:
> k(7):=21.2116:
#----------------------- Calculation for remaining k's---------------------------------------------
--------------
> for i from 8 to 19 do
> h1:=4*i-1:
>
h2:=.25*Pi*h1*(1+2/(Pi^2*h1^2)-62/(3*(Pi^2*h1^2)^2)+15116/(15*(Pi^2*h1^2)^3)-12554474/
(105*(Pi^2*h1^2)^4)+8368654292/(315*(Pi^2*h1^2)^5)):
> k(i):=evalf(h2):
> od:
#==================================================================
```

```
# **********
# *                                VELOCITY CALCULATION BLOCK
# **********
# *
# *                                      AXIAL VELOCITY
# *
> T1(0):=0:
#--------------------------------Outer (n) Loop ---------------------------------------------------------------
--
> for n from 1 to 19 do
> T2:=(k(n)*(x/a)+1)*exp(-k(n)*(x/a))*BesselJ(0,k(n)*r/a)/BesselJ(1,k(n)):
> #----------------------------Inner (m) Loop -------------------------------------------------------------------
--
> t13(0):=0:
> for m from 1 to 38 do
> t1(m):=m*Pi/N:
> t2(m):=t1(m)*r/a:
> t3(m):=BesselI(0,t1(m)):
> t4(m):=BesselI(1,t1(m)):
> t5(m):=BesselI(0,t2(m)):
> t6(m):=BesselI(1,t2(m)):
> t7(m):=t5(m)/t3(m)-(2*t5(m)+t2(m)*t6(m))/(2*t3(m)+t1(m)*t4(m)):
> t8(m):=t4(m)/t3(m)-(t1(m)*t3(m))/(2*t3(m)+t1(m)*t4(m)):
> t9(m):=t7(m)/t8(m):
> t10(m):=t1(m)/(k(n)^2+t1(m)^2):
> t11(m):=exp(-N*k(n))*cos(m*Pi)*(N/2+k(n)/(k(n)^2+t1(m)^2))-k(n)/(k(n)^2+t1(m)^2):
> t12(m):=t11(m)*cos(m*Pi*x/(N*a)):
> t13(m):=t13(m-1)+t9(m)*t10(m)*t12(m):
> od:
#-------------------------------------------------------------------------------------------------------------
--
> T3(n):=A(n)*(T2+4*k(n)/N*t13(38));
> T1(n):=T1(n-1)+T3(n);
> od:
> u0:=T1(19)+2*(1-r^2/a^2):
> u:=U*u0:
> ux:=diff(u,x):
> ur:=diff(u,r):
#-------------------------------------------------------------------------------------------------------------
--
# **********
# *                                      RADIAL VELOCITY
# **********
```

```
# *
#------------------------------Outer (n) Loop -----------------------------------------------------------------------
--
> P1(0):=0:
> for n from 1 to 19 do
> P2:=k(n)*(x/a)*exp(-k(n)*(x/a))*BesselJ(1,k(n)*r/a)/BesselJ(1,k(n)):
#----------------------------Inner (m) Loop ------------------------------------------------------------------------
--
> p13(0):=0:
> for m from 1 to 38 do
> p1(m):=m*Pi/N:
> p2(m):=p1(m)*r/a:
> p3(m):=BesselI(0,p1(m)):
> p4(m):=BesselI(1,p1(m)):
> p5(m):=BesselI(0,p2(m)):
> p6(m):=BesselI(1,p2(m)):
> p7(m):=p6(m)/p3(m)-(p2(m)*p5(m))/(2*p3(m)+p1(m)*p4(m)):
> p8(m):=p4(m)/p3(m)-(p1(m)*p3(m))/(2*p3(m)+p1(m)*p4(m)):
> p9(m):=p7(m)/p8(m):
> p10(m):=p1(m)/(k(n)^2+p1(m)^2):
> p11(m):=exp(-N*k(n))*cos(m*Pi)*(N/2+k(n)/(k(n)^2+p1(m)^2))-k(n)/(k(n)^2+p1(m)^2):
> p12(m):=p11(m)*sin(m*Pi*x/(N*a)):
> p13(m):=p13(m-1)+p9(m)*p10(m)*p12(m):
> od:
> P3(n):=A(n)*(P2+4*k(n)/N*p13(38));
> P1(n):=P1(n-1)+P3(n);
> od:
> v0:=P1(19):
> v:=U*v0:
> vx:=diff(v,x):
> vr:=diff(v,r):
#===================================================================================
# **********
# *                              STRAIN RATE CALCULATION BLOCK
# **********
# *                              SAMPLE CALCULATIONS FOR r/a = 0.1
# **********
# *                           COMPONENTS OF THE STRAIN RATE MATRIX
#
#--------------------------------------------------------------------------------------------------------------------
--
> s11:=vr:
#--------------------------------------------------------------------------------------------------------------------
```

```
--
> s22:=v/r:
#-----------------------------------------------------------------------------------------------------------------
--
> s33:=ux:
#-----------------------------------------------------------------------------------------------------------------
--
> s12:=0:
#-----------------------------------------------------------------------------------------------------------------
--
> s13:=.5*(ur+vx):
#-----------------------------------------------------------------------------------------------------------------
--
> s23:=0:
#-----------------------------------------------------------------------------------------------------------------
--
> r:=.01*a:

#-----------------------------------------------------------------------------------------------------------------
--
> with(linalg):
Warning: new definition for   norm
Warning: new definition for   trace
#-----------------------------------------------------------------------------------------------------------------
--
# **********
# *              LOOP FOR CALCULATING MATRIX AT VARIOUS X
# *            AND GENERATION OF EIGENVALUES AT EACH POINT
# **********

> for x from 0 to 1*a by .1*a do
> x;
> S11:=evalf(s11);
> S22:=evalf(s22);
> S33:=evalf(s33);
> S13:=evalf(s13);
> X:=x*10/a:
> Y:=floor(X):
> G(Y):=matrix(3,3,[S11,0,S13,0,S22,0,S13,0,S33]);
> F(Y):=evalf(Eigenvals(G(Y)));
> F1(Y):=F(Y)[1]:
> F2(Y):=F(Y)[2]:
> F3(Y):=F(Y)[3]:
```

```
> SS:=(max(F1(Y),F2(Y),F3(Y))-min(F1(Y),F2(Y),F3(Y)))/2;
> od;
#==========================================================================
# **********
# *                         SAMPLE OUTPUT
# **********
                    0

                 S11 := 0

                 S22 := 0

               S33 := -.000011

             S13 := -27.35194739

                  X := 0

                  Y := 0

                         [      0       0  -27.35194739     ]
                         [                                  ]
         G(0) :=         [      0       0        0          ]
                         [                                  ]
                         [ -27.35194739  0    -.000011      ]

         F(0) := [ -27.35195289, 0, 27.35194190 ]

              F1(0) := -27.35195289

                 F2(0) := 0

              F3(0) := 27.35194190

               SS := 27.35194740

                 .000016891

              S11 := -453.3531141

              S22 := -453.4381107

              S33 := 906.7911996
```

S13 := -15.91197403

X := 1.000000000

Y := 1

$$G(1) := \begin{bmatrix} -453.3531141 & 0 & -15.91197403 \\ 0 & -453.4381107 & 0 \\ -15.91197403 & 0 & 906.7911996 \end{bmatrix}$$

F(1) := [ -453.5392387, -453.4381107, 906.9773243 ]

F1(1) := -453.5392387

F2(1) := -453.4381107

F3(1) := 906.9773243

SS := 680.2582816

.000033782

S11 := -701.8530336

S22 := -701.8917146

S33 := 1403.744750

S13 := -7.849037901

X := 2.000000000

Y := 2

$$G(2) := \begin{bmatrix} -701.8530336 & 0 & -7.849037901 \\ 0 & -701.8917146 & 0 \\ -7.849037901 & 0 & 1403.744750 \end{bmatrix}$$

F(2) := [ -701.8917146, -701.8822921, 1403.774008 ]

F1(2) := -701.8917146

F2(2) := -701.8822921

F3(2) := 1403.774008

SS := 1052.832861

.000050673

S11 := -785.2911403

S22 := -785.3764812

S33 := 1570.667625

S13 := -1.780563783

X := 3.000000000

Y := 3

$$G(3) := \begin{bmatrix} -785.2911403 & 0 & -1.780563783 \\ 0 & -785.3764812 & 0 \\ -1.780563783 & 0 & 1570.667625 \end{bmatrix}$$

F(3) := [ -785.3764812, -785.2924856, 1570.668971 ]

F1(3) := -785.3764812

F2(3) := -785.2924856

F3(3) := 1570.668971

SS := 1178.022726

.000067564

S11 := -749.1050454

S22 := -749.2402740

S33 := 1498.345323

S13 := .6448513045

X := 4.000000000

Y := 4

$$G(4) := \begin{bmatrix} -749.1050454 & 0 & .6448513045 \\ 0 & -749.2402740 & 0 \\ .6448513045 & 0 & 1498.345323 \end{bmatrix}$$

F(4) := [ -749.2402740, -749.1052304, 1498.345508 ]

F1(4) := -749.2402740

F2(4) := -749.1052304

F3(4) := 1498.345508

SS := 1123.792891

.000084455

S11 := -645.1002359

S22 := -645.2626656

S33 := 1290.362897

S13 := -.1663172205

X := 5.000000000

Y := 5

$$G(5) := \begin{bmatrix} -645.1002359 & 0 & -.1663172205 \\ 0 & -645.2626656 & 0 \\ -.1663172205 & 0 & 1290.362897 \end{bmatrix}$$

F(5) := [ -645.2626656, -645.1002499, 1290.362911 ]

F1(5) := -645.2626656

F2(5) := -645.1002499

F3(5) := 1290.362911

SS := 967.8127883

.000101346

S11 := -516.0393455

S22 := -516.2031022

S33 := 1032.242446

S13 := -3.042676637

X := 6.000000000

Y := 6

$$G(6) := \begin{bmatrix} -516.0393455 & 0 & -3.042676637 \\ 0 & -516.2031022 & 0 \\ -3.042676637 & 0 & 1032.242446 \end{bmatrix}$$

F(6) := [ -516.2031022, -516.0453249, 1032.248425 ]

F1(6) := -516.2031022

F2(6) := -516.0453249

F3(6) := 1032.248425

SS := 774.2257636

.000118237

S11 := -390.0995637

S22 := -390.2458730

S33 := 780.3454378

S13 := -6.785830402

X := 7.000000000

Y := 7

```
         [ -390.0995637        0        -6.785830402 ]
         [                                           ]
G(7) :=  [      0        -390.2458730        0       ]
         [                                           ]
         [ -6.785830402        0        780.3454378  ]
```

F(7) := [ -390.2458730, -390.1389042, 780.3847788 ]

F1(7) := -390.2458730

F2(7) := -390.1389042

F3(7) := 780.3847788

SS := 585.3153259

.000135128

S11 := -281.8726677

S22 := -281.9923455

S33 := 563.8650135

S13 := -10.52343374

X := 8.000000000

Y := 8

```
         [ -281.8726677        0        -10.52343374 ]
         [                                           ]
G(8) :=  [      0        -281.9923455        0       ]
```

```
        [                                            ]
        [ -10.52343374       0        563.8650135 ]

F(8) := [ -282.0035894, -281.9923455, 563.9959353 ]

        F1(8) := -282.0035894

        F2(8) := -281.9923455

        F3(8) := 563.9959353

         SS := 422.9997624

          .000152019

        S11 := -196.2105510

        S22 := -196.3020964

        S33 := 392.5126479

        S13 := -13.77342885

         X := 9.000000000

            Y := 9

        [ -196.2105510       0       -13.77342885 ]
        [                                         ]
G(9) := [      0      -196.3020964       0        ]
        [                                         ]
        [ -13.77342885       0        392.5126479 ]

F(9) := [ -196.5326100, -196.3020964, 392.8347069 ]

        F1(9) := -196.5326100

        F2(9) := -196.3020964

        F3(9) := 392.8347069

         SS := 294.6836585
```

.000168910

S11 := -132.2888581

S22 := -132.3552968

S33 := 264.6441550

S13 := -16.35958410

X := 10.00000000

Y := 10

```
         [ -132.2888581        0        -16.35958410 ]
         [                                           ]
G(10) := [      0        -132.3552968        0       ]
         [                                           ]
         [ -16.35958410        0        264.6441550  ]
```

F(10) := [ -132.9619765, -132.3552968, 265.3172734 ]

F1(10) := -132.9619765

F2(10) := -132.3552968

F3(10) := 265.3172734

SS := 199.1396250

---

## APPENDIX II-A

## COMMUNICATIONS WITH FDI INC.

This appendix includes a partial listing of the communications with FDI Inc., the creators of FIDAP regarding problems encountered while modeling the flow for the original problem.

**Letter 1**

From jcumming@deathloc.cc.binghamton.edu Tue Feb 6 08:43 EST 1996
Received: from deathloc.cc.binghamton.edu (deathloc.cc.binghamton.edu[128.226.1.110])
by bingnfs1 (SMI-8.6/8.6.9) with SMTP id IAA03111 for
<br00340@bingsuns.cc.binghamton.edu>; Tue, 6 Feb 1996 08:43:16 -0500
Received: by deathloc.cc.binghamton.edu (4.1)
id AA01076; Tue, 6 Feb 96 08:56:10 EST
Date: Tue, 6 Feb 1996 08:56:09 -0500 (EST)
From: "John (Jay) Cummings" <jcumming@deathloc.cc.binghamton.edu>
Subject: Strsprint command (fwd)
To: br00340@bingsuns.cc.binghamton.edu
Message-Id: <Pine.3.89.9602060823.A1072-0100000@deathloc.cc.binghamton.edu>
Mime-Version: 1.0
Content-Type: TEXT/PLAIN; charset=US-ASCII
Content-Length: 5027
Status: RO
X-Status:

Manu, here is FDI's resonses. - Jay

---------- Forwarded message ----------
Date: Mon, 5 Feb 96 16:13:17 CST
From: FDI Support Team <support@fdi.com>
To: jcumming@deathloc.cc.binghamton.edu
Subject: Strsprint command

jcumming@deathloc.cc.binghamton.edu
Subject: Strsprint command

FLUID DYNAMICS INTERNATIONAL
500 Davis Street, Suite 600
Evanston, Illinois 60201 U.S.A.

Phone: (847) 491-0200
Fax: (847) 869-6495
E-mail: support@fdi.com

FROM: FDI Support

--------------------------------------------------------------------------------

TO: John Cummings
UNIVERSITY: SUNY

DATE: 5 February 1996 TOTAL PAGES: 1

--------------------------------------------------------------------------------

<DELETED>

**********************************************************

you wrote:
I have attached a copy of my file at the end of this letter. The file includes the changes suggested previously (ie. scaling of sides of slot, instead of creating a small slot to start with) and using a segregated solver.

In an earlier message, I had said that the transverse velocity components are much smaller than expected. However now I have found something even more unexpected :

> The velocity field would not satisfy the continuity equation, the error being quite large.
>
> The geometry is a cuboid, with edges along the three axes. The inlet and outlet have normals in the z direction. Fluid flows into the region at the inlet, with constant uz=-.203
>
> As the flow is incompressible, integral of (uz)*(dA), where dA is (dx)*(dy) should be the same over all planes parallel to the inlet.
>
> However, a plot of UZ on different planes shows that it *decreases* monotonically, from the uniform inlet condition that uz=-.203 m/s at all points as you go downstream!
>
> Thus, more fluid flows into any volume element, than flows out of it.

Could you please look at the thing and see if you can figure out what is causing the problem?

*******************************************************
fdi:
I ran the input file and verified that you are losing mass by checking that the flow rates are not equal at the inlet and at the outlet. You can use the following commands to verify this.

fipost
flow(density,enti="inlet")
flow(density,enti="outlet")

In order to determine your source of error, I suggest that you run the analogous 2-d problem (in the x-z plane). Set up the 2-d problem and check the flow rates at the inlet and the outlet. If they are not equal, you may need to refine the mesh, increase the value of the penalty keyword (currently the default value of 10e-6 is used) or increase the convergence tolerance.

Please let us know if you have any further questions.
Good-luck!
FDI SUPPORT

<DELETED>

**Letter 2**

From support@fdi.com Wed Feb 21 16:01 EST 1996
Received: from hp.fdi.com (hp.fdi.com [192.104.61.84]) by bingnfs1
(SMI-8.6/8.6.9) with ESMTP id QAA23464 for
<br00340@bingsuns.cc.binghamton.edu>;
Wed, 21 Feb 1996 16:01:35 -0500
Received: by hp.fdi.com
(1.37.109.16/16.2) id AA203376424;
Wed, 21 Feb 1996 15:00:24 -0600
Message-Id: <199602212101.QAA23464@bingnfs1>
From: FDI Support Team <support@fdi.com>
Subject: nondimensionalize
To: br00340@bingsuns.cc.binghamton.edu

Date: Wed, 21 Feb 96 15:00:24 CST
Mailer: Elm [revision: 70.85.2.1]
Content-Type: text
Content-Length: 8529
Status: RO
X-Status: jcumming@deathloc.cc.binghamton.edu
br00340@bingsuns.cc.binghamton.edu
Subject: nondimensionalize

FLUID DYNAMICS INTERNATIONAL
500 Davis Street, Suite 600
Evanston, Illinois 60201 U.S.A.

Phone: (847) 491-0200
Fax: (847) 869-6495
E-mail: support@fdi.com

FROM: FDI Support

-------------------------------------------------------------------------------

TO: John Cummings and Manu
UNIVERSITY: SUNY

DATE: 21 February 1996 TOTAL PAGES: 1

-------------------------------------------------------------------------------

John,

I am e-mailing the following to Manu also.

you wrote:

Hello again. I have a grad student here, who has an ongoing problem using Fidap (v7.52, under solaris 2.4). We have communicated with you a few times over the past month, but, apparently the problem persists. I hope I have included enough information (below), so that you may fully analyze the problem, and offer a solution(?)

Thanks. If you require more information about what the student is doing, please contact me, or email the student directly at br00340@bingsuns.cc.binghamton.edu (his name is Manu). If you contact him directly, please CC: me, so I know what is going on.

************************************************************

fdi:

I want to make sure that the units for this problem are consistent. I am concerned that the problems you have faced are due to the small length scales you have used.

Your input file has the following values

dimensions of box: -.1e-3<x<.1e-3
dimensions of box: -.5e-3<y<.5e-3
dimensions of box: 0<z<.15e-3

inlet velocity: .2
density:5500
viscosity:1000

Are the units for these values consistent?
If dimensions are in meters, then velocity should be in m/s, density in kg/m3, viscosity in N-s/m2.

Are you expecting parallel flow at the outlet? If so you need to impose an additional set of boundary conditions for ux and uy at the outlet.

I changed the pressure calculation from the penalty method to the mixed approximation which should give a more accurate solution in your type of problem.

I modified your input file to verify that in the case where all of the above parameters are 1 that continuity is satisfied. The Reynolds number for this problem is also 1. I will send you the input file I used and also the calculation of the flow rate at the inlet and outlet. Since they are both equal, mass is conserved. Since it is NOT conserved with your set of parameters, it is probably due to the differences in scaling. One suggestion is to nondimensionalize so that the lengths for your problem are of the order 1. The Reynolds number will not be 1 however. You can slowly adjust the Reynolds number from 1 (using the input file I am sending you where continuity is conserved at the inlet and outlet) to whatever the actual value for the Reynolds number for your problem is. At each step, make sure that continuity is conserved. If at appears that at a particular value of Reynolds number that continuity is not conserved then you will have to refine the mesh, increase the tolerance or do a combination of the two.

The following is the output from the FIOUT file which shows that continuity is satisfied.
I used the commands

```
fipo
flow(enti="inlet",prin)
flow(enti="outlet",prin)
```

## APPENDIX II-B

## FIDAP PROGRAM FOR CIRCULAR APERTURES

```
TITLE
2-D STEADY STATE ENTRANCE FLOW
/
/THIS PROGRAM CREATES A FINITE ELEMENT MODEL FOR
/A CASE DYNAMICALLY SIMILAR TO THE ANALYTICAL CASE
/
/----------------------------------------------------------
/
/GEOMETRY CREATION AND MESHING OF REGION
/
FI-GEN( ELEM = 1, POIN = 1, CURV = 1, SURF = 1, NODE = 0, MEDG = 1,MLOO = 1,
MFAC = 1, BEDG = 1, SPAV = 1, MSHE = 1, MSOL = 1 )
PGRID( ON )
PGRID( SNAP )
POINT( ADD, COLO = 2, COOR, WIND = 1 )
 0 0 0
 3 0 0
 3 1 0
 0 1 0
WINDOW(CHANGE= 1, MATRIX )
   1.00     .00     .00     .00
    .00    1.00     .00     .00
    .00     .00    1.00     .00
    .00     .00     .00    1.00
   -.08    3.08    -.68    1.68  -10.50   10.50
POINT( SELE, ID, WIND = 1 )
 4
 3
CURVE( ADD, LINE, COLO = 8 )
POINT( SELE, ID, WIND = 1 )
 1
 2
CURVE( ADD, LINE )
POINT( SELE, ID, WIND = 1 )
 1
 4
CURVE( ADD, LINE )
POINT( SELE, ID, WIND = 1 )
```

```
 2
 3
CURVE( ADD, LINE )
CURVE( SELE, ID, WIND = 1 )
 1
 2
MEDGE( ADD, COLO = 7, INTE = 136 )
/MEDGE( ADD, COLO = 7, INTE = 90 )
/MEDGE( ADD, COLO = 7, INTE = 60 )
CURVE( SELE, ID, WIND = 1 )
 4
 3
MEDGE( ADD, FRST, INTE = 90, RATI = 2 )
/MEDGE( ADD, FRST, INTE = 60, RATI = 2 )
/MEDGE( ADD, FRST, INTE = 40, RATI = 2 )
CURVE( SELE, ID, WIND = 1 )
 1
 4
 2
 3
MFACE( WIRE, COLO = 8, EDG1 = 1, EDG2 = 1, EDG3 = 1, EDG4 = 1 )
MFACE( SELE, ID, WIND = 1 )
 1
ELEMENT( SETD, NODE = 9 )
MFACE( MESH, MAP, ENTI = "fluid" )
MEDGE( SELE, ID, WIND = 1 )
 4
ELEMENT( SETD, EDGE, NODE = 3 )
MEDGE( MESH, MAP, ENTI = "inflow" )
MEDGE( SELE, ID, WIND = 1 )
 3
MEDGE( MESH, MAP, GROU = 3, ENTI = "outflow" )
MEDGE( SELE, ID, WIND = 1 )
 2
MEDGE( MESH, MAP, GROU = 4, ENTI = "symmetry" )
MEDGE( SELE, ID, WIND = 1 )
 1
MEDGE( MESH, MAP, GROU = 5, ENTI = "wall" )
END( )
/
/----------------------------------------------------------
/
FIPREP
```

```
/
/DEFINITION OF SOLUTION METHOD
/
PROBLEM( ADD, AXI-, INCO, STEA, LAMI, LINE, NEWT, MOME, ISOT, FIXE, SING )
EXECUTION(NEWJOB)
PRESSURE(MIXED,CONTINUOUS)
/
/IMPOSITION OF BOUNDARY CONDITIONS
/
ENTITY(FLUID,NAME="fluid")
ENTITY(PLOT,NAME="symmetry")
ENTITY(PLOT,NAME="inflow")
ENTITY(PLOT,NAME="outflow")
ENTITY(PLOT,NAME="wall")
BCNODE(URC,ENTITY="symmetry",ZERO)
BCNODE(UZC,ENTITY="inflow", CONS = .203 )
BCNODE(URC,ENTITY="inflow",ZERO)
BCNODE(URC,ENTITY="outflow",ZERO)
BCNODE(VELOCITY,ENTITY="wall",ZERO)
VISCOSITY(CONSTANT=1)
DENSITY(CONSTANT= .000933955)
RENUMBER(PROFILE)
END
/
/----------------------------------------------------------
/

/SOLUTION PHASE
/
CREATE(FISOLV)
RUN( FISOLV, IDEN = "circle", FORE, COMP )
/
/========================================================
/
```

## APPENDIX II-C

**Part 1**

```
***********
*               PROGRAM IDENTIFICATION
***********
*
*    Compute the strain components from velocity data points
*    using finite difference scheme for derivatives
*
***********
*               VARIABLE IDENTIFICATION
***********
*
*    XF       - Multiplier for scaling distance
*    UF       - Multiplier for scaling velocity
*    I        - Index (radial position based)
*    J        - Index (axial position based)
*    XX(J)    - Dimensionless axial position
*    RR(I)    - Dimensionless radial position
*    UU(J,I)  - Dimensionless axial velocity
*    VV(J,I)  - Dimensionless radial velocity
*    X(J)     - Actual axial position
*    R(I)     - Actual radial position
*    U(J,I)   - Actual axial velocity
*    V(J,I)   - Actual radial velocity
*    UX(J,I)  - Differential of axial velocity wrt axial position
*    UR(J,I)  - Differential of axial velocity wrt radial position
*    VX(J,I)  - Differential of radial velocity wrt axial position
*    VR(J,I)  - Differential of radial velocity wrt radial position
*    S11(J,I) - Stress(rr)
*    S22(J,I) - Stress(phi-phi)
*    S33(J,I) - Stress(xx)
*    S12(J,I) - Stress(r-phi)
*    S13(J,I) - Stress(r-x)
*    S23(J,I) - Stress(x-phi)
*
**********
*               TYPE DECLARATION AND STORAGE ALLOCATION
*
     DIMENSION XX(11),RR(13),UU(11,13),VV(11,13),X(11),R(13)
     DIMENSION U(11,13),V(11,13),UX(11,13),UR(11,13)
     DIMENSION VX(11,13),VR(11,13),S11(11,13),S22(11,13)
```

```
      DIMENSION S33(11,13),S12(11,13),S13(11,13),S23(11,13)
*
**********
*              INITIALIZATION BLOCK
**********
*
      OPEN(1,FILE='datlff')
      OPEN(2,FILE='strain')
      OPEN(3,FILE='output')
      XF = 1.651E-4
      UF = .203
*
**********
*              DATA INPUT AND SCALING
**********
*
      DO 100 I = 1,13
        DO 200 J = 1,11
          READ(1,*) RR(I),XX(J),UU(J,I),VV(J,I)
 10        FORMAT(F4.2,4X,F3.1,5X,F7.5,9X,F8.5)
          X(J)=XF*XX(J)
          R(I)=XF*RR(I)
          U(J,I)=UF*UU(J,I)
          V(J,I)=UF*VV(J,I)
 200      CONTINUE
 100    CONTINUE

*
**********
*              CALCULATIONS
**********

      DO 300 I = 2,11
        DO 400 J = 2,9
          UX(J,I) = (U(J+1,I)-U(J-1,I))/(X(J+1)-X(J-1))
          UR(J,I) = (U(J,I+1)-U(J,I-1))/(R(I+1)-R(I-1))
          VX(J,I) = (V(J+1,I)-V(J-1,I))/(X(J+1)-X(J-1))
          VR(J,I) = (V(J,I+1)-V(J,I-1))/(R(I+1)-R(I-1))
          S11(J,I)= VR(J,I)
          S22(J,I)= V(J,I)/R(I)
          S33(J,I)= UX(I,J)
          S12(J,I)= 0
          S13(J,I)= .5*(UR(J,I)+VX(J,I))
```

```
        S23(J,I)= 0
        WRITE(2,*)S11(J,I),S22(J,I),S33(J,I),S13(J,I)
        WRITE(3,*)XX(J),RR(I),S11(J,I),S22(J,I),S33(J,I),S13(J,I)
 400    CONTINUE
 300  CONTINUE
     STOP
     END
```

**Part 2**

This program reads in the shear rates obtained at various points by using a finite difference scheme to generate derivatives for the velocity field. The velocity data points are the ones obtained by Lew & Fung using analytical treatment. Then the shear rate matrix is created and the eigenvalues determined so as to obtain the maximum shear rate, as also to check for continuity violations, by summing the terms of main diagonal,which should be zero.

```
> with(linalg):
> for i from 2 by 1 to 80 do
> A:=readline(strain);
> B:=sscanf(A,` %e %e %e %e`);
> G(i):=matrix(3,3,[B[1],0,B[4],0,B[2],0,B[4],0,B[3]]);
> F(i):=evalf(Eigenvals(G(i)));
> F1(i):=F(i)[1]:
> F2(i):=F(i)[2]:
> F3(i):=F(i)[3]:
> Ch(i):=F1(i)+F2(i)+F3(i);
> S(i):=(max(F1(i),F2(i),F3(i))-min(F1(i),F2(i),F3(i)))/2;
> od;
----------------------------------------------------------------------
```

**Part 3**

RESULTS FOR NUMERICAL DIFFERENTIATION

Columns (1) and (2) define location of point

Column (3) is the maximum shear rate (1/s)

Column (4) is the sum of the main diagonal for the shear rate matrix, and should be zero for continuity to be satisfied.

| x/a | r/a | Max Shear | Cont. Check |
|---|---|---|---|
| .1000000000000000, | .1000000000000000, | 661.5475531, | 160.6419998 |
| .2000000000000000, | .1000000000000000, | 383.0918656, | -1070.084001 |
| .3000000000000000, | .1000000000000000, | 408.4290908, | -1584.593000 |
| .4000000000000000, | .1000000000000000, | 379.8112401, | -1497.786000 |
| .5000000000000000, | .1000000000000000, | 325.9724639, | -1278.432000 |
| .6000000000000000, | .1000000000000000, | 261.2872428, | -1014.507999 |
| .7000000000000000, | .1000000000000000, | 203.1120051, | -761.4649998 |
| .8000000000000000, | .1000000000000000, | 172.9658152, | -546.9070000 |
| .1000000000000000, | .2000000000000000, | 1036.731501, | 330.381000 |
| .2000000000000000, | .2000000000000000, | 1124.273111, | -236.873000 |
| .3000000000000000, | .2000000000000000, | 393.8667515, | -1526.988000 |
| .4000000000000000, | .2000000000000000, | 369.0825570, | -1408.950000 |
| .5000000000000000, | .2000000000000000, | 313.7859798, | -1175.273000 |
| .6000000000000000, | .2000000000000000, | 255.9280709, | -913.5609998 |
| .7000000000000000, | .2000000000000000, | 222.8164378, | -673.6130000 |
| .8000000000000000, | .2000000000000000, | 259.0818773, | -476.5769998 |

.1000000000000000, .3000000000000000, 1136.402188, 614.227000

.2000000000000000, .3000000000000000, 1110.033042, 126.339001

.3000000000000000, .3000000000000000, 1076.136313, -27.011000

.4000000000000000, .3000000000000000, 350.2523264, -1248.840999

.5000000000000000, .3000000000000000, 296.4807022, -997.4989997

.6000000000000000, .3000000000000000, 263.4363798, -745.9930000

.7000000000000000, .3000000000000000, 298.5834197, -532.1729999

.8000000000000000, .3000000000000000, 393.4665544, -366.0600000

.1000000000000000, .4000000000000000, 1192.806908, 537.467000

.2000000000000000, .4000000000000000, 1064.940028, 248.189000

.3000000000000000, .4000000000000000, 984.5833180, 14.938000

.4000000000000000, .4000000000000000, 826.9019785, 9.901000

.5000000000000000, .4000000000000000, 294.7412152, -739.7330001

.6000000000000000, .4000000000000000, 316.3421844, -516.8140000

.7000000000000000, .4000000000000000, 448.5173682, -347.3808000

.8000000000000000, .4000000000000000, 579.4344566, -227.1304008

.1000000000000000, .5000000000000000, 1155.599069, 328.291000

.2000000000000000, .5000000000000000, 917.5468200, 99.878000

.3000000000000000, .5000000000000000, 841.6150015, 80.3900005

.4000000000000000, .5000000000000000, 664.5419524, 115.0494000

.5000000000000000, .5000000000000000, 510.9572501, 19.6727000

.6000000000000000, .5000000000000000, 499.6195426, -241.8294001

.7000000000000000, .5000000000000000, 678.9953850, -139.4684004

.8000000000000000, .5000000000000000, 820.7220193, -78.3593999

.1000000000000000, .6000000000000000, 1183.023724, 75.594000

.2000000000000000, .6000000000000000, 797.0826241, -26.4769998

.3000000000000000, .6000000000000000, 683.7293663, 310.3610002

.4000000000000000, .6000000000000000, 607.0792881, 360.8140000

.5000000000000000, .6000000000000000, 599.1834552, 232.8580001

.6000000000000000, .6000000000000000, 821.1949712, -.4713000

.7000000000000000, .6000000000000000, 989.7860225, 58.690999

.8000000000000000, .6000000000000000, 1114.692069, 54.592001

.1000000000000000, .7000000000000000, 1101.871975, 70.375000

.2000000000000000, .7000000000000000, 723.6308095, 517.3629999

.3000000000000000, .7000000000000000, 753.8078535, 766.4450003

.4000000000000000, .7000000000000000, 819.8937075, 708.287000

.5000000000000000, .7000000000000000, 1049.993833, 481.381000

.6000000000000000, .7000000000000000, 1251.841747, 209.015500

.7000000000000000, .7000000000000000, 1346.206906, -17.600300

.8000000000000000, .7000000000000000, 1451.459636, 142.689800

.1000000000000000, .8000000000000000, 1358.250735, 845.672999

.2000000000000000, .8000000000000000, 1133.417042, 1337.694000

.3000000000000000, .8000000000000000, 1299.985954, 1273.102000

.4000000000000000, .8000000000000000, 1534.789104, 954.675001

.5000000000000000, .8000000000000000, 1678.442162, 612.381100

.6000000000000000, .8000000000000000, 1755.288522, 308.849901

.7000000000000000, .8000000000000000, 1791.106945, 88.435601

.8000000000000000, .8000000000000000, 1813.226800, -94.445099

.1000000000000000, .9000000000000000, 2489.231551, 1479.025999

.2000000000000000, .9000000000000000, 2348.735810, 1590.559001

.3000000000000000, .9000000000000000, 2363.470178, 1202.535100

.4000000000000000, .9000000000000000, 2301.187334, 764.908301

.5000000000000000, .9000000000000000, 2227.365938, 530.416999

.6000000000000000, .9000000000000000, 2146.788644, 345.177500

.7000000000000000, .9000000000000000, 2150.734902, 196.428600

.8000000000000000, .9000000000000000, 2061.403414, 145.100990

.1000000000000000, .9500000000000000, 5086.591456, 1655.901704

.2000000000000000, .9500000000000000, 4004.112670, 1357.326400

.3000000000000000, .9500000000000000, 3338.179082, 702.681800

.4000000000000000, .9500000000000000, 2732.429198, 363.891100

.5000000000000000, .9500000000000000, 2613.826378, 319.924751

.6000000000000000, .9500000000000000, 2436.079882, 215.383579

.7000000000000000, .9500000000000000, 2321.481300, 47.571660

## APPENDIX III

```
/input file which creates a brick by mshells and fi-bc for boundary conditions
TITLE( )
CASE1
/NEWTONIAN FLUID, FLAT ENTRANCE PROFILE
/
/---------------------------------------------------------------
/PARAMETERS FOR THE PROBLEM
/---------------------------
/
/*****GEOMETRY DEFINITION*****
/
/APERTURE LENGTH
$l = 1.016
/APERTURE BREADTH
$b = 5.08
/APERTURE HEIGHT
$h = 1.524
/
/*****FLUID PARAMETERS*****
/
/DENSITY
$d=.000000005500
/VISCOSITY
$v=.0000203
/*****FLOW PARAMETERS*****
/
/INLET VELOCITY IN Z DIRECTION
/$z=.203
$z=.203
/
/*****MESH DEFINITION*****
/
/   WALL
/NO OF DIVISIONS
$w1=20
/RATIO 1
$w2=1
/RATIO 2
$w3=1
/PCENTER
```

```
$w4=.5
/
/    INLET
/NO OF DIVISIONS
$i1=15
/RATIO 1
$i2=1.25
/RATIO 2
$i3=1.25
/PCENTER
$i4=.5
/
/    OUTLET
/NO OF DIVISIONS
$o1=15
/RATIO 1
$o2=1.25
/RATIO 2
$o3=1.25
/PCENTER
$o4=.5
/
/------------------------------------------------------------------
/MODEL GENERATION
/-----------------
/
FI-GEN( ELEM = 1, POIN = 1, CURV = 1, SURF = 1, NODE = 0, MEDG = 1, MLOO = 1,
MFAC = 1, BEDG = 1, SPAV = 1, MSHE = 1, MSOL = 1 )
WINDOW(CHANGE= 1, MATRIX )
   1.000000   0.000000   0.000000   0.000000
   0.000000   1.000000   0.000000   0.000000
   0.000000   0.000000   1.000000   0.000000
   0.000000   0.000000   0.000000   1.000000
  -10.00000   10.00000   -7.50000    7.50000   -7.50000    7.50000
POINT( ADD, COOR, WIND =1)
$l  $b  0
$l  -$b  0
-$l -$b  0
-$l  $b  0
$l  $b  $h
$l  -$b  $h
-$l -$b  $h
-$l  $b  $h
```

```
POINT( SELE, COOR, WIND =1)
$l  $b  0
$l -$b  0
CURVE(ADD, LINE)
POINT( SELE, COOR, WIND =1)
$l -$b  0
-$l -$b  0
CURVE(ADD, LINE)
POINT( SELE, COOR, WIND =1)
-$l -$b  0
-$l $b  0
CURVE(ADD, LINE)
POINT( SELE, COOR, WIND =1)
-$l $b  0
$l  $b  0
CURVE(ADD, LINE)
POINT( SELE, COOR, WIND =1)
$l  $b  $h
$l -$b  $h
CURVE(ADD, LINE)
POINT( SELE, COOR, WIND =1)
$l -$b  $h
-$l -$b  $h
CURVE(ADD, LINE)
POINT( SELE, COOR, WIND =1)
-$l -$b  $h
-$l $b  $h
CURVE(ADD, LINE)
POINT( SELE, COOR, WIND =1)
-$l $b  $h
$l  $b  $h
CURVE(ADD, LINE)
POINT( SELE, COOR, WIND =1)
$l  $b  0
$l  $b  $h
CURVE(ADD, LINE)
POINT( SELE, COOR, WIND =1)
$l -$b  0
$l -$b  $h
CURVE(ADD, LINE)
POINT( SELE, COOR, WIND =1)
-$l -$b  0
-$l -$b  $h
```

```
CURVE(ADD, LINE)
POINT( SELE, COOR, WIND =1)
-$l $b 0
-$l $b $h
CURVE(ADD, LINE)
CURVE(SELE, ID, WIND =1)
1
2
3
4
MFACE(WIRE)
CURVE(SELE, ID, WIND =1)
5
6
7
8
MFACE(WIRE)
CURVE(SELE, ID, WIND =1)
1
10
5
9
MFACE(WIRE)
CURVE(SELE, ID, WIND =1)
10
6
11
2
MFACE(WIRE)
CURVE(SELE, ID, WIND =1)
11
7
12
3
MFACE(WIRE)
CURVE(SELE, ID, WIND =1)
12
4
9
8
MFACE(WIRE)
MEDGE(SETD)
CURVE(SELE, ID, WIND =1)
```

```
1
2
3
4
MEDGE(ADD, INTE=$i1, RATI=$i2, 2RAT=$i3, PCEN=$i4)
CURVE(SELE, ID, WIND =1)
5
6
7
8
MEDGE(ADD, INTE=$o1, RATI=$o2, 2RAT=$o3, PCEN=$o4)
CURVE(SELE, ID, WIND =1)
9
10
11
12
MEDGE(ADD, INTE=$w1, RATI=$w2, 2RAT=$w3, PCEN=$w4)
MFACE(SELE, ID, WIND=1)
1
2
3
4
5
6
MSHELL(ADD)
MSHELL(SELE, ID, WIND=1)
1
MSOLID(ADD)
ELEMENT(SETD)
MSOLID(SELE, ID, WIND=1)
1
MSOLID(MESH,MAP, ENTI="fluid")
END
/-----------------------------------------------------------------
FI-BC( )
WINDOW(CHANGE= 1, MATRIX )
  -0.707107  -0.408248   0.577350   0.000000
   0.707107  -0.408248   0.577350   0.000000
   0.000000   0.816497   0.577350   0.000000
   0.000000   0.000000   0.000000   1.000000
  -6.57280    6.57280   -2.48011    7.37909   -3.42080  6.88490
BGADD(SELE, FACE, ID, WIND=1)
6
```

```
BGADD(ADD, ENTI="inlet")
BGADD(SELE, FACE, ID, WIND=1)
3
BGADD(ADD, ENTI="outlet")
BGADD(SELE, FACE, ID, WIND=1)
5
4
1
2
BGADD(ADD, ENTI="wall")
BCSENTITY( BCNO )
BCSENTITY( SELE, ID , WIND = 1 )
2
BCNODE( UX, GSEL, ZERO )
BCNODE( UY, GSEL, ZERO )
BCNODE( UZ, GSEL, CONS =-$z)
UTILITY( UNSE, ALL)
BCSENTITY( SELE, ID , WIND = 1 )
3
/BCNODE( PRES, GSEL, ZERO )
BCNODE( UX, GSEL, ZERO )
BCNODE( UY, GSEL, ZERO )
UTILITY( UNSE, ALL)
BCSENTITY( SELE, ID , WIND = 1 )
4
BCNODE(VELO, GSEL, ZERO)
END( )
FIPREP( )
/----------------------------------------------------------------
DATAPRINT( ADD, CONT )
EXECUTION( ADD, NEWJ )
PRINTOUT( ADD, NONE, BOUN )
PROBLEM( ADD, 3-D, INCO, STEA, LAMI, LINE, NEWT, MOME, ISOT, FIXE,
SING )
pres(mixe,disc)
SOLUTION( ADD, s.s. = 10 )
ENTITY( ADD, NAME = "fluid", FLUI )
ENTITY( ADD, NAME = "wall", PLOT )
ENTITY( ADD, NAME = "inlet", PLOT )
ENTITY( ADD, NAME = "outlet", PLOT )
/DENSITY( ADD, SET = 1, CONS = $d )
/VISCOSITY( ADD, SET = 1, CONS = $v )
END( )
```

```
/
/----------------------------------------------------------------
/SOLUTION
/--------
CREATE( FISO )
READFILE()
```